The work submitted in this dissertation is the result of my own investigation, except where otherwise stated.

Ich erkläre hiermit, dass ich die vorgelegte Dissertation selbst verfasst und mich dabei keiner anderen als der von mir ausdrücklich bezeichneten Quellen und Hilfen bedient habe.

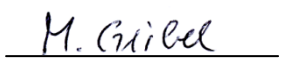

Mirjam Geibel, Edinburgh 24.09.2011

Dissertation
submitted to the
Combined Faculties for the Natural Sciences and for Mathematics
of the Ruperto-Carola University of Heidelberg, Germany
for the degree of
Doctor of Natural Sciences

Presented by

Mirjam Geibel (B.Sc., M.Sc.)
Born in: Karlsruhe, Germany
Oral examination: 14.11.2011

Defining the role of TrkB signalling in CCK-expressing neurons

Referees: Dr. Paul Heppenstall
Prof. Dr. Stephan Frings

Summary

The neurotrophin receptor TrkB has been shown to regulate neuronal survival, migration, differentiation and innervation in the peripheral and central nervous system. In the mature nervous system, it can modulate synaptic plasticity and excitatory neuron-specific deletion of *Trkb* results in compromised learning ability and impaired long-term potentiation. TrkB is also expressed in interneurons and was reported to regulate interneuron differentiation, synapse assembly, maintenance and development of inhibitory networks. Given the heterogeneity of interneurons, cell-specific approaches are required to study the function of TrkB in different interneuronal subtypes.

This study investigates the role of TrkB in a specific subset of interneurons that express cholecystokinin (CCK). *Trkb* was specifically deleted from CCK-neurons by crossing a transgenic BAC-Cre mouse line that expresses Cre under the CCK-promotor (*BAC-CCK-Cre* line) to a T*rkb*-floxed mouse line. CCK-Cre specific *Trkb*-knockout mice ($Trkb^{CCK\text{-}KO}$ mice) develop mature-onset central obesity and show hyperactivity of the HPA axis with peripheral signs of hypercortisolism. Analysis of food intake revealed that central obesity is not associated with hyperphagia but is a cause of hypercortisolism. Furthermore, we show that hypercortisolism-induced obesity is associated with increased leptin and insulin levels. Hyperactivity of the HPA axis in $Trkb^{CCK\text{-}KO}$ mice is associated with increased activity of the central HPA axis regulator, the paraventricular nucleus of the hypothalamus (PVN). PVN activity is strictly regulated by surrounding inhibitory interneurons and glucocorticoid feedback inhibition. We show that GABAergic interneurons in the vicinity of the PVN are recombined in the *BAC-CCK-Cre* line and colocalize with the glucocorticoid receptor GR. Furthermore, we present data indicating an impaired glucocorticoid feedback inhibition in $Trkb^{CCK\text{-}KO}$ mice. TrkB was previously shown to interact directly with the GR leading to enhanced phosphorylation of PLCγ1 by TrkB. Analysis of mice with a mutation in either the PLC or SHC adaptor site of TrkB reveals that the phenotype observed here is dependent on PLCγ1 signalling. Therefore we conclude that TrkB signalling in hypothalamic CCK-interneurons integrates glucocorticoid feedback inhibition and is required for inhibitory control of PVN activity.

Zusammenfassung

Der Neurotrophinrezeptor TrkB reguliert Neuritenwachstum und Überleben, Migration und Differenzierung von Neuronen im peripheren und zentralen Nervensystem. Außerdem moduliert TrkB synaptische Plastizität im adulten Organismus. Das spezifische Entfernen dieses Rezeptors aus exzitatorischen Neuronen in Mäusen führt zu verminderter Lernfähigkeit und Langzeit-Potenzierung. TrkB wird auch in Interneuronen exprimiert und spielt eine wichtige Rolle in der Differenzierung, Synapsenbildung und -erhaltung dieser Zellen und in der Entwicklung und dem Erhalt von inhibitorischen Neuronennetzwerken. Da Interneuronen eine äußerst heterogene Gruppe bilden, sind zellspezifische Methoden notwendig, um die Funktion von TrkB in den verschiedenen Subtypen von Interneuronen zu untersuchen.

Diese Arbeit untersucht die Rolle von TrkB in einem spezifischen Subtyp von Interneuronen, die Cholecystokinin (CCK) exprimieren. *Trkb* wurde spezifisch aus CCK-exprimierenden Neuronen entfernt, indem eine BAC transgene Mauslinie, die die Cre-Rekombinase unter dem CCK-Promotor exprimiert (*BAC-CCK-Cre* Linie), mit einer *Trkb*-gefloxten Mauslinie gekreuzt wurde. CCK-Cre spezifische *Trkb*-Knockout Mäuse ($Trkb^{CCK\text{-}KO}$ Mäuse) entwickeln altersabhängige zentrale Fettleibigkeit, Hyperaktivität der Hypothalamus-Hypophysen-Nebennierenrindenachse (HHNA) und chronischen Hypercortisolismus. Fettleibigkeit ist in diesen Mäusen nicht mit vermehrter Nahrungsaufnahme assoziiert, sondern ist eine Folge des Hypercortisolismus und von erhöhten Leptin- und Insulinwerten begleitet. Hyperaktivität der HHNA in $Trkb^{CCK\text{-}KO}$ Mäusen geht mit einer erhöhten Aktivität des zentralen Regulators der HHNA, dem Nucleus Paraventricularis (PVN), einher. Die Aktivität des PVN wird strikt durch lokale inhibitorische Interneurone und negative Rückkopplung durch Glukokortikoide reguliert. Wir zeigen hier, dass GABAerge Neuronen in der Nähe des PVN in der BAC-CCK-Cre Linie rekombiniert sind und mit dem Glukokortikoidrezeptor (GR) kolokalisieren. Das Entfernen von *Trkb* aus diesen Neuronen in $Trkb^{CCK\text{-}KO}$ Mäusen beeinträchtigt die hemmende Wirkung von Glukokortikoiden auf die Aktivität der HHNA. TrkB kann mit dem GR interagieren und dies verstärkt die Signaltransduktion über die PLC-Adaptorstelle des TrkB-Rezeptors. Die Analyse von

Mauslinien mit einer Punktmutation der PLC- oder SHC-Adaptorstelle des TrkB-Rezeptors zeigt, dass die Regulierung der HHNA von einer funktionalen PLC-Adaptorstelle abhängig ist. Folglich ist die Signaltransduktion über TrkB in CCK-exprimierenden Interneuronen des Hypothalamus notwendig, um die Glukokortikoidrückkopplung im ZNS zu integrieren und die Aktivität der HHNA zu regulieren.

Acknowledgements

It is a pleasure to thank the many people who made this thesis possible.

First of all, I would like to express my gratitude to my PhD supervisor, Dr. Liliana Minichiello, who has supported me throughout my thesis with her knowledge, encouragement and understanding.

I would like to thank the members of my TAC, Prof. Dr. Stephan Frings, Dr. Paul Heppenstall and Dr. Paul Bertone for constructive advice.

For the pleasant and stimulating environment as well as their technical help I would like to thank all present and former members of the Minichiello lab. In particular, I am grateful to Dr. Sylvia Badurek for her support in taking over this project and for teaching me histological techniques, genotyping and handling of mice. Many thanks also go to the present members of the lab, Dr. Jacqui Horn, Juraj Koudelka and Dr. Dario Besusso, whose help, patience and encouragement, particularly during the last months, was invaluable.

Furthermore, I would like to thank Dr. Claus Nerlov and his group for helpful advice during the common seminars. I am also grateful to Dr. Valeria Berno for her assistance with confocal microscopy, to Dr. Mumna Al Banchaabouchi and Dominika Farley for help with behavioural tests and to Giuseppe Chiapparelli, Lynn Morrison and Jenni Rennie for taking care of the mice.

The support and encouragement of many friends has been indispensable, and I would like to particularly thank Catarina Catela and Paschalis Kratsios who were great flatmates in Rome and Anne Desmazieres and Julien Tailleur for many evenings spent together discussing the world and enjoying the pleasures of good food and drink.

There are many more people who have supported me during this time. I will thank them personally when possible.

Special thanks to my family for their love, support and encouragement. Finally, I most want to thank my partner Thomas for his patience, love and endless support throughout the last years.

TABLE OF CONTENTS

Table of Contents

1 Introduction

1.1 Neurotrophins and neurotrophin receptors

1.1.1 Structure and interaction of neurotrophins and their receptors

Neurotrophins are a small family of soluble growth factors that are important regulators of vertebrate nervous system development and maintenance. They were originally characterized by their role in target tissue innervation in the periphery. Innervating sensory and sympathetic neurons are dependent on neurotrophin support and thus the limited amount of neurotrophin expressed by a particular target tissue determines the extend of innervation of this tissue (Levi-Montalcini and Booker, 1960; Bibel and Barde, 2000; Huang and Reichardt, 2001). Moreover, neurotrophins are also expressed by most neurons where they regulate diverse functions including development, survival, axon outgrowth, neuronal function and synaptic plasticity (Reichardt, 2006).

Four members of the neurotrophin family have been characterized in mammals – nerve growth factor (NGF), brain-derived neurotrophic factor (BDNF), neurotrophin 3 (NT3) and 4/5 (NT4/5) and two more members were found in fish – NT6 and NT7 (Huang and Reichardt, 2001). The mature neurotrophins form stable non-covalently associated homodimers and are structurally very similar. They contain a structure referred to as 'cysteine knot', which consists of three disulfide bonds forming an actual knot between highly conserved β-strands that build the interface for dimerization. Receptor specificity is conferred by the highly variable N-terminus and other more spread residues (McDonald et al., 1991; Butte, 2001). Neurotrophins are initially synthesized as longer proforms (proneurotrophins) that rapidly homodimerize and are cleaved by furin and proconvertases into the mature form in the ER and Golgi. Proneurotrophins can also be secreted and have signalling capacity of their own that has opposing effects from their mature forms (discussed below). Moreover, proneurotrophins can be cleaved after secretion by enzymes in the extracellular space such as matrix metalloproteases or plasmin adding a further regulatory mechanism (Seidah et al., 1996; Lee et al., 2001; Teng et al., 2010).

Neurotrophins bind two different types of receptors (Figure 1.1 A): all proneurotrophins and, with lower affinity, mature neurotrophins can bind the p75 neurotrophin receptor ($p75^{NTR}$). In contrast, binding to the different Trks (tropomyosin-receptor kinase), a subfamily of tyrosine kinase receptors, is specific to the different mature neurotrophins: NGF binds TrkA, BDNF and NT4/5 bind TrkB, and NT3 binds TrkC with high affinity and TrkA and TrkB with lower affinity (Bibel and Barde, 2000; Huang and Reichardt, 2001; Lee et al., 2001).

The $p75^{NTR}$ receptor

The $p75^{NTR}$ receptor is part of the tumour necrosis factor superfamily (TNFR-SF) (Huang and Reichardt, 2001) that is characterized by an extracellular ligand binding domain consisting of four repeats of a cysteine-rich domain (Figure 1.1 A) (Johnson et al., 1986). Dimerization of $p75^{NTR}$ is a prerequisite for neurotrophin-induced signalling and occurs via a disulfide bridge between cysteine residues in the transmembrane domain. Binding of neurotrophins to the dimer induces separation of the two intracellular domains enabling interaction with intracellular signalling molecules (Vilar et al., 2009a, 2009b). The intracellular domain of p75NTR has no catalytic activity but contains a death domain and interacts, depending on the ligand and cellular context, with different adaptor proteins (Reichardt, 2006).

For instance, $p75^{NTR}$ can interact with sortilin leading to formation of a complex with high affinity for proneurotrophins. Activation of this complex by proneurotrophins induces apoptotic signalling (Lee et al., 2001; Nykjaer et al., 2004; Teng et al., 2005). Adaptor proteins binding to $p75^{NTR}$ include TRAF6 (TNF receptor associated factor), NRIF (neurotrophin interacting factor) and other factors that then induce Jun kinase signalling, p53 activation and apoptosis (Reichardt, 2006). Moreover, similar to the β-amyloid precursor protein, the intracellular domain of $p75^{NTR}$ can undergo proteolytic sequential cleavage by α- and β- secretase. This releases part of the intracellular domain (ICD) together with NRIF that can subsequently translocate into the nucleus and activate transcription (Kenchappa et al., 2006). This pathway was proposed to be involved in axon

growth cone collapse via ICD dependent activation of the GTPase RhoA and myelin-associated inhibitory factors as well as in axon repellent guidance cues via semaphorin and ephrin signalling (Schecterson and Bothwell, 2010). On the other hand $p75^{NTR}$ binding by neurotrophins can also induce activation of NF-κB (nuclear factor kappa-light-chain-enhancer of activated B cells) and subsequent transcription of prosurvival genes (Reichardt, 2006).

$P75^{NTR}$ also interacts with mature neurotrophins and their respective receptors. This interaction increases specificity for NGF and BDNF compared to NT3 and NT4/5 and activates Trk-dependent survival signalling (Bibel et al., 1999). Moreover, interaction of $p75^{NTR}$ and Trks could be involved in regulating retrograde transport, ubiquitination and endocytosis of Trk receptors (Skaper, 2008).

As interaction of proneurotrophin with $p75^{NTR}$ and sortilin leads to apoptosis while interaction of mature neurotrophins with $p75^{NTR}$ and Trk receptors leads to prosurvival signalling the processing of proneurotrophins by proteases is an important regulatory step to switch between these two modes (Lee et al., 2001).

The Trk receptors and mechanisms regulating Trk receptor signalling

The tyrosine kinase Trk receptors are transmembrane glycoproteins that only dimerize upon ligand binding. This induces auto-crossphosphorylation of intracellular kinase domains and activation of downstream signalling pathways (Barbacid, 1995). The extracellular domain of Trk receptors consist of a cysteine-rich cluster, three leucine-rich repeats, a second cysteine-rich cluster and two Ig-like domains the second of which confers ligand specificity (Barbacid, 1995; Urfer et al., 1995). All Trks have a short transmembrane domain and a highly conserved intracellular tyrosine kinase domain (Figure 1.1 A) (Barbacid, 1995). Signalling via Trk receptors activates MAPK (mitogen-activated protein kinase), PI3K (phosphatidylinositol 3-kinase), PLCγ1 (phospholipase C-γ1) and their respective downstream effectors (Huang and Reichardt, 2003). Trk receptor signalling pathways and functions will be discussed in detail in chapters 1.1.2, 1.1.3 and 1.1.4.

Alternative splicing influences Trk signalling. Deletion of a short amino acid sequence of the juxtamembrane domain of the extracellular domain of TrkA and TrkB increases specificity for NGF and BDNF respectively (Skaper, 2008). Also truncated forms without the intracellular catalytic domain exist for TrkB and TrkC. These can dimerize with the full length form and inhibit signalling (Eide et al. 1996) but are also able to induce signalling by interaction with intracellular scaffold proteins (Schecterson and Bothwell, 2010). Whereas the full-length isoforms of TrkB and TrkC are predominant during development the truncated forms are more abundant in the mature brain (Fryer et al., 1996).

Another important feature of neurotrophin signalling is endocytosis and retrograde axonal transport. Retrograde transport of the ligand/receptor complex or downstream effectors is required to translate events at a distal axon into changes in nuclear transcription. Endocytosis of neurotrophin/$p75^{NTR}$/Trk complexes could regulate receptor availability on the cell surface but might also allow for prolonged signalling via the internalized complex (Wu et al., 2009). As components of downstream signalling pathways are differentially distributed in vesicles sorting of TrkB into different vesicles can also determine which downstream pathways are activated (Huang and Reichardt, 2003).The detailed mechanism of Trk receptor endocytosis, retrograde transport and degradation is however still controversial. Endocytosis of Trk receptor complexes was shown to occur through clathrin-dependent and independent mechanisms as well as through macropinocytosis and complexes were found to be localized to stable early and late endosomes, multivesicular bodies and macroendosomes (Wu et al., 2009).

Finally, Trk receptors can also be transactivated by zinc, the low-density lipoprotein 1 LRP1 and several G-protein coupled receptors (GPCR) as the A2a adenosine receptor, the PAC1 receptor (pituitary adenylate cyclase-activating polypeptide type I receptor isoform 1) and endocannabinoid receptors. GPCR induced Trk activation can occur intracellularly before receptors exit the Golgi and might inhibit trafficking of the receptors to the cell surface (Schecterson and Bothwell, 2010). Transactivation of Trk

receptors seems to be dependent on activation of Fyn (Rajagopal et al. 2006; Huang et al. 2008).

1.1.2 Signalling pathways downstream of Trk receptors

This part will concentrate on canonical signalling pathways downstream of Trk receptors induced by binding of mature neurotrophins. Binding of neurotrophins to Trk receptors induces dimerization of the receptor and subsequent cross-autophosphorylation of tyrosine residues by the intracellular kinase domain. Phosphorylated tyrosine residues serve as docking sites for cytoplasmic adaptor proteins containing PTB (phosphotyrosine-binding) or SH2 (Src homology 2) domains which activate downstream signalling cascades (Bibel and Barde, 2000; Alberts et al., 2002). Two main tyrosine adaptor sites have been characterized in all Trk receptors: one for the adaptor proteins SHC (Sh2-domain containing) and FRS2 (fibroblast growth factor receptor substrate 2) at Y490 (TrkA), Y515 (TrkB) or Y516 (TrkC) that activates Ras-MAP-kinase and PI3-kinase signalling cascades and one for PLCγ1 at Y785 (TrkA), Y816 (TrkB) or Y789 (TrkC) (Figure 1.1 B) (Huang and Reichardt, 2003).

Tyrosine residues other than these were reported to bind adaptor proteins and activate downstream signalling cascades. Phosphorylated tyrosines in the activation loop for instance can bind rAPS (receptor associated protein of the synapse) and SH2-B leading to activation of the Ras-MAPK signalling cascade (Huang and Reichardt, 2003).

Ras - MAP-kinase signalling

Activation of the Ras-MAPK signalling cascade by neurotrophins promotes neuronal differentiation, migration, and survival of subpopulations of neurons and is generally mediated by binding of SHC or FRS2 to the SHC adaptor site (Figure 1.1 B) (Medina et al., 2004; Reichardt, 2006). Both adaptor proteins bind to phosphorylated tyrosines via a PTB domain and are then phosphorylated in turn. Phosphorylated SHC or FRS2 recruit GRB2 (growth factor receptor-bound protein 2) that is associated with SOS (son of sevenless) via an SH3 domain. SOS is a guanine nucleotide exchange factor (GEF) that activates small GTPases like Ras. Ras activates then PI3K (discussed in next

subchapter) and the MAPK cascade via one of the serine/threonine kinases Raf, MEKK2/3 (MAP kinase kinase kinase 2/3) or p38 MAPK. Activation of Raf or MEKK initiates sequential phosphorylation and activation of members of the MEK (MAP kinase kinase), ERK (extracellular signal-regulated kinase, a MAP kinase) and finally RSK (ribosomal s6 kinase) families of serine/threonine protein kinases. RSK phosphorylates and activates the transcription factor CREB (cAMP responsive element binding protein) (Alberts et al., 2002; Reichardt, 2006; Minichiello, 2009). Activation of MAP-kinase activated protein kinase-2 by p38 directly activates CREB (Xing et al., 1998). CREB regulates expression of genes involved in neuronal differentiation and survival (Bonni et al., 1999; Riccio et al., 1999). Activation of the MAPK cascade can be modulated by its own downstream effectors as activated ERK and RSK can induce dissociation of SOS from GRB2 by phosphorylation (Douville and Downward, 1997).

Neurotrophin induced MAPK signalling can be enhanced by different factors. For instance, FRS2 recruitment to the SHC adaptor site of TrkA was reported to induce prolonged activation of MAPK signalling via Crk (CT-10 related kinase 3), C3G (also RAPGEF, a GEF) and Rap1 (Ras-related protein, a small GTPase) (Kao et al., 2001; Wu et al., 2001). MAPK signalling can also be facilitated by recruitment of the protein phosphatase SH-PTP2 (protein-tyrosine phosphatase 2C) by GRB2, most probably leading to inactivation of an inhibitory factor (Reichardt, 2006), or by binding of CHK (homolog of cytoplasmic tyrosine kinase CSK) to the PLCγ docking site of TrkA (Yamashita et al., 1999).

BDNF not only activates MAPK signalling pathways but can also modulate signal strength by modulating the subcellular distribution and nuclear translocation of activated MAP kinases (Patterson et al., 2001).

Phosphatidylinositol 3-kinase signalling

As discussed in the previous chapter, docking of adaptor proteins to the SHC site of Trk receptors can activate PI3K signalling promoting neuronal survival (Bibel and Barde, 2000). PI3K can be activated by Ras or by GAB1 (GRB2-associated-binding

protein 1)-recruitment to GRB2 (Holgado-Madruga et al., 1997) or Trk-dependent phosphorylation of IRS1/2 (insulin receptor substrate 1/2) (Figure 1.1 B) (Yamada et al., 1997).

PI3K phosphorylates the cytoplasmic inositol ring of membrane-anchored phosphatidylinositols, thus generating the phosphoinositides phosphatidylinositol phosphate (PIP), phosphatidylinositol bisphosphate (PIP2) and phosphatidylinositol trisphosphate (PIP3). Phosphoinositides recruit inositide-dependent protein kinase (PDK-1) and protein kinase Akt (protein kinase B, PKB) via their pleckstrin homology (PH) domain to the membrane. PDK-1 then phosphorylates and activates Akt (Leevers et al., 1999; Alberts et al., 2002). Akt phosphorylates several downstream effectors involved in apoptotic signalling including BAD, a Bcl2-family member, and FKHRL1, a transcription factor regulating proapoptotic genes (Datta et al., 1997; Brunet et al., 1999). Upon phosphorylation by Akt both proteins are sequestered by 14-3-3 proteins preventing them from exerting their proapoptotic actions (Datta et al., 2000; Brunet et al., 2002). Akt also phosphorylates the NF-κB inhibitor I-κB, initiating the release and prosurvival signalling of NF- κB (Maggirwar et al., 1998) and S6 kinases that regulate translation of certain mRNAs (Kimball et al., 2002). The phosphoinosites generated by PI3K can moreover recruit GEFs for Rho family proteins that regulate organization of the F-actin cytoskeleton and might therefore be involved in growth cone guidance (Wang et al., 2002; Yuan et al., 2003).

PLCγ signalling

Binding of PLCγ1 to the PLC docking site of activated Trk receptors induces phosphorylation and activation of PLCγ1 by the receptor (Figure 1.1 B) (Reichardt, 2006). PLCγ1 then hydrolyzes phosphatidylinositol 4,5-bisphosphate into inositol 1,4,5-trisphosphate (IP3) and diacylglycerol (DAG) (Alberts et al., 2002). IP3 induces release of Ca^{2+} from internal stores (endo- and sarcoplasmic reticulum) into the cytoplasm by binding to IP3-gated Ca^{2+}-release channels. Free Ca^{2+} is bound by calmodulin and Ca^{2+}-calmodulin complexes then activate Ca^{2+}/calmodulin-dependent protein kinase II and IV

(CaMKII and CaMKIV) (Alberts et al., 2002). Both kinases are involved in regulating synaptic plasticity, LTP and learning. CaMKIV phosphorylates CREB inducing transcription of genes involved in survival signalling, neuronal differentiation but also synaptic plasticity (Finkbeiner et al., 1997). Regulation of synaptic plasticity and LTP by neurotrophins via CREB induced transcription was shown to be dependent on activation of the PLCγ1 activated pathways, but not the MAPK activated pathways (Minichiello et al., 2002). CaMKII regulates synapse formation and remodelling, synaptic plasticity and short and long-term memory formation by phosphorylation of members of the postsynaptic density (PSD) like the GluR1 subunit of the AMPA receptor and the NMDA receptor, both ionotropic glutamate receptors, and transcription of different genes (for instance of BDNF). CaMKII can sustain its own activity via autophosphorylation which might play an important role in generation of LTP and long-term memory (Soderling, 2000). DAG, on the other hand, activates PKC isoforms that have also been involved in synaptic plasticity and learning (Saito and Shirai, 2002). It is however not clear if this pathway is specifically activated downstream of TrkB signalling (Gärtner et al., 2006). PLCγ1 activation also results in activation of protein kinase C-δ which can activate ERK1/2 in a Ras-independent way (Corbit et al., 1999).

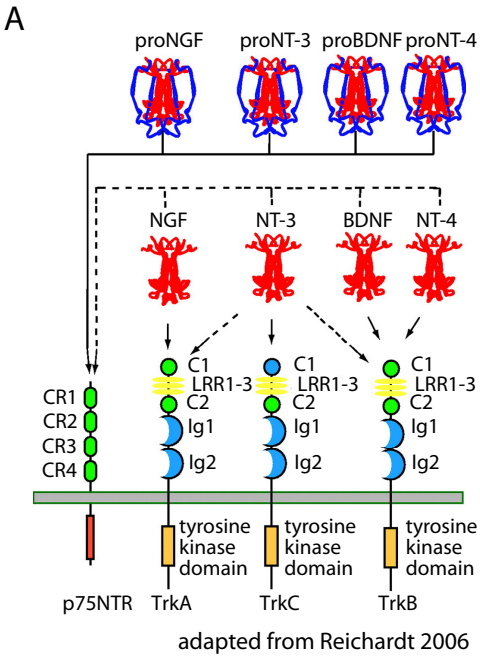

Figure 1.1 Neurotrophins and their receptors (A) and neurotrophin signalling pathways (B). A All proneurotrophins bind the $p75^{NTR}$ whereas the mature neurotrophins bind specifically to their respective receptor. CR cysteine-rich motif, C1/2 cysteine-rich cluster, LRR leucine-rich repeat, Ig1/2 immunoglobin-like domain. B Signalling pathways activiated by neurotrophins, at the example of BDNF and TrkB. Ligand binding induces receptor dimerization and auto-crossphosphorylation. Phosphorylation and docking to Y515 activates mitogen-activated protein kinase (MAPK) and phosphatidylinositol-3-kinase (PI3K) pathways that mediate survival, growth and differentiation. Docking of PLCγ1 to phosphorylated Y816 induces release of internal Ca^{2+} stores and activation of Ca^{2+}/Calmodulin (CaM)-dependent kinases (CamK) that regulate synaptic plasticity and thus behaviour. Additional details and abbreviations are provided in the main text.

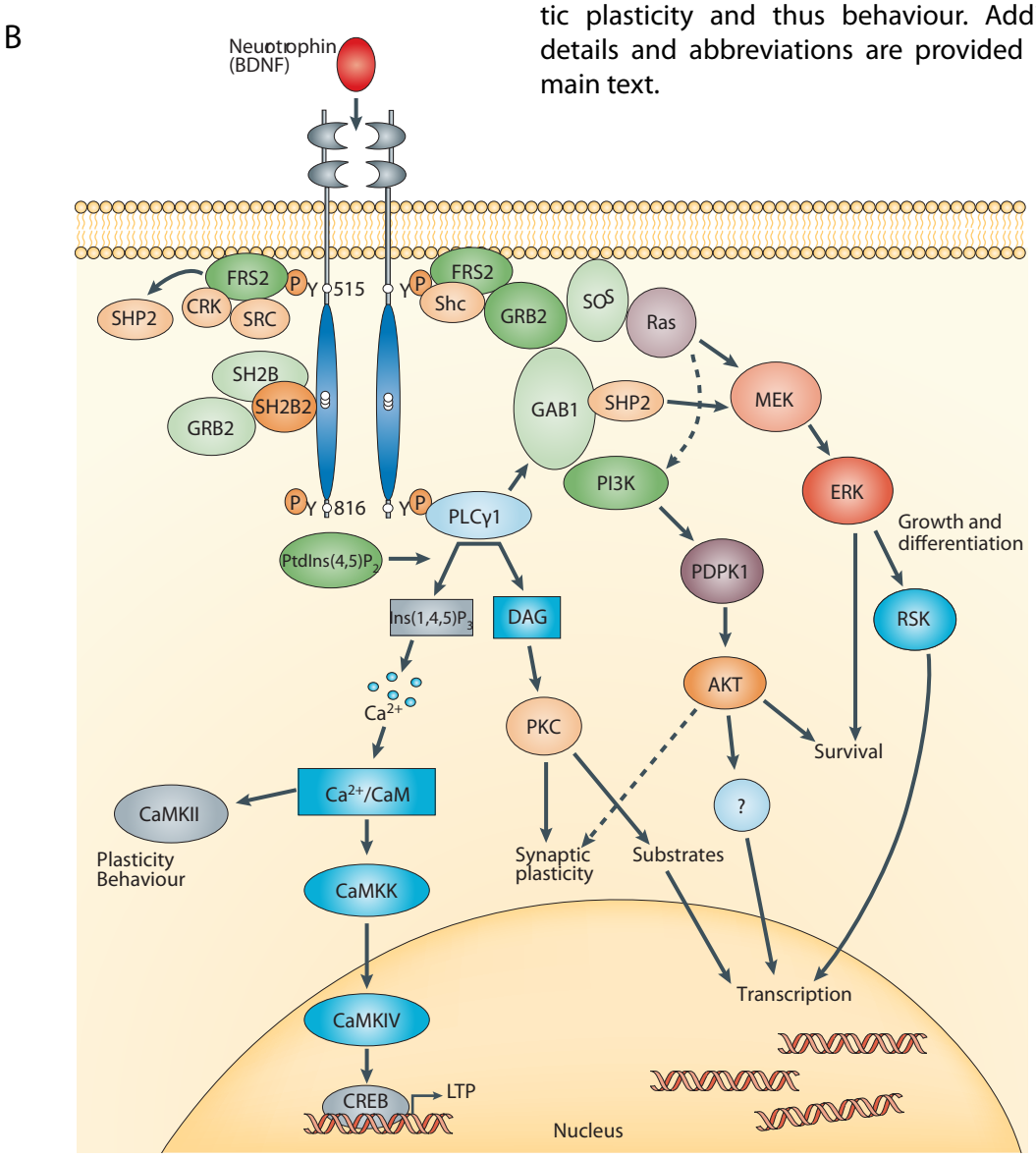

1.1.3 Functions of Trk receptors in development

Neurotrophins and their receptors regulate survival of neurons in the PNS and, to a much smaller extent, in the CNS, but regulate also neuronal migration, differentiation and neurite outgrowth.

Neurotrophins control the survival of neurons in the PNS and CNS

Trk receptors promote survival of sensory and sympathetic neurons in the peripheral nervous system whereas neurons of the central nervous system are less dependent on neurotrophin signalling. All three Trk receptors are highly expressed during development and are expressed in different combinations. Accordingly, different subpopulations of neurons are dependent on one or several neurotrophins (Bibel and Barde, 2000).

Trk receptors promote survival of sensory neurons in the trigeminal (facial sensory nerves), the dorsal root (sensory nerves of the body), the vestibular and cochlear (sensory nerves from ear), the geniculate (sensory nerves from taste buds) and the nodose-petrosal ganglia (visceral sensory nerves from organs).

In the trigeminal and dorsal root ganglia (DRG) sensory neurons are generally dependent on one specific Trk receptor. Nociceptive DRG neurons express TrkA and are almost completely lost in *Trka* and *Ngf* mutants (Crowley et al., 1994; Smeyne et al., 1994). Proprioceptive DRG neurons are dependent on NT-3 and TrkC from early neurogenesis on and are lost in *Nt*-3 and *Trkc* mutants (Fariñas et al., 1994). Proprioceptive neurons in the mesencephalic nucleus of the trigeminal ganglion are either dependent on BDNF/TrkB or on NT-3/TrkC and are partially lost in absence of one of these factors and completely lost in *Nt-3/Nt-4/Bdnf* triple mutants (Fan et al., 2000; Matsuo et al., 2000). In mutant mice, the targets innervated by these neurons can be affected by the lack of innervation. For instance muscle spindles innervated by proprioceptive DRG neurons are lost in *Nt*-3 and *Trkc* mutants (Fariñas et al., 1994), and cutaneous receptors (for instance D-hair receptors) are affected by loss of NT-3, NT-4 and a point mutation of the SHC docking sit in TrkB (Minichiello et al., 1998; Huang and Reichardt, 2001). Sensory neurons in the vestibular ganglion are dependent on

BDNF/TrkB signalling (Ernfors et al., 1994; Jones et al., 1994; Minichiello et al., 1995; Schimmang et al., 1995). In the cochlear ganglion sensory neurons express both TrkB and TrkC and, with exceptions, BDNF and NT3 are redundant. As BDNF is not expressed in the basal turns of the cochlea at the time of neurotrophin dependency *Nt-3* mutants show loss of neurons innervating this region (Fariñas et al., 2001). Sensory neurons in the nodose-petrosal ganglion that innervate viscera are dependent on either BDNF or NT-4 and are partially lost in the single mutant mice but completely lost in *Trkb* or *Bdnf/Nt-4* double mutants (Conover et al., 1995; Minichiello et al., 1998). The geniculate ganglion contains sensory neurons that innervate the tongue and palate. These are, comparable to nodose-petrosal neurons, dependent on either BDNF or NT-4 and 90-95% are lost in double mutants, but only around 50% in the single mutants (Conover et al., 1995; Liu et al., 1995).

In contrast to parasympathetic neurons that develop normal in absence of neurotrophins or their receptors, sympathetic neurons are strongly dependent on neurotrophic support. In *Trka* mutants most sympathetic neurons die perinatally starting around E17.5 (Fagan et al., 1996). Comparable phenotypes were observed in *Ngf* and *Nt-3* mutants and it is believed that NT-3 acts through TrkA in this case (Crowley et al., 1994; Smeyne et al., 1994).

In the CNS a role for neurotrophins in supporting survival of neurons is much less apparent. Even though all neurotrophins (with exception of NGF) increase the survival rate of motorneurons *in vitro*, a triple mutant of *Nt-3, Nt-4 and Bdnf* shows only a 20% reduction in spinal and facial motor neurons (Liu and Jaenisch, 2000; Huang and Reichardt, 2001). *Trkb* mutant mice show apoptosis of dentate gyrus neurons during postnatal development (Alcántara et al., 1997) and reduced expression of TrkB and TrkC in double mutant mice causes extensive death of dentate gyrus and cerebellar granule neurons. This shows that TrkB and TrkC cooperate in supporting survival of specific CNS neurons during postnatal development (Minichiello and Klein, 1996).

Neurotrophins control neurite outgrowth

Neurotrophins not only support survival of neurons during development but regulate also growth of axons and dendrites. All neurotrophins can induce neurite outgrowth *in vitro* in responsive neurons (Huang and Reichardt, 2001). NGF was found due to its ability to induce growth of sympathetic neurons (Levi-Montalcini and Angeletti, 1968) and sympathetic ganglia respond to NGF administration by increasing the number and length of neurites. Moreover, innervating preganglionic axons are also increased in numbers (Schäfer et al., 1983). The ability of all four neurotrophins to steer axon outgrowth was demonstrated by placing beads containing NGF, BDNF, NT-3 or NT-4 ectopically on limb buds of E10.5 mice. Sensory axons and few motor axons were derouted and grew towards the beads. Administration of function-blocking antibodies inhibited outgrowth of both nerve types (Tucker et al., 2001).

In the central nervous system neurotrophins were shown to control dendrite growth. For instance, application of BDNF, NT-3 or NT-4 to organotypic cultures of ferret visual cortex increased the arborisation and length of pyramidal neurons (McAllister et al., 1995). Mice that lack truncated and full-length forms of TrkB in pyramidal neurons show a reduction in the length of pyramidal cell dendrites (Xu et al., 2000).

BDNF/TrkB promote neuron migration and differentiation

Apart from regulating survival and outgrowth of neurons, BDNF and TrkB were also shown to promote migration and differentiation of neurons in the CNS. BDNF mutants show impaired differentiation of some CNS neurons (Jones et al., 1994) and both *Bdnf* and *Trkb* mutants display impaired dendritic differentiation of cerebellar Purkinje cells (Schwartz et al., 1997; Minichiello et al., 1998).

Brain-specific deletion of TrkB or point mutation of the SHC and PLCγ docking sites cause delayed migration of cortical neurons leading to accumulation of neurons in the superficial layers of the cortex. Moreover, defects in differentiation were observed even though it is unclear whether these are due to lack of TrkB or due to changes in the environment caused by the delay in migration (Medina et al., 2004).

1.1.4 Functions of Trk receptors in the adult organism

Neurotrophin signalling is not only required during development of the nervous system but was also shown to influence function of neurons in the adult PNS and CNS by modulating synapse number and transmission.

For instance, Nja and Purves showed early on that sympathetic neurons of the PNS required NGF to maintain incoming synapses (Njå and Purves, 1978). Moreover, NGF can acutely sensitize sensory nociceptive neurons. Part of this effect depends on mast cell activation by NGF and secretion of further factors by mast cells, but NGF and also BDNF and NT-4 were also shown to act directly on sensory neurons in mast cell-free cultures *in-vitro* (Shu and Mendell, 1999). Administration of NT-3 can prevent long-term synaptic deficiencies after transection of sensory nerves suggesting a requirement of these neurons for NT-3 to maintain their synapses (Mendell, 1999).

In the adult central nervous system TrkB and TrkC are widely expressed by most neurons (Klein et al., 1990; Tessarollo et al., 1993), whereas TrkA expression is generally restricted to cholinergic neurons in the forebrain (Holtzman et al., 1995). A role for NT-3 signalling through TrkC in adult CNS function is still uncertain. Neuron-specific deletion of *Nt-3* does not cause any changes in synaptic transmission or long-term potentiation and these mice did not show any apparent phenotype up to the age of 1.5 years (Ma et al., 1999). Moreover, *Trkc* heterozygous mice, in contrast to *Trkb* heterozygous mice, do not show any changes in hippocampal spine morphology (von Bohlen und Halbach et al., 2008).

NGF/TrkA signalling was proposed to be required for maintenance and function of cholinergic neurons. Infusion of NGF increases expression of choline-o-acetyltransferase (ChAT), the enzyme that synthesizes acetylcholine (Hefti et al., 1989). Moreover, *Ngf* heterozygous mice show partial loss of septal cholinergic neurons and have deficits in memory acquisition and retention which can be improved by long-term infusion of NGF (Chen et al., 1997).

Nt-4 knockout mice show normal basal transmission and short-term memory formation in the hippocampus but deficits in long lasting long-term potentiation (LTP) and fear conditioning (Xie et al., 2000).

Involvement of BDNF/TrkB signalling in modulation of synaptic plasticity has been extensively studied. BDNF is primarily packaged into vesicles of the regulated secretion pathway (the other neurotrophins to a smaller extend) and this allows for activity-dependent secretion (Mowla et al., 1999; Brigadski et al., 2005). Activity-dependent secretion of BDNF at axon terminals and from dendrites has been demonstrated by overexpression of green fluorescent protein (GFP)-tagged BDNF, but has also been confirmed for endogenous BDNF (Brigadski et al., 2005; Nakajima et al., 2008). BDNF and TrkB are localized at glutamatergic synapses (Drake et al., 1999) and BDNF expression in the hippocampus is increased in response to neuronal activity and LTP (Patterson et al., 1992).

Bdnf knockout mice have less and less well defined synapses and show impaired LTP (Pozzo-Miller et al., 1999). Generation of LTP has been correlated to memory formation and, accordingly, *Bdnf* heterozygous mice show learning deficits (Linnarsson et al., 1997). Defects in LTP in *Bdnf* mutants are reversible by re-introduction of BDNF which proves that this is not a consequence of developmental defects but that BDNF has a role in regulation of synaptic plasticity per se (Korte et al., 1996; Patterson et al., 1996). This was confirmed by the finding that postnatal deletion of *Trkb* in the forebrain results in impaired LTP in the CA3-CA1 region and compromised learning ability (Minichiello et al., 1999). TrkB involvement in the regulation of synaptic plasticity is mediated by PLCγ signalling since mice with a point mutation in the PLCγ docking site show a comparable phenotype whereas no deficits in LTP or learning were observed in mice with a point mutation in the SHC adaptor site (Minichiello et al., 2002). PLCγ was proposed to mediate early LTP by phosphorylation of CaMKII and induce late LTP by CAMKIV-mediated activation of CREB (Minichiello, 2009). Morover, pre- and postsynaptic signalling by the TrkB-PLC site was reported to support hippocampal LTP (Gärtner et al.,

2006). An involvement of both TrkB adaptor sites was found for fear learning and amygdalar synaptic plasticity (Musumeci et al., 2009).

BDNF/TrkB signalling is not only involved in memory formation but can also influence behaviour. BDNF expression in the hippocampus of human post mortem tissue is reduced in association with depressive behaviours and upregulated in response to antidepressant treatment (Martinowich et al., 2007) However, disruption of BDNF/TrkB signalling in mice does not cause depression-like behaviour. *Bdnf* heterozygous mice show clear aggressive behaviour and are hyperactive (Lyons et al., 1999; Kernie et al., 2000). Also mice with a specific deletion of *Bdnf* in principal neurons are more aggressive and active (Rios et al., 2001). Whereas in this first publication the line was described as more anxious, a second publication using a comparable line found decreased anxiety but increased depressive behaviour in females but not males (Monteggia et al., 2007). Finally, principal neuron-specific deletion of *Trkb* causes hyperactivity but no change in anxiety or depressive behaviour (Zorner et al., 2003). Taken together, these results suggest that at least permanent changes in BDNF/TrkB signalling rather influence locomotion and aggression than depressive behaviour. It should be noted that even though BDNF might not be involved in depressive behaviour it seems to be required for the action of antidepressants (Martinowich et al., 2007).

Involvement of BDNF/TrkB signalling in control of energy intake and the hypothalamic-adrenal axis will be discussed in the respective chapters (1.3.2 and 1.4.2).

1.2 TrkB signalling in Interneurons

1.2.1 Interneuron characterization and function

The function of neuronal networks relies on the interaction of two major neuron classes – principal excitatory neurons with long projections, and interneurons that innervate local regions and mainly use the inhibitory neurotransmitter GABA (γ-aminobutyric acid). Interneurons control and synchronize the output of populations of excitatory neurons but also integrate input from different regions and different neurotransmitter systems. Thus, they are essential to keep neuronal networks in balance (Freund, 2003). In the cortex and hippocampus interneurons constitute 15-20% of all neurons. Interneurons have a less negative rest potential than principal neurons and have therefore a lower spike threshold, i.e. react more sensitive to excitatory input. Accordingly, interneurons react faster than principal neurons to excitatory input and some interneuron subgroups are characterized by high-frequency firing – a feature important for regulation and synchronization of principal neuron activity (Jonas et al., 2004; Somogyi and Klausberger, 2005).

Impaired function of interneurons and the GABAergic system has been associated with various disorders of the nervous system, most notably with schizophrenia and epilepsy, but also with Huntington, Parkinson disease and the Tourette syndrome (DeFelipe, 1999; Lewis et al., 2005; Woo and Lu, 2006).

The inhibitory neurotransmitter GABA

GABA is, next to glycine, the main inhibitory neurotransmitter in the brain. GABA binds to postsynaptic ionotropic $GABA_A$ receptors that are ligand-activated chloride channels. The GABA-induced chloride influx leads to hyperpolarisation and inhibition of the target neuron (Kandel et al., 2000). GABAergic synapses can be found on dendrites, soma and the axon initial segment (AIS) of neurons. GABAergic synapses onto dendrites of principal neurons modulate specific glutamatergic inputs into that dendritic domain whereas synapses onto the soma and AIS (also referred to as perisomatic region) rather regulate responsiveness, output and thus synchrony of principal neurons (Figure

1.2 A) (Freund and Katona, 2007). Apart from ionotropic receptors, GABA can also bind to G-protein coupled metabotropic $GABA_B$ receptors that mediate slow long-lasting inhibition of network activity (Kohl and Paulsen, 2010). Under some circumstances, GABA has an excitatory instead of an inhibitory effect on target neurons. For instance, during development GABA is generally excitatory due to the lack of the chloride gradient typical for mature neurons (Rivera et al., 1999).

Interneuron development

Interneurons differ from principal neurons in their developmental origin. Principal cortical neurons are generated in the subventricular zone of the cortical neuroepithelium and then migrate radially into the cortical layers in an inside-out fashion. Thus earlier born neurons are located in the deeper layers and later born neurons are located in the outer layers of the cortex (Kandel et al., 2000). In contrast, interneurons are generally generated in the ganglionic eminences and only in primates also partially in the subventricular zone (Marín and Rubenstein, 2001; Letinic et al., 2002; Gelman and Marín, 2010). The ganglionic eminences are structured into the lateral, the medial and the caudal ganglionic eminence (LGE, MGE and CGE) and each of these generate specific subtypes of interneurons (Figure 1.2 B). The LGE mainly generates olfactory, striatal medium spiny and lateral cortical interneurons (Wonders and Anderson, 2005). The MGE is the primary source for cortical interneurons and gives rise to most parvalbumin (PV) and somatostatin (SST) expressing interneurons whereas the CGE generates reelin, calretinin (CR) and vasointestinal protein (VIP) expressing cortical interneurons (Gelman and Marín, 2010). Recently also the preoptical area (POA) has been proposed to generate a small proportion of cortical interneurons (Gelman and Marín, 2010). Generation of interneurons in the mouse MGE starts at E9.5 and peaks as E13.5 whereas CGE-derived interneurons are generated from E12.5 on and peak at E15.5 (Miyoshi and Fishell, 2010). Newly generated interneurons migrate from the ganglionic eminences tangentially into the cortex and only then migrate radially to their final position (Marín and Rubenstein, 2001; Huang et al., 2007). MGE-derived interneurons mirror the age-

dependent inside-out order of principal neurons, whereas CGE-derived interneurons are spaced throughout the cortical layers independent of their birth date (Miyoshi and Fishell, 2010). Interneuron subtypes are specified in the ganglionic eminences before migration (Xu et al., 2003b) but the final morphological features are developed once the neurons reaches the final location in the cortex (Huang et al., 2007).

Interneuron classification

Interneurons are a very heterogeneous group but are generally characterized by several common features. They use the inhibitory neurotransmitter GABA and therefore express glutamate decarboxlases (Gad65 and Gad67), the enzymse that synthesize GABA from glutamate. Moreover, interneurons generally have short axons and type II synapses (or symmetric synapses). The dendritic morphology is generally simpler than that of principal neurons and most interneurons do not have dendritic spines (Woo and Lu, 2006; Ascoli et al., 2008). The axonal arbors of interneurons are very elaborate, branch often and have class-specific morphological characteristics (Figure 1.2 A) (Huang et al., 2007). However, there are exceptions to this characterization as there are interneurons with long projections and interneurons that use other neurotransmitters than GABA (for instance glycine, or the excitatory neurotransmitter acetylcholine). Also GABA does not always lead to inhibition of target neurons and, as already mentioned, especially not during development (Maccaferri and Lacaille, 2003; Mott and Dingledine, 2003). The large diversity of hippocampal and cortical interneurons has prompted diverse attempts to classify interneurons of the hippocampus and cortex into subgroups. A unifying nomenclature for classification of cortical interneurons has only recently been published by the Petilla Interneuron Nomenclature Group (Ascoli et al., 2008). According to this scheme interneurons should be classified by defined morphological (soma, dendrite, axon morphology and connections), molecular (expression of neurotransmitter, neuropeptides and other markers) and physiological (electrophysiological properties) terms.

The most recent classification of interneurons that took all three features (morphology, molecular markers, physiology) into account found 21 subclasses in the

A

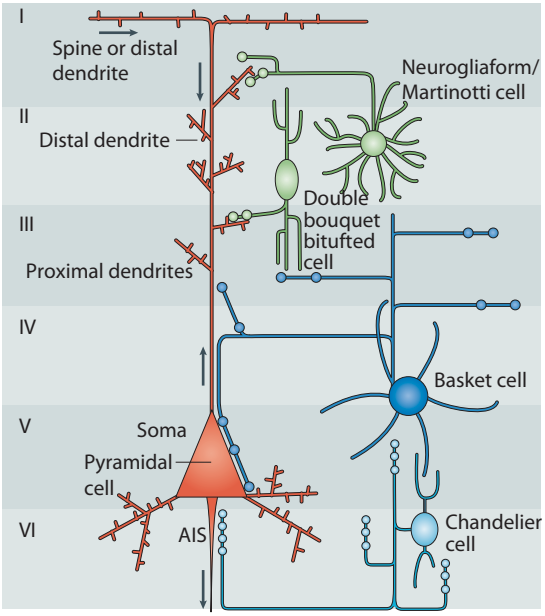

adapted from Huang et al., 2007

B

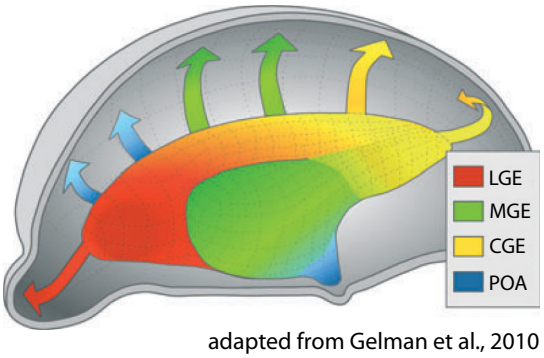

adapted from Gelman et al., 2010

C

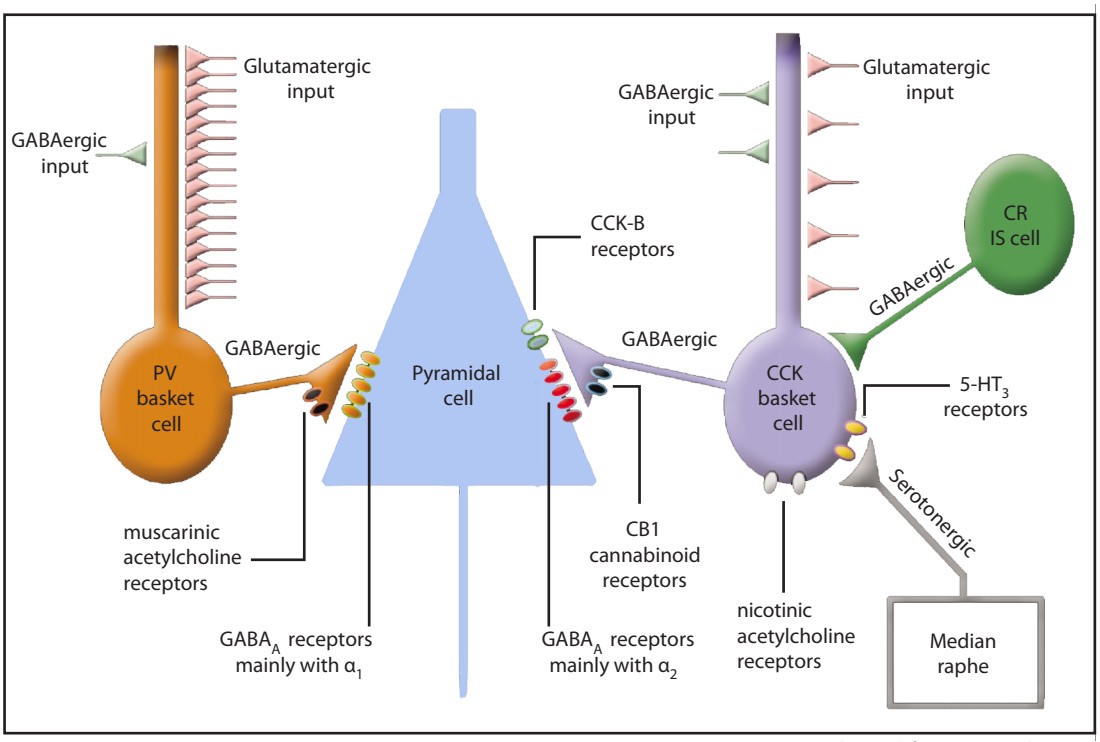

adapted from Freund, 2003

Figure 1.2 A Innervation of pyramidal neurons (red) by different types of interneurons (green and blue) in the cortex. Interneurons have distinct axonal morphologies and innervate different domains (distal or proximal dendrites, soma and axon initial segment (AIS)) of pyramidal neurons. I-VI: cortical layers I-VI. B Developmental origin of interneurons. Interneurons are generated in the lateral, medial or caudal ganglionic eminence (LGE, MGE and CGE) or the preoptic area (POA) from where they migrate tangentially into the cortex. C Comparison of parvalbumin (PV) basket cells that receive strong glutamatergic input and synchronize pyramidal cell firing and cholecystokinin (CCK) basket cells that receive more diverse input and integrate information from different regions and neurotransmitter systems.

CA1 region of the hippocampus (Klausberger and Somogyi, 2008), an extensive description of most of these can be found in Somogyi et al (Somogyi and Klausberger, 2005). Gelman and colleagues (Gelman and Marín, 2010) proposed that cortical interneurons can be described by just four classes that differ in their developmental origin, expression of transcription factors during development and in the adult in expression of different markers. These four classes are

(1) fast-spiking, PV-containing basket or chandelier cells from the ventral MGE;

(2) SST-containing interneurons with either intrinsic burst spiking or adapting non-fast-spiking profiles; originate in the dorsal MGE and often have long axons;

(3) CR and/or VIP expressing cells with bipolar or double-bouquet morphologies that rapidly adapt and are generated in the CGE;

(4) NPY and/or reelin but not SST expressing, rapidly adapting interneurons with multipolar morphologies that originate in the CGE and the POA.

1.2.2 CCK-expressing neurons

Cholecystokinin (CCK) is expressed in numerous classes of interneurons (Klausberger and Somogyi, 2008). CCK was initially identified as a gut peptide hormone involved in gallbladder motility and pancreatic enzyme secretion but is one of the most abundant neuropeptides in the brain (Vanderhaeghen et al., 1980; Beinfeld, 2001; Giacobini and Wray, 2008). It is expressed as a 115 amino acid long pre-pro-form that is modified by signal peptide cleavage, sulfation and carboxyamdiation and then cleaved into several active peptides (CCK-83, CCK-58, CCK-33, CCK-22, CCK-8) of which CCK-8 is the predominant form found in neurons (Rehfeld et al., 2003). Peripheral and central CCK has been implicated in satiety signalling. Peripheral CCK is released from the duodenum in response to gastric filling and stimulates vagal afferents that target the NTS (nucleus tractus solitarius) in the brainstem (Berthoud et al., 2006; Fan et al., 2004). Central CCK is expressed in the NTS and several hypothalamic nuclei, both sites for control of food intake (Beinfeld, 2001; Vanderhaeghen et al., 1980). The actual mechanism of central CCK in food intake control is controversial (Fink et al., 1998), but

CCK knockout mice show changes in the daily rhythm of food intake even though the average amount is normal (Lo et al., 2008). CCK has also been implicated in anxiety-related behaviour and accordingly CCK knockout mice show increased anxiety but also impaired spatial memory (Rotzinger and Vaccarino, 2003; Lo et al., 2008).

CCK was reported to be expressed in numerous brain regions during embryogenesis and adulthood. First expression can be detected around E8.5 (mouse) in neural crest and neural tube cells. At E12.5 expression is detectable in the spinal cord, trigeminal ganglion, the primordium of the anterior pituitary and encephalic regions. At E14.5 *Cck* mRNA is additionally found in the median eminence, the anterior amygdala, anterior hypothalamus and the thalamus. By E17.5 expression has spread to most brain areas including cortical regions, the hippocampus and most hypothalamic nuclei. At that age, expression in the pituitary was restricted to cells directly adjacent to the median eminence (Giacobini and Wray, 2008). In adult rats *Cck* mRNA expression was found in the olfactory bulb, the cerebral cortex in layers II/III and V/VI (pyramidal neuron in deeper layer), the piriform cortex, the amygdala (especially basolateral and medial ventral amygdala), the subiculum, the hippocampus (especially pyramidal neurons in CA1), most hypothalamic nuclei (para- and periventricular nucleus, supraoptic, dorsomedial and supramammillary nuclei and few cells in the posterior area and the medial mammillary nucleus), the thalamus, midbrain (ventral tegmental area, interfascicularis nucleus, substantia nigra, linearis rostralis, central gray, edinger-westphal nucleus, superior and inferior colliculus) and few cells in the cerebellum (reticular formation, parabrachial nucleus) (Schiffmann and Vanderhaeghen, 1991). Absence of expression was reported for the white matter, the striatum, and the arcuate and ventromedial nucleus of the hypothalamus, cortex and deep nuclei of the cerebellum and brainstem (Schiffmann and Vanderhaeghen, 1991), but expression in the rostral striatum and nucleus accumbens was reported by Hökfelt and colleagues (Hökfelt et al., 1985).

Originally, CCK was thought to be exclusively expressed in interneurons (Hendry et al., 1984; Nunzi et al., 1985; Sloviter and Nilaver, 1987), however exceptions have been

found where CCK is expressed in pyramidal projection neurons. Expression of *Cck* mRNA in pyramidal neurons in cortex and the hippocampus was shown by *in-situ* hybridization (Schiffmann and Vanderhaeghen, 1991) and several tracing studies revealed a subset of cortical principal neurons with cortical, striatal and thalamic projections that contain *Cck* mRNA (Burgunder and Young 3rd, 1990; Senatorov et al., 1995). CCK positive projections can also be found in the amygdala (Mascagni and McDonald, 2003). In this publication it was reported that in pyramidal neurons only the bigger CCK precursor forms are present in the soma and get quickly transported into axons where they are further processed. Thus pyramidal neurons often do not show immunolabeling for CCK unless axonal transport is blocked by colchicine treatment (Mascagni and McDonald, 2003).

Even though CCK-positive neurons are found in most brain regions only CCK-interneurons of the hippocampus have been characterized further: Most CCK-interneurons in the CA1 region are basket cells that innervate the soma and proximal/basal dendrites of pyramidal cells and interneurons and partially express VIP and vGlut3 (Somogyi and Klausberger, 2005). Other subtypes of CCK-interneurons were described that also innervate distal/apical dendrites, for instance Schaffer collateral associated cells (Somogyi and Klausberger, 2005). Cortical and hippocampal CCK-interneurons originate in the CGE and hippocampal CCK-interneurons were shown to be born in two waves between E9.5 to E12.5 and E12.5 to E16.5 (Morozov et al., 2009; Tricoire et al., 2011). In contrast to PV expressing basket cells that receive strong glutamatergic input and are thought to regulate network activity and synchrony (the 'rhythm'), CCK basket cells were proposed to be able to integrate more diverse inputs (Figure 1.2 C). They receive less glutamatergic but more GABAergic and also serotonergic input and receive projections from distal (subcortical) regions. CCK-interneurons in the CA1 express receptors for serotonin (5-HT3), acetylcholine, GABA, endocannabinoids and estrogen. Therefore, they are ideally suited for integration of subcortical inputs (Freund, 2003) and have been suggested to fine-tune the emotional, metabolic and

physiological state of an animal (Freund and Katona, 2007). However, it should be considered that all these characteristics were only described for the CA1. The function and characteristics of CCK-expressing neurons in other regions are mostly unknown.

1.2.3 TrkB signalling in Interneurons

BDNF/TrkB signalling plays an important role in the regulation of interneuron development and function. It is generally accepted that BDNF itself is not expressed in mature interneurons (Cellerino et al., 1996; Gorba and Wahle, 1999; Pascual et al., 1999), even though one publication suggests that it is expressed in cortical interneurons upon neurodegeneration of adjacent pyramidal neurons (Wang et al., 1998). Interneurons do however express TrkB (Zachrisson et al., 1996; Gorba and Wahle, 1999; Pascual et al., 1999) and can thus respond to BDNF released from principal neurons. Pyramidal neurons can release BDNF from dendrites (postsynaptically) where it would act on axons and synapses of interneurons (presynaptically) or from axon terminals where it would act on the postsynapses of several interneurons (Huang et al., 2007).

Analysis of *Bdnf* knockout mice gave a first indication for a role of BDNF/TrkB signalling in interneurons. These mice did not show any gross morphological changes in the cortex but had reduced expression of the interneuron markers NPY, PV and calbindin in the cortex (Jones et al., 1994). Also *Trkb* knockout mice show impairments in the GABAergic system even though the number of active interneurons is normal (Carmona et al., 2006). This suggests, that BDNF/TrkB signalling might play a role in differentiation of interneurons but is not required for survival. Overexpression of *Bdnf* was reported to accelerate maturation of the inhibitory cortical network in mice (Huang et al., 1999).

During development, TrkB signalling has been involved in the regulation of interneuron migration, neurite outgrowth, differentiation, synaptogenesis, but also in regulation of network activity and synchronization.

A role for TrkB in interneuron migration has so far only been shown *in vitro*. TrkB activation can induce PI3K-dependent tangential migration of MGE- derived interneurons (Polleux et al., 2002) and can also induce migration of PV and CCK

interneurons (Berghuis et al., 2005) *in vitro*. However, specific deletion of *Trkb* from early postmitotic GABAergic neurons does not lead to any changes in number or position of cortical interneurons suggesting that at least *in vivo* TrkB is not required for survival or migration of cortical interneurons (Sánchez-Huertas and Rico, 2011).

Involvement of BDNF/TrKB signalling in interneuron neurite outgrowth has only been demonstrated *in vitro*. Administration of BDNF to neuron cultures increases dendritic length and branching in an activity-dependent way but not the number of interneurons (Jin et al., 2003). This effect was also shown specifically for cultures of PV- or CCK-positive interneurons (Berghuis et al., 2004, 2005).

There is clear evidence that TrkB signalling is important for proper differentiation of interneurons as it was shown to regulate expression of several interneurons markers essential for proper interneuron function. For instance, overexpression of *Bdnf* in mice increases *Gad67* mRNA levels (Aguado et al., 2003) and accordingly, *Trkb* knockout mice show reduced *Gad67* mRNA levels (Carmona et al., 2003). Specific deletion of *Trkb* from cortical GABAergic interneurons results in reduced levels of Gad65, Gad67 and VGAT (vesicular GABA transporter) that are all imperative for GABAergic function. This publication also demonstrated that TrkB directly regulates Gad65 expression via MAPK-dependent activation of CREB which binds to the Gad65 promotor (Sánchez-Huertas and Rico, 2011). Moreover, treatment of neuronal cultures with BDNF increases expression of PV, another interneuron marker (Berghuis et al., 2004).

Numerous *in-vitro* experiments demonstrate that BDNF promotes the formation of GABAergic synapses in hippocampal and cortical cultures (Woo and Lu, 2006; Huang et al., 2007). Moreover, specific removal of *Trkb* from cerebellar precursor cells causes a marked decrease in GABAergic synapses even though interneurons are present in normal numbers (Rico et al., 2002). Overexpression of *Bdnf* during mouse development results in increased synapse numbers (GABAergic and non-GABAergic) (Aguado et al., 2003) whereas deletion of *Trkb* leads to a reduction of GABAergic synapses in the hippocampus (Carmona et al., 2006). Finally, promotion of synaptic adhesion by signalling via the

TrkB-PLC site was shown to be required for assembly and maintenance of GABAergic synapses (pre- and postsynaptic) in the cerebellum (Chen et al., 2011).

Spontaneous network activity is an important feature of the developing hippocampus and cortex and was suggested to control synapse formation and synchronization (Ben-Ari, 2001). In *Trkb* knockout mice, the impairment in GABAergic differentiation and synaptogenesis leads to reduced spontaneous network activity at P2/3 (when GABA is still excitatory) and hyperexcitability at P8/9 when GABA is inhibitory (Carmona et al., 2003, 2006). Also, early overexpression of *Bdnf* causes premature spontaneous activity and synchronization (Aguado et al., 2003) confirming the importance of BDNF/TrkB signalling for this developmental step.

Even though this is not an interneuron-specific function, BDNF/TrkB signalling has also been implicated in the developmental switch that alters the response of a postsynaptic cell to GABA. During development GABA is excitatory and only later becomes inhibitory when the K^+/Cl^- cotransporter KCC2 is expressed in postsynaptic neurons (Rivera et al., 1999; Ben-Ari, 2001). BDNF/TrkB signalling was shown to upregulate KCC2 expression during development (Aguado et al., 2003) and it might have the reverse effect in adult neurons (Woo and Lu, 2006).

In the adult brain, BDNF/TrkB signalling is not only required for maintenance of GABAergic synapses but might also regulate adult synaptic transmission by altering expression of receptors in postsynaptic clusters. In hippocampal neuron cultures, BDNF administration increased the number of $GABA_A$ and NMDA receptor clusters in postsynaptic densities. The increase of NMDA receptor-positive clusters was dependent on prior $GABA_A$ activation, suggesting that BDNF/TrkB signalling could thus balance inhibitory and excitatory inputs (Elmariah et al., 2004). TrkB might also regulate receptor composition as *Trkb* knockout mice have a different composition of AMPA and $GABA_A$ receptors which could alter electrophysiological characteristics (Carmona et al., 2003). Apart from acting postsynaptically, BDNF/TrkB signalling also regulates expression of presynaptic markers. BDNF administration can upregulate expression of syntaxin,

synaptobrevin and synaptophysin (Woo and Lu, 2006) and chronic application of BDNF increases GABA vesicle release by changing calcium channel distribution (Baldelli et al., 2005). Impaired GABAergic function has been implicated in the pathogenesis of schizophrenia and since patients show reduced levels of Gad67, PV, BDNF and TrkB mRNA also BDNF/TrkB signalling might be involved (Hashimoto et al., 2005).

1.3 BDNF, TrkB and the central control of energy homeostasis

1.3.1 Central control of energy intake

The brain contains two major centers that receive and integrate information about short- and long-term changes in energy homeostasis and then adapt energy intake correspondingly; these are the hypothalamus and the dorsal vagal complex (DVC) in the brainstem which contains the nucleus tractus solitarius (NTS), the area postrema and the dorsal motor nucleus of the vagus nerve (Figure 1.3 A) (Lebrun et al., 2006). The arcuate nucleus of the hypothalamus (ARC) and the area postrema have fenestrated capillaries (they are not separated from the peripheral blood circulation by the blood brain barrier) and can therefore sense glucose and other metabolites in the blood (Cone et al., 2001; Price et al., 2008). The NTS receives short-term satiety information from the gastrointestinal system over the vagal nerve and gustatory information from taste receptors (Morton et al., 2006) and controls short-term energy intake by regulating meal size independent of the hypothalamus (Gao and Horvath, 2008).

The hypothalamus can also sense short-term signals as glucose, but more importantly, can sense adiposity-related signals and regulates long-term energy intake. Adipocytes secrete the hormone leptin and serum levels of leptin are proportional to the amount of adipose tissue (Zhang et al., 1994; Gao and Horvath, 2008). Also insulin, which is secreted from beta-cells in the pancreas to regulate glucose homeostasis (Schwartz et al., 2000) shows an increase in serum levels in response to weight gain (Schwartz et al., 2000). Leptin and insulin act on two different populations of neurons in the ARC (Figure 1.3 B). One population expresses pro-opiomelanocortin (POMC) and cocaine- and amphetamine-regulated transcript (CART) and is activated by leptin and insulin whereas the other population expresses agouti-related protein (AgRP), NPY and is inhibited by leptin and also insulin (Schwartz et al., 2000; Morton et al., 2006). Upon activation, POMC/CART neurons secrete the melanocortin α-MSH, one of the peptides synthesized from POMC. α-MSH in turn activates neurons expressing MC4R receptors that have anorexigenic (food intake suppressing) effects (Figure 1.3 A,B) (Cone, 2005). Neurons

expressing MC4R were reported in the ARC itself, the lateral hypothalamus (LHA), paraventricular nucleus of the hypothalamus (PVN), the dorsomedial hypothalamus (DMH) and ventromedial hypothalamus (VMH) (Figure 1.3 A) (Morton et al., 2006; Gao and Horvath, 2008). AgRP/NPY neurons are GABAergic and suppress activity of POMC/CART and other anorexigenic neurons and therefore have an orexigenic (food intake promoting) effect unless inhibited by leptin and insulin (Figure 1.3 B) (Cowley et al., 2001; Gropp et al., 2005; Luquet et al., 2005).

The medial PVN receives input from arcuate POMC and NPY neurons (Cowley et al., 1999) and corticotropin-releasing hormone (CRH) and urocortin, that are both expressed in the PVN, can inhibit food intake (Spina et al., 1996; Richard et al., 2000). CRH is upregulated in response to leptin (Uehara et al., 1998) and might act through suppression of the orexigenic NPY-system (Heinrichs et al., 1993). An involvement of the PVN downstream of leptin and melanocortin signalling was also proven by specific reexpression of MC4R in this region on a MC4R knockout background. This restored partially the obesity and almost completely the hyperphagia (excessive hunger and food intake) found in MC4R knockout mice but not the decreased energy expenditure (Balthasar et al., 2005). It is noteworthy that the downstream effector of CRH in the hypothalamic-pituitary-adrenal axis (HPA axis), corticosterone, has an orexigenic effect, most probably through suppression of CRH expression (Nieuwenhuizen and Rutters, 2008).

The VMH expresses receptors for leptin, α-MSH and NPY and receives inputs from the ARC. Specific deletion of leptin receptors in the VMH leads to obesity and hyperphagia suggesting the VMH is involved in anorexigenic signalling downstream of leptin (Gao and Horvath, 2008). Excitatory VMH neurons might act as a positive feedback to the ARC and increase the activity of ARC POMC neurons (Sternson et al., 2005). Neurons in the LH control food intake and arousal and have in general an orexigenic effect whilst neurons in the DMH have an anorexigenic effect (Gao and Horvath, 2008).

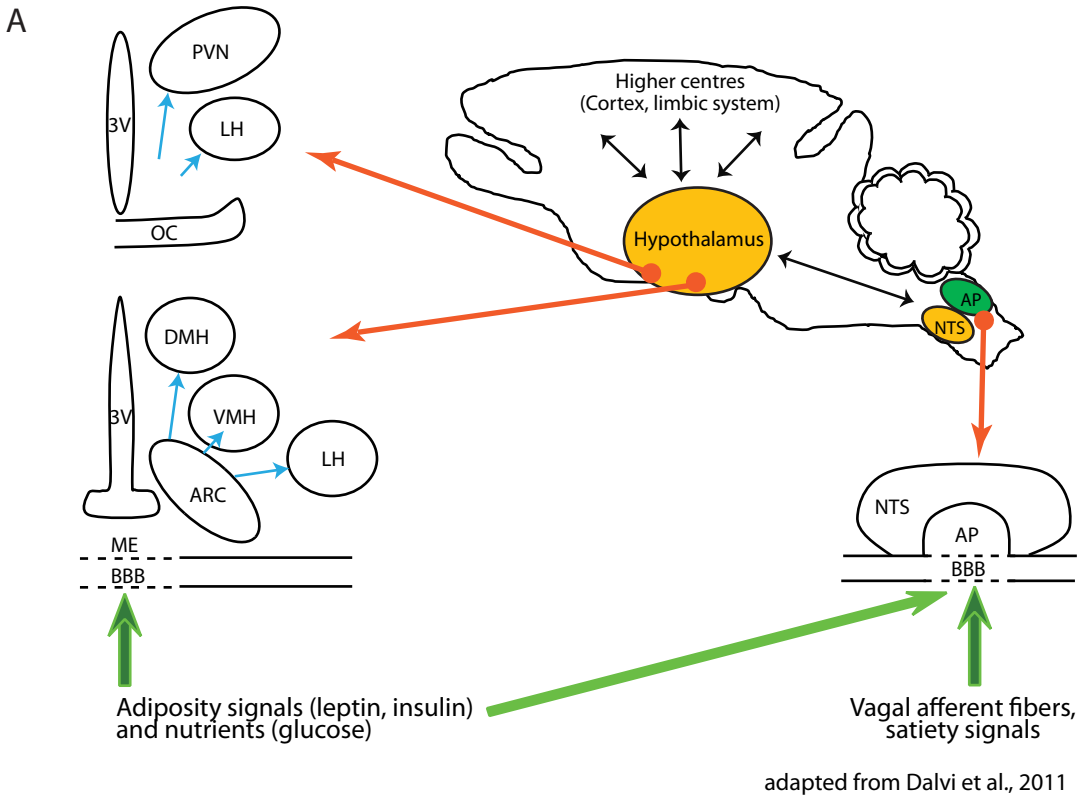

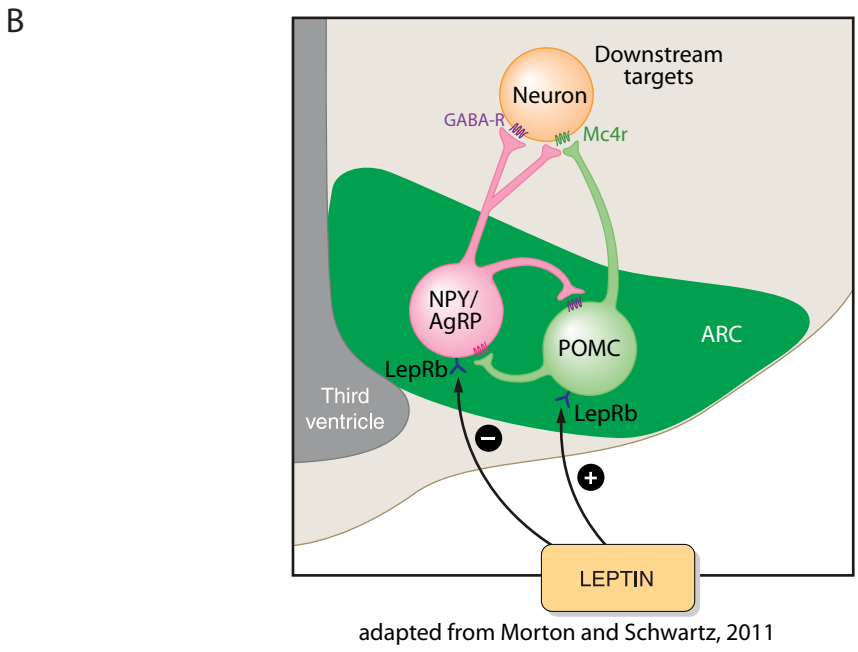

Figure 1.3 A Schematic overview of regions involved in central regulation of food intake and coronal sections of single regions. Adiposity signals and nutrients act on the arcuate nucleus (ARC) and the nucleus tractus solitarius (NTS) as the blood-brain barrier (BBB) is disrupted at the level of the median eminence (ME) and the area postrema (AP). Neurons in the ARC act then on downstream targets in the ventromedial, dorsomedial and paraventricular nucleus of the hypothalamus (VMH, DMH and PVN) and the lateral hypothalamus (LH). 3V third ventricle, OC optic chiasm. B The ARC contains two populations of leptin-responsive neurons, NPY/AgRP (neuropeptide Y, agouti-related peptide) gabaergic neurons that are inhibited by leptin and suppress activity of downstream targets, and POMC (proopiomelanocortin) neurons that are activated by leptin and act on downstream targets via melanocortin signalling. GABA-R γ-aminobutyric acid receptor, LepRb leptin receptor, Mc4r melanocortin receptor 4

Obesity and the metabolic syndrome

Disregulation of leptin/melanocortin signalling can lead to hyperphagia, weight gain and obesity. Increase in adipose tissue is generally accompanied by increased insulin and leptin levels (hyperinsulinemia and hyperleptinemia) and resistance to both hormones (Belgardt and Brüning, 2010).

As already mentioned, leptin is secreted by adipocytes and therefore leptin secretion and serum leptin levels are proportional to the amount of adipose tissue. Obesity-induced leptin resistance might partially be due to decreased transport of leptin through the blood brain barrier but also due to increase in C-reactive protein in obese patients, which binds to leptin and abolishes thus binding to the leptin receptor. Moreover, signalling downstream of the leptin receptor is inhibited by phosphatases that were found to be upregulated in obese individuals (Belgardt and Brüning, 2010). Central resistance to insulin is based on the same mechanisms as leptin resistance (Belgardt and Brüning, 2010). Obesity also induces resistance to insulin in the periphery leading to increased insulin secretion, hyperinsulinemia and finally to hyperglycemia and development of diabetes type II (Schwartz et al., 2000; Martyn et al., 2008). Obesity is not only associated with development of diabetes type II but is also often accompanied by further symptoms such as hypertension, dyslipidemia (abnormal lipid levels – fat or cholesterol), a risk for coronary heart disease and increased mortality (Spiegelman and Flier, 2001).

This set of metabolic disorders is known as metabolic syndrome (also syndrome X, the insulin resistance syndrome or the deadly quartet). Even though the precise definition is still controversial, the metabolic syndrome is generally characterized by 1) glucose intolerance/insulin resistance, 2) hypertension, 3) dyslipidemia and 4) central obesity (Eckel et al., 2010).

1.3.2 BDNF and TrkB are involved in the central control of energy intake

Numerous studies show that BDNF/TrkB signalling is implicated in the central control of energy homeostasis. First experiments showed that long-, but not short-term

infusion of BDNF into the lateral ventricle of rats strongly suppresses food intake and leads to weight loss (Pelleymounter et al., 1995). Further indications for a role of BDNF and TrkB in anorexigenic signalling came from analysis of genetically modified mouse lines. *Bdnf* heterozygous (*Bdnf*$^{+/-}$) mice and mice that express *Trkb* at reduced levels are hyperphagic and have increased body weight (Lyons et al., 1999; Xu et al., 2003a). A later study showed that only a certain percentage of *Bdnf*$^{+/-}$ mice developed obesity. This segregation correlated with BDNF expression in the LHA and VMH. Non-fat *Bdnf*$^{+/-}$ mice showed decreased expression of BDNF in the LHA in comparison to fat *Bdnf*$^{+/-}$ mice and an altered distribution of BDNF in the VMH. Moreover, obesity in *Bdnf*$^{+/-}$ mice is accompanied by increased insulin and leptin but not increased glucose levels and is reversible by infusion of BDNF into the third ventricle (Kernie et al., 2000). This is a central and development-independent function of BDNF as specific postnatal deletion of *Bdnf* in principal neurons of the forebrain also results in hyperphagia, obesity, hyperleptinemia, hyperinsulinemia and hyperglycemia (Rios et al., 2001).

Xu and colleagues (Xu et al., 2003a) first showed that BDNF might regulate anorectic signalling downstream of melanocortin (α-MSH) signalling in the VMH. They showed that BDNF expression in the VMH is regulated by melanocortin signalling in response to the nutritional state and that BDNF infusion can rescue the hyperphagia and weight gain that melanocortin-signalling-deficient mice show. A role for BDNF in acute anorectic signalling in the VMH was confirmed by a study using mice with a viral-mediated knockdown of *Bdnf* in the VMH and DMH. These mice developed hyperphagia and obesity with hyperleptinemia, hyperinsulinemia and hyperglycemia but with normal energy expenditure (Unger et al., 2007). Dietary restriction reverses the metabolic abnormalities found in these and also in *Bdnf*$^{+/-}$ mice (Duan, 2003; Unger et al., 2007) confirming that hyperphagia is the actual cause of obesity in these mice.

In the VMH, BDNF is expressed by excitatory neurons that project to numerous other nuclei. A direct action of BDNF in the feedback mechanism of VMH neurons to the ARC is unlikely, as TrkB does not colocalize with either POMC/CART nor NPY/AgRP

neurons in the ARC (Xu et al., 2003a). However, the VMH projects also to the DVC. BDNF expression in the DVC is, as in the VMH, regulated by nutritional state (Bariohay et al., 2005), and pharmacological blockade of TrkB signalling in the DVC blocks the anorexigenic effect of melanocortin signalling (Bariohay et al., 2009). Therefore, BDNF from the VMH and DVC might be involved in food intake regulation in the DVC downstream of melanocortin signalling.

Also the PVN has been suggested as a side where BDNF might regulate food intake. Injection of BDNF into the PVN suppressed feeding in rats, modulated NPY expression in the ARC and suppressed NPY-induced feeding (Wang et al., 2007). Chronic infusion of BDNF into the lateral ventricle or into the PVN upregulated expression of the anorectic peptides CRH and urocortin and moreover decreased food intake and body weight. This effect of BDNF could be abolished by blocking the CRH-R2 receptor that is activated by CRH and urocortin. Therefore, long-term regulation of food intake by BDNF might be mediated by CRH/urocortin signalling through CRH-R2 (Toriya et al., 2010). However, no changes in peptide expression in the PVN were found in any of the obese BDNF or TrkB mutants (Kernie et al., 2000; Rios et al., 2001; Xu et al., 2003a)

1.4 The hypothalamic-pituitary-adrenal axis and BDNF/TrkB signalling

1.4.1 The hypothalamic-pituitary-adrenal axis

The hypothalamic-pituitary-adrenal (HPA) axis is the system that regulates basal and stress-induced glucocorticoid secretion (corticosterone in rodents, cortisol in humans). The paraventricular nucleus of the hypothalamus (PVN) is considered the 'master regulator' of HPA axis activity as it contains the parvocellular neurons that express and secrete corticotropin–releasing hormone (CRH) (Herman et al., 2008). CRH is also expressed by other neurons in the CNS and can act as neurotransmitter, but only parvocellular neurons project to the median eminence and release CRH as a hormone into the portal bloodstream (Drolet and Rivest, 2001). The portal bloodstream is a system of blood vessels that connect the median eminence directly with the anterior pituitary. Here, CRH induces release of adrenocorticotropic hormone (ACTH), one of the peptides cleaved from POMC, into the peripheral bloodstream. ACTH then stimulates glucocorticoid synthesis and secretion from the zona fasciculata of the adrenal cortex (Felig and Frohman, 2001; Herman and Mueller, 2006; Ulrich-Lai and Herman, 2009). After secretion into the peripheral bloodstream glucocorticoids can inhibit PVN activity in the hypothalamus and ACTH secretion from the pituitary in a negative feedback loop (Figure 1.4 A) (Watts, 2005) that will be discussed in more detail in the next subchapter.

The effect of CRH on ACTH secretion can be potentiated by co-secretion of arginine-vasopressin (AVP) from parvocellular neurons (Volpi et al., 2004). Apart from colocalizing with CRH in parvocellular neurons, AVP is also expressed by other neurons in the PVN, the magnocellular neurons, which project directly to the posterior pituitary (also called neurohypophysis) from where they release AVP into the peripheral blood stream for blood pressure control (de Wardener, 2001).

Changes in AVP and CRH secretion are difficult to measure directly but their expression levels in the PVN mirror parvocellular neuron activity and are therefore used

as marker for PVN activity (Watts, 2005). A further marker for PVN activity is enkephalin that is expressed in an unnamed nucleus laterally to the PVN and only upon conditions of elevated HPA axis activity in the PVN itself (Dumont et al., 2000; Viau and Sawchenko, 2002; Watts, 2005).

ACTH and corticosterone are secreted in a daily rhythm that precedes activity. Therefore, ACTH and corticosterone reach their basal, lowest levels at the beginning of the rest phase (early evening in humans, early morning in rodents) and peak shortly before the onset of the active phase (early morning in humans, early evening in rodents). The circadian rhythm is based on hourly bursts (or more frequent depending on individual and species) of ACTH and corticosterone secretion that persist through rest and active phase and only changes in amplitude (Figure 1.4 B) (Watts, 2005; Lightman and Conway-Campbell, 2010). CRH secretion is not required for maintenance of this ultradian rhythm (Lightman and Conway-Campbell, 2010) but CRH expression in the PVN shows an inverse relationship as it is low at the beginning of the active phase and then increases (Watts, 2005). Binding of glucocorticoids to the glucocorticoid receptor GR follows the hourly burst suggesting that GR activity is involved in regulating the ultradian rhythm (Lightman and Conway-Campbell, 2010). However, CNS-specific deletion of the *Gr* in mice did not influence the circadian rhythm per se (Tronche et al. 1999). Thus, the origin of the circadian rhythm is still controversial with mechanism involving GR signalling in the hippocampus, the clock in the suprachiasmatic nucleus, and the adrenal itself being proposed (Watts, 2005; Lightman and Conway-Campbell, 2010; Son et al., 2011).

Response to a stressor involves the autonomic nervous system, the HPA axis and the limbic system. Whilst the sympathetic autonomic nervous systems reacts in seconds to a stressor by increasing heart rate, blood pressure and secreting adrenalin, the HPA axis reacts more slowly. ACTH is released after seconds (Watanabe and Orth, 1987) but corticosterone is only secreted 10-15 minutes after the stressor. However, elevated glucocorticoid levels are maintained longer and can therefore adapt body functions to

cope with stress by increasing energy metabolism and blocking immune and inflammatory responses (de Kloet et al., 2005; Ulrich-Lai and Herman, 2009). The hypothalamic nuclei controlling HPA axis activity integrate catecholaminergic input from the autonomic nervous system but also inputs from the limbic system and are therefore ideally positioned to adapt the reaction to a specific stressor (Jankord and Herman, 2008; Ulrich-Lai and Herman, 2009). Processing of psychogenic and systemic stressors requires the limbic system (mainly the amygdala, the hippocampus and the prefrontal cortex). The limbic system receives and integrates input from cortical areas that are involved in sensory processing and memory and input from brainstem areas (locus coeruleus, raphe nuclei) that regulate attention and arousal (Ulrich-Lai and Herman, 2009). The limbic system is not directly connected to the PVN but via a bisynaptic network over different inhibitory GABAergic nuclei (see next subchapter) (Cullinan et al., 2008; Jankord and Herman, 2008).

Central control of HPA axis activity: glucocorticoid feedback and GABAergic neurons

Activity of the HPA axis is tightly regulated on a central level by GABAergic inhibitory interneurons and glucocorticoid feedback (Figure 1.4 A,C).

Glucocorticoids act in a negative feedback loop and suppress HPA axis activity at the level of the pituitary and the brain (Watts, 2005). Mineralocorticoid as well as glucocorticoid receptors (MR and GR) are activated by glucocorticoids but differ in their affinity and expression pattern and therefore also in their function. MRs have a high affinity for glucocorticoids and are occupied at basal glucocorticoid serum levels. Glucocorticoid receptors (GR) have a 10-fold lower affinity and only bind glucocorticoids after bursts of secretion (de Kloet et al., 2005). Both receptors dimerize upon ligand binding and translocate to the nucleus where they act as transcription factors (Müller and Holsboer, 2006) but can both also function without dimerization but by interacting with other receptors and transcription factors (Reichardt et al., 1998; de Kloet et al., 2005). CNS expression of MRs is generally restricted to neurons of the limbic system, especially the hippocampus, but GRs are widely expressed in neurons and glia (de Kloet et al., 2005;

Berger et al., 2006). MRs are occupied at basal glucocorticoid levels and were suggested to regulate the basal HPA axis tone. However, neither forebrain-specific deletion of *Mr* nor *Mr* overexpression caused significant changes in daily or stress-related HPA axis activity but resulted rather in cognitive impairment or decreased anxiety, respectively (Berger et al., 2006; Kolber et al., 2008). Therefore, MR-involvement in the regulation of HPA axis activity is rather limited.

As GRs only bind glucocorticoids at elevated serum levels and their occupation correlates with the circadian cycle they were suggested to mediate feedback inhibition (Joëls and Baram, 2009; Ulrich-Lai and Herman, 2009). Indeed, CNS-specific deletion of the *Gr* in mice causes a marked hyperactivity of the HPA axis even though the circadian rhythm was still present (Tronche et al., 1999). Deletion of *Gr* in principal neurons in the forebrain in mice resulted in impaired negative glucocorticoid feedback but ACTH and corticosterone were only elevated from around four months of age on (Boyle et al., 2005). Both mouse models also show decreased anxiety behaviour and the latter also decreased depression-like behaviour suggesting these functions of the GR are linked to the limbic system (Tronche et al., 1999; Boyle et al., 2005, 2006). Mutation of the GR dimerization domain in mice causes elevated basal corticosterone levels but no changes in stress response, CRH expression or ACTH secretion, suggesting that these are regulated by a DNA-binding independent mechanism (Reichardt et al., 1998). As GRs are widely expressed in the brain it is still controversial if they act directly on parvocellular neurons or rather on GABAergic neurons that control PVN activity or even in limbic regions. CRH expression shows an inverse relationship with serum glucocorticoid levels, particularly at glucocorticoid levels between 10 to 150 ng/ml. *In vitro* studies suggested a direct action of glucocorticoids on CRH expression in parvocellular neurons but corticosterone administration into the PVN *in vivo* had little effect on PVN CRH expression (Watts 2005). Also the finding that mutation of the GR dimerization domain does not alter CRH expression (Reichardt et al. 1998, see above) indicates another mechanism than direct inhibition of CRH expression by the GR.

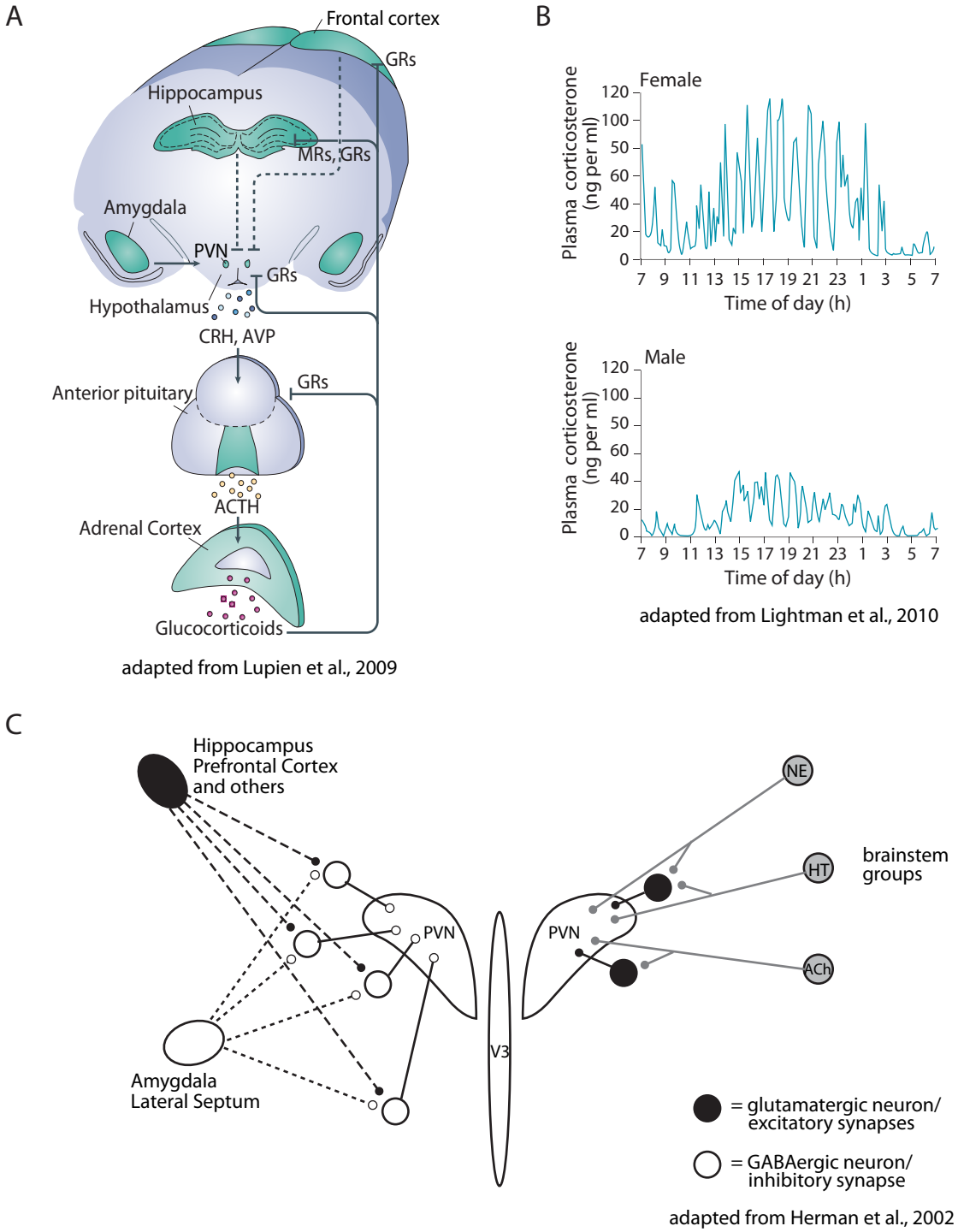

Figure 1.4 A Overview of the HPA axis. Parvocellular neurons in the paraventricular nucleus (PVN) secrete CRH and AVP into the portal blood stream. This induces secretion of ACTH from the pituitary which in turn induces release of glucocorticoids from the adrenal cortex. Glucocorticoids act in a negative feedback loop on the pituitary and several brain regions by binding to mineralo- and glucocorticoid receptors (MR, GR). Hippocampus and prefrontal cortex inhibit and amygdala projections activate PVN neurons. B Ultradian rhythm of corticosterone plasma levels in female and male rodents. C The PVN is under tonic inhibitory input from local gabaergic interneurons which in turn receive glutamatergic input from the hippocampus and prefrontal cortex and GABAergic input from the amygdala. Excitatory input into the PVN is much weaker and mainly originates from noradrenergic (NE), serotonergic (HT) and acetylcholinergic (ACh) brainstem nuclei that innervate the PVN either directly or via local glutamatergic neurons.

Activity of parvocellular neurons is also tightly regulated by local GABAergic interneurons. It should be mentioned that these interneurons do not originate in the ganglionic eminences like cortical and hippocampal interneurons, but from the intra-hypothalamic diagonal, a zone between the anterior dorsal and posterior ventral regions of the hypothalamus (Blackshaw et al., 2010). GABAergic interneurons that innervate parvocellular neurons were found in the peri-PVN (includes the subparaventricular zone, neurons directly dorsal and lateral to the PVN and neurons in the dorsomedial anterior hypothalamic area (dmAHN) and the perifornical nucleus (Herman et al., 2002), but also in the dorsomedial hypothalamus (DMH), the preoptic area and nucleus (POA) and the bed nucleus of the stria terminalis (BST) thus building an inhibitory ring around the PVN (Figure 1.4 C) (Cullinan et al., 1993, 2008; Bowers et al., 1998; Herman et al., 2002). Microinjections of a GABA antagonist into the PVN induce an increase in corticosterone levels in unstressed animals. This response is blunted in stressed animals suggesting that inhibitory interneurons exert tonic inhibition over the PVN that is only lifted upon stress (Cole and Sawchenko, 2002; Hewitt et al., 2009; Wamsteeker and Bains, 2010).

Apart from exerting tonic inhibition over the PVN, local GABAergic interneurons also serve as a gateway for afferent limbic inputs (Figure 1.4 C). As already mentioned, the limbic system has few direct inputs into the PVN but rather innervates GABAergic nuclei in the vicinity of the PVN. Projections from the hippocampus and prefrontal cortex are mainly glutamatergic and activate GABAergic interneurons leading to suppression of HPA axis activity. In contrast to this, projections from the amygdala are rather GABAergic and inhibit interneurons leading to disinhibition of the PVN (Herman et al., 2002; Herman, 2003; Cullinan et al., 2008; Jankord and Herman, 2008). Hence, the ring of inhibitory interneurons in the hypothalamus and BST integrates excitatory and inhibitory inputs from the limbic system, a mechanism that was suggested to be especially important for anticipatory responses and habituation to repeated stress (Jankord and Herman, 2008).

Hypercortisolism: Cushing's syndrome and the metabolic syndrome

Disregulation of the HPA axis can cause numerous diseases. For instance, chronically elevated glucocorticoid levels result in development of Cushing's syndrome. In humans the cause of Cushing's syndrome is generally a pituitary or adrenal tumor leading to increased ACTH and/or cortisol secretion or prolonged glucocorticoid treatment. Cushing's syndrome is characterized by central obesity with increased visceral fat mass in the abdominal and trunk area, as well as fat accumulation in the neck/shoulder region and the face. This is accompanied by increased leptin and insulin levels, hyperglycemia, hypertension and development of diabetes type II. Increased glucocorticoid production by the adrenal cortex results in adrenal hypertrophy and the chronically elevated glucocorticoid levels cause muscle atrophy, thinning skin with decreased subcutaneous fat mass and a decrease in bone density. Also psychological disturbances as emotional lability, increased irritability, anxiety, depression and cognitive deficits are often found in Cushing's patients (Felig and Frohman, 2001; Nieuwenhuizen and Rutters, 2008; Fernandez-Rodriguez et al., 2009).

Cushing's syndrome can be modeled in mice, for instance by overexpression of *Crh* (Stenzel-Poore et al., 1992; Groenink et al., 2002), altered posttranslational processing of ACTH (Saiardi and Borrelli, 1998; Westphal et al., 1999) or brain-specific deletion of the *Gr* (Tronche et al., 1999). These models show a subset of the symptoms seen in humans, depending on the method used.

Some of the symptoms observed in Cushing's syndrome, especially central obesity, hyperleptinemia, hyperinsulinemia, hyperglycemia, diabetes type II and hypertension, are reminiscent of the metabolic syndrome suggesting that disregulation of the HPA axis and glucocorticoid secretion could contribute to the development of this disease (Peeke and Chrousos, 1995; Pasquali et al., 2006; Anagnostis et al., 2009). A state of 'functional hypercortisolism' has been described in obese individuals with subtle increases in HPA axis activity and increased activity of glucocorticoids in peripheral tissues, especially adipose tissue (Pasquali et al., 2006; Anagnostis et al., 2009). Chronic administration of

corticosterone causes hyperphagia in mice leading to development of a full metabolic syndrome (Karatsoreos et al., 2010). Glucocorticoids were suggested to have an orexigenic effect and to alter food preference towards more fat and sugar-containing food. The orexigenic effect might be based on glucocorticoid suppression of CRH which has anorexigenic effects (see chapter 1.3.1) (Nieuwenhuizen and Rutters, 2008). Glucocorticoids might alter fat distribution by direct action on adipose tissue. For instance, increased availability of glucocorticoids in fat tissue by overexpression of 11β-hydroxysteroid dehydrogenase-1 (*11β-Hsd1*), a glucocorticoid-converting enzyme, leads to obesity (Masuzaki et al., 2001). Furthermore, glucocorticoids were shown to upregulate NPY receptors in adipose tissue resulting in abdominal obesity under conditions of stress-induced NPY release (Kuo et al., 2007).

1.4.2 Indications for a role of BDNF/TrkB signalling in the control of HPA axis activity

Both BDNF and TrkB are expressed in the pituitary and the hypothalamic nuclei involved in HPA axis control (Tapia-Arancibia et al., 2004). HPA axis activity and the ability to cope with stress has been associated with the Val66Met mutation of the *Bdnf* locus in humans (Schule et al., 2006; Shalev et al., 2009; Vinberg et al., 2009).

Most studies involving BDNF directly in the regulation of HPA axis activity originate from just one lab. This group showed that acute immobilization stress increases *Bdnf* mRNA and peptide levels in the pituitary (Givalois et al., 2001), PVN (Rage et al., 2002), hippocampus (Marmigère et al., 2003) (decrease after longer stress stimuli), and median eminence of rats (Givalois et al., 2004a). Furthermore, they demonstrated that one injection of BDNF into the lateral ventricle acutely increases serum ACTH and corticosterone levels and later also *Crh* mRNA expression in the PVN (Givalois et al., 2004b). Chronic infusion of BDNF into the lateral ventricle increased PVN CRH and AVP mRNA and peptide levels. However, the net effect on HPA axis activity was unclear as serum ACTH levels were decreased but corticosterone levels increased (Naert et al., 2006). Finally, they showed that exposure of rats to chronic stress leads to upregulation of

BDNF peptide levels in hippocampus, hypothalamus and pituitary, to increased PVN CRH and AVP mRNA and peptide levels and increased serum ACTH and corticosterone levels (Naert et al., 2010). Electrophysiological analysis of GABAergic synapses onto PVN neurons suggests that BDNF decreases GABAergic input by removal of $GABA_A$ receptors via a postsynaptic mechanism (Hewitt and Bains, 2006).

BDNF and TrkB were also suggested to interact with glucocorticoid feedback. Corticosterone was shown to regulate expression of BDNF and TrkB in the hippocampus, hypothalamus and , at least for BDNF, in the pituitary (Schaaf et al., 1997; Tapia-Arancibia et al., 2004). Furthermore, the GR can directly interact with TrkB *in vitro* enhancing BDNF-dependent signalling via the PLC docking site of TrkB (Numakawa et al., 2009).

Yet, in the *Bdnf* or *Trkb* mutant mouse lines in which HPA axis activity was analyzed no changes were apparent. For instance, $Bdnf^{+/-}$ mice have normal corticosterone levels (Kernie et al., 2000) and conditional deletion of *Trkb* in principal neurons of the forebrain did not cause any changes in HPA axis activity suggesting that, if TrkB has any role in regulation of the HPA axis, it is not dependent on principal neurons (Zorner et al., 2003).

1.5 Aim of this Project

This project aims at characterizing the role of the neurotrophin receptor TrkB in a specific subset of interneurons that express CCK. To specifically ablate *Trkb* from these neurons, we have generated a transgenic BAC-Cre mouse line that expresses Cre under the CCK-promoter and crossed it to a T*rkb*-floxed mouse line.

Little is known concerning the role of CCK-positive interneurons outside of the hippocampus and cortex, but CCK is also found in numerous other regions of the brain. For instance, analysis of recombination in the *BAC-CCK-Cre* mice revealed a high number of recombined neurons in the hypothalamus in regions involved in control of energy intake or regulation of hypothalamic-pituitary-adrenal (HPA) axis activity. Intriguingly, BDNF/TrkB signalling has been involved in both central metabolic control and regulation of the HPA axis.

This study investigates the involvement of TrkB signalling in CCK-expressing interneurons in control of energy intake and modulation of HPA axis activity. CCK-Cre specific *Trkb*-knockout mice develop central obesity and have elevated ACTH and corticosterone levels indicating HPA axis hyperactivity. Therefore, body weight gain, fat accumulation and food intake on normal and high-fat diet will be analyzed. Also obesity-related changes in serum levels of major metabolic hormones as leptin and insulin will be described. Peripheral consequences of increased HPA axis activity will be investigated by morphological analysis of the adrenal cortex and analysis of fat distribution. A possible association of increased HPA axis activity with altered anxiety behaviour will be studied by testing anxiety behaviour. The central regulator of HPA axis activity is the paraventricular nucleus of the hypothalamus (PVN). Changes in PVN function will be assessed by *in-situ* hybridization for markers of PVN activity. The distribution of recombined CCK-neurons in nuclei involved in HPA axis regulation will be analyzed as well as their potential to integrate glucocorticoid feedback inhibition. To verify which downstream pathways of TrkB are involved in the phenotypes observed, mice with point mutations in the TrkB-SHC or TrkB-PLC adaptor site will be analyzed as well.

2 MATERIALS AND METHODS

2.1 Standard chemicals and consumables

All chemicals were purchased from Sigma Aldrich (Sigma-Aldrich Ltd, Gillingham, UK and Sigma-Aldrich Chemie GmbH, Munich, Germany) or VWR (VWR International, Lutterworth, UK and VWR International GmbH, Darmstadt, Germany) in molecular biology grade unless otherwise stated.

Consumables were purchased from Roth (Carl Roth GmbH, Karlsruhe, Germany), Eppendorf (Eppendorf UK Limited, Cambridge, UK), BD (BD, Oxford, UK), Greiner (Greiner Bio-One Ltd., Stonehouse, UK), Thermo Fisher Scientific (Fisher Scientific UK Ltd., Loughborough, UK and Fisher Scientific GmbH, Schwerte, Germany), Gilson (Gilson UK, Luton, UK) and Rainin (Anachem Ltd, Luton, UK).

2.2 Buffers

All buffers were prepared with ultrafiltered water unless stated otherwise. Water was purified using the "Milli-Q-water purification system" from Millipore (Millipore Ltd, Watford, UK). For *in-situ* hybridization water and PBS were treated with DMPC (dimethylpyrocarbonate), a less carcinogenic alternative to DEPC (diethylpyrocarbonate) in order to inactivate RNases. DMPC was added at a dilution of 0.1 % (v/v), solutions incubated at 37 °C for at least one hour and then autoclaved in order to inactivate DMPC.

Buffers in alphabetical order:

Acidic Alcohol:

0.25% HCl in 70% ethanol (676 µl of 37% HCl for 100 ml)

100% avertin stock:

10 g of 2,2,2-tribromoethyl alcohol (Sigma-Aldrich) were dissolved in 10 ml of tert-amyl alcohol (Sigma-Aldrich) by stirring over night at 37 °C and then kept at 4 °C protected from light.

Bluing Solution:

0.3% ammonium hydroxide in distilled water

Cresyl Violet (CV) buffer:

2 g sodium acetate, 3 ml glacial acetic acid for 1 litre

Cresyl Violet stock solution:

2% (w/v) cresyl violet in water, stir o/n

Cryoprotection buffer for floating sections:

30% (w/v) sucrose, 30% (v/v) ethylene glycol, 1% (w/v) polyvinyl-pyrrolidone (PVP-40) in 0.1 M PB pH 7.4

(for 1 l: add 10 g PVP-40 to 500 ml PB, stir until dissolved, slowly add 300 g sucrose until dissolved, add 300 ml ethylene glycol and add up to 1 litre with PB, store at -20 °C)

10x DNA loading buffer:

50% glycerol, 0.2% OrangeG (Sigma, O-1625), in 1xTAE or 1xTBE

Hybridization buffer:

2x buffer from Sigma (Hybridization Solution I, #53754), dilute 1:1 with formamide, contains then 50% formamide, 5x SSC, 5x Denhardt's solution, 100 µg/ml salmon sperm; add 250 µg/ml tRNA

LB/LB Agar:

10 g Bacto-tryptone, 5 g Bacto-yeast extract, 10 g NaCl per 1 l (add 15 g Agar for plates)

NTMT buffer:

100 mM Tris-HCl pH 9.5, 100 mM NaCl, 100 mM MgCl2, 0.1% Tween-20

PB:

100 mM PB, pH 7.4 (77.4 ml of 1 M Na_2HPO_4, 22.6 ml of 1 M NaH_2PO_4 for 1 litre)

PBS:

0.01 M phosphate buffer, 0.0027 M potassium chloride and 0.137 M sodium chloride, pH 7.4 (was prepared from Sigma PBS tablets - P4417)

10x PCR buffer:

100mM Tris-HCl pH9.0, 500mM KCl, 1% Triton X-100

4% PFA:

For 1 litre final solution 40 g of paraformaldehyde (Sigma, stored at 4 °C) were dissolved in 800 ml PB buffer (pH 7.4) by heating to 60 °C. The solution was cooled down to room temperature, adjusted to pH 7.4 with sodium hydroxide if necessary, and filtered through a 50 µm syringe filter. Aliquots were stored at -20 °C, for experiments the required amount was thawed at 56 °C and then cooled to 4 °C.

Ponceau solution:

0.1% Ponceau S, 5% acetic acid

5x Protein loading buffer for SDS-PAGE:

313 mM Tris pH 6.8, 50% glycerol, 10% SDS, 0.05 % bromophenol blue, add 5% β-mercaptoethanol just before use

Protein lysis buffer for blotting:

50 mM Tris pH 8.0, 150 mM NaCl, , 1% NP-40, 0.1% SDS, 1 tablet of SigmaFast proteinase inhibitor cocktail per 100 ml (S8820, Sigma-Aldrich, final concentration: 2 mM AEBSF, 0.3 µM Aprotinin, 130 µM Bestatin, 1 mM EDTA, 14 µM E-64 and 1 µM Leupeptin), aliquot and store at -20°C

Protein lysis buffer for ELISA:

25 mM HEPES pH 7.4, 160 mM KCl, 1% Triton-X100, 1 tablet of SigmaFast proteinase inhibitor cocktail per 100 ml (as for protein lysis buffer for blotting)

5x SDS-PAGE Running Buffer:

will give 1x: 25 mM Tris, 192 mM glycine, 0.1% SDS

(for 1 l of 5x: 15.5 g Tris base, 72.1 g glycine, 5 g SDS)

50x TAE:

2 M Tris, 1 M glacial acetic acid, 50 mM EDTA, pH 8.0

Tail lysis buffer:

100 mM Tris, 1 mM EDTA, 250 mM NaCl, 0.2% SDS, pH 7.5

10x TBE:

890 mM Tris, 890 mM boric acid, 20 mM EDTA, pH 8.3

TB:

50 mM Tris, pH 8.3

TBS:

50 mM Tris, 150 mM NaCl, pH 7.5

TE:

10 mM TrisHCl, 1 mM EDTA, pH7.5

10x Transfer Buffer:

will give 1x: 50 mM Tris, 40 mM glycine, 0.02% SDS, 10% methanol

(for 1 l of 10x: 60.6 g Tris base, 30 g glycine, 2 g SDS, methanol is only added to diluted buffer just before use)

Tris-Azide:

40 mM Tris, 10 mM phosphate, 0.7% NaCl, 0.05 % NaN_3

(for 1l: 4.85 g Tris base, 1.5 g Na_2HPO_4 x $2H_20$ or 8.4 ml of 1 M Na_2HPO_4 x $2H_20$, 0.22 g NaH_2PO_4 x H_2O or 0.8 ml of 2 M NaH_2PO_4 x H_2O, 7 g NaCl, 0.5 g NaN_3)

2.3 Animals

All animal procedures at the Mouse Biology Unit of EMBL Monterotondo were conform to national and international laws and policies (EEC Council Directive 86/609, OJ L 358, 1, December 12, 1987; NIH Guide for the Care and Use of Laboratory Animals, NIH Publication No. 85-23, 1985 revised in 1995). All procedures performed at the Centre for Neuroregeneration, Edinburgh, UK were conform to UK legislation (Scientific procedures ACT 1986) and the University of Edinburgh ethical review committee policy.

2.3.1 Mouse lines

Mouse line	Description	First reference
BAC-CCK-Cre	BAC transgenic line expressing Cre recombinase and lacZ from the CCK promoter	PhD thesis of Sylvia Badurek/this study
Trkb-floxed	Line for conditional deletion of *Trkb*, loxP sites flank the second exon of the kinase domain	(Minichiello et al., 1999)
Trkb-CCK-KO	Cross of the *BAC-CCK-Cre* line and the *Trkb-floxed* line	PhD thesis of Sylvia Badurek/this study
Z/EG	Transgenic reporter line switching from lacZ expression to EGFP expression (under the pCAGGS promoter) upon Cre-mediated recombination	(Novak et al., 2000)
R26R-EYFP	Knockin reporter line expressing EYFP from the Rosa-26R locus upon Cre-mediated removal of a stop cassette	(Srinivas et al., 2001)
$Trkb^{PLC}$	Line with a single point mutation in the PLC docking site (Y816F)	(Minichiello et al., 2002)
$Trkb^{WT}$	Wildtype knockin mice, used as wildtype control for the $Trkb^{PLC}$ line since this line was generated by a cDNA knockin approach	(Minichiello et al., 2002)
$Trkb^{SHC}$	Line with a single point mutation in the SHC docking site (Y515F)	(Minichiello et al., 1998)

2.3.2 Generation of the *BAC-CCK-Cre* line

The *BAC-CCK-Cre* line was generated by Sylvia Badurek, a former PhD student in the lab. Since this line is not officially published yet the generation of the line will be summarized here.

The plasmid (pIZKeoX1) containing the Cre-recombinase cassette was generated by Che Serguera in E.coli for subsequent insertion into BACs. The cassette consists of a hybrid intron (HI) followed by the Cre-recombinase gene. After the Cre-recombinase

gene an internal ribosomal entry site (IRES) followed by the beta-galactosidase gene (lacZ) was inserted in order to allow for faster identification of transgene expression by X-gal staining. A neomycin/kanamycin cassette (neo) for selection of E.coli containing the modified BAC was inserted (Figure 2.1).

BAC no. RPCI23-26B6 (256125bp) containing the *Cck* gene was chosen for targeting by Sylvia Badurek and ordered from BACPAC resources (Children's Hospital, Oakland, USA). Jeannette Rientjes and Annett Spanner from the Gene Expression Service at EMBL-Monterotondo cloned the 50 bp homology arms and added these to the Cre-construct. The Cre-recombinase construct was then inserted into the first coding ATG of the *Cck* gene of the BAC via ET recombination in E.coli and the neo cassette was removed using a Flp-recombinase. Circular BAC DNA was injected at 1-2 ng/µl into pronuclei of CBA/C57 hybrid oocytes by José Gonzalez and his team from the Transgenic Service Facility at EMBL-Monterotondo.

The resulting pups were screened by Sylvia Badurek for presence of the transgene by PCR for the Cre-recombinase. Several founders were analyzed by beta-galactosidase staining and crossing to the *Z/EG* reporter line. The founder line with an expression best corresponding to published expression patterns of *Cck* was then used for all experiments.

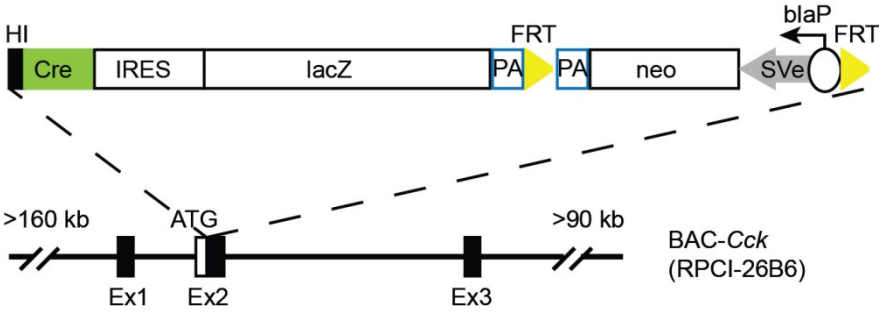

Figure 2.1 Cre-recombinase construct and insertion site in the CCK-BAC. blaP beta-lactamase promoter; Cre Cre-recombinase; Ex exons of the *Cck* gene; FRT flpe recognition site; HI hybrid intron; IRES internal ribosome entry site; lacZ *beta-galactosidase* gene; neo neomycin/ kanamycin gene; PA polyadenylation site; SVe SV40 early enhancer/promoter region

2.3.3 Animal handling and colony organization

The *Trkb*^{PLC}, *Trkb*^{WT}, *Trkb*^{SHC} and *R26R-EYFP* mice were maintained on a mixed genetic background (C57B6/129), *Z/EG* mice were maintained on a C57B6/129/CD1 mixed background and *Trkb-floxed* mice on a C57B6 background. The *BAC-CCK-Cre* transgenic founder was a CBA/C57B6 hybrid that was crossed back to C57B6 mice for at least five generations. For the *Trkb-CCK-KO* line male heterozygous mice (*CCK-Cre*$^{tg/+}$,*Trkb*$^{lx/+}$) were crossed to floxed females (*CCK-Cre*$^{+/+}$,*Trkb*$^{lx/lx}$ or *Trkb*$^{lx/lx}$) as full knockout mice did not breed well.

At EMBL Monterotondo all basic animal handling was performed by animal caretaker Giuseppe Chiapparelli, at the Centre for Neuroregeneration in Edinburgh animal handling was performed by caretakers Jenni Rennie and Lynn Morrison. Female and male mice were housed separately with a maximum of five animals per cage. In the case of males only littermates were housed together whereas females were combined from several litters if possible. Mice were only kept alone if males had no littermates, were removed from a breeding, or if corticosterone or ACTH serum levels were to be determined from these animals. In this case mice were kept separately for at least two weeks before the experiment. For all other behavioural experiments mice were always kept with company.

For breeding one male was kept with two females, in the Centre for Neuroregeneration the first female to litter was generally separated in order to reduce stress. The minimal breeding age for males was 8 weeks and for females 6 weeks. Pups were separated from their mother at about P20. At EMBL Monterotondo animals were identified by eartagging with metal eartags from Hauptner (Hauptner Instrumente GmbH, Dietlikon-Zürich, Switzerland) and tail biopsies were taken for genotyping by me. At the Centre for Neuroregeneration ear punches were taken by the technicians according to the Universal mouse numbering system (Dickie, 1975) and were used for identification and as biopsies for genotyping.

Adult mice were sacrificed either by cervical dislocation or by gassing them with CO_2; young animals were sacrificed by decapitation unless stated otherwise in the respective method.

2.4 Genotyping

2.4.1 DNA purification

Genotyping samples from weaned mice were obtained either by tail clipping or ear punching and kept at -20 °C until processed. Biopsies were lysed for at 4 hours to overnight at 56°C in a waterbath (Grant Instruments, Shepreth, UK) in 200 µl of tail lysis buffer (see chapter 2.2) with 4 µl of Proteinase K (20 mg/ml stock, Sigma-Aldrich)(half the volume was used for ear notches). To inactivate the Proteinase K samples were then incubated for 10 minutes at 95 °C in a heatblock (Grant Instruments, Shepreth, UK).

For quick purification 600 µl ddH_2O was added to tail samples whereas ear punch samples were left undiluted. Tubes were centrifuged for 5 minutes at 8000 g (Eppendorf 5417R centrifuge) in order to precipitate hair and not lysed tissue. Samples were stored at 4 °C until genotyped and then transferred to -20 °C.

For cleaner purification the Qiagen DNeasy Kit (Qiagen, Hilden, Germany) was used with a modified protocol. After digestion samples were vortexed (Vortex genie 2, Scientific industries) for 10-15 seconds, 400 µl of a 1:1 mix of QIAGEN buffer AL and 99% ethanol was added and samples again vortexed for 10-15 seconds. Samples were then transferred to DNeasy mini columns with a collection tube and centrifuged (Eppendorf 5417R centrifuge) at 8000 rpm at RT for 1 min. The collection tube was exchanged, columns washed with 500 µl of QIAGEN wash buffer AW1 and centrifuged at 8000 rpm at RT for 1 min. Again, the collection tube was exchanged and the column washed with 500 µl of QIAGEN wash buffer AW2 and centrifuged at 13 000 rpm at RT for 3 min. The columns were then placed into normal tubes, 150 µl ddH_2O was applied directly onto the membrane and left to incubate for 1 min. Genomic DNA was eluted by centrifugation at

8000 rpm at RT for 1min. Samples were stored at 4°C until genotyping and then transferred to -20 °C.

For genotyping of embryos yolk sacs were used. Tissue was stored at -20 °C until processed. Lysis was performed as for tail samples. DNA was purified by ethanol precipitation. To 200 µl of lysate 24 µl of 5 M NaCl (final concentration 200 mM) and 400 µl (2 Vol) of 100 % ethanol were added and samples incubated at -20 °C for 30 minutes. Samples were then centrifuged for 20 minutes at 20.000 g at 4 °C. The DNA pellet was washed with 70% ethanol, pellets were air-dry, resuspended in 40 µl ddH_2O and stored at 4 °C.

2.4.2 Primers, Reaction setup and PCR conditions

Primers were ordered in lyophilized form from Metabion or Sigma, reconstituted with ddH_2O to 100 µM and stored at -20 °C. Unless otherwise stated, PCR reactions were set up in 50 µl (49 µl mastermix and 1 µl DNA) with 5 µl 10x buffer (see chapter 2.2), 3 µl $MgCl_2$ (25m M stock), 8 µl dNTPs (1.25 mM stock, 1.25 mM per nucleotide type), 0.5 µl of each primer, 31.5 µl ddH_2O and 0.5 µl Taq polymerase (Proteomics Core Facility at EMBL-Heidelberg). All PCRs were performed on a PTC-200 Peltier Thermal Cycler (MJ Research) or on a BioRad DNAEngine Peltier Thermal Cycler.

Cre PCR:

Primers: Cre1 5'- GCC TGC ATT ACC GGT CGA TGC AAC GA -3'

Cre2 5'- GTG GCA GAT GGC GCG GCA ACA CCA TT -3'

Product size: 726 bp

Cycling conditions: 94 °C 3 min, 94 °C 30 sec, 67 °C 1min, 72 °C 1min, go to step 2: 35 times, 72 °C 5 min, 4 °C 10 min

Quick or clean DNA preparation

R26R-EYFP PCR:

The R26R-EYFP PCR was set up as 20 µl reaction with 2 µl 10x buffer, 2 µl dNTP (1.25 mM per nucleotide), 1.2 µl $MgCl_2$ (25mM stock), 0.2 µl of each primer (100 µM), 0.5 µl Taq polymerase, 7.9 µl ddH_2O and 6 µl DNA.

Primers: PK40 5'- AAA GTC GCT CTG AGT TGT TAT -3'
PK41 5'- GCG AAG AGT TTG TCC TCA ACC -3'
PK42 5'- GGA GCG GGA GAA ATG GAT ATG -3'

Product size: WT band (PK40 + PK42): 600 bp
KI band (PK40 + PK41): 300 bp

The two PCR reactions were performed separately.

Cycling conditions: 94 °C 3 min, 94 °C 30 sec, 58 °C 30 sec, 72 °C 1min, go to step 2: 40 times, 72 °C 5 min, 4 °C 10 min

Only clean DNA preparation

Trkb-floxed allele:

Primers: prSYB2 5'- AGC ACG AGC ACA TTG TCA AG -3'
prSYB3 5'- AAG GTG ATC AAC AGC CCA AG -3'

Product size: floxed band: 933 bp
WT band: 850 bp

Cycling conditions: 94 °C 3 min, 94 °C 30 sec, 55° C 1min, 72 °C 1min, go to step 2: 35 times, 72 °C 5 min, 4 °C 10 min

Quick or clean DNA preparation

Trkb-PLC and Trkb-WT-control PCR:

Primers: LM8 5'- CAG CTT CGG TCA TCA GCA ACG -3'
LM9 5'- GCC CAG CAG GAG ACA GAC -3'
LM10 5'- CTC TTG ATG TGC TGA ACA AAT GTG -3'

Product size: WT band: 370bp

mutant band: 180bp

The two reactions were performed together.

Cycling conditions: 94 °C 3 min, 94 °C 30 sec, 63° C 1min, 72 °C 1min, go to step 2: 35 times, 72 °C 5 min, 4 °C 10 min

Quick or clean DNA purification

Trkb-SHC PCR:

Primers: LM8 5'- CAG CTT CGG TCA TCA GCA ACG -3'

LM9 5'- GCC CAG CAG GAG ACA GAC -3'

LM33 5'- GAT GTG GAA TGT GTG CGA GGC C -3'

Product size: WT band (LM8 + LM9): 370 bp

mutant band (LM9 + LM33): 580 bp

The two PCR reactions were performed separately.

Cycling conditions: 94 °C 3 min, 94 °C 30 sec, 60 °C (wt)/55 °C (mut) 30 sec, 72 °C 1min, go to step 2: 40 times, 72 °C 5 min, 4 °C 10 min

Quick or clean DNA purification

Z/EG PCR:

Primers: EGFPgen1 5' AAG TTC ATC TGC ACC ACC G 3'

EGFPgen2 5' TCC TTG AAG AAG ATG GTG CG 3'

EGFPgenWT1 5' CTA GGC CAC AGA ATT GAA AGA TCT 3'

EGFPgenWT2 5' GTA GGT GGA AAT TCT AGC ATC ATC C 3'

Product size: EGFP: 173 bp

WT (IL-2 locus): 324 bp

The two PCR reactions were performed separately.

Cycling conditions: 94 °C 1 min 30 sec, 94 °C 30 sec, 59 °C 45 sec, 72 °C 45 sec, go to step 2: 34 times, 72 °C 7 min, 4 °C forever

Clean DNA preparation only

2.4.3 Agarose gel electrophoresis

PCR reactions were run on 1% or 2% agarose gels. Gels were prepared with agarose from Sigma in 1x TAE or 1X TBE buffer (see chapter 2.2). Agarose was melted in a commercial microwave oven until completely dissolved, cooled down and 2.5 µl of a 10 mg/ml ethidium bromide stock solution (Sigma) per 100 ml was added before pouring the gel (gel apparatus from EMBL workshop). 5 µl of 10x DNA loading buffer (chapter 2.2) was added to the samples and 20 µl of each sample loaded. A 1kb DNA ladder (Invitrogen) was used as marker. Gels were run at 140 – 200 V until the bands were properly separated. Bands were visualized with a Gel Document Illuminator (Uvitech Cambridge).

2.5 Biochemistry

2.5.1 Antibodies

Antibodies used for western blotting were a monoclonal rabbit-anti-TrkB (1:500, clone 80E3, Cell Signalling), a monoclonal mouse-anti-TUJ.1 (1:10000, Ab14545, Abcam) and HRP-conjugated secondary antibodies (1:10.000, Jackson Lab).

2.5.2 Tissue collection and preparation of lysates for blotting

For biochemistry experiments mice were perfused with PBS in order to remove as much blood as possible from the brain. Mice were anesthetized with avertin (500 mg kg^{-1} i.p., Sigma-Aldrich) or Euthanal® (50 µl, i.p.) and after 3 minutes responsiveness was tested by pinching the paw until mice were completely unresponsive. At this point a tail sample was taken for genotyping. Mice were fixed on a plastic lid placed at an angle in a box to allow liquids to flow down into the box. The chest was opened and a cut performed in the right atrium to allow liquid to flow out. For perfusion a pump (Masterflex Economy, easy-load II, with tube L/S 13, Cole Parmer) was used with a 30G needle (BD Microlance 3 20G x 1 ½ inch) fixed to the tube. Mice were then perfused with PB, pH 7.4 through the left ventricle of the heart until only clear liquid left the atrium and the liver was pale (around 7.5 ml). The head was removed and the brain and pituitary extracted.

Dissections were performed as quick as possible on a metal plate placed on ice and tissue placed immediately on dry ice. First the cerebellum, hindbrain and the olfactory bulbs were removed. Then the two cortices were carefully separated from the rest of the brain by following the corpus callosum. The hippocampus and striatum were removed from the cortices. Finally the hypothalamus was dissected from the rest of the brain. Tissues were stored at -80°C until further processed.

Before lysis samples were weighed frozen. Then tissues were quickly transferred into 10 volumes (vol/wt) protein lysis buffer (see chapter 2.2) in a tissue grinder (VWR) on ice. Tissue was disrupted by 10 slow strokes with the dounce of the grinder or until no big particles were visible. Afterwards lysates were homogenized by sonicating three times for 30 seconds at 10 % strength with 10 second breaks on ice (Branson digital sonifier). To get rid of remaining particles samples were centrifuged for one hour at 20.000 rpm at 4°C. The supernatant was split into a 40 µl aliquot and into a second aliquot which was frozen on dry ice and stored at -80 °C. The 40 µl aliquot was mixed with 10 µl protein loading buffer (see chapter 2.2) and stored at -20°C for blotting.

2.5.3 Measurement of protein concentration

Protein concentration was determined with a BCA (bicinchoninic acid) assay (#23227, BCA Protein Assay Kit, Pierce/Thermo Scientific, Cramlington, UK) since it is less sensitive to the presence of detergents as Triton X-100 and NP-40 in the lysis buffer than other tests.

The assay was performed according to manufacturer's instructions. Briefly a working solution from the two reagents in the kit was prepared. 50 volumes of reagent A (1% BCA-Na_2, 2% $Na_2CO_3 \cdot H_2O$, 0.16% Na_2 tartrate, 0.4% NaOH, 0.95% $NaHCO_3$) were mixed with 1 volume of reagent B (4% $CuSO_4 \cdot 5H_2O$ in ddH_2O). Standards were prepared from albumin provided with the kit with the respective lysis buffer in the following concentrations: 2,000 µg/ml, 1,500 µg/ml, 1,000 µg/ml, 500 µg/ml, 250 µg/ml, 125 µg/ml, 25 µg/ml and 0 µg/ml (blank). 10 µl of each standard or sample were applied to a 96-well plate in duplicate and 200 µl of working solution was added. The plate was incubated for

half an hour at 37°C, then absorption was measured at 562 nm in plate reader (Tecan). If the colour reaction was too strong samples were diluted 1:10.

2.5.4 SDS- gel electrophoresis, blotting and detection of proteins

Polyacrylamide gels were prepared and run in a miniVE Mini Vertical Electrophoresis Unit (Hoefer, Holliston, US). For a 10% separating gel 6.227 ml ddH_2O, 3.25 ml 40% polyacrylamid, 3.25 ml 1.5 M Tris pH 8.8, 130 µl 10% SDS, 130 µl 10% APS and 13 µl TEMED were mixed. After casting, the gel was overlayed with 100% ethanol in order to insure an even surface. Once the gel had polymerized the ethanol was removed and a stacking gel cast (4%: 3.145 ml ddH_2O, 0.5 ml 40% polyacrylamid, 1.25 ml 0.5 M Tris pH 6.8, 50 µl 10% SDS, 50 µl 10% APS and 5 µl TEMED). The finished gels were transferred into the gel chamber with 1x SDS page running buffer. Samples had been mixed with protein loading buffer before freezing and were now just thawed and boiled for 5 minutes at 95 °C. 20 µl of sample was loaded per well and 5 µl of Benchmark marker (Invitrogen). Gels were run at 120 V until the dye had passed the stacking gel and then at 140 V until the dye ran out of the bottom of the gel.

Blotting was performed by wet transfer using a Mini Trans-Blot Cell (Biorad). The sandwich for blotting was prepared in a box filled with 1x transfer buffer with 10% methanol. One layer of blotting paper was placed on a foam pad, then a nitrocellulose membrane (GE healthcare) in the size of the gel, the gel, another layer of blotting paper and a second foam pad were placed on top. Air bubbles were removed by carefully rolling a plastic pipette over the sandwich. The holder was closed (white site towards the membrane) and placed into the transfer chamber with the buffer. The transfer was performed for 16 hours at 4°C at 30 V.

After blotting the membrane was rinsed in ddH_2O, then Ponceau solution (see chapter 2.2) was added for two minutes in order to see if the transfer had worked and all samples were equally loaded. The staining was washed out with TBS and the membrane was cut in half between the 64 and 80 kDa band. The lower part was used for TUJ.1 (~50 kDa) and the upper part for TrkB (~145 kDa full length, ~95 kDa truncated).

All washing and incubation steps were performed on a rocking platform at RT unless otherwise stated. Membranes were blocked in 5% skimmed milk in TBS for one hour and then incubated with primary antibodies as stated in chapter 2.5.1 over night at 4°C on a rocking platform. Afterwards membranes were washed three times ten minutes with TBS and incubated with HRP-conjugated secondary antibody as stated in chapter 2.5.1 for two hours. Three TBS washes of 15 minutes were performed. Bands were detected by incubating membranes in 1 ml of a 1:1 mixture of the reagents of the SuperSignal West Pico Chemiluminescent Substrate System (Pierce). Membranes were placed in a film cassette, covered with Saran wrap and films (BioMax Light Films, Kodak) were exposed in the dark room for the 10 seconds, 1 and 5 minutes. Films were developed for 2.5 minutes in developing solution (4153, developer for Curix 60, Agfa), washed thoroughly in water, fixed 3 minutes in fixative solution (4354 rapid fixer, Agfa), washed again and were then dried.

2.5.5 Quantification of immunoblots

Films were scanned using a commercial scanner (Epson) in grey-scale with a resolution of 1200 dpi and 8 bit. Bands in immunoblots were quantified using ImageJ and a method published by Luke Miller (Miller, 2010). Briefly, the rectangular selection tool was used to define the position of the bands and a profile of each band was plotted. The baseline of each peak (corresponding to one band) was defined by closing of the peak with the straight line tool and the area of each peak was measured. The area was expressed as percentage of the total area of all peaks (all bands at one size). The relative density was calculated by dividing this number by the average percentage of the bands of the control animals. The relative density of the TUJ.1 bands was used to normalize the relative density of full-length and truncated TrkB bands for differences in loading.

2.6 Immunoassays and assays for metabolites

2.6.1 Assays used

Hormone	Type	Manufacturer/Catalogue Number
ACTH	competitive EIA	Phoenix Pharmaceuticals/EK-001-21
ACTH	competitive ^{125}I RIA	Diasorin/24065
CCK	competitive EIA	Phoenix Pharmaceuticals/EK-069-04
Corticosterone	competitive EIA	Immunodiagnostic Systems/AC-14F1
Glucose	direct colour reaction	BioAssay Systems/DIGL-100
Insulin	Sandwich ELISA	Millipore/EZRMI-13K
Leptin	Sandwich ELISA	Millipore/EZML-82K

EIA enzyme immunoassay; ELISA enzyme-linked immunosorbent assay;
RIA radioimmunoassay

2.6.2 Blood withdrawal and serum extraction

Blood was withdrawn by cardiac puncture from the right ventricle. For this, a 1 ml syringe with a broad needle (22 Gauge) was filled with 50 µl of 0.5 M EDTA (final dilution: 50 mM) as anticoagulant. Mice were sacrificed by CO_2, the chest opened and blood was slowly drawn from the right ventricle of the heart until the needle was filled to 500 µl. The needle was removed from the syringe and the blood transferred into a 1.5 ml tube, mixed well and kept on ice. When all mice were processed, the blood was centrifuged for 10 minutes at 2000 rpm and 4 °C to separate the serum. The serum (supernatant) was transferred to fresh tubes, frozen on dry ice and kept at -80 °C.

For measurement of glucose, insulin and leptin mice were fastened for six hours before the experiment in order to exclude variations due to food intake.

For measurement of ACTH and corticosterone it is important to not disturb or stress animals before the experiment since this would induce elevated levels of both hormones. Animals were therefore separated into single cages at least 2 weeks before the experiment (to avoid changes in hormone levels due to social interaction) and animals were sacrificed as quickly as possible from the moment the cage was taken out.

For morning ACTH levels, animals were quickly decapitated and trunk blood was collected in plastic vials with 50 µl 0.5 M EDTA and stored on ice. For centrifugation blood was transferred to Eppendorf tubes and then processed as described above.

2.6.3 Tissue collection and lysis for ELISA

For tissue collection for ELISA mice were sacrificed by CO2. Brains were extracted, frozen on dry ice and stored at -80°C. Before lysis, brains were weighed frozen and then transferred into 5 volumes (vol/wt) of protein lysis buffer for ELISA (see chapter 2.2) on ice. Tissue was sonicated three times for 15 seconds with 45 seconds break at 20% output strength (Branson digital sonifier). Samples were rotated at 4 °C for one hour to extract proteins and then centrifuged for 20 minutes at 16.000 g at 4 °C. The supernatant was aliquoted into 400 µl per tube, frozen on dry ice and stored at -80°C.

2.6.4 CCK EIA

For determination of brain CCK content a competitive EIA from Phoenix Pharmaceuticals was used. For competitive assays, the wells of a microtiter plate or strip are precoated with a secondary antibody specific for the species of the primary antibody. The primary antibody (in this case to CCK) is incubated together with the sample or standard and biotinylated CCK. The CCK in the standards or samples and the biotinylated CCK compete for binding to the primary antibody – the more CCK present in the standard/sample, the less biotinylated CCK binds. The primary antibody – CCK complexes are captured to the wells by the precoated secondary antibody. The amount of bound biotinylated CCK is then detected by incubation with SA-HRP (streptavidin-horseradish peroxidase) followed by the substrate for HRP (TMB = 3.3',5,5'-tetra-methylbenzidine). A blue coloured product forms that is turned into yellow by adding a stop solution (hydrochloric acid). Absorption is measured at 450 nm and the background at 620 nm in a plate reader (Tecan). The intensity of the final yellow product is proportional to the amount of biotinylated peptide bound and therefore inversely proportional to the amount of CCK present in the standard or sample.

Brain lysates were prepared as described in chapter 2.6.3, thawed quickly at 37°C and transferred to ice just before use. A dilution of 1:2 in assay buffer was used. Standards with concentrations of 0.01, 0.1, 1, 10 and 100 ng/ml were prepared from the stock solution provided with the kit. All reagents were reconstituted according to the manufacturer's instructions. 50 µl of standard, positive controls or sample were added in duplicate to the 96-well plate strips provided with the kit. The primary antibody to CCK and the biotinylated CCK peptide were added and plates incubated for 2 hours at RT on a rocking platform. Wells were washed 5 times with wash buffer and then incubated with a SA-HRP solution for one hour at RT on a rocking platform. Wells were again washed five times with wash buffer to remove unbound SA-HRP and then the substrate for HRP was added. Plates were covered and incubated on a rocking platform for one hour at RT and then stop solution was added and absorption measured.

For analysis the background OD (optical density) and then the blank value (no assay buffer, no primary antibody, no biotinylated CCK) were subtracted for each well from the OD at 450 nm. Then all values were normalized to the value of total binding (assay buffer plus primary antibody plus biotinylated antibody, gives therefore maximum colour reaction). Since the standard curve for competitive assays is not linear but sigmoidal a log-logit was used for curve fitting. For this the logit (ln(n/1-n)) of each normalized OD was calculated and the logit of the standards was plotted over the concentration. In this way the sigmoidal curve is transformed into a logarithmic curve and logarithmic regression can be performed with Microsoft Excel. (If the x-axis is transformed to a logarithmic scale the curve is transformed into a straight line, however excel still needs to perform a logarithmic regression). The logarithmic regression gives an equation in the form of $y=a*\ln(x)+b$ where y is the logit, x the concentration, a the slope and b the y-intercept. The concentration of the samples can therefore be calculated by $x=\exp(y-b/a)$. The resulting concentration was multiplied with the dilution factor to obtain the final concentration. Values were not used when duplicates differed more than 15% or when positive controls were not inside the acceptable range.

2.6.5 Glucose Assay

For measurement of serum glucose, the QuantiChrom™ Glucose Assay Kit from BioAssay Systems was used. A standard was prepared according to manufacturer's instructions from a glucose stock provided with the kit with concentrations of 0, 50, 100, 200 and 300 mg/dl glucose. 5 µl of each standard and sample were mixed with 500 µl of provided reagent in a 1.5 ml centrifuge tube, boiled for 8 minutes in a heat block at 95 °C and cooled down in ice water for 4 minutes. Since glucose concentration in mouse serum often reaches 300 mg/dl samples were generally diluted 1:2 in ddH_2O beforehand. The reagent contains o-toluidine which reacts with the aldehyde group of glucose in hot glacial acetic acid (also in the provided reagent) and forms a colour product with an absorption maximum at 630 nm. Formation of the colour product is proportional to glucose concentration. After cooling down 200 µl of the reaction was transferred in duplicate to a 96-well plate and absorption measured at 620 nm in a plate reader (Tecan).

For analysis, the blank OD (0 mg/dl standard) was subtracted from all measured values. The OD of the standards was then plotted over the concentration and the slope was determined using linear regression, i.e. fitting a linear curve with Microsoft Excel. The concentration of the samples was determined by dividing the respective OD value by the slope. Values were only used for further statistical analysis if the duplicates did not show a difference of more than 15%.

2.6.6 Insulin ELISA

For determination of serum insulin levels, a sandwich ELISA from Millipore was used. In this case the wells of the microtiter plate are precoated with a monoclonal primary antibody that captures the insulin in the sample or standard. A second primary (polyclonal) antibody to insulin is added that is conjugated to biotin. The amount of bound biotinylated antibody is determined by adding SA-HRP and then a substrate to HRP as described for the competitive immunoassay (see chapter 2.6.4). In this case the colour development and therefore absorption is proportional to the amount of insulin present in the sample or standard.

Serum was prepared as described in chapter 2.6.2, quickly thawn at 37°C and kept on ice. Reagents were prepared according to manufacturer's instructions. All incubation steps were performed at RT on a rocking platform unless otherwise stated. Plates were prewashed and then 10 µl of standards (concentration: 0.2, 0.5, 1, 2, 5 and 10 ng/ml), quality controls, samples or assay buffer as blank were added in duplicate together with 10 µl matrix solution (to avoid background from serum components). The detection antibody (the biotinylated polyclonal primary antibody) was added and the plate incubated for 2 hours. Wells were washed three times, incubated for 30 minutes with SA-HRP and washed six times. The substrate solution was added and after 15 minutes incubation the stop solution. Absorption was measured at 450 nm and background at 620 nm. Concentrations of unknown samples was determined by a log-logit fit as described in chapter 2.6.4. Values were only used if the concentration of the quality control was in the accepted range and if duplicates did not differ more than 15%.

2.6.7 Leptin ELISA

Serum leptin was determined with a sandwich ELISA from Millipore. The principle of this assay is described in the above chapter (2.6.6) with the difference that the wells for this assay were precoated with a secondary antibody and that the first primary antibody was incubated with the standard and samples and captured by the coated wells. The second primary antibody was only added in the next incubation step.

The experiment and analysis was performed as described in chapter 2.6.6 with the following differences. Standards were 0.2, 0.5, 1, 2, 5, 10, 20 and 30 ng/ml and 10 µl of standards, samples or quality controls were mixed with 10 µl of matrix solution, 30 µl of assay buffer and the first primary antibody. Serum from obese animals was diluted 1:5. Plates were incubated for 2 hours, washed three times and the detection antibody was added and incubated for one hour. Plates were washed three times and SA-HRP, substrate incubations and analysis performed as described in chapter 2.6.6.

2.6.8 Corticosterone EIA

Serum corticosterone was determined with a competitive EIA from Immunodiagnostic systems. This assay is based on the same principles as the competitive CCK EIA (see chapter 2.6.4) but the primary antibody to corticosterone is directly coated to the wells and the competing corticosterone is directly labelled with HRP instead of using a biotin-streptavidin system.

Serum was prepared as described in chapter 2.6.2, quickly thawn at 37°C and then kept on ice. Reagents were prepared according to manufacturer's instructions. All incubation steps were performed at RT on a rocking platform unless otherwise stated. 100 µl of standard (0, 1.0, 2.4, 7.0, 17.9, 49.1, 179 ng/ml but slightly different depending on lot), positive control or samples were added to wells in duplicate. The HRP-conjugated corticosterone was added and plates were incubated over night (16-24 hours) at 4 °C on a rocking platform. Wells were then washed three times, substrate solution was added, incubated for 30 minutes and then the stop solution added. Absorption was measured at 450 nm and background at 620 nm. Analysis was performed using a log-logit fit as described for the CCK EIA (see chapter 2.6.4) and values were only used if the positive controls were in the right range and duplicates did not differ more than 15%.

2.6.9 ACTH EIA

Serum levels of ACTH were determined with an ACTH enzyme immunoassay from Phoenix Pharmaceuticals. We also tested a radioimmunoassay for ACTH (see next chapter) but this proved to be more work intensive, required the use of radioactivity and was not more sensitive. Therefore all ACTH sera were analyzed with this enzyme immunoassay, apart from the AM ACTH levels that were determined by RIA.

This assay is a competitive assay that works exactly as the CCK assay and was therefore performed and analyzed exactly the same way (see chapter 2.6.4). The only difference were the concentrations of the standards which were 0.04, 0.2, 1, 5, 25 ng/ml. It is important to use fresh serum aliquots (that were not thawn before) for determination of ACTH as it is rapidly degraded.

2.6.10 ACTH RIA

The ACTH radioimmunoassay from Diasorin was used for the morning ACTH levels but then not used any more since it proved to be not more sensitive than the EIA (previous chapter) but requires the use of radioactivity and is more work intensive.

The ACTH RIA is a competitive assay, comparable to the competitive EIAs only that radioactive ACTH is used as competitor instead of biotinylated ACTH. The samples or standards were incubated with an ACTH primary antibody and the ^{125}I-labeled ACTH (referred to as tracer). The antibody-ACTH complexes were then captured by a secondary antibody that is bound to beads. These were precipitated and radioactivity of the precipitate was measured. The radioactivity is then proportional to the amount of tracer and inverse proportional to the amount of ACTH in the standard or sample.

Fresh sera were used, quickly thawn and kept on ice. All reagents were prepared as described in the manufacturer's instructions. 100 µl of standards (0, 11.9, 42.5, 96.1, 212 and 462 pg/ml), positive controls or samples were incubated over night (16.24 hours) with 200 µl of tracer and 200 µl of ACTH antiserum in glass vials. Then the beads with the secondary antibody were added, incubated for 20 minutes at RT and precipitated by centrifugation for 20 minutes at 760 x g at RT. The supernatant was decanted and radioactivity was measured in a gamma scintillation counter. For analysis a hill fit was performed with Origin (OriginLab) and sample values were read from the fitted curve.

2.7 Histology and Immunohistochemistry

2.7.1 Collection, weighing and imaging of fat pads

Shoulder fat pad were imaged with a commercial digital camera (Panasonic). The skin of mice that had been perfused for other purposes was removed from the shoulder/neck region and pictures were taken.

For analysis of gonadal and mesenteric fat the fat tissue was carefully dissected. The mesenteric fat pad lines the intestines and can be removed by separating the pancreas and then pulling the fat apart from the intestine. The gonadal fat is easily identifiable as it is the big fat pad lying on top of the intestine that is immediately visible when opening the

abdomen. It is attached to the gonads and can be dissected by carefully removing these from the fat. Fat pads were weighed either freshly or were frozen on dry ice and weighed later (only one method was used for one batch of mice). Fat pad weight was expressed as percentage of body weight.

2.7.2 Analysis of adrenals

For analysis of adrenal morphology adrenals were removed, transferred to ice-cold 4% PFA in an eppendorf tube and fixed over night at 4 °C. We tried to weigh adrenals after dissection but since they often only weigh around 1 mg no balance was sensitive enough. After fixation adrenals were embedded in paraffin. All steps were performed on a rotating wheel or, for the xylene steps, a rotating platform. Adrenals were washed for one hour in PBS, one hour in 0.85% NaCl at 4 °C and then dehydrated for one hour at 4 °C in each 50%, 70%, 85%, 95% and 2x 100% EtOH (dilutions with 0.85 % NaCl). Either the 70% or the 100% step was performed over night, and at this point also remaining fat was dissected from the adrenals at it is very well distinguishable at this point. Adrenals were then transferred to glass vials and dehydrated in two changes of xylene for one hour each. Paraffin (at 60 °C) was added to give a 1:1 mixture (by eye) of paraffin to xylene and adrenals incubated for 1 hour at 60 °C. Adrenals were then kept in paraffin over night at 60 °C and on the next day paraffin was exchanged for 4-5 times every hour. Finally, adrenals and the last change of paraffin were transferred to plastic molds, adrenals positioned and the molds were cooled down and kept at 4°C.

Adrenals were sectioned into 8 µm serial sections on series of 4 slides (always 4 consecutive sections on one slide, then 4 on the next slide and so on) on a microtome (Leica). Slides were stored at 4 °C until further use.

Adrenal morphology was visualized by haematoxylin/eosin staining. For this sections were dewaxed for 20 minutes in xylene, rehydrated through a series of 100%, 90%, 70%, 50% ethanol (dilution in water) and tap water for two minutes each. Sections were incubated for five minutes in haematoxylin (Accustain Harris Haematoxylin solution, modified, Sigma HHS16), washed two minutes in tap water, dipped for 15

seconds in acidic ethanol (see buffers, chapter 2.2), washed two minutes in tap water, dipped for 30 seconds in bluing solution (see buffers), washed two minutes in tap water, dipped 30 seconds in acidic eosin (Accustain Eosin Y Solution aqueous, Sigma HT110216, plus 0.5 ml glacial acidic acid per 100 ml), washed two minutes in water and were quickly dehydrated for 30 seconds in 95% ethanol (short since eosin is ethanol soluble), two minutes in 100% ethanol, six minutes in xylene and mounted with DPX. Haematoxylin stains nuclei by binding to lysine residues of histones under acidic conditions. The acidic alcohol is used for this purpose and also to remove excessive haematoxylin staining (referred as 'differentiation') and turns the staining red. The bluing solution stops the differentiation process as it has a basic pH and turns the staining blue. Eosin stains cytoplasm in red (Lillie, 1965).

Brightfield images were taken from adrenal cortices with an Axio Scope (Carl Zeiss) mounting 10x/0.3 NA, 20x/0.8 NA and 40x/0.75 NA plan-apochromat objectives (Carl Zeiss) connected to an AxioCam ICC1 colour camera (Carl Zeiss). For each adrenal three pictures were taken from sections through the middle of the adrenal. These pictures covered most of the adrenal cortex. The thickness of the zona fasciculata was measured with the measurement tool in Image J (Abramoff et al., 2004; Rasband, 2011) or the measurement tool in Photoshop in nine locations per adrenal (three per picture) and in both adrenals of each mouse. The nine measurements per adrenal were averaged, and then the values of both adrenals per mouse were averaged.

2.7.3 Collection and sectioning of brains and pituitaries

For immunohistochemistry brains and pituitaries were prefixed by perfusion. Mice were perfused with PBS as described in chapter 2.5.2, but perfusion with PBS was followed by perfusion with 7.5- 10 ml of 4% PFA/PB, pH7.4. Brains and pituitaries were quickly removed and transferred to 4% PFA/PB on ice and postfixed for 3 hours. Initially, tissues were postfixed over night, but we realized that most antibodies work better on less strongly fixed tissue. After postfixation tissues were washed twice in PBS and then cryoprotected in 30% sucrose in Tris-Azide buffer (see buffers in chapter 2.2). Pituitaries

were left in sucrose over night and brains for 2-3 days until they were sunk to the bottom of the tubes. Tissues were then embedded in OCT in plastic molds and frozen on dry ice (pituitaries) or in precooled isopentane on dry ice for one minute and stored at -80 °C.

For sectioning tissues were calibrated to -20 °C for several hours or overnight in a commercial freezer. They were then transferred to a cryostat (Leica) and mounted on holders with OCT. Pituitaries were sectioned to 10 µm, directly placed on superfrost plus slides, dried for several hours at RT and then stored at -80°C. Brains were either stored as floating sections or on slides. For floating sections, brains were sectioned into 30 µm sections that were shortly washed in PBS, transferred to 96-well plates with Tris-Azide buffer (200 µl per well) and then stored at 4°C. In this way, sections can be stored for 2-3 months. Alternatively, sections can also be stored in cryoprotection buffer (see buffers in chapter 2.2) at -20 °C for much longer. For sections on slides, brains were sectioned into 10 or 15 µl sections that were placed immediately on superfrost-plus slides, dried for at least four hours to over night at RT and then kept at -80 °C.

2.7.4 Preparation of gelatine-coated slides

Gelatine-coated slides were used for mounting floating sections as sections stick too strongly to superfrost-slides to allow for wrinkle-free mounting. 0.5% (w/v) gelatine was dissolved in water at 70 °C, the solution was cooled to RT and 0.05% (w/v) alum chrome (chromium potassium sulphate) was added. The solution was cooled to 4°C and immediately used. Normal untreated glass slides (VWR) were placed into plastic slide holders and washed two times ten minutes in bidistilled water. Slides were placed into the gelatine solution for 5 minutes and bubbles carefully removed. Afterwards, the holders were placed on paper towels and tilted to that excess solution could run off. Slides were dried in this way under a hood over night or at 100 °C for one to two hours and then stored in a sealed box for not more than two months.

2.7.5 Nissl staining

Nissl staining which stains the somata of neurons and glia was used to analyze general morphology of the brain. For this, floating sections from perfused brains (chapter

2.7.3) were placed on gelatine-coated slides (chapter 2.7.4) and dried over night under a hood. Sections were then fixed for five minutes in ice-cold 4% PFA and washed twice for 5 minutes in PBS. In order to permeabilize membranes for cresyl violet, sections were incubated in a glass jar in xylene for 30 minutes. A cresyl violet working solution was prepared by diluting the cresyl violet stock solution 1/100 in cresyl violet buffer (see buffers chapter 2.2). After incubation in xylene, sections were rehydrated in 100% EtOH (1 min), 90% EtOH (1 min), 70% EtOH (40 sec) and 50% EtOH (20 sec) and then placed into cresyl violet working solution for 20 minutes. Sections were quickly dipped into PBS (10 sec) and then dehydrated through 50% EtOH (30 sec to 1 min depending on strength of stain), 80%, 95% and 100% EtOH (1 min each) and placed into xylene for at least 10 minutes. Slides were coverslipped with Eukit or DMX (Sigma) and dried for several hours under a hood. Pictures were taken with a brightfield microscope (Leica) with a 10x/0.3 NA plan-apochromat objective and a Leica camera.

2.7.6 Antibodies for immunohistochemistry

Antibody	Manufacturer/Catalogue no.	Dilution/Comments
gp-α-AVP (pAb)	Peninsula Laboratories/T-5048	1:2000
m-α-CCK (mAb)	Cure Centre UCLA/#9303	1:100 (use 0.05% Tween not Triton)
rb-α-c-fos (pAb)	Santa Cruz/sc-52	1:1000
gp-α-CRF (CRH) (pAb)	Peninsula Laboratories/T-5007	1:1000
rat-α-Ctip2 (pAb)	Abcam/ab18465	1:200
rb-α-GABA (pAb)	Sigma/A2052	1:1000
ch-α-GFP (pAb)	Abcam/ab13970	1:2000
rb-α-GFP (pAb)	Abcam/ab6556	1:1000
rb-α-GR (pAb)	Santa Cruz/sc-1004	1:1000
rb-α-p133-Creb (pAb)	Upstate/06-519	1:200
rb-α-PV (pAb)	Abcam/45542	1:1000

g = goat, gp = guinea pig, m = mouse, rb = rabbit
mAb = monoclonal antibody, pAb = polyclonal antibody

2.7.7 Immunofluorescence staining and analysis of colocalization

For immunofluorescence 30 µm floating sections or 10-15 µm sections on slides were used. For floating sections, sections were transferred to 24-well plates (1-2 sections per well for sagittal sections and 1-4 sections per well for coronal sections) where all steps were performed. 500 µl were used for washing steps, and 200 µl for antibody incubations. All steps were performed at RT on a rocking platform unless otherwise stated. Sections were washed twice with PB for 15 minutes, three times with TBS for 15 minutes and then blocked for one hour in 10% NGS, 0.3% Carrageenan (0.9% stock solution in TBS), 0.5% Triton-X100 in TBS. If high background is observed, this can sometimes be removed by quenching for one hour in 0.1 M glycine/0.1 M ammonium chloride after the PB washes. Sections were then incubated with primary antibody (dilutions see previous chapter) diluted in 1% NGS, 0.3% Carrageenan, 0.1% Triton-X100 in TBS for 36-60 hours at 4°C on a rocking platform. Afterwards, sections were washed three times with TBS for ten minutes and incubated with secondary antibody (Alexa488/555/633-conjugated goat secondary antibodies, Invitrogen) diluted 1:1000 in TBS with 0.1% Triton-X100 for two to three hours in the dark. Sections were washed three times in TBS for 10, 15 and 30 minutes in the dark. For counterstaining with DAPI, sections were rinsed with PBS, incubated for five minutes with DAPI in PBS (0.5 µg/ml from 5 mg/ml stock), washed three minutes with PBS and transferred to fresh PBS. Sections were placed on gelatine-coated slides (chapter 2.7.4) and dried over-night under a hood in the dark. Slides were then coverslipped with Vectashield (Vector Labs) and stored at 4°C in the dark.

Fluorescent staining on sections on slides was performed the same way with the following differences. If sections were from perfused brains, they were removed from the -80°C freezer and dried for 30 minutes. If sections were from fresh frozen brains, they were removed from the -80°C freezer, warmed up 3-5 minutes and fixed in 4% PFA for at least 15 minutes. These sections have to be treated with care as they are easily destroyed. Washing steps were all shortened to five minutes. For blocking and primary antibody incubations no carrageenan but 1% BSA was used. Primary antibody incubations were

performed for 12 to 36 hours, secondary antibody incubations were performed for one hour and 2.5% BSA was added.

For fluorescent imaging either standard fluorescent microscopes (Leica and Zeiss) were used with 10x/0.3 NA and 20x/0.8 NA plan-apochromat objectives and monochrome cameras or confocal microscopes (Leica SP6 or Zeiss LSM710 Meta confocal microscope) with plan-apochromat 10x/0.45 M27, 20x/0.8 M27, 40x/1.3 Oil DIC M27 and 63/1.40 Oil DIC M27 objectives.

As the staining for CCK shows high background and requires high antibody concentrations specificity of the antibody was tested by using a blocking peptide. For this, the primary antibody was incubated with a five-fold excess of a blocking peptide (CCK peptide from Santa Cruz) for two hours at RT in TBS before application to the sections. As the CCK antibody is a monoclonal antibody from ascite supernatant, a concentration of 1 mg/ml was assumed. The final concentration for this antibody would therefore be 10 µg/ml and accordingly 50 µg/ml of the blocking peptide were used.

For analysis of YFP/CCK and YFP/GABA colocalization, cell counts were performed on three non-consecutive sections (spaced 80 -100 µm) per mouse and three mice in total. Counts were done manually as the quality of both the CCK- and GABA-staining is not good enough to allow for automatic analysis. An area of 0.124 mm2 was analyzed per sections and only clearly labelled cells were counted.

2.7.8 DAB (3'3-diaminobenzidine) staining

For DAB staining 30 µm floating sections were used. Sections were transferred to 24-well plates (1-2 sections per well for sagittal sections and 1-4 sections per well for coronal sections) where all steps were performed. 500 µl were used for washing steps, and 200 µl for antibody incubations. All steps were performed at RT on a rocking platform unless otherwise stated. Sections were washed three times with PB for 15 minutes and then peroxidase activity was quenched by incubating for 20 minutes in 2% H_2O_2 (diluted in water). Two 15 minute washes in TBS were performed and then sections were blocked with 10% NGS, 0.3% Carrageenan (0.9% stock solution in TBS), 0.5% Triton-X100 in TBS

for one hour. Sections were incubated with primary antibody (dilutions chapter 2.7.6) diluted in 1% NGS, 0.3% Carrageenan, 0.1% Triton-X100 in TBS for 36-60 hours at 4°C on a rocking platform. Afterwards, sections were washed three times with 1% NGS, 0.5% Triton-X100 in TBS for 15 minutes. Secondary antibodies (biotinylated secondary antibodies, Vector Labs) were applied at a dilution of 1:200 in 1% NGS, 0.3% Carrageenan, 0.5% Triton-X100 and sections incubated over night at 4 °C. Sections were washed three times 15 minutes with 1% NGS, 0.5% Triton-X100 in TBS. For the next step the peroxidase Vectastain ABC system from Vector Labs was used. This system contains avidin and biotinylated peroxidase that were preincubated for half an hour with 1% NGS (1:100 dilution of each reagent A, B and NGS in TBS) to form avidin-biotin-peroxidase complexes. These were then incubated with the sections for one hour to allow the free biotin-binding sites of avidin to bind to the biotinylated secondary antibody on the sections. Sections were washed three times 15 minutes with TBS and two times 15 minutes with TB. For the colour reaction DAB (3'3-diaminobenzidine) was used that is converted to a brown precipitate by the peroxidase in the presence of hydrogen peroxide. Tablets from Sigma were used that give a ready-to-use solution when dissolved in water. Sections were incubated for 30 seconds to 10 minutes until staining was visible without background. For some stainings cobalt chloride was added (also available as tablets) which amplifies the signal and gives a dark blue to black colour. The colour reaction was stopped by washing three times with ice-cold TB and sections were mounted on gelatine-coated slides (see chapter 2.7.4) and dried over night. Sections were dehydrated for one minute in each 90% and 100% EtOH, incubated 10 minutes in xylene and then coverslipped with DMX or Eukit.

Brightfield images were taken with a Leica Stereo Microscope or a Leica DMI microscope mounting 10x and 20x Leica objectives.

2.8 *In-situ* hybridization

2.8.1 Probes

gene	primers	restriction enzyme and RNA polymerase for antisense/ sense probe	location and length of probe
Avp	5'-GGA GAG AGA ATT CAT GCT CGC CAG GAT GCT C 5-'GAG AGG ATC CCT TGG CAG AAT CCA CGG AC	EcoRI and SP6/ BamHI and T7	exon 1-3 492 nt
Crh	5'-GAG AGA ATT CAG AGA GCG CCC CTA ACA TG 5'-AGA GAG AAG CTT AGC ATG GGC AAT ACA AAT AAC G	EcoRI and SP6/ HindIII and T7	exon 2 807 nt
Penk	5'-TTC CTG AGG CTT TGC ACC 5'-TCA CTG CTG GAA AAG GGC	EcoRI and SP6/ BamHI and T7	exon 1-2 816 nt
Trkb	5'-TCA GCA TAT CAA GAG ACA C 5'-CTG TAC ACA TCT CGG GAC AT	EcoRI and SP6/ BamHI and T7	exon 20 – 21 520 nt

2.8.2 Preparation of plasmids containing the probes

For in-situ hybridization RNA probes were used. The plasmids containing the probes for *Penk* and *Trkb* were designed and prepared by Emerald Perlas from the Histology Service at the EMBL in Monterotondo. The *Penk* probe is one of the probes published for *Penk* by the Allen Brain Atlas project (Riboprobe ID: RP_060315_01_A07, (Lein et al., 2007)).

Plasmids and probes for *Avp* and *Crh* were designed and cloned by me, the *Avp* probe corresponds to the probe published by the Allen Brain Atlas project (Riboprobe ID: RP_Baylor_102643), the *Crh* probe is slightly modified as the Allen Brain Atlas probe (Riboprobe ID: RP_Baylor_102704) contains an intron sequence. Glycogen stocks containing the plasmids with the respective cDNA clone were obtained from Open Biosystems (Avp clone 5683720, Crh clone 40126240). The probe sequence was subcloned from these plasmids into a pGEM-3ZF(+) vector that contains SP6 and T7 RNA polymerase start sites. For this, the probe sequence was amplified by PCR directly from colonies obtained from the glycerol stock with the primers listed in chapter 2.8.1. These contain the actual primer sequence for amplification, the restriction site for subcloning plus several AG repeats to improve the restriction digest and to balance the GC-content.

PCR was performed with two different annealing temperatures and started with a 10 minute incubation at 95 °C to disrupt bacterial cells. For the first 5 cycles a lower temperature of 53 °C was used that is adapted to the actual primer without restriction sites and AG-repeats to allow for efficient amplification of the cDNA. For the next 30 cycles a higher annealing temperature of 65 °C, adapted to the whole primers, was used to ensure specificity. The PCR reaction was separated on a 1.5% agarose gel and the band corresponding to the PCR product was cut out and DNA purified using the Geneclean II Kit (MP Biomedicals) according to manufacturer's instructions. The pellet was resuspended in 20 µl water and 5 µl were digested with 10 units EcoRI and BamHI (Avp) or EcoRI and HindIII (Crh) in the respective buffers (all New England Biolabs) for three hours at 37 °C. Also 1 µl of the pGEM plasmid was digested in the same way. The digests were separated on an agarose gel and the bands corresponding to the digested PCR product (the insert) and the linearized plasmid, respectively, were cut out and purified from the gel using the Geneclean II Kit. The plasmid was resuspended in 100 µl water and the insert in 20 µl water. For ligation 10 ng of plasmid and insert (6 times molar ratio) and 20 units of T4 DNA ligase were incubated for three hours at RT and ligation was stopped by incubating the reaction for ten minutes at 65 °C.

1 µl of the ligation reaction was transformed into XL-1 blue competent cells (Stratagene) by heat shock according to manufacturers instruction and cells were plated on agar containing 100 µg/ml ampicillin and covered with 200 µl of 10 mM IPTG (isopropyl thiogalactoside) and 40 µl of 2% x-Gal (5-bromo-4-chloro-3-indolyl-beta-D-galactopyranoside). The XL-1 strain expresses ß-galactosidase unless a sequence is inserted in the multiple cloning site, disrupting the ß-galactosidase gene. When grown on agar with IPTG and x-Gal (inducer and substrate for ß-galactosidase) colonies without insert turn blue whereas colonies containing an insert stay white. Colonies were grown over night at 37 °C and several white colonies were picked and transferred to 5 ml LB with 100 µg/ml ampicillin and grown over night at 37 °C with shaking. A 4 ml aliquot of each culture was used for DNA purification using the Qiagen Miniprep Kit and 0.8 ml of each

culture was mixed with 0.8 ml sterile 40% glycogen and frozen at -80°C for storage. 1 µl of the purified plasmid was tested for the right insert by a restriction digest (as described above).

2.8.3 Preparation of probes

Digoxigenin (DIG)-labelled probes were generated from the pGEM plasmids containing the probe sequence by run-off transcription. Solution were kept RNase-free from phenol-chloroform purification on. For this, solutions were treated with DMPC or prepared in DMPC-treated water (preparation see chapter 2.2) and all equipment was cleaned with 0.5 % SDS followed by 3% H_2O_2 or baking at 300 °C for two hours (only glassware).

5 µl of the plasmid were linearized with 30 units of either EcoRI (for antisense) or BamHI (*Avp* sense) or HindIII (*Crh* sense) in a 50 µl reaction for three hours at 37 °C. For run-off transcription, the digestion has to be complete, therefore, 2 µl of the reaction were run on a gel to verify this. The rest of the linearized plasmid was purified by phenol/chloroform purification. The volume of the restriction digest was increased to 500 µl with DMPC-treated water and 500 µl of phenol/chloroform/isoamyl alcohol (25:24:1) was added. Tubes were vortexed, and phases separated by centrifugation (10 min at 10000 x g). 500 µl of the upper, anorganic phase was transferred to a new tube, 500 µl chloroform was added, tubes vortexed and centrifuged again as above. 400 µl of the upper, anorganic phase was transferred to a new tube, 40 µl of sodium acetate (3 M, pH 5.2) and 880 µl 100% ethanol were added and tubes left at -20 °C for 30 minutes to let DNA precipitate. DNA was then pelleted by centrifugation (20 minutes at 4 °C at maximum speed = 20000 x g). The ethanol was decanted and the pellet washed with 95% ethanol. This was also decanted, the pellet air-dried for three to five minutes and then resuspended in 20 µl DMPC-treated water and stored at -20 °C.

The antisense probe was then generated by run-off transcription with SP6 RNA-polymerase on the EcoRI-linearized plasmid and the sense probe by transcription with T7 RNA-polymerase on the BamHI/HindIII-linearized plasmid. 20 µl of the linearized

plasmid was mixed with 3 µl of 10x transcription buffer, 3 µl DIG-labelling mix, 3 µl RNA polymerase and 1 µl RNase-inhibitor (all reagents from Roche). The DIG labelling mix contains ATP, CTP, GTP, UTP and DIG-labelled UTP so that every 20-25 th nucleotide of the final probe is DIG-labelled. The reaction was run for two hours at 37 °C and then stopped by adding 3 µl of 0.2 M EDTA. RNA was purified by precipitation with 3.3 µl 4 M lithium chloride and 72 µl 100% ethanol (chilled to -20°C) for 30 minutes at -20 °C. RNA was pelleted by centrifugation at 20.000 x g at 4 °C for 20 minutes (this should give a clearly visible pellet). The ethanol was decanted, the pellet washed with 95% ethanol, the ethanol decanted, the pellet quickly air-dried and resuspended in 50 µl nuclease free water from the DNA-free kit (Ambion) used for the next step.

As the DNA:RNA content is roughly 1:10 after run-off transcription and DNA might give background staining during the *in-situ* hybridization, probes was Dnase treated using the DNA-free kit from Ambion according to manufacturer's instructions. 1 µl of RNase inhibitor was added to the final probe, RNA concentration and purity measured at a nanodrop (usually between 100 – 1000 ng/µl), the proper size checked on an agarose gel and 5-10 µl aliquots of the probes stored at -80°C. Probes were usually first tested at 400 ng/ml and concentration only changed if necessary.

2.8.4 *In-situ* hybridization

The *in-situ* hybridization protocol used here was developed and tested by me from standard protocols. For simple *in-situ* hybridization (*Penk*, *Avp* and *Crh*) brains were used fresh-frozen, not prefixed. For this, mice were sacrificed with CO_2 or per decapitation. Brains were quickly removed, snap frozen for 25 seconds in isopentane on dry ice, wrapped in aluminium foil and stored in falcon tubes at -80 °C. For sectioning, brains were embedded in OCT in the cryostat and sectioned to 8-10 µm on superfrost plus slides. Sections were allowed to dry for 30 seconds at RT, apart from this slides were stored in the cryostat and then at -80 °C. For in-situ hybridization plus immunostaining brains were prefixed by perfusion as described in chapter 2.7.3 and postfixed for one to three

hours (longer postfixation requires very strong digestion of the tissue). Brains were processed as in 2.7.3 and sectioned as described above.

All buffers used up to the hybridization step were either DMPC-treated or prepared in DMPC-treated water. All steps were either performed on the slides placed on a support in a plastic container or in coplin glass jars.

Slides were removed from -80 °C and dried shortly. Sections from fresh-frozen brains were fixed for 15 minutes in 4% PFA/PBS, whereas sections from prefixed brains were washed twice in PBS for five minutes, digested with 10 µg/ml Proteinase K (Roche) in PBS for 6 min at 37 °C (slides were covered with parafilm for this step), washed again twice five minutes in PBS and refixed for ten minutes in 4% PFA/PBS. All sections were then washed twice with PBS for five minutes and equilibrated for 5 min in 0.1 M triethanolamine pH 8.0. Amine groups were acetylated to avoid background by incubation in 0.25% acetic anhydride in 0.1 M triethanolamine pH 8.0 for 10 min. Sections were washed twice in PBS for five minutes and then prehybridized for two hours at 58 °C with hybridization buffer (see buffers, chapter 2.2). To avoid drying of the sections slides were covered with coverslips for prehybridization and hybridization and the plastic box containing the slides was humidified with 50% (vol/vol) formamide/5x SSC and closed. Probes were diluted to 400 ng/ml in hybridization buffer, incubated for 5 min at 80 °C and then chilled in ice-water. 150 µl of probes was applied per slide and hybridized at 58 °C for 24-40 hours.

Slides were checked for dried sections and transferred to a glass jar with 2x SSC to let coverslips come off. Coverslips were removed after roughly ten minutes and slides incubated for another 20 minutes at RT in 2x SSC. Sections were then washed twice for 30 minutes in 2x SSC at 65 °C, twice for 30 minutes in 0.1x SSC at 65 °C, transferred to warmed PBS (else the glass jar breaks) and gradually cooled down with PBS to RT and rinsed twice for five minutes with PBS. Sections were then blocked in 10% normal sheep serum and 0.1% Tween-20 in TBS, pH 7.5 for one hour at RT. An alkaline phosphatase-conjugated anti-DIG antibody (Roche) diluted 1:1000 in blocking solution was applied,

slides covered with parafilm and incubated over night at 4°C in a box humidified with water. Sections were then washed three times 20 minutes in TBS plus 0.1% Tween-20, equilibrated five minutes in NTMT buffer (see buffers, chapter 2.2) and five minutes in NTMT buffer with 5 mM levamisole to block endogenous alkaline phosphatases. For colour development the alkaline phosphatase substrate BCIP/NTB was used that produces a blue precipitate. Section were incubated with NTMT buffer containing 3.75 µl/ml BCIP, 5 µl/ml NBT, 0.1% Tween-20 and 5 mM levamisole for two hours to overnight in a humid chamber at RT until a signal was visible. The *Avp* and *Penk* signal develops rather quickly (several hours) whereas the signal for *Crh* and *TrkB* can take one day to develop and might require several changes of developing buffer. Colour development was stopped by washing slides in PBS containing 1 mM EDTA for ten minutes. The staining was cleared in 95% ethanol for several hours, precipitates were then removed by washing 15 minutes in PBS and finally slides were mounted with Vectashield. An aqueous mounting medium was used here as the NBT/BCIP precipitate can crystallize in xylene-based mounting media and is then not visible any more.

For immunofluorescence double-labelling the primary anti-GFP antibody was added 1:500 to the anti-DIG antibody solution. Afterwards sections were washed three times for ten minutes in PBS with 0.1% Tween, the Alexa488-conjugated secondary antibody was added diluted 1:1000 in PBS and incubated for two hours at RT. Sections were then washed and processed for colour development as described above. This protocol worked well for both anti-GFP antibodies (see 2.7.6), for other antibodies the staining might have to be performed separately after the colour development. In this case, depending on the antibody, the ethanol step might have to be omitted.

The same microscope used for analysis of the adrenals (see chapter 2.7.2) was used here. Staining density and integrated density was measured with ImageJ (Abramoff et al., 2004; Rasband, 2011). For this, a threshold in the YUV colour space identifying the BCIP/NBT signal was defined with the 'Threshold Color' plugin as described by Swanson and colleagues (Swanson et al., 2006). The measurement tool was then used to restrict

analysis to areas bigger than 25 μm^2 and to measure stained area and staining density. For analysis of *Avp*, *Crh* and *Penk* three sections through the PVN spaced 80 μm were analyzed per mouse.

2.9 Behavioural Studies

2.9.1 Measurement of food intake

Food intake was measured in LabMaster metabolic cages from TSE Systems (Bad Homburg, Germany) that are equipped with sensors that measure food and water intake in ten second intervals. Mice were transferred to the cages at 2-3 months of age and were then housed separately. Food and water was provided *ad libitum*. Food intake was first measured on a normal diet for three weeks and then changed to a high fat diet for three weeks. Food intake was measured for so long to take short- and longterm changes in food intake into account. At the EMBL in Monterotondo, the normal diet was the '2018 Teklad Rodent Diet' (60% calories from carbohydrates, 23% from protein and 17% from fat, 3.3 Kcal/g digestible energy) and at the Centre for Neurodegeneration in Edinburgh the 'Rat and Mouse No.3 Breeding' diet from Special Diets Services (61.2% calories from carbohydrates, 27.3% from protein and 11.5% from fat, 2.9 Kcal/g digestible energy). As high-fat diet the Harlan Teklad diet TD.06414 was used with 34% total fat content and 21.3% calories from carbohydrates, 18.4% from protein and 60.3% from fat with 5.1 kcal/g energy. Two experiments with each three controls and three mutant mice were performed, one of them with males, in Monterotondo, the other one with females in Edinburgh.

2.9.2 Analysis of immobilization stress-induced changes in HPA-axis activity

In order to measure HPA axis activity in response to immobilization stress, animals were placed in restrainers (4x12 cm tubes) for 20 minutes. Animals were then killed immediately with CO_2 and blood and brains collected as described in chapters 2.6.2 and 2.7.3.

2.9.3 Analysis of locomotion, anxiety and exploratory behaviour

These behaviour tests were performed with one batch of male animals that were housed together as single housing might change behaviour. The tests were performed in the order they are listed here. The testing equipment (all from TSE, Bad Homburg, Germany) was set up by Mumna Al Banchaabouchi and Dominika Farley from the EMBL-Monterotondo Phenotyping Core Facility and tests were performed and analyzed by me.
Mice were transferred to the behaviour facility one week before starting the tests and habituated to the respective test room one hour before each test. Mice were marked with felt tips with differently coloured rings around the tail to avoid stress through checking the eartag. All test equipment was sprayed and wiped with water followed by ethanol between each mouse.

Dark-Light Box

The Dark-Light Box paradigm is used to test anxiety and exploratory behaviour. The same arena as for the open field is used, but half of it is covered by a black box that has only a small hole in the middle to allow the mouse to enter. The mouse is placed in the open part (light box) and then tracked for 30 minutes by an automatic videotracking program (TSE VideoMot2) through a camera placed over the box. As the mouse can only be tracked in the light box the time it is not traceable is calculated as the time it spends in the dark box. The more often a mouse enters the light box and the more time it spends there the less anxious and more exploratory it is considered.

Elevated Plus Maze

The Elevated Plus Maze tests anxiety and consists of four elevated arms that build a cross and two of which have opaque walls (closed arms) whereas the two others do not (open arms). The more time an animal spends in the open arms the less anxious it is considered. The animals were placed in the centre of the cross and videotraced (same programme as above) for five minutes. The program automatically calculates the time spent in open and closed arms and in the centre.

Open Field

The Open Field tests anxiety, locomotion and exploratory behaviour. Here, the test was also repeated with each animal on four consecutive days to test for habituation to a novel and stressful environment. The animals were placed separately in the middle of an open arena (50x50x22 cm) illuminated evenly with 150-200 Lux and are tracked for 30 minutes (program as described above). Rearing is measured by light-beam frames placed around the arena. Time spent in the border and centre, number of visits to the centre, distance travelled and rearings are automatically calculated.

Inframot

The Inframot tests for activity of animals in a home cage by sensing the body displacement via infrared radiation (body heat). Animals were separately placed into inframot cages containing bedding and food and water *ad libitum*. Activity was recorded by the IRMOT programme for four days and nights without prior habituation.

2.10 Statistical analysis

All experiments and analysis were carried out blind to the genotype and with at least three animals per genotype unless stated otherwise. All results are indicated as mean ± standard error of the mean unless stated otherwise. Significance between samples was assessed by Student's t-test and one or two-way ANOVA and Fisher's PLSD post-hoc test. Differences were considered significant when $p<0.05$.

3 RESULTS

3.1 Characterization of the *BAC-CCK-Cre* mouse line

The *BAC-CCK-Cre* mouse line was generated and first analyzed by another PhD student in the Minichiello lab, Sylvia Badurek. As the construct for this line contains a *beta-galactosidase* gene, she analyzed expression of the line by staining for beta-galactosidase (data not shown here). Moreover, she also analyzed recombination by crossing the *BAC-CCK-Cre* line with two different reporter lines, the *Z/AP* and *Z/EG* reporter lines (Lobe et al., 1999; Novak et al., 2000) that express alkaline-phosphatase or EGFP upon Cre-mediated recombination. However, these lines were found to have a low recombination efficiency and show an incomplete recombination pattern (data not shown here), therefore we repeated this analysis using a Rosa26R-EYFP reporter line .

3.1.1 Recombination pattern of the BAC-CCK-Cre line

The recombination pattern of the *BAC-CCK-Cre* line was characterized by crossing the line to a R26R reporter line that expresses EYFP under the Rosa 26-promoter after Cre-mediated removal of a stop cassette (*R26R-EYFP*). The EYFP signal was detected by diamino benzidine (DAB) immunostaining or fluorescent immunostaining with an anti-GFP antibody that also binds EYFP. The endogenous fluorescent signal of EYFP is detectable by confocal microscopy but rather low as the Rosa 26-promotor is not very strong, therefore fluorescent immunostaining was used to amplify the signal.

In adult *BAC-CCK-Cre:R26R-EYFP* mice recombined cells were found in the cortex, hippocampus, olfactory bulb, striatum, thalamus, inferior and superior colliculus, amygdala, hypothalamus, midbrain, brainstem and cerebellum (Figure 3.1). In the cortex, many recombined cells were found in the more caudal parts as the subiculum, the visual and somatosensory cortex and less in the frontal/somatomotor and prefrontal cortex with exception of the orbital cortex that also showed a high number of recombined cells (Figure 3.1 A). Recombined cells were mainly found in layers V and VI but also in layers II-IV. Notably, some of the recombined cells in layer V and VI had the appearance of pyramidal neurons with clearly visible apical dendrites (Figure 3.1 B). In the hippocampus

scattered recombined cells were found in the dentate gyrus and CA3, and numerous recombined cells with the appearance of pyramidal neurons were found in the CA1 (Figure 3.1 B). The nature of these cells was further characterized by colocalization studies (see below and Figure 3.5). Numerous recombined cells were found in the thalamus, the caudal basal forebrain in the bed nucleus of the stria terminalis, and in most of the hypothalamic nuclei, including the medial preoptic area, the anterior hypothalamic nucleus, the paraventricular nucleus and the ventromedial and dorsomedial nucleus (Figure 3.1 B page 2). In the midbrain recombined cells were found in the ventral tegmental area, the inferior and superior colliculus and the periaqueductal gray (Figure 3.1 A, B page 2). The cerebellum showed strong recombination in all cell types and also the brainstem showed widespread recombination, especially in the dorsal vagal complex (Figure 3.1 A, B page 2). The striatum was generally devoid of recombined cells with exception of a small number of cells in the rostral striatum (Figure 3.1 B page 2). In the olfactory bulb a cluster of recombined neurons was found in the accessory olfactory bulb but only few scattered cells were found in the olfactory bulb in the glomerular layer (Figure 3.1 B page 2). Also in the amygdala only few recombined cells were found (Figure 3.1 A coronal section).

In order to verify recombination at earlier stages and during development, recombination in the *BAC-CCK-Cre:R26R-EYFP* line was analyzed by DAB and immunofluorescence staining of sections from P7 brains and E12.5 embryos (Figure 3.2).

At P7 recombination was found in the same regions as in the adult and especially already in the thalamus and hypothalamus. There seemed to be less recombined neurons in cortical regions and the hippocampus than in adult mice (Figure 3.2 A). At E12.5 recombination was seen in the spinal cord, the heart and in single scattered cells in the periphery (data not shown). In the brain, recombined cells were found in the future midbrain, especially the future colliculus, in the hindbrain (future brainstem) and scattered cells in the future preoptic area and hypothalamus. No recombined cells were found in the future cortex (Figure 3.2 B).

As we are investigating HPA axis activity in the *Trkb-CCK-KO* line and changes in adrenal and pituitary function would influence corticosterone and adrenocorticotropic hormone (ACTH) levels recombination was analyzed in these tissues by DAB immunostaining for EYFP (Figure 3.3). Stained sections from mice that do not have the *Cre-recombinase* transgene but the *R26R-EYFP* allele are shown as control. Pituitaries were almost devoid of recombined cells and only few scattered recombined cells were found in the anterior pituitary from where ACTH and other hormones are secreted and posterior pituitary from where oxytocin and vasopressin are secreted. Numerous recombined cells were found in the adrenal medulla that synthesizes catecholamines whereas the three zones of the adrenal cortex (zona glomerulosa, synthesizes mineralocorticoids, zona fasciculata, synthesis glucocorticoids and zona reticularis, synthesizes androgens) showed generally no recombination except in a few single cells.

Sylvia Badurek had analyzed recombination in heart, lung, spleen and kidney of BAC-CCK-Cre:Z/EG mice and found recombination in the heart and single cells in the spleen but no recombination in lung and kidney (data not shown here).

3.1.2 Cell type-specificity of recombination

We next verified that Cre-mediated recombination in the *BAC-CCK-Cre* line was restricted to CCK-expressing cells. Brain sections of *BAC-CCK-Cre:R26R-EYFP* were double- stained for EYFP and CCK by immunofluorescence staining and confocal images were taken. As the CCK antibody gives a rather weak and punctate staining with high background, specificity was tested by preincubating the antibody with CCK-8 peptide. This abolished staining confirming that the antibody used specifically binds to CCK (not shown). Images from different brain regions show that cells expressing EYFP usually also express CCK (Figure 3.4) confirming that recombination is restricted to CCK-positive cells. In most areas the majority of CCK-positive cells also expresses EYFP, only in the cortex a bigger fraction of CCK cells was not targeted. CCK-EYFP colocalization was quantified in the hypothalamus and will be discussed below (see also Figure 3.6).

CCK was described to be expressed in a subpopulation of GABAergic interneurons, however several publications also reported CCK expression in principal neurons (see Introduction, chapter 1.2.2). We therefore analyzed coexpression of EYFP and GABA by immunofluorescence staining and confocal imaging (Figure 3.5 A). In the CA1 EYFP positive neurons in the stratum pyramidale (the layer of dense EYFP-expressing neurons, arrows) do not express GABA whereas recombined neurons in other layers are also GABA-positive (arrowheads). In the CA3 recombined neurons generally also express GABA. In the cortex two different populations can be distinguished. The recombined neurons that have clear apical dendrites do not express GABA (arrows) whereas other EYFP-positive neurons do (arrowheads). In the prefrontal cortex all recombined neurons are GABAergic. Also in the hypothalamus the vast majority of recombined neurons is GABAergic (Figure 3.6). Colocalization of GABA and EYFP was quantified in the hypothalamus (see text below and Figure 3.6).

Further colocalization studies were performed to characterize the principal neuron-shaped recombined neurons in the hippocampus and cortex (Figure 3.5 B, D). In the cortex coexpression of EYFP with CTIP2, a marker for corticospinal motorneurons (that are principal neurons), was analyzed (Figure 3.5 B). Recombined neurons with stained apical dendrites colocalize with CTIP2 (arrows) whereas other recombined neurons do not express CTIP2 (arrowheads). The experiments for the hippocampus were performed by Sylvia Badurek. She analyzed coexpression of EGFP and CFP in the hippocampus of mice of the *BAC-CCK-Cre:Z/EG* line crossed to a line that expresses a CamKII-CFP fusion protein (C. Serguera and L. Minichiello, unpublished). As CamKII is specific to principal neurons, CFP highlights principal neurons, and EGFP indicates Cre-mediated recombination. The endogenous fluorescent signal was used in this case as anti-GFP antibodies would bind both EGFP and CFP. As can be seen in Figure 3.5 (D), the recombined neurons in the CA1 were also positive for CFP. Finally, colocalization of EYFP and parvalbumin was analyzed (Figure 3.5 C). Parvalbumin highlights a subpopulation of interneurons that do generally not overlap with CCK-expressing

interneurons. Confocal images of the CA1 and the cortex confirmed that, with a few exceptions, recombined neurons do generally not express parvalbumin.

As the phenotype described for the *Trkb-CCK-KO* line is dependent on hypothalamic neurons, colocalization of EYFP with GABA and CCK was analyzed and quantified in the peri-PVN region (Figure 3.6). Colocalization was quantified in sections from three mice in total, and in three sections per mouse. Colocalization with GABA showed that 41.1 ± 5.9 % (mean ± standard deviation, SD) of GABAergic neurons were recombined in the hypothalamus (left graph, red bar representing GABAergic neurons in comparison to yellow bar representing double-stained neurons). Of the recombined neurons, 86.1 ± 2.6 % (mean ± SD) were GABAergic (left graph, green bar representing recombined EYFP expressing neurons in comparison to yellow bar representing double-stained neurons). Colocalization with CCK showed that 80.2 ± 7.5 % (mean ± SD) of CCK-positive neurons expressed also EYFP and were thus successfully targeted (right graph, red bar representing CCK-positive neurons in comparison to yellow bar representing double-stained neurons). Of recombined neurons 96.9 ± 0.8 % (mean ± SD) were positive for CCK (right graph, green bar representing recombined EYFP expressing neurons in comparison to yellow bar representing double-stained neurons).

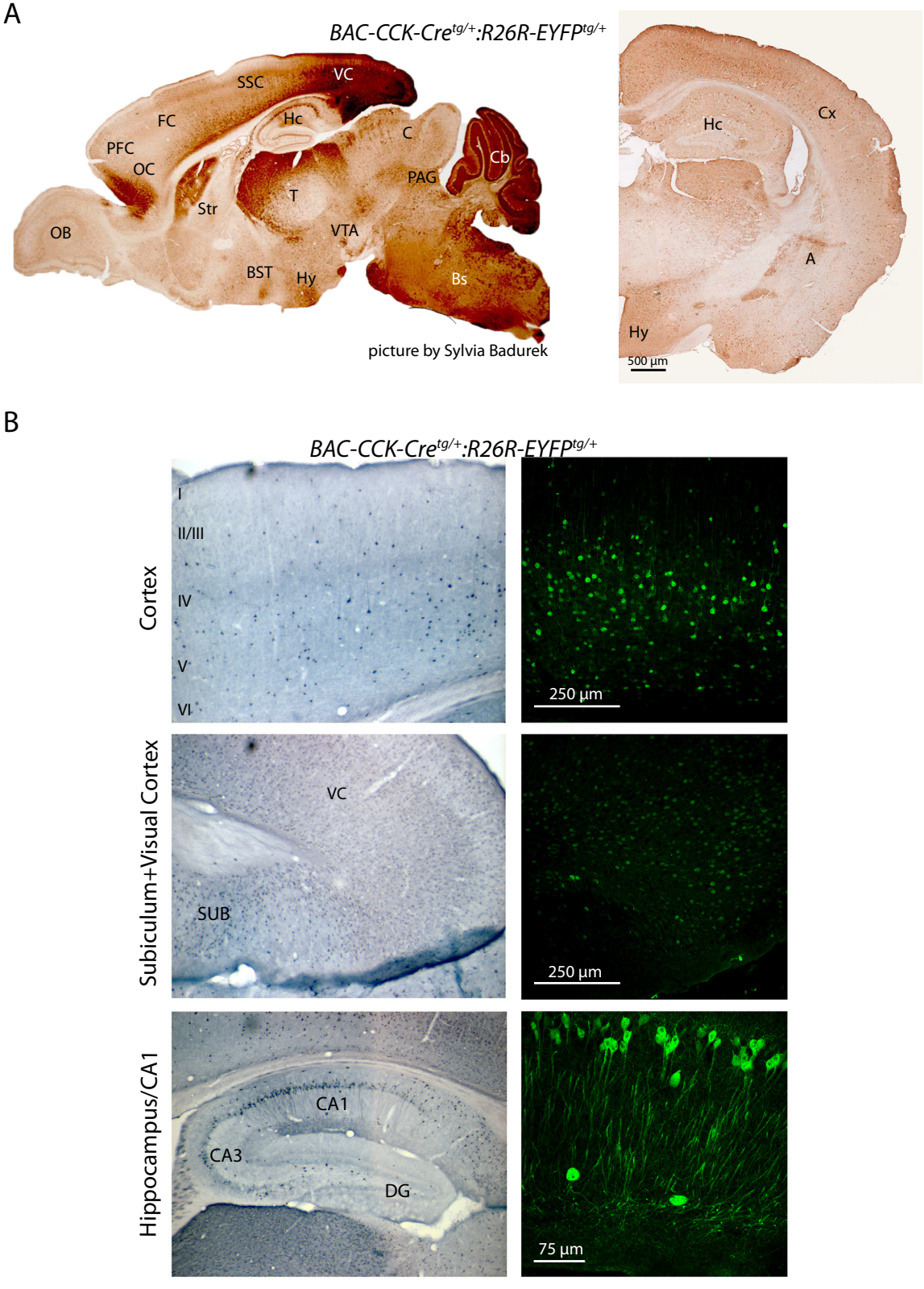

Figure 3.1 Recombination pattern of the *BAC-CCK-Cre:R26R-EYFP* line, brightfield and confocal images of DAB and fluorescent anti-G/YFP staining. A Sagittal and coronal overview (sagittal section stained and imaged by S. Badurek) B Recombination is detected in cortex, hippocampus, hypothalamus, midbrain/VTA, brainstem/NTS, striatum (only rostral, arrow), thalamus, colliculus, cerebellum and in the olfactory bulb. A amygdala; AHN anterior hypothalamic nucleus; AOB accessory olfactory bulb; Bs brainstem; BST bed nucleus of the stria terminalis; C colliculus; Cb cerebellum; DG dentate gyrus; DMH dorsomedial hypothalamic nucleus;

B

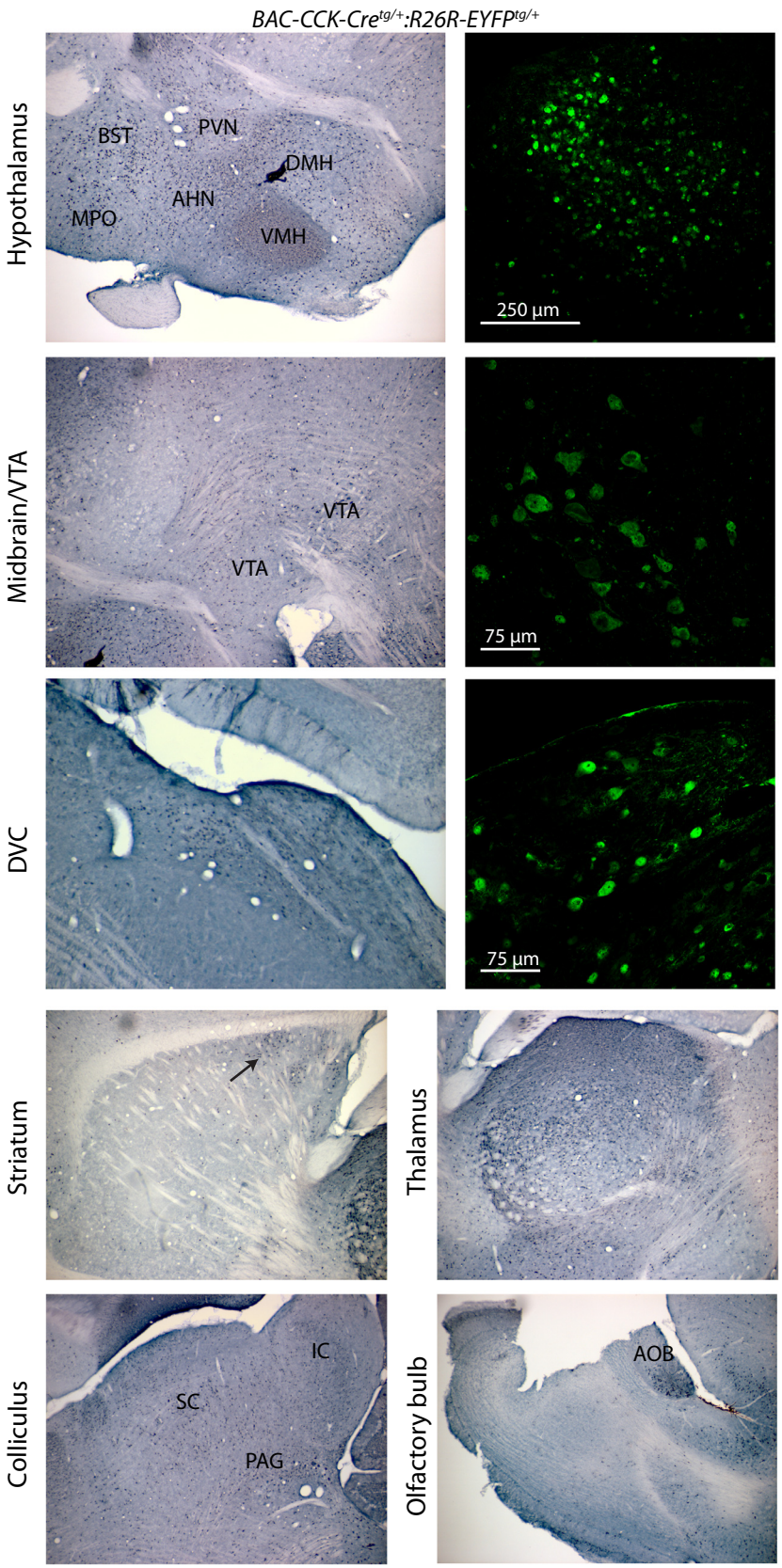

DVC dorsal vagal complex; FC frontal/somatomotor cortex; IC inferior colliculus; Hc hippocampus; Hy hypothalamus; MPO medial preoptic area; OB olfactory bulb; OC orbital cortex; PAG periaqueductal grey; PFC prefrontal cortex; PVN paraventricular nucleus of the hypothalamus; SC superior colliculus; SSC somatosensory cortex; SUB subiculum; VC visual cortex; VMH ventromedial hypothalamic nucleus; VTA ventral tegmental area

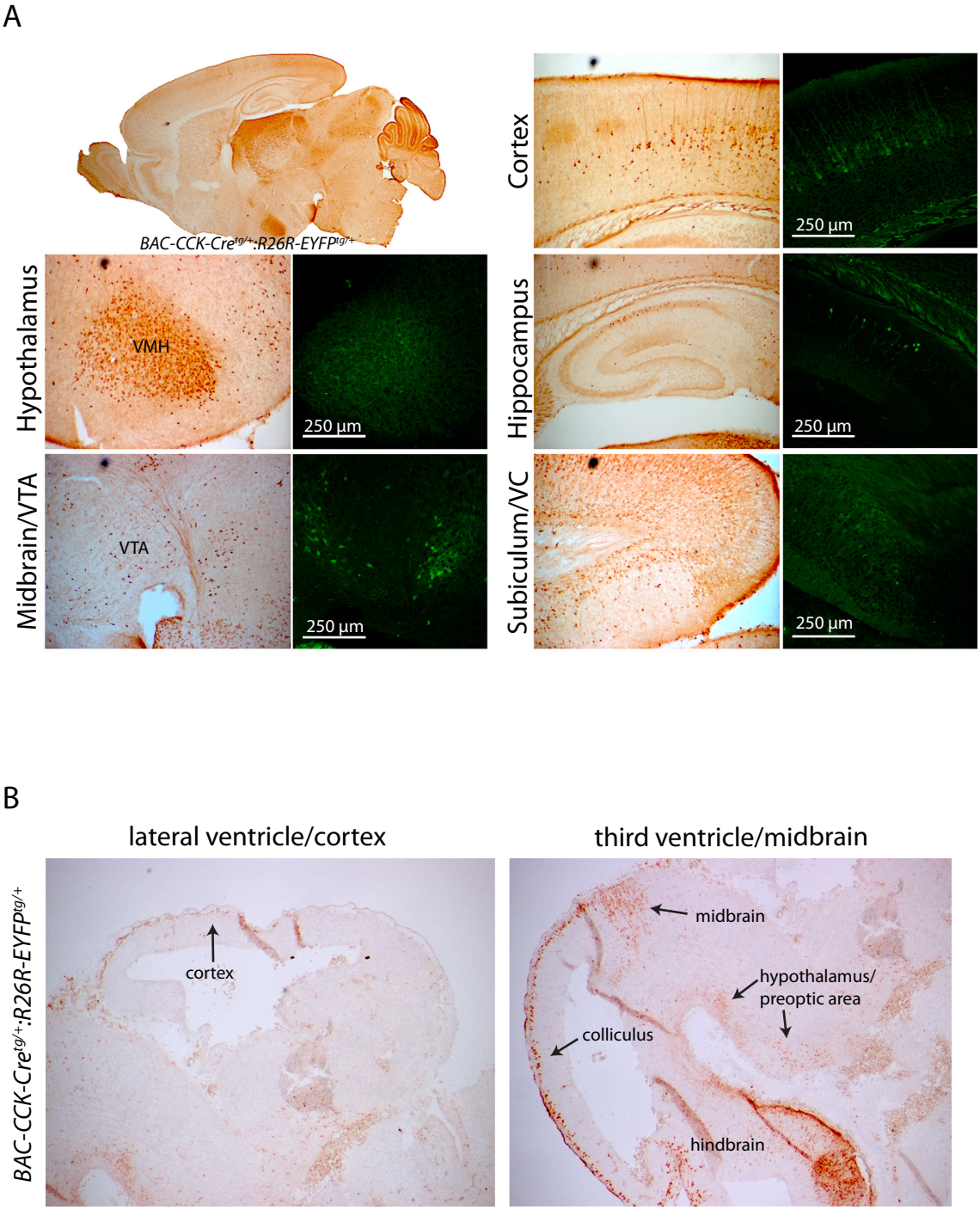

Figure 3.2 Recombination Pattern of the *BAC-CCK-Cre:R26R-EYFP* line at P7 (A) and E12.5 (B), DAB and fluorescent anti-G/YFP staining, brightfield and confocal images. A Recombination at postnatal day 7 is comparable to the adult and detectable in cortex, hippocampus, thalamus, hypothalamus, midbrain, olfactory bulb and cerebellum. B Recombination at E12.5 is restricted to hindbrain, hypothalamus, preoptic area, midbrain and colliculus. No recombined cells are visible in the future cortex. VC visual cortex; VMH ventromedial nucleus of the hypothalamus; VTA ventrat tegmental area

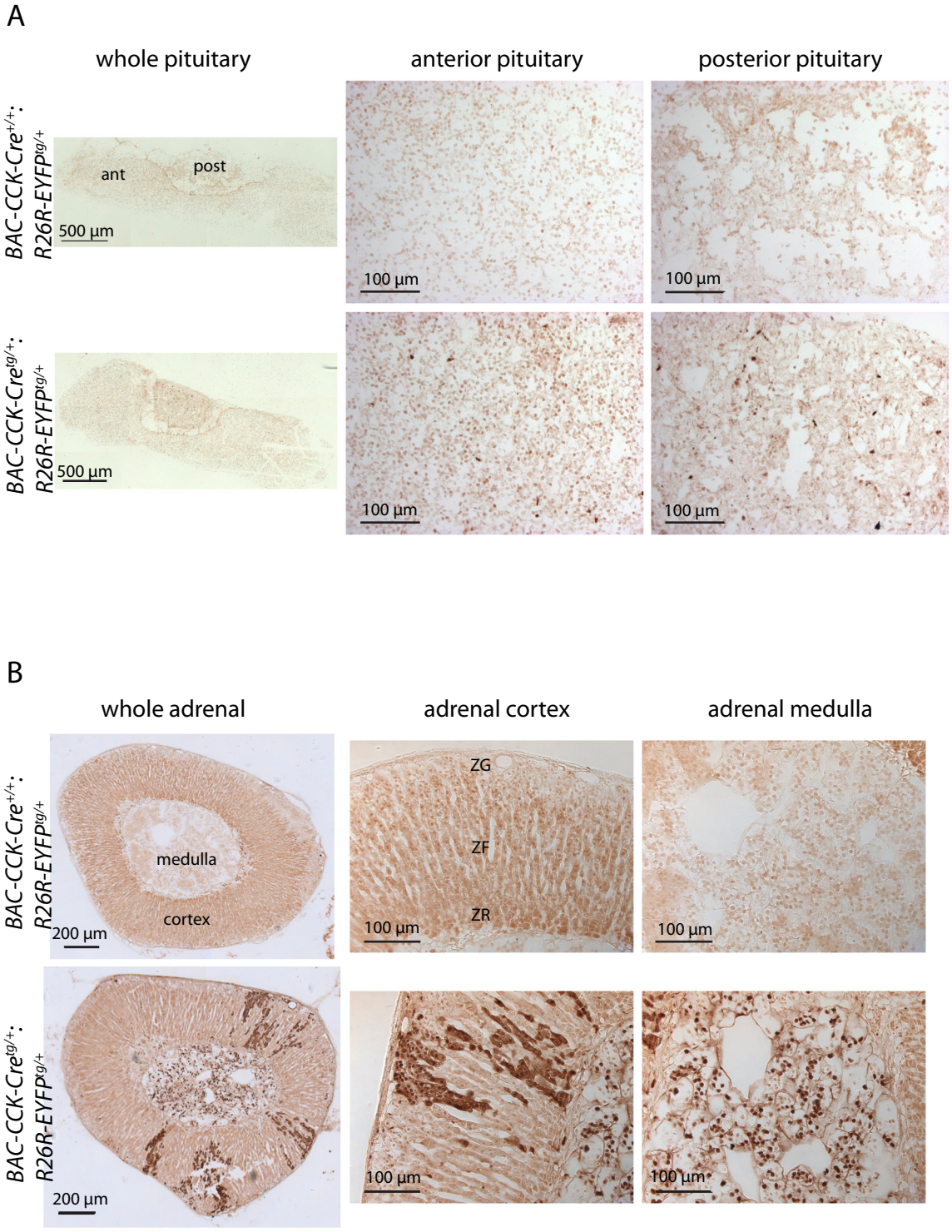

Figure 3.3 Recombination pattern of the *BAC-CCK-Cre:R26R-EYFP* line in pituitary (A) and adrenal (B), brightfield images of DAB anti-G/YFP staining. In each case the upper panels are control tissues from mice without the Cre-transgene. A Only few single cells are recombined in the anterior and posterior pituitary. B Chromaffine cells of the adrenal medulla show recombination. There is generally no recombination in the adrenal cortex apart from single cells in all three zones. ZF zona fasciculata, ZG zona glomerulosa, ZR zona reticularis

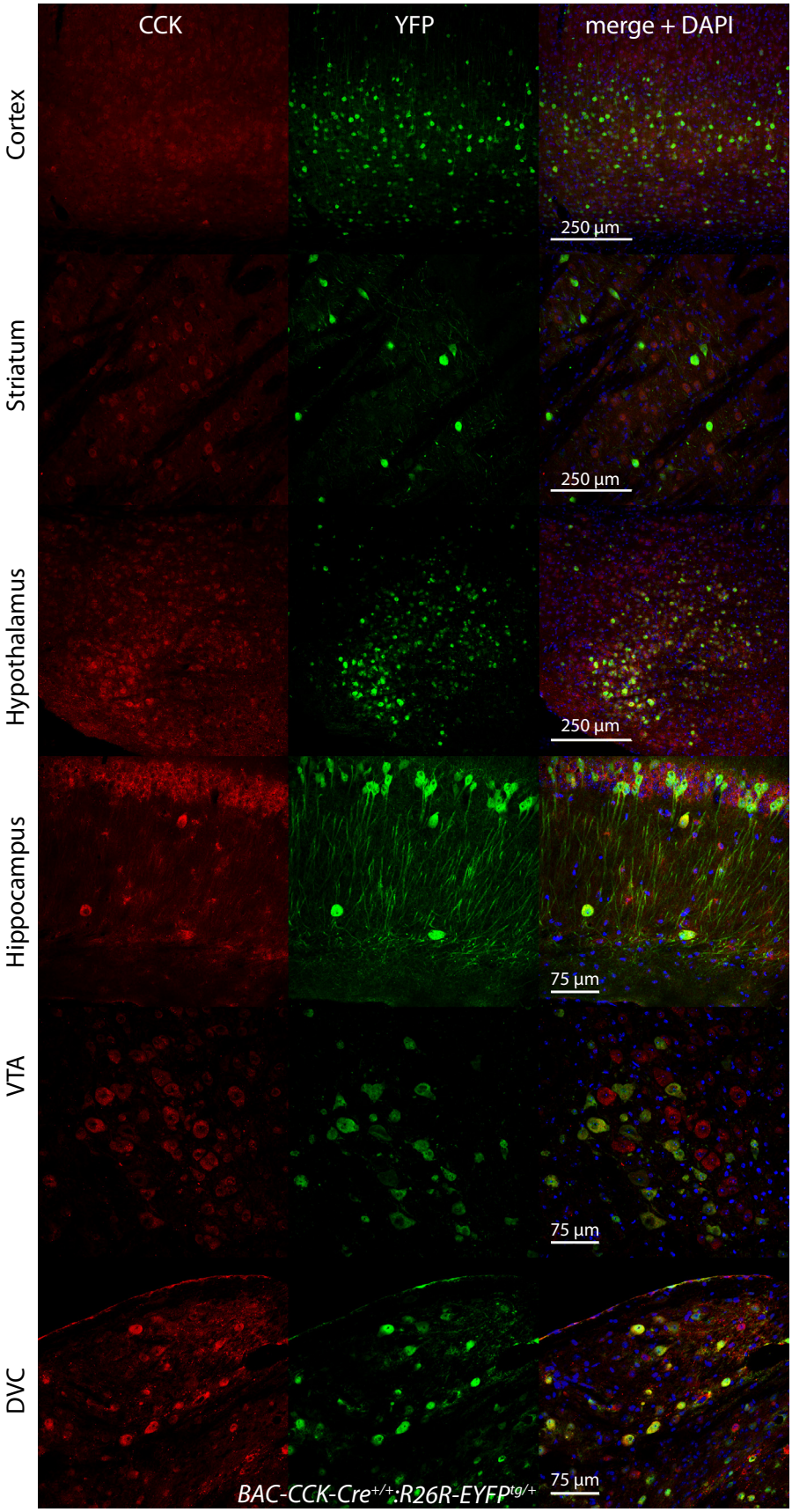

Figure 3.4 Colocalization of CCK and YFP in different brain regions in the *BAC-CCK-Cre:R26R-EYFP* line, confocal pictures of fluorescent anti-CCK and anti-G/YFP immunostaining. DVC dorsal vagal complex; VTA ventral tegmental area

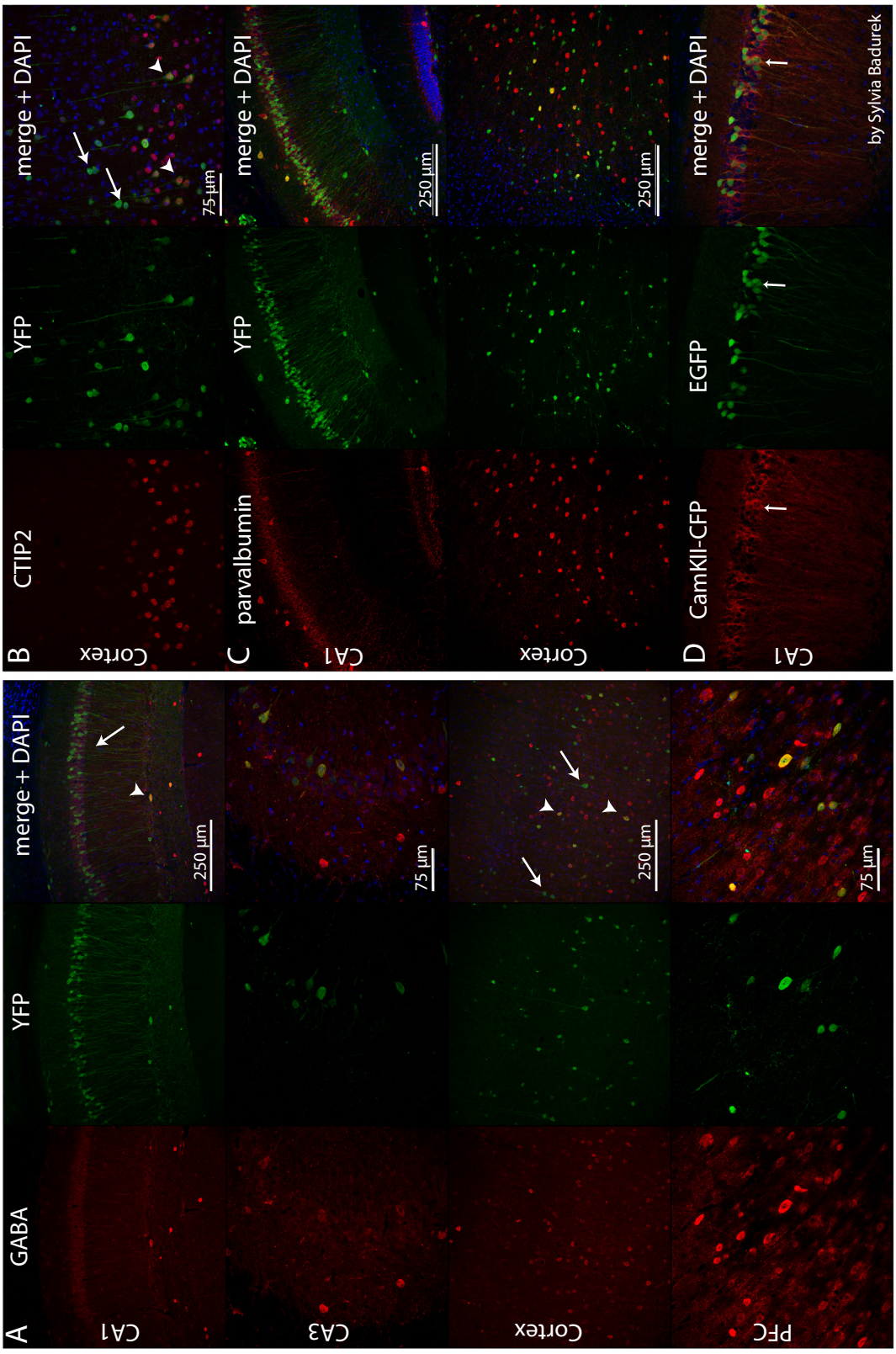

Figure 3.5 Colocalization of different neuronal markers with YFP in the *BAC-CCK-Cre:R26R-EYFP* line, fluorescent anti-G/YFP staining plus respective marker (A, B, C), or colocalization of endogenous EGFP and CFP in the BAC-CCK-Cre:Z/EG:CamKII-CFP line (D), confocal images. A Colocalization with the interneuron marker GABA (arrows: absence of colocalization, arrowheads: colocalization). B Colocalization with CTIP2, a marker for corticospinal motorneurons in principal neurons of the cortex (arrows: absence of colocalization, arrowheads: colocalization) C Colocalization with parvalbumin, a marker of another subtype of interneurons D Colocalization with a CamKII-CFP fusion protein that highlights principal neurons.

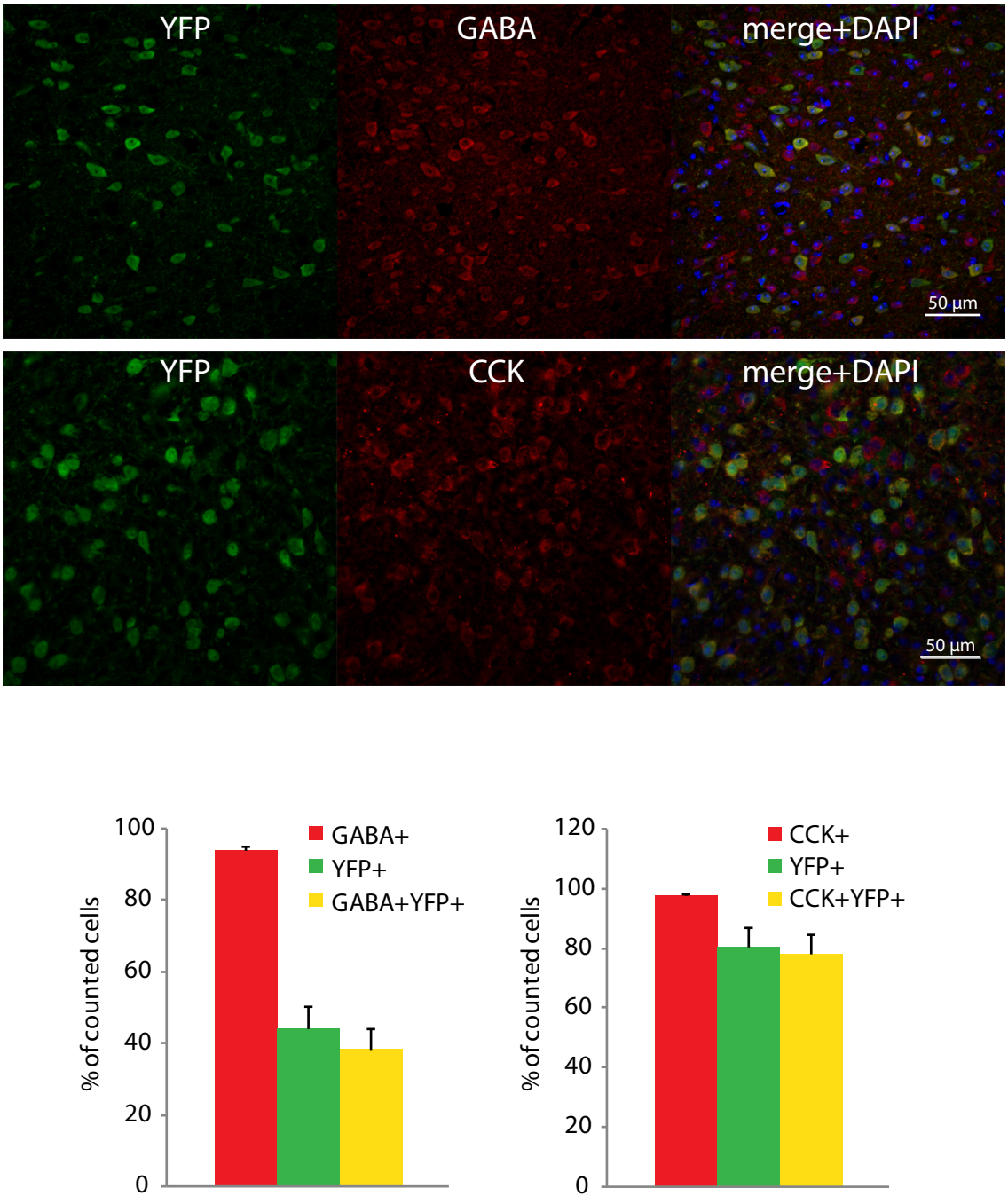

Figure 3.6 Analysis of CCK and GABA coexpression with the EYFP signal of recombined neurons in the rostromedial anterior hypothalamus (peri-PVN) in the *BAC-CCK-Cre:R26R-EYFP* line. Confocal pictures of fluorescent anti-GABA or anti-CCK plus anti-G/YFP staining. Colocalization was analyzed in sections of three mice and expressed as % of the counted cells. 41% of the GABAergic neurons in the hypothalamus show Cre- mediated recombination, and 86% of recombined neurons express GABA. Of the CCK-expressing neurons 80% show recombination and 97% of recombined neurons show clear expression of CCK.

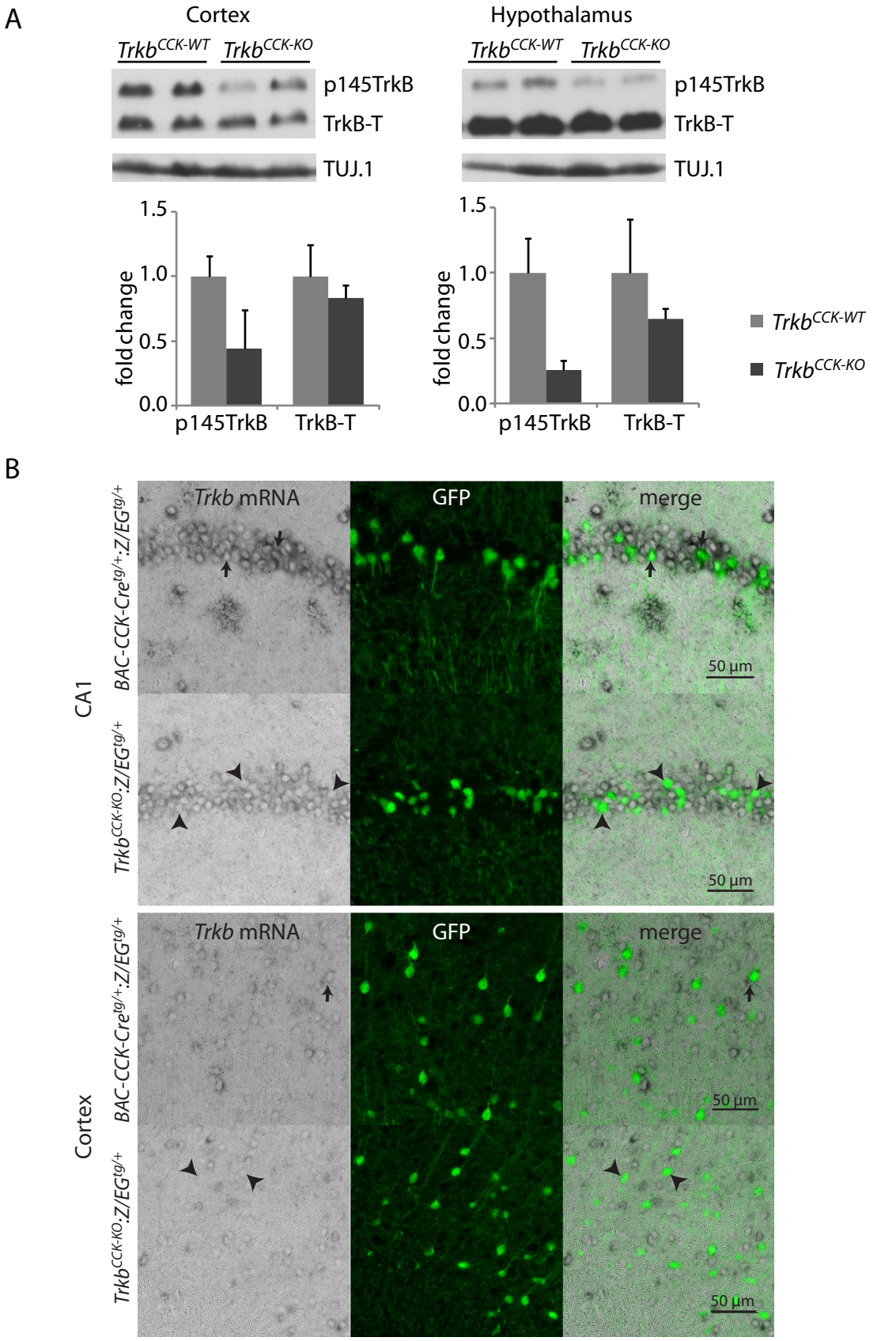

Figure 3.7 Cre-mediated removal of full-lenghthTrkB in the *Trkb-CCK-KO* line shown by immunoblot (A) and *in-situ* hybridization. A Immunoblot and quantification for full length (p145TrkB and truncated (TrkB-T) TrkB and TUJ.1 as loading control. See text for values. B *Trkb* mRNA *in-situ* hybridization and anti-GFP double labeling shows expression of *Trkb* in targeted neurons (arrows) in the *BAC-CCK-Cre:Z/EG* line and removal of *Trkb* in these cells in the *Trkb*$^{CCK\text{-}KO}$*:Z/EG* line (arrowheads).

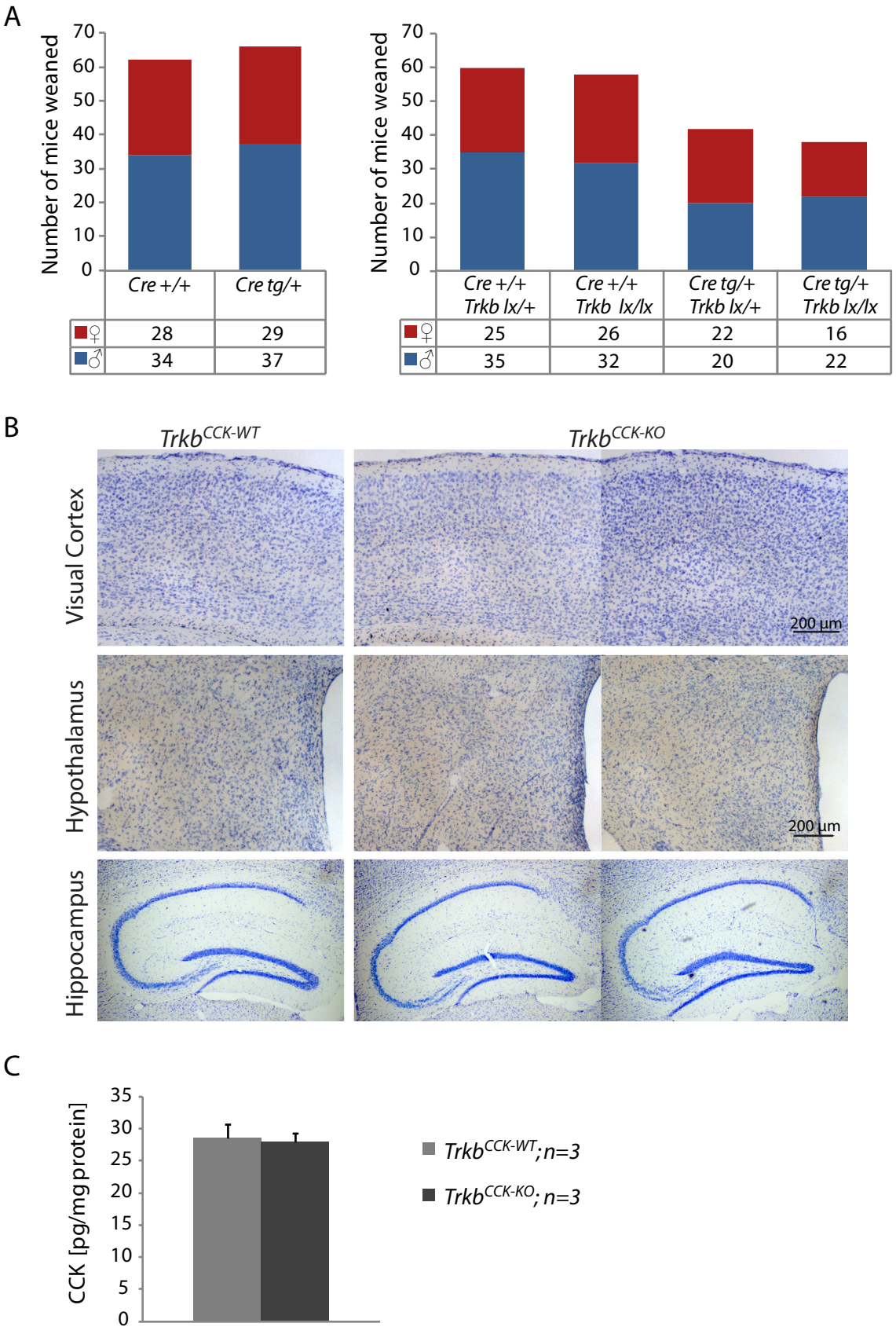

Figure 3.8 Analysis of *Trkb*$^{CCK\text{-}KO}$ mice. A Distribution of genotype and gender of mice from *BAC-CCK-Cre* and *Trkb-CCK-KO* breedings at weaning. B Cresyl violet staining demonstrates that *Trkb*$^{CCK\text{-}KO}$ mice do not show any general morphological changes in the brain. C Brain CCK-levels are unchanged in *Trkb*$^{CCK\text{-}KO}$ mice.

3.2 Generation of CCK neuron-specific *Trkb* knockout mice

To specifically ablate *Trkb* from CCK-expressing neurons, the *BAC-CCK-Cre* line was crossed to the *Trkb-floxed* line (line descriptions see Materials and Methods, chapter 2.3.1). The CCK-specific *Trkb* knockout mice resulting from these crosses (CCK-$Cre^{tg/+}$,$Trkb^{lx/lx}$) will be referred to as $Trkb^{CCK\text{-}KO}$ mice, the floxed controls (CCK-$Cre^{+/+}$,$Trkb^{lx/lx}$) as $Trkb^{CCK\text{-}WT}$ mice. In some cases *Trkb-floxed* mice were included in $Trkb^{CCK\text{-}WT}$ control groups, this is then stated in the figure legend. Also wildtype and transgenic mice from the *BAC-CCK-Cre* line were used as controls, referred to as *WT* and *Cre* mice. As *Cre* and $Trkb^{CCK\text{-}KO}$ mice originate from different breedings, *WT* mice were used as control for *Cre* and $Trkb^{CCK\text{-}WT}$ as controls for $Trkb^{CCK\text{-}KO}$ mice and data is represented in separate graphs.

3.2.1 Removal of *Trkb* by Cre-mediated recombination in $Trkb^{CCK\text{-}KO}$ mice

Successful removal of TrkB protein in knockout mice was verified by western blot on lysates of cortex and hypothalamus of adult $Trkb^{CCK\text{-}WT}$ and $Trkb^{CCK\text{-}KO}$ mice. Specific expression of *Trkb* mRNA in recombined cells was analyzed by double-staining for *Trkb* mRNA by *in-situ* hybridization and EGFP by immunofluorescence staining on brains of adult *BAC-CCK-*$Cre^{tg/+}$*:Z/EG-*$EGFP^{tg/+}$ mice and specific deletion in the presence of Trkb-floxed alleles was analyzed on brains of adult $Trkb^{CCK\text{-}KO}$*:Z/EG-*$EGFP^{tg/+}$ mice. We attempted to repeat this with the *R26R-EYFP* reporter line instead of the *Z/EG* reporter line, but failed so far to obtain mice of the $Trkb^{CCK\text{-}KO}$*: R26R-*$EYFP^{tg/+}$ genotype.

Western-blot for TrkB was performed on cortex and hypothalamic lysates of two mice per genotype and quantified with ImageJ (Figure 3.7 A). The antibody used binds the full-length (p145TrkB) and truncated (TrkB-T) isoforms of TrkB, thus giving a double band. Both bands were analyzed separately and normalized to TUJ.1 (neuron-specific class III β-tubulin) as loading control. In the cortex expression of full-length TrkB was slightly but not significantly reduced and expression of the truncated isoforms was unchanged (p145TrkB: $Trkb^{CCK\text{-}KO}$ 0.45±0.29 vs $Trkb^{CCK\text{-}WT}$ 1.00±0.16, p = 0.071; TrkB-T: $Trkb^{CCK\text{-}KO}$ 0.84±0.10 vs $Trkb^{CCK\text{-}WT}$ 1.00±0.24, p = 0.233; expressed as ratio of $Trkb^{CCK\text{-}WT}$,

values are mean ± SD). In the hypothalamus expression of full-length TrkB was reduced significantly to 25% and expression of the truncated isoforms was slightly but not significantly lower (p145TrkB: $Trkb^{CCK\text{-}KO}$ 0.25±0.08 vs $Trkb^{CCK\text{-}WT}$ 1.00±0.26, p = 0.031; TrkB-T: $Trkb^{CCK\text{-}KO}$ 0.65±0.08 vs $Trkb^{CCK\text{-}WT}$ 1.00±0.41, p = 0.176; expressed as ratio of $Trkb^{CCK\text{-}WT}$, values are mean ± SD). One should note that expression of the truncated forms is very high in the hypothalamus, therefore this blot was exposed for a shorter time than the blot with cortical lysates. If exposed for the same time, expression levels of the full-length form is comparable in cortex and hypothalamus.

Double staining for *Trkb* mRNA and EGFP in CA1 and cortex of *BAC-CCK-Cre*$^{tg/+}$*:Z/EG-EGFP*$^{tg/+}$ mice confirmed expression of *Trkb* in EGFP-positive cells on a wildtype background (Figure 3.7 B, arrows). On the knockout background (*Trkb*$^{CCK\text{-}KO}$*:Z/EG-EGFP*$^{tg/+}$) recombined EGFP expressing cells were clearly devoid of *Trkb* mRNA expression (Figure 3.7 B, arrowheads). Analysis of hypothalamic neurons was attempted but was impossible as very few neurons showed EGFP expression in the *BAC-CCK-Cre:Z/EG* line.

3.2.2 *Trkb*$^{CCK\text{-}KO}$ mice are viable and have normal brain morphology

Trkb$^{CCK\text{-}KO}$ mice are viable and show no increased mortality rate from weaning to seven months of age (the maximum age they were kept to so far). The distribution of gender and genotypes was analyzed at weaning in litters from *BAC-CCK-Cre* and *Trkb-CCK-KO* lines (Figure 3.8 A). For the *BAC-CCK-Cre* line 128 mice were analyzed in total and no differences were found between *WT* and *Cre* mice (Chi-Square test p = 0.723) or males and females (Chi-Square test p = 0.216) or gender and genotype considered together (Chi-Square test p = 0.194)(for numbers see figure). For the *Trkb-CCK-KO* line 198 mice were counted in total and no difference was found between males and females (Chi-Square test p = 0.155) or between genotypes (Chi-Square test p = 0.059). There was a deviation from the expected distribution when analyzing genotype and gender together (Chi-Square test p = 0.011) and, as visible in the graph, the number of heterozygous (*CCK-Cre*$^{tg/+}$*,Trkb*$^{lx/+}$) and *Trkb*$^{CCK\text{-}KO}$ mice found at weaning age was slightly lower than

the number of *CCK-Cre*$^{+/+}$,*Trkb*$^{lx/+}$ control mice, and the number of female mice was lower than the number of male mice. This is most probably a random effect that will disappear when more mice are counted.

General brain morphology was analyzed by Nissl staining (Cresyl-violet staining) (Figure 3.8 B). No differences were found between the visual cortex, hypothalamus and hippocampus of *Trkb*$^{CCK\text{-}WT}$ and *Trkb*$^{CCK\text{-}KO}$ mice.

We next planned to verify whether targeted neurons were present in normal numbers in *Trkb*$^{CCK\text{-}KO}$ mice. Absence of CCK-expressing neurons would lead to decreased CCK brain levels, as they are the only source of CCK in the brain. We therefore analyzed CCK levels in total brain lysates from *Trkb*$^{CCK\text{-}WT}$ and *Trkb*$^{CCK\text{-}KO}$ mice by ELISA (Figure 3.8 C). The CCK-concentration was normalized to the protein content in each lysate. No difference in CCK levels was found (*Trkb*$^{CCK\text{-}KO}$ 27.9 ± 1.47 pg/mg protein vs *Trkb*$^{CCK\text{-}WT}$ 28.6 ± 2.18 pg/mg protein, n=3 for both groups, p = 0.410).

3.3 Disruption of TrkB in CCK-positive neurons results in obesity

3.3.1 *Trkb*$^{CCK\text{-}KO}$ mice develop mature-onset obesity

Trkb$^{CCK\text{-}KO}$ mice develop clearly visible obesity from around four months of age on. To characterize weight gain in *Trkb*$^{CCK\text{-}KO}$ mice male *WT*, *Cre*, *Trkb*$^{CCK\text{-}WT}$ and *Trkb*$^{CCK\text{-}KO}$ mice were weighed regularly from 1.5 to 5 months of age (Figure 3.9 A and numbers in C). Male *WT* and *Cre* mice did not show any difference in body weight at any time point, but *Trkb*$^{CCK\text{-}KO}$ mice started to be significantly heavier than *Trkb*$^{CCK\text{-}WT}$ controls from four months of age on and were clearly heavier at five months of age. Female *WT*, *Cre*, and *Trkb*$^{CCK\text{-}KO}$ mice were only analyzed at five months of age and again *Trkb*$^{CCK\text{-}KO}$ mice were significantly heavier as controls (Figure 3.9 B, numbers in C).

Sagittal pictures of the recombination pattern in the *BAC-CCK-Cre:R26R-EYFP* line had shown widespread recombination in the hypothalamic nuclei involved in metabolic control. As these nuclei can be better identified in coronal sections, coronal sections from brains of *BAC-CCK-Cre:R26R-EYFP* mice were stained for EYFP and

analyzed for recombination. As shown later (Figure 3.13 E), the arcuate nucleus, that contains the major leptin-responsive neuronal populations (see Introduction, chapter 1.3.1) was devoid of recombined cells. However, the VMH, in which BDNF was shown to play a role downstream of melanocortin signalling (Introduction, chapter 1.3.2), showed numerous recombined neurons.

To verify that body weight gain was due to increased adiposity (accumulation of fat tissue) we next dissected and weighed the gonadal and mesenteric fat pads from mice of all four genotypes (Figure 3.10). Part of the fat pads were dissected and weighed by the research assistant Jacqui Horn. These are the two major visceral fat pads of the abdomen and lead to what is known as central obesity in humans. Weight of the fat pads was normalized to the body weight and is expressed as % of body weight. The gonadal fat pad was significantly enlarged by a factor of 2.2 in female $Trkb^{CCK\text{-}KO}$ mice in comparison with controls and enlarged, even if not significantly, by a factor of 1.3 in male $Trkb^{CCK\text{-}KO}$ mice (Figure 3.10 A, numbers in C). The mesenteric fat pad was significantly enlarged by a factor of 2.8 in female $Trkb^{CCK\text{-}KO}$ mice in comparison with controls and by a factor of 1.6 in male $Trkb^{CCK\text{-}KO}$ mice. No differences were observed between *WT* and *Cre* male or female mice.

3.3.2 Food intake on normal and high fat diet in $Trkb^{CCK\text{-}KO}$ mice

As other models of TrkB or BDNF deficiency show hyperphagia (overeating)-induced obesity we next analyzed food intake in $Trkb^{CCK\text{-}KO}$ and $Trkb^{CCK\text{-}WT}$ mice. Mice were kept separately in metabolic cages and had free access to food and water. The food containers were connected to sensors that measured weight of the container and thus removal of food every 10 seconds (see also Materials and Methods, chapter 2.9.1). Food intake was analyzed in one group of male mice (3 control and 3 knockout mice, 3 months old at the start of the experiment) that were kept on a normal diet for three weeks and then changed to a high-fat diet for three weeks, and in one group of female mice (3 control and 3 knockout mice, 2-3 months old at the start of the experiment) that were just kept on a normal diet for six weeks.

Food intake was analyzed during the active (dark) and resting (light) period for one week (Figure 3.11 A and B). No difference between *Trkb*$^{CCK\text{-}KO}$ and *Trkb*$^{CCK\text{-}WT}$ mice was found in the accumulated food intake during that week in either period or in total (Figure 3.11 A, includes numbers). Also when looking at single day and night intake, no difference was visible in food intake or diurnal rhythm (Figure 3.11 B). Next, the accumulated food intake over several weeks was analyzed to see if there was any long-term difference (Figure 3.11 C). After three weeks *Trkb*$^{CCK\text{-}KO}$ male mice had eaten the exact same amount in comparison to *Trkb*$^{CCK\text{-}WT}$ mice (*Trkb*$^{CCK\text{-}KO}$ 76.8 ± 2.2 g vs *Trkb*$^{CCK\text{-}WT}$ 77.0 ± 2.1 g, n=3 for each group, p = 0.478, mean ± SEM, for other numbers see figure 3.11 C) and also *Trkb*$^{CCK\text{-}KO}$ female mice did not eat significantly more that *Trkb*$^{CCK\text{-}WT}$ control mice after five weeks (*Trkb*$^{CCK\text{-}KO}$ 152.3 ± 8.9 g vs *Trkb*$^{CCK\text{-}WT}$ 142.4 ± 5.6 g, n=3 for each group, p = 0.200, mean ± SEM, for other numbers see figure 3.11 C). Figure 3.11 D shows the average daily food intake of female *Trkb*$^{CCK\text{-}KO}$ and *Trkb*$^{CCK\text{-}WT}$ mice in comparison to the weight that these mice gained in exactly that week. Despite eating the same amount of food (*Trkb*$^{CCK\text{-}KO}$ 4.0 ± 0.2 g vs *Trkb*$^{CCK\text{-}WT}$ 4.4 ± 0.2 g, n=3 for each group, p = 0.157, mean ± SEM), *Trkb*$^{CCK\text{-}KO}$ mice gained significantly more weight (*Trkb*$^{CCK\text{-}KO}$ 0.9 ± 0.1 g vs *Trkb*$^{CCK\text{-}WT}$ 0.6 ± 0.0 g, n=3 for each group, p = 0.003, mean ± SEM).

The only difference found in food intake was in females during the first two hours after they were transferred for the first time into metabolic cages. Whereas the control group reacted to this stressful new environment by not eating anything, *Trkb*$^{CCK\text{-}KO}$ female mice did eat significantly more during that period (Figure 3.11 E)(*Trkb*$^{CCK\text{-}KO}$ 0.30 ± 0.04 g vs *Trkb*$^{CCK\text{-}WT}$ 0.01 ± 0.01 g, n=3 for both groups, p = 0.0009). Three days later at the same time no difference was found (Figure 3.11 E) (*Trkb*$^{CCK\text{-}KO}$ 0.28 ± 0.09 g vs *Trkb*$^{CCK\text{-}WT}$ 0.37 ± 0.06 g, n=3 for both groups, p = 0.213). This behaviour was also seen after changing the bedding of cages, but was not found in male *Trkb*$^{CCK\text{-}KO}$ mice (not shown).

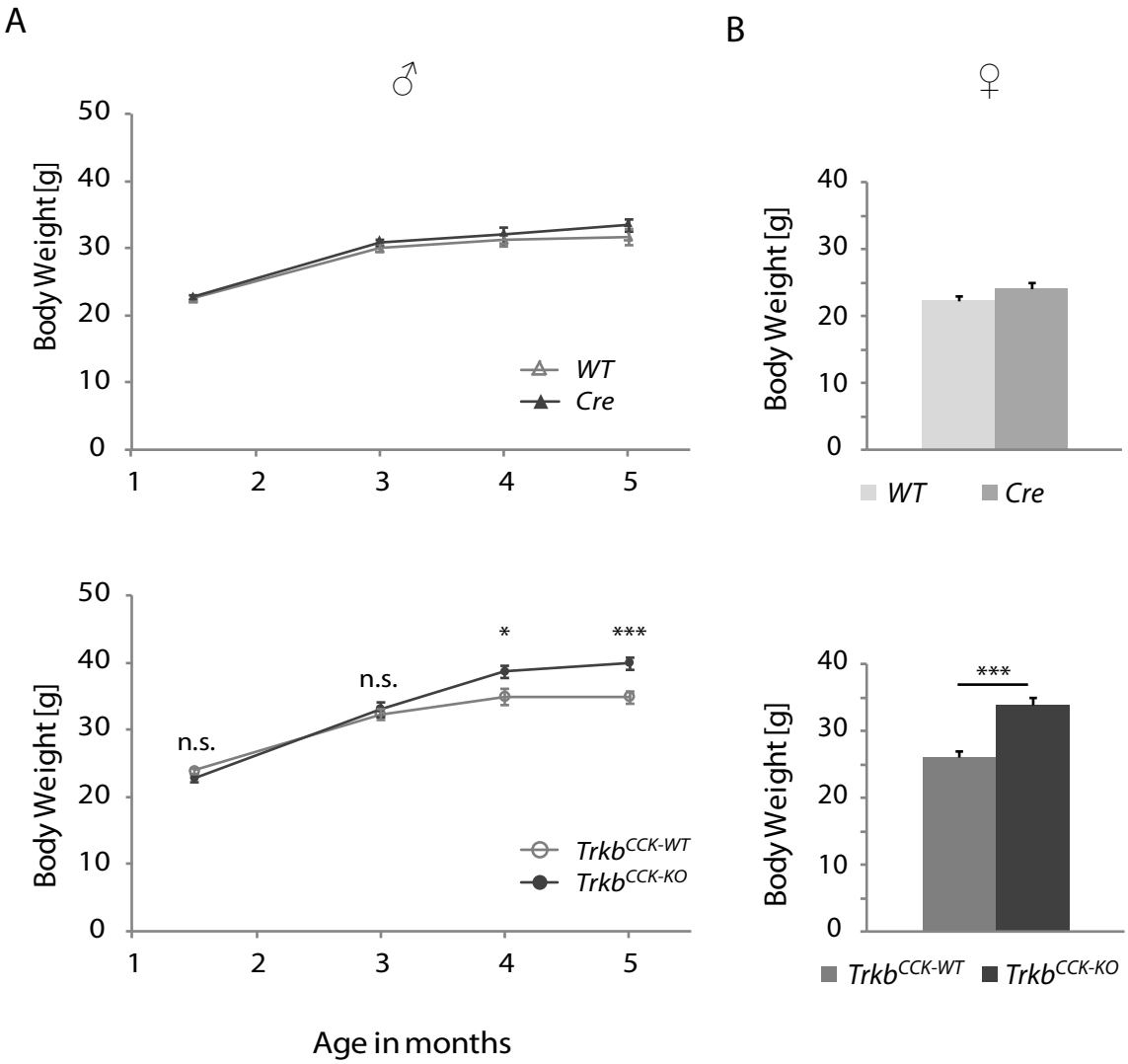

C

		Body Weight ± SEM [g] / number of animals								p (t-test)	
gender/age [months]		*WT*	n	*Cre*	n	*Trkb*$^{CCK-WT}$	n	*Trkb*$^{CCK-KO}$	n	*WT: Cre*	*Trkb*^{WT}:*Trkb*^{KO}
males	1.5	22.6 ± 0.4	9	22.9 ± 0.3	12	24.0 ± 0.4	6	22.9 ± 0.6	8	0.307	0.108
	3	30.1 ± 0.5	13	30.9 ± 0.5	20	32.3 ± 0.8	11	33.1 ± 1.1	16	0.133	0.296
	4	31.3 ± 0.9	12	32.0 ± 1.1	12	35.0 ± 1.3	9	38.7 ± 1.0	13	0.340	0.015
	5	31.8 ± 1.3	13	33.4 ± 0.9	12	35.0 ± 0.9	11	40.0 ± 0.9	17	0.148	0.0003
females	5	22.4 ± 0.6	4	24.2 ± 0.9	11	26.2 ± 0.8	24	34.0 ± 1.1	27	0.136	0.0000004

Figure 3.9 *TrkB*$^{CCK-KO}$ mice gain more weight than control mice. A Body weight of male *WT* and *Cre* control mice and *Trkb*$^{CCK-WT}$ control and *Trkb*$^{CCK-KO}$ mice from the age of six weeks to five months. B Body weight of female WT and Cre control mice and female *Trkb*$^{CCK-WT}$ control and *Trkb*$^{CCK-KO}$ mice at the age of five months. C Table showing body weight, number of animals weighed and significance levels for the data shown in A and B.

A

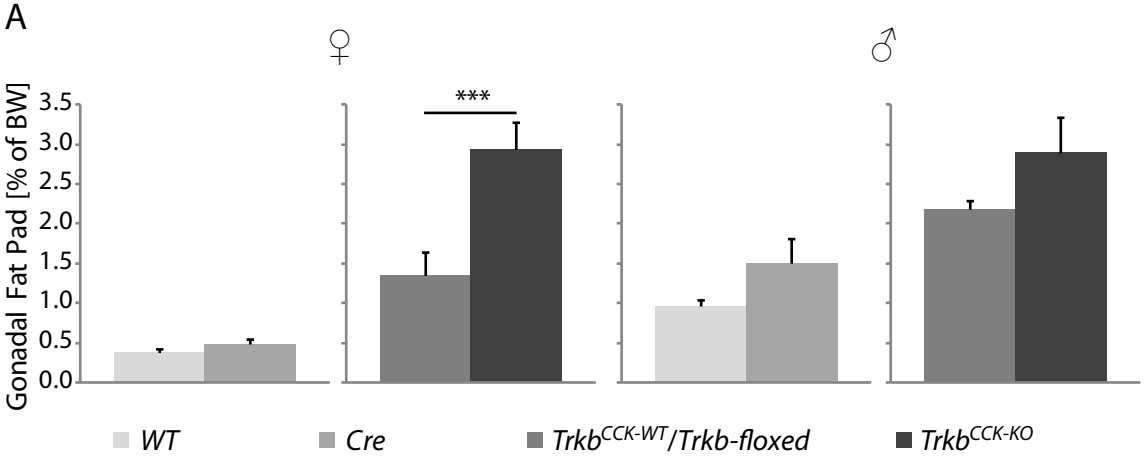

B

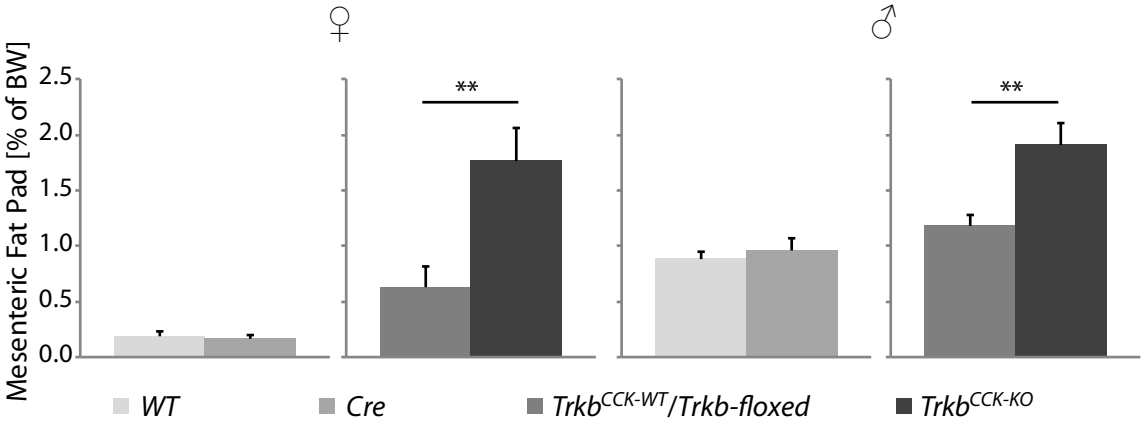

C

		Fat Pad ± SEM [% of BW] / number of animals				p (t-test)	
Fat Pad/Gender		*WT*	*Cre*	*Trkb*$^{CCK-WT/lx}$	*Trkb*$^{CCK-KO}$	*WT:Cre*	*Trkb*^{WT}:*Trkb*^{KO}
gonadal	females	0.37 ± 0.05	0.49 ± 0.06	1.35 ± 0.29	2.94 ± 0.33	0.098	0.001
	n	4	5	9	8		
	males	0.97 ± 0.07	1.51 ± 0.30	2.18 ± 0.11	2.89 ± 0.46	0.062	0.069
	n	5	5	5	4		
mesenteric	females	0.02 ± 0.04	0.17 ± 0.04	0.63 ± 0.19	1.77 ± 0.30	0.312	0.002
	n	4	5	11	10		
	males	0.89 ± 0.06	0.97 ± 0.10	1.19 ± 0.10	1.91 ± 0.20	0.298	0.002
	n	5	8	10	10		

Figure 3.10 Fat accumulation in visceral fat pads is increased in *Trkb*$^{CCK-KO}$ mice. A Weight of gonadal fat pads in percent of body weight in female and male *WT* and *Cre* control mice and *Trkb*$^{CCK-WT}$ and *Trkb-floxed* (3 females) control and *Trkb*$^{CCK-KO}$ mice. B Weight of mesenteric fat pads in percent of body weight in female and male *WT* and *Cre* control mice and *Trkb*$^{CCK-WT}$ and *Trkb-floxed* (3 females) control and *Trkb*$^{CCK-KO}$ mice. C Values with standard error of the mean, numbers and significance levels for data shown in A and B.

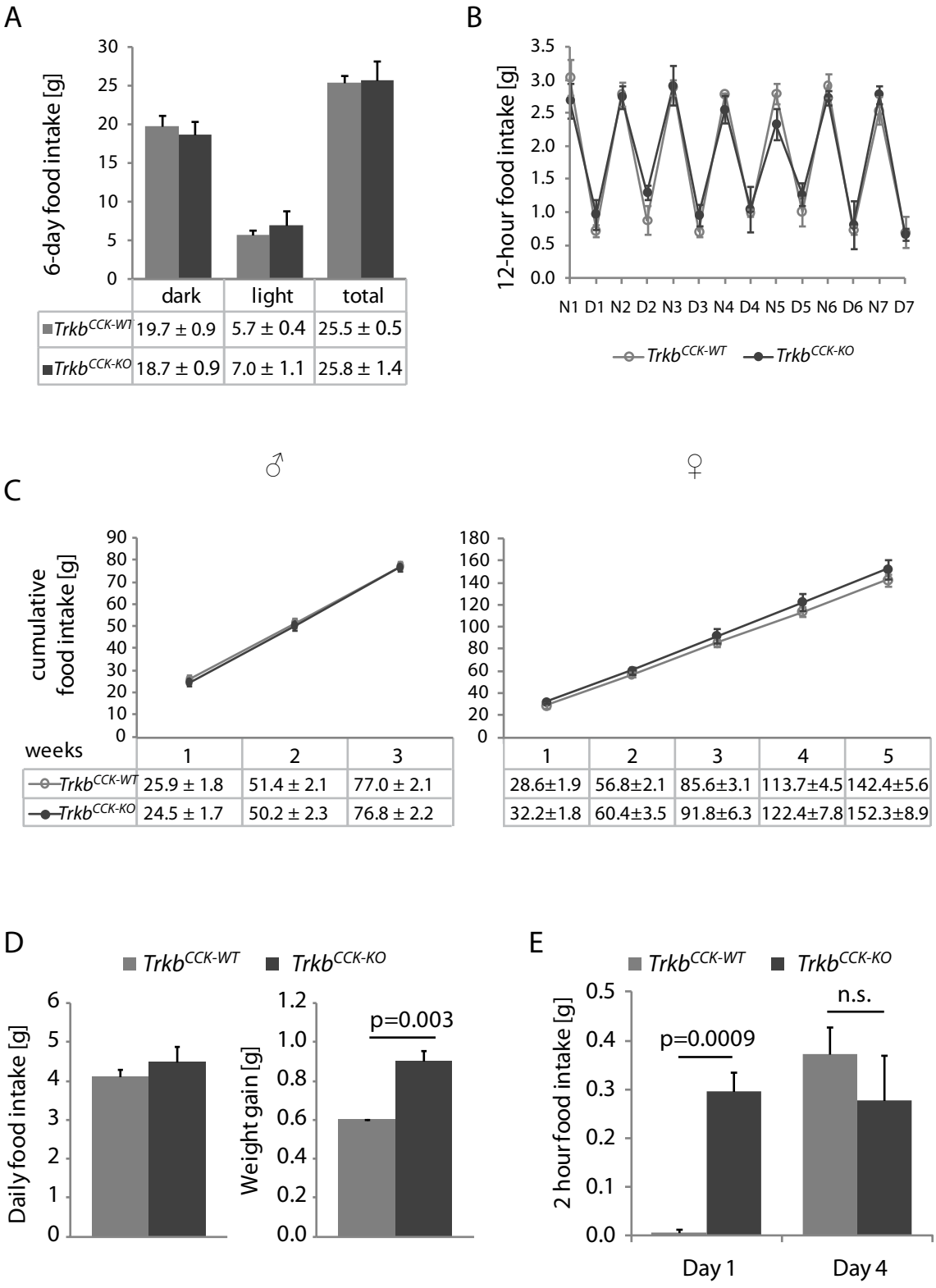

Figure 3.11 Food intake in control and *Trkb*$^{CCK\text{-}KO}$ mice (both groups n=3 in all experiments). A Food intake over 6 days in total and during the dark (active) and light (rest) period in male *Trkb*$^{CCK\text{-}KO}$ and *Trkb*$^{CCK\text{-}WT}$ mice B Pattern of food intake during one week in the dark period (N) and light period (D), same animals as A. C Cumulative food intake over three (males, left) and five (females, right) weeks. D Average daily food intake during one week and body weight gain in the same week in female *Trkb*$^{CCK\text{-}KO}$ and *Trkb*$^{CCK\text{-}WT}$ control mice. E Food intake in the first two hours after animals were transfered to metabolic cages and during two hours at the same time three days later.

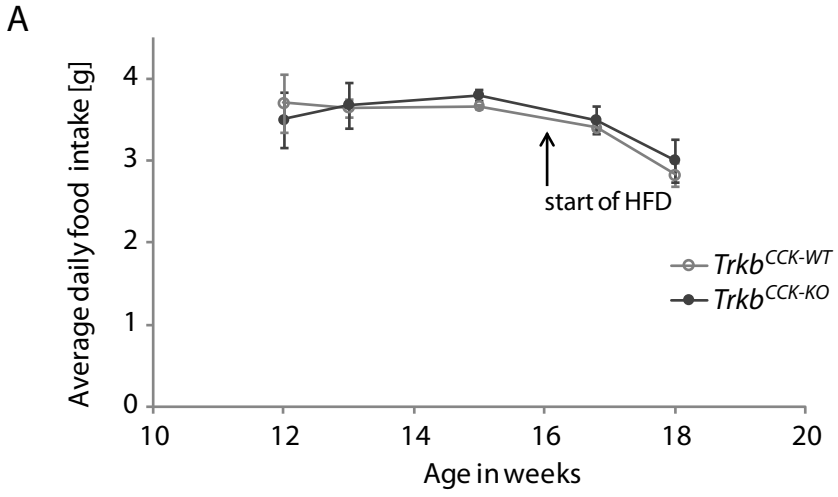

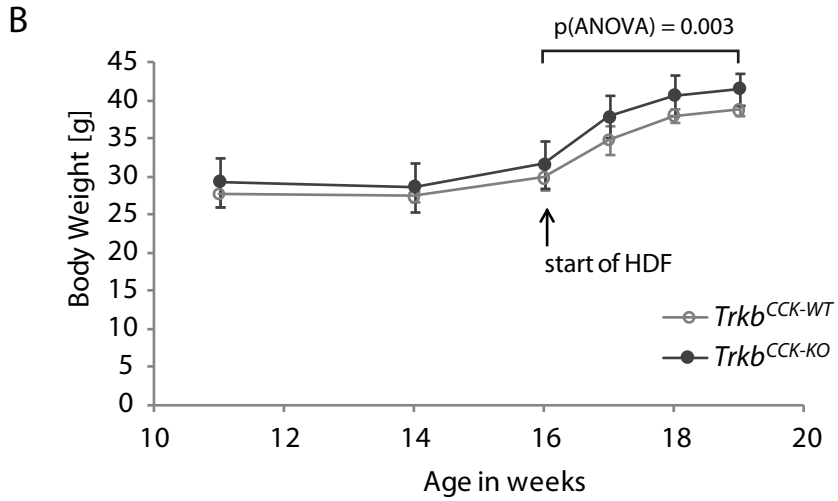

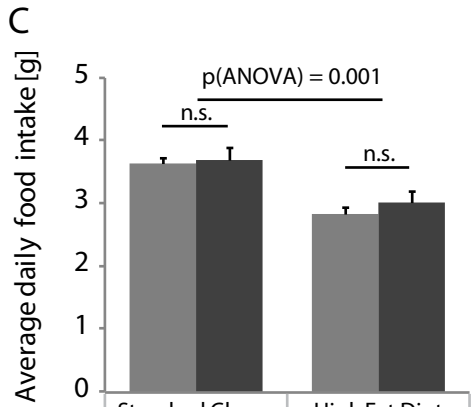

	Standard Chow	High Fat Diet
Trkb^{CCK-WT}	3.64 ± 0.08	2.83 ± 0.10
Trkb^{CCK-KO}	3.68 ± 0.20	3.00 ± 0.18

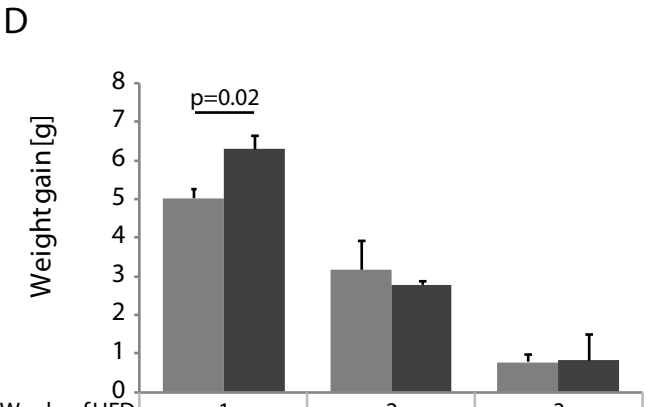

Weeks of HFD	1	2	3
Trkb^{CCK-WT}	5.0 ± 0.3	3.2 ± 0.8	0.8 ± 0.2
Trkb^{CCK-KO}	6.3 ± 0.4	2.8 ± 0.1	0.8 ± 0.7

Figure 3.12 Food intake and weight gain on high-fat diet (HFD) in male *Trkb*$^{CCK-WT}$ control and *Trkb*$^{CCK-KO}$ mice (both groups n=3). A Development of average daily food intake on normal and high-fat diet, arrow indicates start of high-fat diet, for numbers see C and main text. B Development of body weight on normal and high-fat diet, arrow indicates start of high fat diet, for numbers see main text. C Comparison of average daily food intake on normal and high fat diet (third week of HFD), values are mean ± SEM. D Weekly weight gain after start of high-fat diet, values are mean ± SEM.

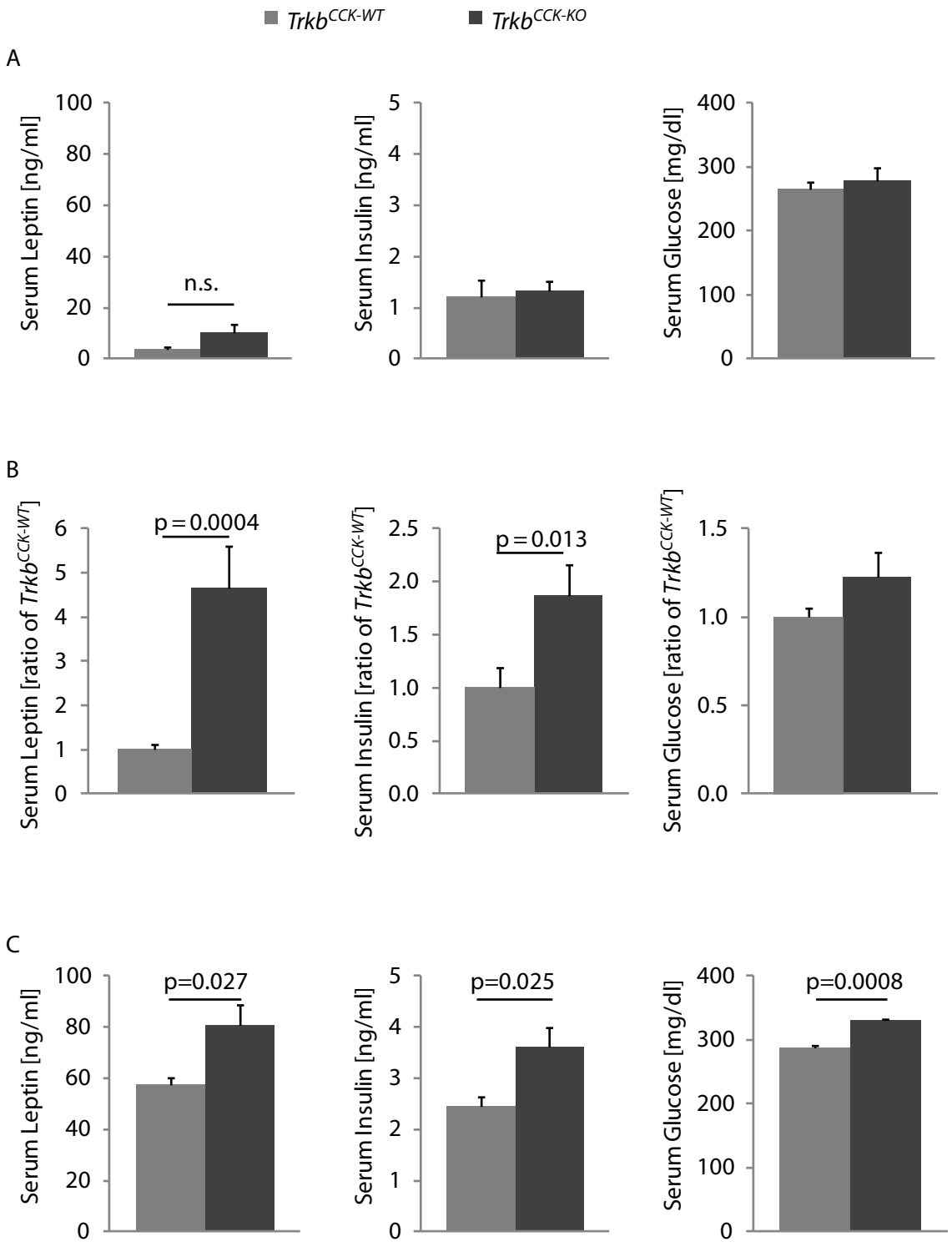

Figure 3.13 A-D Serum leptin, insulin and glucose levels in *Trkb*$^{CCK\text{-}WT}$ control and *Trkb*$^{CCK\text{-}KO}$ mice at different stages and on different diets. A 2.5 months old male mice B 5 months old male and female merged. Note that data was normalized to controls before combining genders, and is therefore given here as ratio of *Trkb*$^{CCK\text{-}WT}$ and not as concentration as in B and C. C 5 months old males on high-fat diet for 3 weeks.

D

			Leptin [ng/ml]	Insulin [ng/ml]	Glucose [mg/dl]
2.5 months	♂	*Trkb*$^{CCK\text{-}WT}$	3.6 ± 1.2	1.2 ± 0.3	265.8 ± 11.4
		n	3	3	3
		Trkb$^{CCK\text{-}KO}$	10.3 ± 3.3	1.3 ± 0.2	278.2 ± 21.3
		n	3	3	3
		p	0.066	0.375	0.317
5 months	♀	*Trkb*$^{CCK\text{-}WT}$	6.1 ± 1.9	0.6 ± 0.1	233.3 ± 30.5
		n	3	3	3
		Trkb$^{CCK\text{-}KO}$	38.2 ± 1.7	0.9 ± 0.3	265.3 ± 35.7
		n	3	2	3
		p	0.0001	0.151	0.267
	♂	*Trkb*$^{CCK\text{-}WT}$	8.1 ± 1.0	1.5 ± 0.5	188.9 ± 6.3
		n	5	4	4
		Trkb$^{CCK\text{-}KO}$	24.4 ± 10.6	3.5 ± 0.0	258.4 ± 54.9
		n	3	2	2
		p	0.042	0.030	0.059
	♂	*WT*	3.1 ± 0.6	0.6 ± 0.1	221.8 ± 30.2
		n	3	3	3
		Cre	5.0 ± 1.1	1.3 ± 0.4	167.7 ± 26.4
		n	5	5	5
		p	0.131	0.113	0.120
HFD	♂	*Trkb*$^{CCK\text{-}WT}$	57.6 ± 2.7	2.4 ± 0.2	287.1 ± 5.2
		n	3	3	3
		Trkb$^{CCK\text{-}KO}$	80.6 ± 8.1	3.6 ± 0.4	330.0 ± 2.2
		n	3	3	3
		p	0.027	0.025	0.0008
			Leptin [ratio]	Insulin [ratio]	Glucose [ratio]
5 months	♂+♀	*Trkb*$^{CCK\text{-}WT}$	1.00 ± 0.13	1.00 ± 0.19	1.00 ± 0.05
		n	8	7	7
		Trkb$^{CCK\text{-}KO}$	4.65 ± 0.95	1.87 ± 0.30	1.23 ± 0.14
		n	6	4	5
		p	0.0004	0.013	0.054

E

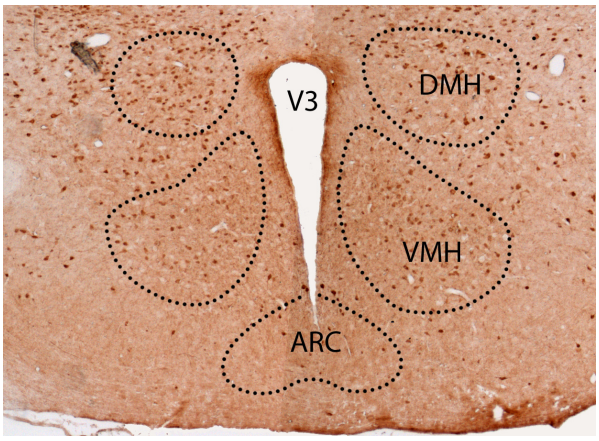

D Values for serum leptin, insulin and glucose levels for data in A-C. Values are shown as mean ± SEM and the number of mice used (n) and significance level (p) are shown.
E Recombination pattern in the *BAC-CCK-Cre:R26R-EYFP* line in hypothalamic regions involved in metabolic control. ARC arcuate nucleus; DMH dorsomedial nucleus of the hypothalamus; VMH ventromedial nucleus of the hypothalamus; V3 third ventricle

We next tested whether *Trkb*$^{CCK\text{-}KO}$ mice were able to downregulate their food intake in response to a high fat diet (HFD). Food intake and weight gain were analyzed in male mice that were fed a HFD with high calorie content for three weeks (see Materials and Methods, chapter 2.9.1). In Figure 3.12 A the average daily food intake is shown at three time points on a normal diet and then at two time points after changing to HFD. Both *Trkb*$^{CCK\text{-}KO}$ and *Trkb*$^{CCK\text{-}WT}$ mice clearly reduced their food intake and no difference was found between genotypes. The average daily food intake of *Trkb*$^{CCK\text{-}KO}$ and *Trkb*$^{CCK\text{-}WT}$ mice on normal diet ('standard chow') and on the last time point on HFD was compared (Figure 3.12 C). No difference in food intake was measured between genotypes but food intake was significantly reduced independent of genotype after changing to HFD (ANOVA for diet $p = 0.001$, ANOVA for genotype $p = 0.486$, ANOVA for diet x genotype effect $p = 0.663$; for other numbers see figure 3.12 C).

Body weight was measured weekly on normal and HFD (Figure 3.12 B). Note that animals were too young (3 months old) at the beginning to show differences in weight. Moreover, after transferring animals into metabolic cages they tend to lose weight in the first week, most probably due to stress that is inflicted by being alone and in a new environment. *Trkb*$^{CCK\text{-}KO}$ males started to gain more weight than controls just before changing to HFD. HFD induced a clear weight gain in both genotypes and ANOVA analysis revealed a diet x genotype dependent effect. Further analysis by Student's t-test showed a significant weight gain in both the *Trkb*$^{CCK\text{-}KO}$ and *Trkb*$^{CCK\text{-}WT}$ group but no significant differences between genotypes at the two time points (*Trkb*$^{CCK\text{-}WT}$ normal diet 29.8 ± 1.1 g vs HFD 38.8 ± 0.5 g, $p = 0.001$; *Trkb*$^{CCK\text{-}KO}$ normal diet 31.6 ± 2.2 g vs HFD 41.5 ± 1.5 g, $p = 0.023$, ANOVA for diet x genotype effect $p = 0.003$, no significant difference between genotypes with t-test, normal diet $p = 0.259$, HFD $p = 0.074$, n=3 for each group). Weight gain on HFD was also analyzed for every single week (Figure 3.12 D). This revealed that *Trkb*$^{CCK\text{-}KO}$ mice gained more weight after one week of HFD, but afterwards weight gain was comparable between the two groups and also decreased due to the downregulation of food intake.

3.3.3 Changes in the metabolic profile of *Trkb*$^{CCK\text{-}KO}$ mice

Obesity is generally associated with elevated serum leptin levels and leptin resistance as leptin is secreted from adipose tissue. Often this is accompanied by insulin resistance and elevated serum insulin and glucose levels leading to development of diabetes type II (see Introduction, chapter 1.3.1). Therefore, we next verified if obesity in *Trkb*$^{CCK\text{-}KO}$ mice was associated with changes in serum leptin, insulin and glucose levels.

Serum leptin, insulin and glucose levels were tested in young still lean and older already obese *Trkb*$^{CCK\text{-}KO}$ mice and controls. Furthermore, serum leptin, insulin and glucose levels were also measured in the male mice that had been fed a high-fat diet for three weeks (see previous chapter).

For the first group, 2.5 months old *Trkb*$^{CCK\text{-}WT}$ and *Trkb*$^{CCK\text{-}KO}$ male mice were used that did not show any significant differences in body weight even though the *Trkb*$^{CCK\text{-}KO}$ male mice were already slightly heavier (*Trkb*$^{CCK\text{-}KO}$ 30.0 ± 0.3 g vs *Trkb*$^{CCK\text{-}WT}$ 27.4 ± 2.1 g, n=3 both groups, p = 0.081). Serum leptin levels were slightly but not significantly elevated in *Trkb*$^{CCK\text{-}KO}$ mice and insulin and glucose levels were comparable in both groups (Figure 3.13 A and D).

For the second group, serum levels were measured in five months old *Trkb*$^{CCK\text{-}KO}$, *Trkb*$^{CCK\text{-}WT}$, *Cre* and *WT* male mice and in five months old female *Trkb*$^{CCK\text{-}WT}$ and *Trkb*$^{CCK\text{-}KO}$ mice. In this case *Trkb*$^{CCK\text{-}KO}$ mice were already significantly heavier (see chapter 3.3.1 and Figure 3.9). The data of male and female groups was combined after normalization to the mean of the respective *Trkb*$^{CCK\text{-}WT}$ group to reach high enough numbers (Figure 3.13 B, data for combined and single groups in D), therefore the graphs show the ratio to control groups and not the concentration as the graphs for younger animals and animals on HFD. Serum leptin levels were significantly elevated by a factor of 4.7 in *Trkb*$^{CCK\text{-}KO}$ mice in comparison to *Trkb*$^{CCK\text{-}WT}$ mice and also serum insulin was significantly elevated by a factor of 1.9. Serum glucose was elevated in *Trkb*$^{CCK\text{-}KO}$ mice but not significantly. When analyzing the genders separately (data in Figure 3.13 D), it becomes apparent that female *Trkb*$^{CCK\text{-}KO}$ mice showed a stronger and more consistent increase in leptin levels than male

Trkb$^{CCK\text{-}KO}$ mice (p = 0.0001 in female mice vs p = 0.042 in male mice) whereas serum insulin and glucose levels were more increased in male than female *Trkb*$^{CCK\text{-}KO}$ mice. The female group was raised at the EMBL in Monterotondo whereas the male group at the CNR in Edinburgh. The rodent diet fed in Monterotondo had a higher calorie and fat content than the diet fed in Edinburgh (see Materials and Methods, chapter 2.9.1) and animals were on average 4 grams lighter in Edinburgh and also had smaller fat pads which might influence leptin levels. For the five months old male group also WT and Cre controls were added to ensure that Cre expression had no influence on the metabolic profile (data in Figure 3.13 D). No differences were found between the two groups.

The HFD groups did not show significant changes in body weight as both *Trkb*$^{CCK\text{-}WT}$ and *Trkb*$^{CCK\text{-}KO}$ mice gained a comparable amount of weight (see previous chapter and Figure 3.12). However, *Trkb*$^{CCK\text{-}KO}$ mice had significantly elevated serum leptin, insulin and glucose levels in comparison to *Trkb*$^{CCK\text{-}WT}$ mice. The HFD had also an effect on serum levels of *Trkb*$^{CCK\text{-}WT}$ mice as leptin was elevated by a factor of 7 and insulin by a factor of 1.6 in comparison to *Trkb*$^{CCK\text{-}WT}$ mice on a normal diet (data table in Figure 3.13 D).

3.4 Hyperactivity of the HPA axis and chronic hypercortisolism in *Trkb*$^{CCK\text{-}KO}$ mice

3.4.1 Corticosterone and ACTH serum levels in *Trkb*$^{CCK\text{-}KO}$ mice

As we found recombination in several nuclei in the hypothalamus that are involved in hypothalamic-pituitary-adrenal axis (HPA axis) regulation we next assessed whether HPA axis activity was changed in *Trkb*$^{CCK\text{-}KO}$ mice. For this, we first analyzed serum levels of the two peripheral components of the HPA axis, adrenocorticotropic hormone that is secreted from the pituitary and corticosterone that is secreted from the zona fasciculata of the adrenal cortex (see also Introduction, chapter 1.4.1).

ACTH and corticosterone serum levels were measured in the morning one hour after lights were switched on (AM) and in the late afternoon (PM). Furthermore, both

hormones were analyzed separately for each gender as female rodents have higher average levels of both hormones and show higher amplitudes (see Introduction, chapter 1.4.1 and Figure 1.4).

Serum ACTH was significantly elevated in female Trkb$^{CCK\text{-}KO}$ mice in comparison to female *Trkb*$^{CCK\text{-}WT}$ mice at both time points (Figure 3.14 A, with data table). Also male *Trkb*$^{CCK\text{-}KO}$ mice had slightly elevated serum ACTH levels at both time points in comparison to male *Trkb*$^{CCK\text{-}WT}$ mice but this difference was not significant (p (AM) = 0.114 and p (PM) = 0.128, for other data see Figure 3.14 A).

Serum corticosterone basal (AM) levels were normal in male and female *Trkb*$^{CCK\text{-}KO}$ mice but PM levels were significantly elevated in male *Trkb*$^{CCK\text{-}KO}$ mice (Figure 3.14 B, with data table). Serum corticosterone PM levels in female *Trkb*$^{CCK\text{-}KO}$ mice were not significantly different from female *Trkb*$^{CCK\text{-}WT}$ controls (Figure 3.14 B, with data table, p = 0.099).

Serum ACTH and corticosterone PM levels were also measured in male and female *WT* and *Cre* mice to exclude any influence of the Cre transgene. No differences were found in either serum ACTH (female *Cre* 0.482 ± 0.025 ng/ml vs *WT* 0.524 ± 0.039 ng/ml, n = 4 for both groups, p = 0.200; male *Cre* 0.618 ± 0.070 ng/ml vs *WT* 0.483 ± 0.031 ng/ml, n = 5/3, p = 0.105) or serum corticosterone levels (female *Cre* 38.9 ± 9.4 ng/ml vs *WT* 29.3 ± 7.9 ng/ml, n = 5/4, p = 0.239; male *Cre* 33.9 ± 5.2 ng/ml vs *WT* 29.2 ± 4.6 ng/ml, n = 5 both groups, p = 0.259).

The HPA axis does not only control the daily fluctuations in ACTH and corticosterone levels but also secretion of both hormones in response to stress. To test the hormonal stress response in *Trkb*$^{CCK\text{-}KO}$ mice, we measured serum ACTH and corticosterone in female *Trkb*$^{CCK\text{-}KO}$ and *Trkb*$^{CCK\text{-}WT}$ mice after a 20 minutes restraint (description of experiment see Materials and Methods, chapter 2.9.2). Restraint stress caused a marked increase in serum ACTH and corticosterone levels in both groups when compared to unstressed groups (Figure 3.14 A-C for females). In the *Trkb*$^{CCK\text{-}WT}$ control group serum ACTH was elevated by a factor of 1.7 and serum corticosterone was elevated

by a factor of almost 10 in comparison to unstressed PM serum levels. However, there was no difference in either ACTH or corticosterone serum levels between stressed $Trkb^{CCK\text{-}KO}$ and $Trkb^{CCK\text{-}WT}$ mice.

3.4.2 Signs of chronic hypercortisolism in the periphery in $Trkb^{CCK\text{-}KO}$ mice

Chronic hypercortisolism as for instance found in Cushing's Syndrome is associated with obesity, increased central fat accumulation, diabetes type II, but also hypertrophy of the adrenal cortex and fat accumulation in the shoulder and neck region (see Introduction, chapter 1.4.1).

Obesity and central fat accumulation is present in $Trkb^{CCK\text{-}KO}$ mice as was shown in chapter 3.3.1 and Figure 3.10. Furthermore, these mice have increased leptin and insulin levels, a sign for developing insulin resistance and diabetes type II (chapter 3.3.3 and respective discussion and Figure 3.13).

A more specific sign for chronic hypercortisolism is hypertrophy of the zona fasciculata of the adrenal cortex. Therefore, brightfield images of the cortex of haematoxylin/eosin-stained adrenals of *WT*, *Cre*, $Trkb^{CCK\text{-}WT}$ and $Trkb^{CCK\text{-}KO}$ male and female mice were analyzed (Figure 3.15 A). A clear increase in the thickness of the zona fasciculata was found in male and female $Trkb^{CCK\text{-}KO}$ mice. For quantification the thickness of the zona fasciculata was measured in nine locations per adrenal, in both adrenals per mouse and three to four animals per genotype (graphs and numbers in Figure 3.15 A). This confirmed a significant increase in the thickness of the zona fasciculata in male and female $Trkb^{CCK\text{-}KO}$ mice in comparison to $Trkb^{CCK\text{-}WT}$ mice. No difference was found between *WT* and *Cre* groups.

We next analyzed fat accumulations in the neck/shoulder region of $Trkb^{CCK\text{-}WT}$ and $Trkb^{CCK\text{-}KO}$ male and female mice. For this, mice were culled, the skin was removed from the back and pictures were taken with a commercial digital camera (Figure 3.15 B). Increased fat accumulations were apparent in female $Trkb^{CCK\text{-}KO}$ mice in comparison to $Trkb^{CCK\text{-}WT}$ mice, in male mice the difference was less clear.

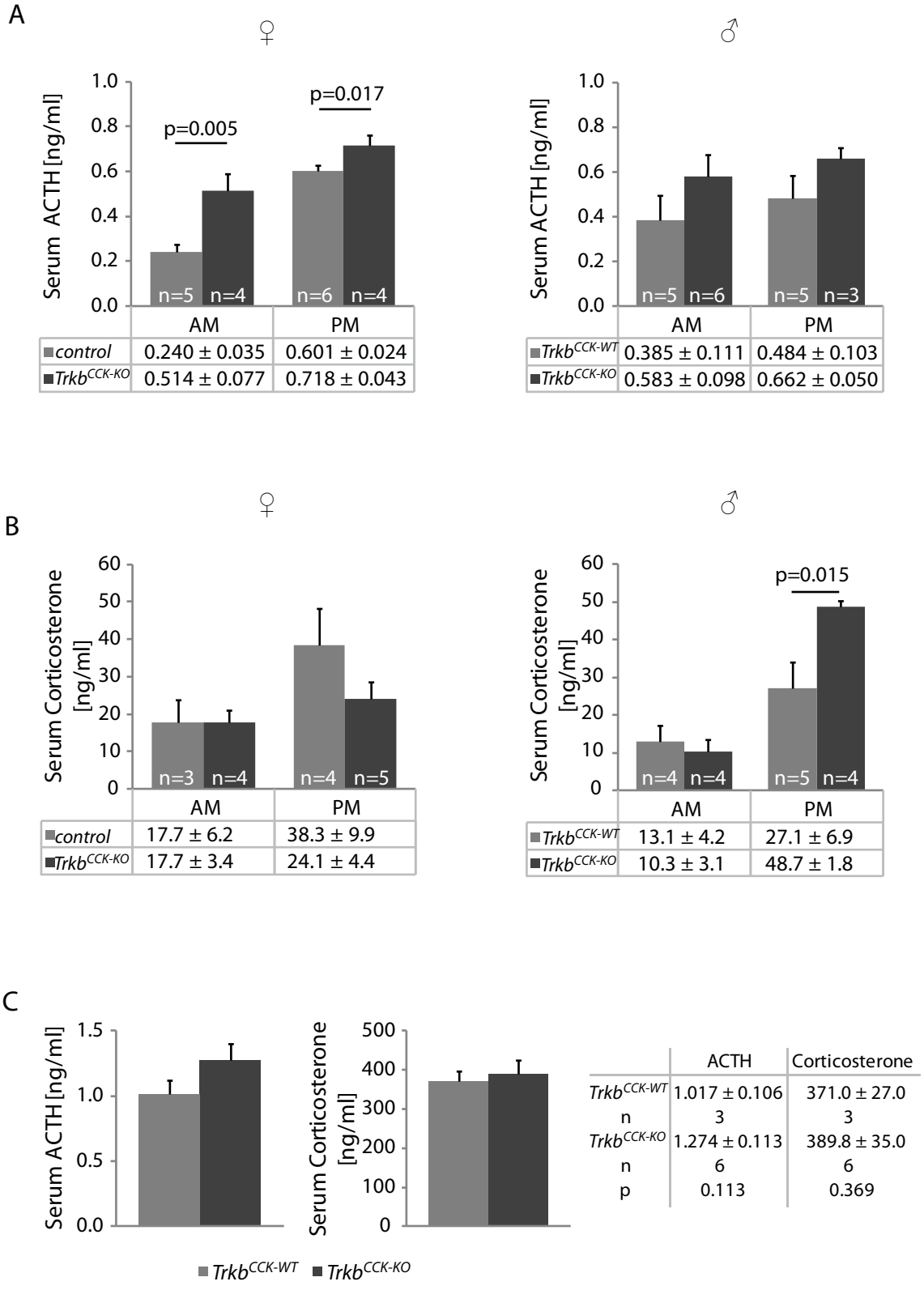

Figure 3.14 Serum ACTH (A) and corticosterone (B) levels in male and female control and *Trkb*$^{CCK\text{-}KO}$ mice and female control and *Trkb*$^{CCK\text{-}KO}$ mice after 20 minutes restraint (C). The female PM group contained both *Trkb*$^{CCK\text{-}WT}$ and *Trkb-floxed* mice. All values are mean ± SEM. For data of *WT* and *Cre* mice see main text. A Morning (AM) and afternoon (PM) serum ACTH levels in female (left) and male (right) mice. B Morning (AM) and afternoon (PM) serum corticosterone levels in female (left) and male (right) mice. C Serum ACTH (left) and corticosterone (right) levels in female mice after 20 minute restraint.

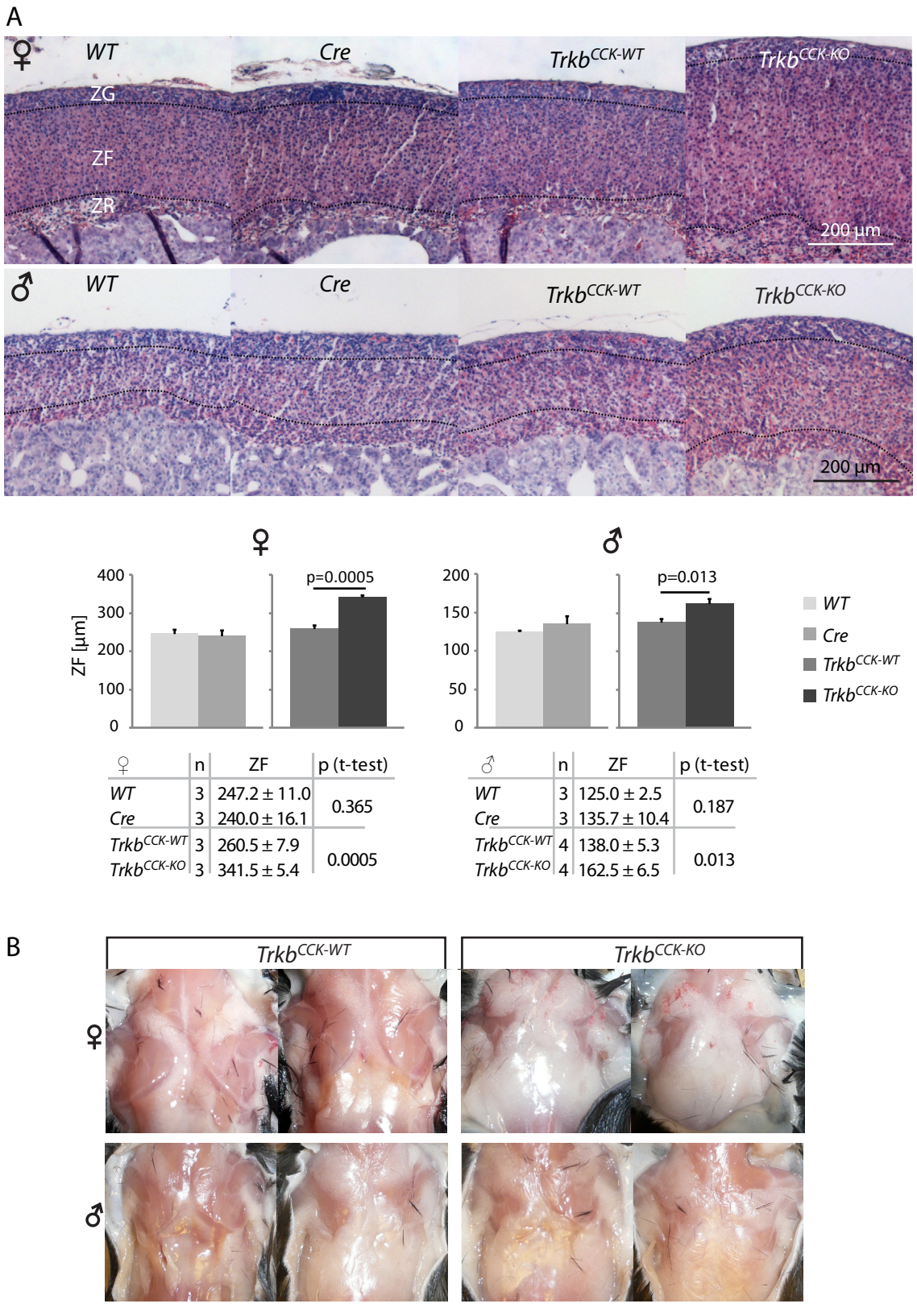

Figure 3.15 Thickness of zona fasciculata and fat accumulation in the neck/shoulder region in in male and female *WT*, *Cre* and *Trkb*$^{CCK\text{-}WT}$ control and *Trkb*$^{CCK\text{-}KO}$ mice. A Brightfield images of adrenal cortex, H&E staining. Zones of the adrenal cortex are indicated in the first picture (ZR zona reticularis, ZF zona fasciculata, ZG zona glomerulosa). Thickness of the ZF was quantified as shown in the graphs, data is given in the tables as mean ± SEM with the p-values. B Pictures of fat accumulations in the shoulder-neck region with the skin removed.

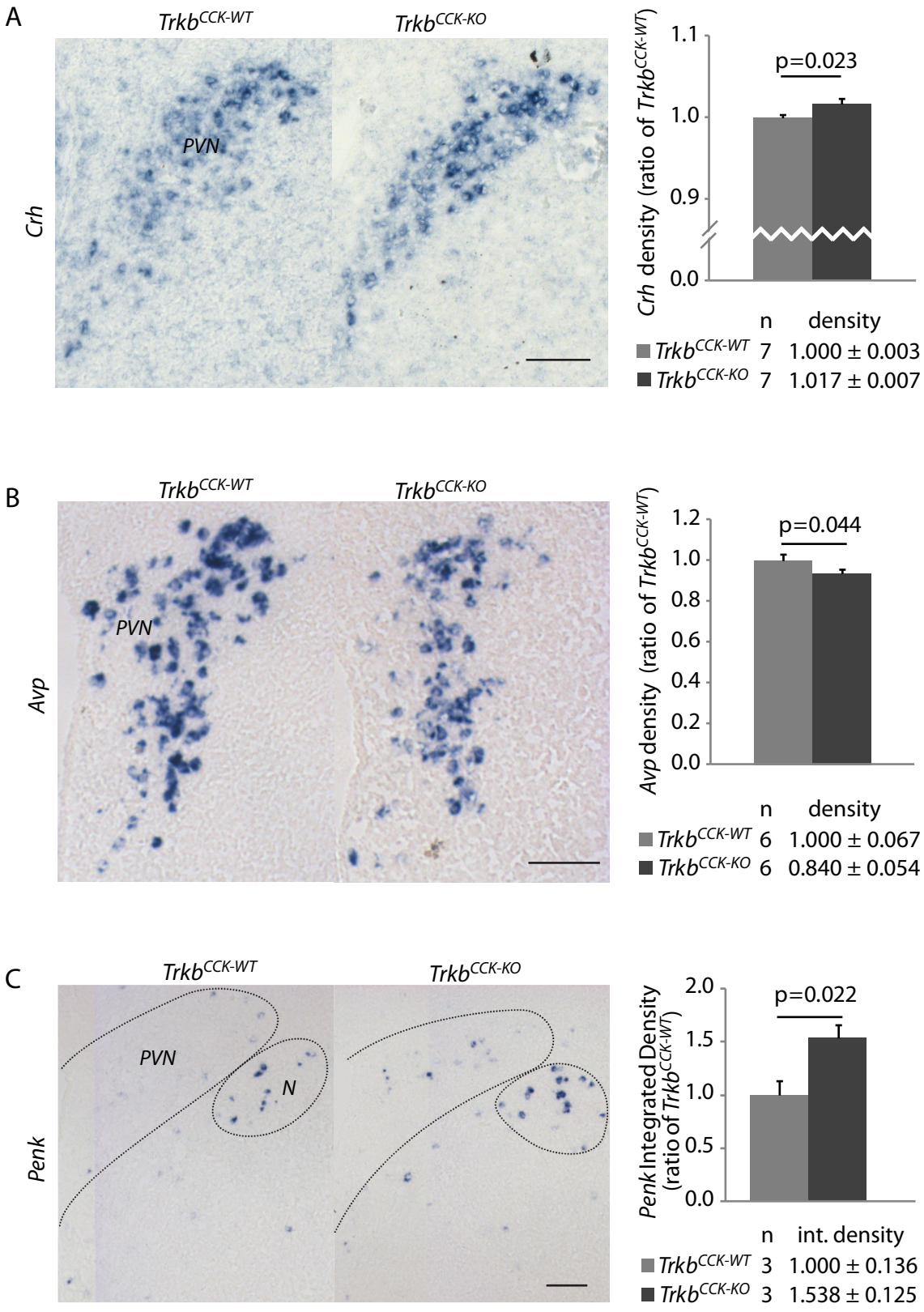

Figure 3.16 *In-situ* hybridization for the HPA axis activity markers *Crh* (A) , *Avp* (B) and enkephalin (*Penk*, C) in the PVN and adjacent regions. Density (A,B) or integrated density (C) of staining was quantified in male and female *Trkb*$^{CCK\text{-}WT}$ control and *Trkb*$^{CCK\text{-}KO}$ mice separately, normalized to the expression level in *Trkb*$^{CCK\text{-}WT}$ control mice and then combined as no difference between genders was found. Levels are expressed as mean ± SEM, n is the numbers of mice used for each analysis . N unnamed nucleus laterally to PVN; PVN paraventricular nucleus

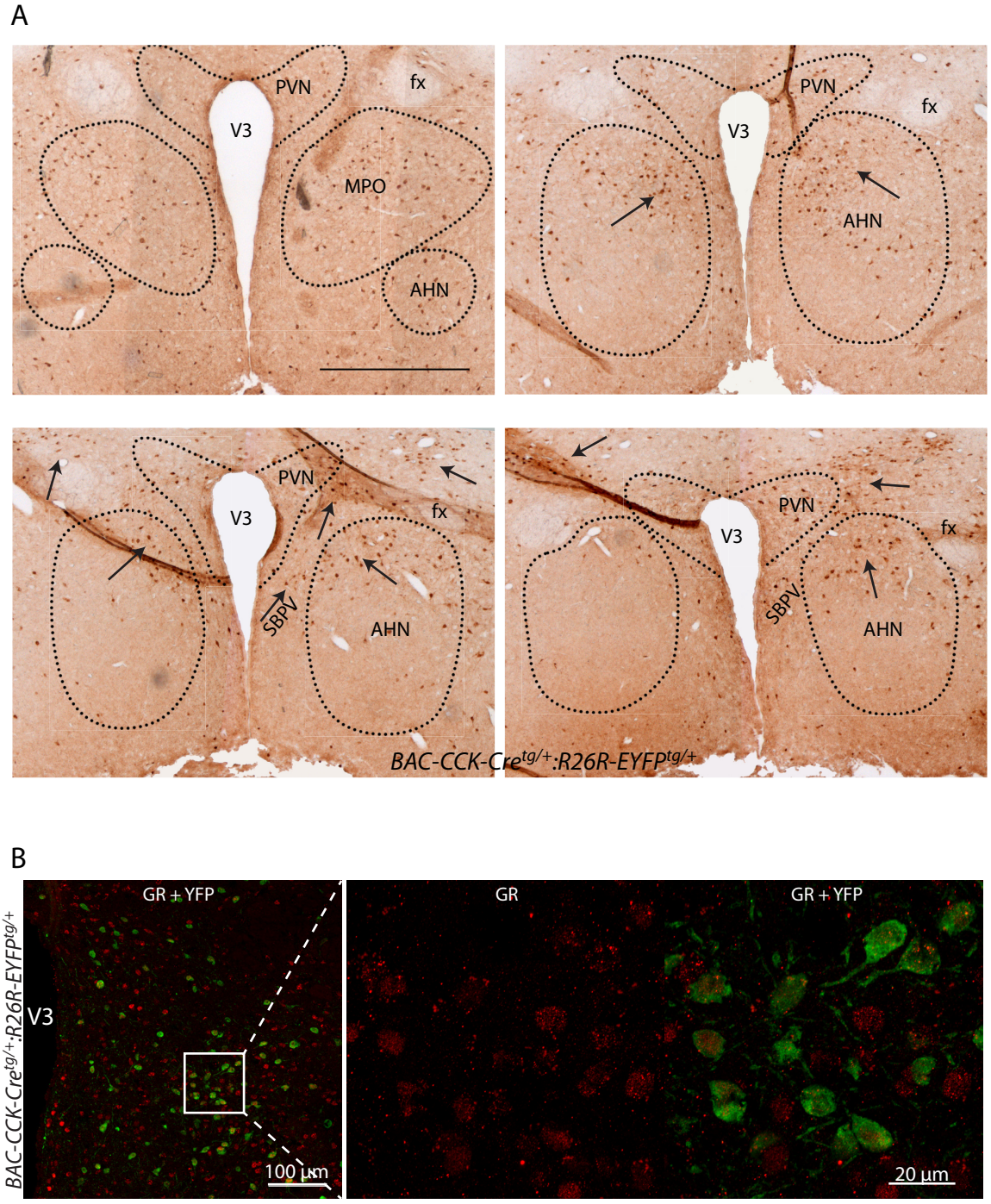

Figure 3.17 A Detailed recombination pattern of the *BAC-CCK-Cre:R26R-EYFP* line in the hypothalamus at the level of the PVN, the four images are from coronal sections that are separated by 80-100 µm. Targeted neurons are found in nuclei known to exert inhibitory control over the PVN such as the MPO (first picture) and the peri-PVN (indicated by arrows, includes dorsomedial AHN, perifornical regions (around the fornix), subparaventricular zone and cells immediately dorsal and lateral to the PVN). B Colocalization of GR immunostaining with EYFP in recombined neurons in the *BAC-CCK-Cre:R26R-EYFP* line in the hypothalamus. Targeted neurons in the peri-PVN do express the glucocorticoid receptor GR (B). AHN anterior hypothalamic nucleus; fx fornix; MPO medial preoptic area; PVN paraventricular nucleus; SBPV subparaventricular zone; V3 third ventricle

3.4.3 Increased expression of markers of PVN activity in *Trkb*$^{CCK\text{-}KO}$ mice

The central regulator of HPA axis activity is the paraventricular nucleus of the hypothalamus (PVN), which contains parvocellular neurons that secrete CRH into the portal blood stream. CRH then induces secretion of ACTH from the pituitary, which in turn induces secretion of glucocorticoids from the adrenal cortex (see Introduction, chapter 1.4.1).

To show that hyperactivity of the HPA axis in *Trkb*$^{CCK\text{-}KO}$ mice is caused by central changes we next investigated PVN activity. For this, expression of *Crh*, *Avp* and *Penk* (pro-enkephalin) mRNA, all markers of PVN activity, was analyzed by *in-situ* hybridization on coronal sections of brains of male and female *Trkb*$^{CCK\text{-}WT}$ and *Trkb*$^{CCK\text{-}KO}$ mice. Density of staining and integrated density (density x area) were analyzed separately for each gender in three 80 µm spaced sections per mouse, normalized to the level in the respective *Trkb*$^{CCK\text{-}WT}$ group and then data from both genders was combined as no differences were visible. *Penk* mRNA was only analyzed in female mice.

Density of the *Crh* signal was only slightly but significantly elevated in *Trkb*$^{CCK\text{-}KO}$ mice in comparison to the *Trkb*$^{CCK\text{-}WT}$ group (Figure 3.16 A, with data table). In contrast, density of *Avp* was decreased in *Trkb*$^{CCK\text{-}KO}$ mice compared to the *Trkb*$^{CCK\text{-}WT}$ mice (Figure 3.16 B, with data table). In both cases only the density but not the integrated density (data not shown) was significantly changed indicating that expression levels, but not the number of *Avp* or *Crh* expressing neurons in the PVN had changed. *Penk* was almost not detectable in the PVN of *Trkb*$^{CCK\text{-}WT}$ mice and ventral to the PVN but was expressed in these regions in *Trkb*$^{CCK\text{-}KO}$ mice (Figure 3.16 C). As the PVN is not as clearly distinguishable in *Penk* stainings as in *Crh* and *Avp* stainings, the location of the PVN in *Penk*-stained sections was determined by overlaying the pictures with pictures of adjacent, *Crh*-stained sections (all *in-situs* were done on the same series of sections).

In the unnamed nucleus laterally to the PVN (for explanation see Introduction, chapter 1.4.1) enkephalin positive cells were visible in *Trkb*$^{CCK\text{-}WT}$ mice and staining was to be increased in *Trkb*$^{CCK\text{-}KO}$ mice. Density and integrated density of the *Penk* signal was

analyzed in the PVN and surrounding regions together. Mean density was not significantly changed (not shown), but integrated density was significantly elevated in *Trkb*$^{CCK\text{-}KO}$ mice (data in Figure 3.16 C). This reflects a more spread *Penk* expression (i.e. not only in the unnamed nucleus but also in the PVN and ventral to the PVN) in *Trkb*$^{CCK\text{-}KO}$ mice.

We also attempted to analyze PVN activity by staining for further markers of neuronal activity as c-Fos and p-Creb. However, both proteins were not expressed in the PVN of naïve unstressed animals (not shown). As the restrained-stressed *Trkb*$^{CCK\text{-}KO}$ and *Trkb*$^{CCK\text{-}WT}$ animals had similar serum ACTH and corticosterone levels it is improbable that any differences in c-Fos, p-Creb or *Crh* mRNA would be found. Indeed, *in-situ* hybridization for *Crh* mRNA did not show any apparent differences (not shown). Immunostaining for c-Fos and p-Creb was attempted but showed in most animals high background so that staining and background was difficult to separate. This is most probably due to the fact that these animals had to be quickly culled after restrained and brains were only perfused after animals were already dead and blood had been taken, leading to suboptimal perfusion.

3.4.4 Recombination pattern in hypothalamic nuclei controlling PVN activity and colocalization with the glucocorticoid receptor

As hyperactivity of the HPA axis in *Trkb*$^{CCK\text{-}KO}$ mice was associated with increased activity in the PVN we next investigated which hypothalamic region would be involved in this deregulation. For this, the recombination pattern in the hypothalamus of *BAC-CCK-Cre:R26R-EYFP* mice was analyzed in more detail in coronal sections stained for EYFP. Four sections on the rostro-caudal axis through the PVN, separated by 80-100 µm and stained for EYFP are shown in Figure 3.17 A. The PVN proper contained only few recombined cells. However, numerous recombined cells were visible in the medial preoptic area (MPO), the dorsomedial part of the anterior hypothalamic nucleus (AHN), the subparaventricular zone (SBPV), around the fornix and directly adjacent to the PVN. The last four regions (dorsomedial AHN, SBPV, perifornical regions and regions directly

adjacent to the PVN) are also described as peri-PVN (see Introduction, chapter 1.4.1, part "Central control of HPA axis activity") and are known, as well as the MPO, to exert tonic inhibition over the PVN. Two further regions known for inhibitory inputs into the PVN also show recombination, even if not visible on these sections here – the dorsomedial hypothalamic nucleus (DMH, see Figure 3.13 E) and the bed nucleus of the stria terminalis (BST, see Figure 3.1 A and B second page).

Recombined and GABAergic neurons in the peri-PVN were further analyzed in the first part of this study (see chapter 3.1.2 and Figure 3.6). This revealed that 86% of recombined neurons in this region were clearly GABAergic, and represented 41% of the total number of GABAergic neurons found.

PVN activity is also regulated by negative feedback of corticosterone via central glucocorticoid receptors (GR), but the region and mechanism mediating this effect is still unknown (see Introduction, chapter 1.4.1). Colocalization studies for GR and EYFP in the peri-PVN in brains of *BAC-CCK-Cre:R26R-EYFP* mice were performed to test whether targeted CCK-neurons could be involved in glucocorticoid feedback inhibition. All recombined neurons expressed the GR (Figure 3.17 B) even though numerous other cells expressing the GR were found as well.

3.4.5 Behavioural analysis of *Trkb*$^{CCK\text{-}KO}$ mice

Hyperactivity of the HPA axis as in Cushing's syndrome is often associated with psychological disturbances as anxiety. CCK and thus CCK-expressing neurons have been implicated in anxiety behaviour (see Introduction, chapter 1.2.2). The Dark-Light Box Test (DLT), Elevated Plus-Maze (EPM) and Open Field (OF) were used to test innate anxiety behaviour in adult male *Trkb*$^{CCK\text{-}WT}$ and *Trkb*$^{CCK\text{-}KO}$ mice. Mice were tested in the Open Field for four consecutive days to test habituation to a stressful environment. For a more detailed description of behaviour tests see Materials and Methods, chapter 2.9.3.

In the DLT the time an animal spent in the light (or dark) box, the distance travelled in the light box and the number of visits to the dark box was analyzed. The more time an animal spends in the light box the less anxious it is considered. The distance

travelled in the light box shows rather how much an animal moves and explores and the number of visits between the two boxes is also an indicator for exploration. No difference was found between $Trkb^{CCK\text{-}WT}$ and $Trkb^{CCK\text{-}KO}$ mice in the three instances (Figure 3.18 A, with data table). Visits between the two boxes seemed elevated in $Trkb^{CCK\text{-}KO}$ mice but shows a very high variation in the control group (numbers in the control group vary between 1 and 57).

The EPM tests only anxiety behaviour – the more time an animal spends in open arms the less anxious it is considered. Time spent in open and closed arms and the centre as well as number of visits into open and closed arms was measured. No difference was found between genotypes (Figure 3.18 B, with data table).

In the Open Field the time spent in the border or centre region, the number of visits into the centre, the total distance travelled and the number of rearings was measured. The more time a mouse stays in the border region the more anxious it is considered. An increased number of visits to the centre and rearings indicate decreased anxiety and increased exploratory behaviour and rearing is also an indicator of arousal. The total distance travelled is an indicator of locomotor activity and arousal. Mice were tested on four consecutive days, this enables animals to get used to the box resulting in decreased overall locomotor activity (distance travelled) .

No differences between $Trkb^{CCK\text{-}WT}$ and $Trkb^{CCK\text{-}KO}$ mice were found in time spent in the border and centre region (Figure 3.19 A, with data table) and visits to the centre (Figure 3.19 B, with data table). These numbers also did not change significantly over the four days tested. As expected, locomotor activity decreased after the first day in the control group and was significantly decreased when comparing distance travelled at day 1 to day 4. $Trkb^{CCK\text{-}KO}$ mice were significantly more active on all days except the first trial/day and did not show a significant decrease in locomotor activity at day 4 in comparison to day 2 (Figure 3.19 C, with data table). ANOVA could not be used to analyze these data, as variances were not homogeneous.

A

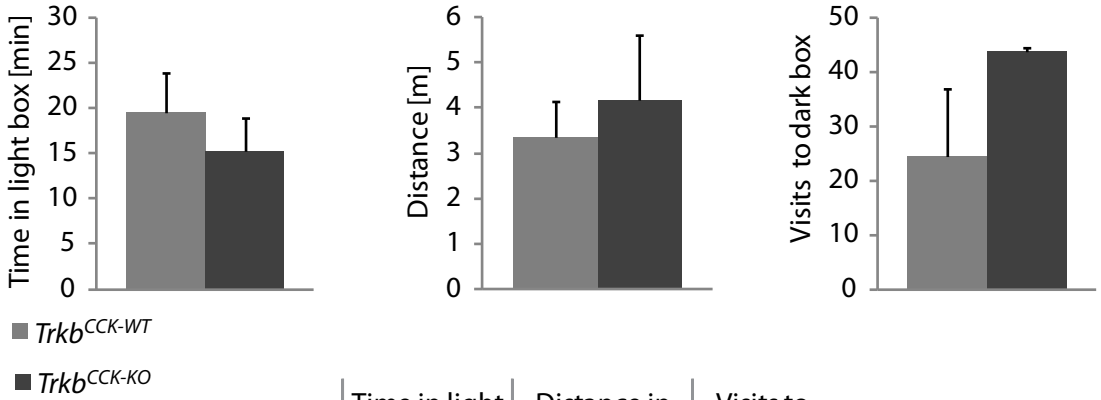

	Time in light box [min]	Distance in light box [m]	Visits to dark box
Trkb$^{CCK\text{-}WT}$	19.5 ± 4.3	3.4 ± 0.8	25 ± 12
n	5	5	4
Trkb$^{CCK\text{-}KO}$	15.2 ± 3.7	4.2 ± 1.4	44 ± 1
n	3	3	3
p	0.261	0.299	0.122

B

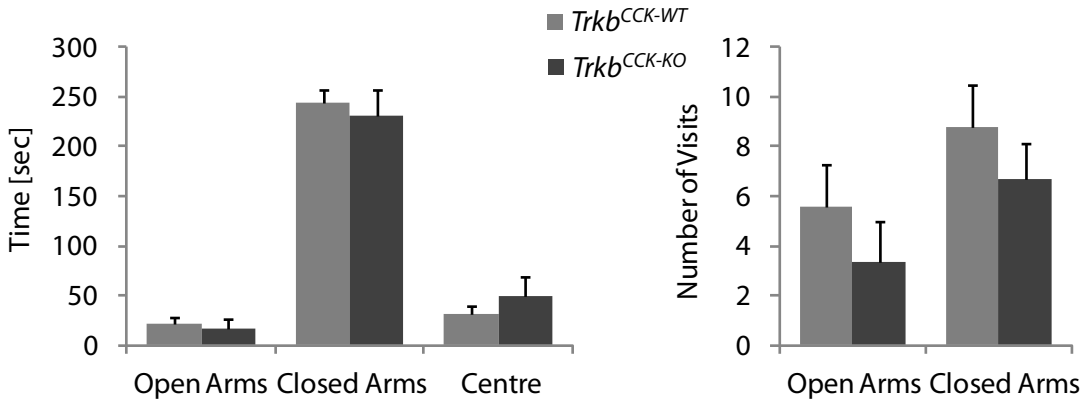

	Time in open arms [sec]	Time in closed arms [sec]	Time in centre [sec]	Visits to open arms	Visits to closed arms
Trkb$^{CCK\text{-}WT}$	21.2 ± 7.6	244.5 ± 13.4	31.8 ± 7.8	6 ± 2	9 ± 2
n	5	5	5	5	5
Trkb$^{CCK\text{-}KO}$	17.2 ± 8.6	230.8 ± 27.1	48.7 ± 21.0	3 ± 2	7 ± 1
n	3	3	3	3	3
p	0.375	0.313	0.198	0.205	0.209

Figure 3.18 Results of the dark-light box test (DLT) (A) and elevated plus-maze (EPM) (B) tested in male *Trkb*$^{CCK\text{-}WT}$ and *Trkb*$^{CCK\text{-}KO}$ mice (B). A Graphs representing results from DLT - time spent in the light box, distance travelled in the light box and visits to the dark box. Data is given in the table as mean ± SEM, n gives the number of animals tested for each group and experiment. B Graphs representing results from EPM - time spent in centre, open or closed arms, and the number of visits from the centre into an open or closed arm. Data is given in the table as mean ± SEM, n gives the number of animals tested for each group and experiment.

A

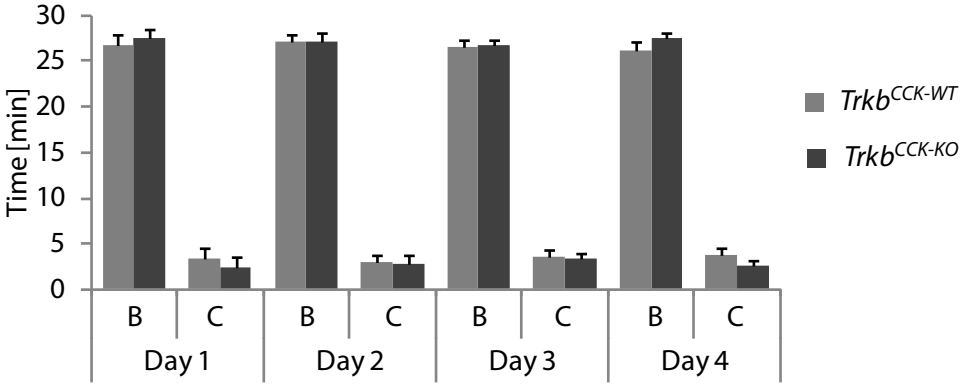

Time [min] spent in:	n	Day 1 Border	Day 1 Centre	Day 2 Border	Day 2 Centre
Trkb$^{CCK\text{-}WT}$	5	26.7 ± 1.2	3.3 ± 1.2	27.1 ± 0.9	2.9 ± 0.9
Trkb$^{CCK\text{-}KO}$	3	27.5 ± 1.0	2.5 ± 1.0	27.1 ± 1.0	2.9 ± 1.0
p		0.318	0.317	0.477	0.478

Time [min] spent in:	n	Day 3 Border	Day 3 Centre	Day 4 Border	Day 4 Centre
Trkb$^{CCK\text{-}WT}$	5	26.5 ± 0.9	3.5 ± 0.9	26.2 ± 0.8	3.8 ± 0.8
Trkb$^{CCK\text{-}KO}$	3	26.7 ± 0.7	3.3 ± 0.7	27.5 ± 0.6	2.5 ± 0.6
p		0.237	0.237	0.168	0.169

B

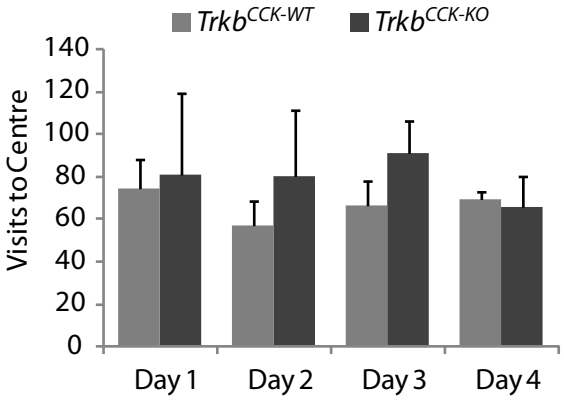

Visits to Centre:	n	Day 1	Day 2
Trkb$^{CCK\text{-}WT}$	5	74.4 ± 13.9	57.2 ± 11.4
Trkb$^{CCK\text{-}KO}$	3	80.7 ± 38.4	80.0 ± 31.7
p		0.429	0.221

Visits to Centre:	n	Day 3	Day 4
Trkb$^{CCK\text{-}WT}$	5	66.4 ± 11.4	69.2 ± 4.0
Trkb$^{CCK\text{-}KO}$	3	91.3 ± 15.2	66.0 ± 14.6
p		0.117	0.399

Figure 3.19 Results of Open Field tested in male *Trkb*$^{CCK\text{-}WT}$ control and *Trkb*$^{CCK\text{-}KO}$ mice on four consecutive days. Data is given in the tables as mean ± SEM, n gives the number of animals tested for each group and p the significance level. A Time in minutes spent in the border and centre on each day (B Border, C Centre). B Number of visits to the centre on each day.

C

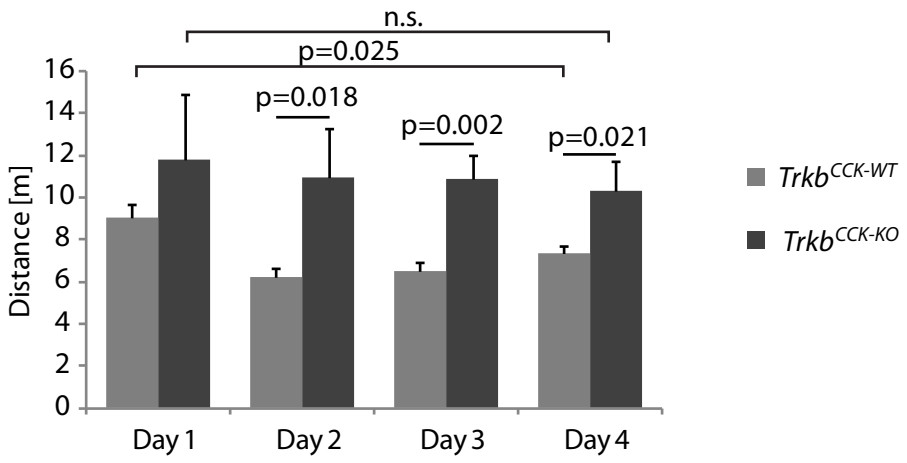

Distance travelled [m]:	n	Day 1	Day 2	Day 3	Day 4
Trkb^{CCK-WT}	5	9.0 ± 0.6	6.2 ± 0.4	6.5 ±0.4	7.4 ± 0.4
Trkb^{CCK-KO}	3	11.8 ± 3.1	11.0 ± 2.3	10.9 ± 1.1	10.3 ± 1.4
p		0.147	0.018	0.002	0.021

D

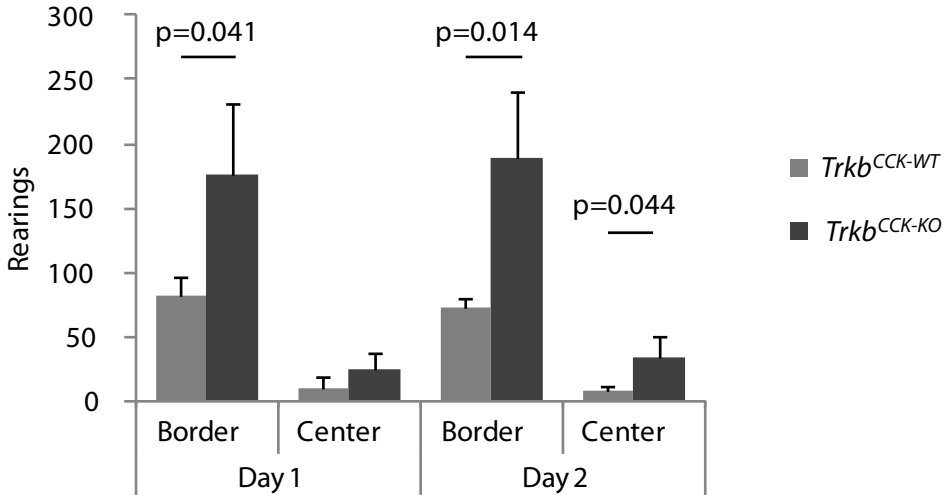

		Day 1		Day 2	
Rearings:	n	Border	Centre	Border	Centre
Trkb^{CCK-WT}	5	81.8 ± 14.8	9.8 ± 8.1	72.0 ± 8.6	7.6 ± 4.2
Trkb^{CCK-KO}	3	176.0 ± 55.8	23.7 ± 13.0	188.0 ± 53.3	34.0 ± 16.0
p		0.041	0.187	0.014	0.044

C Distance in meters travelled on each day. ANOVA could not be used to compare a genotype-day effect as variances were not homogeneous, p values are calculated by Studen't t-test. D Number of rearings in border and centre regions on day one and two.

Furthermore, *Trkb*$^{CCK\text{-}KO}$ mice reared significantly more in the border region during the first day and in both border and centre region during the second day (Figure 3.19 D, with data table).

We planned to measure homecage locomotor activity in inframot cages, but this experiment did not deliver reliable results as activity counts varied by a factor of over 10 in control mice, most probably because sensors were not calibrated properly.

Another indication for changed behaviour of *Trkb*$^{CCK\text{-}KO}$ mice was found in females after placing them for the first time in metabolic cages. During the first two hours female *Trkb*$^{CCK\text{-}KO}$ mice ate significantly more than the control group (this was the only time any difference in food intake was found) (see chapter 3.3.2, Figure 3.11 E).

During handling *Trkb*$^{CCK\text{-}KO}$ mice became easily aroused and reacted more aggressively, i.e. generally tried to bite immediately.

3.5 Analysis of mice with a mutation of the PLC-docking site of TrkB

TrkB activates downstream signalling pathways via two intracellular docking sites, the TrkB-SHC site that activates MAPK and PI3K pathways, and the TrkB-PLC site that activates PLCγ1 and calcium/calmodulin kinase pathways (see Introduction, chapter 1.1.2 and Figure 1.1).

To assess which of these sites was involved in regulation of HPA axis activity we analyzed body weight and thickness of the zona fasciculata of the adrenal cortex in lines with heterozygous point mutations in either site (*Trkb*^{SHC} and *Trkb*^{PLC} mice). For these experiments mice were weighed by Jenni Rennie from the animal facility in Edinburgh, and adrenals were embedded, sectioned and stained by a PhD student, Juraj Koudelka.

Trkb$^{S/+}$ mice did not show any signs of increased body weight compared to *Trkb*$^{+/+}$ control mice at an age of five months (females, 5 months old, *Trkb*$^{S/+}$ 28.1 ± 0.9 g vs *Trkb*$^{+/+}$ 32.1 ± 2.4 g, n = 7/3, p = 0.042; males 5 months old, *Trkb*$^{S/+}$ 39.1 ± 3.1 g vs *Trkb*$^{+/+}$ 37.3 ± 1.3 g, n = 6/4, p = 0.332) and also no changes in the thickness of the zona fasciculata of the adrenal cortex (male mice, *Trkb*$^{S/+}$ 116.8 ± 8.5 µm vs *Trkb*$^{+/+}$ 123.4 ± 16.1 µm, n = 3/2, p = 0.357).

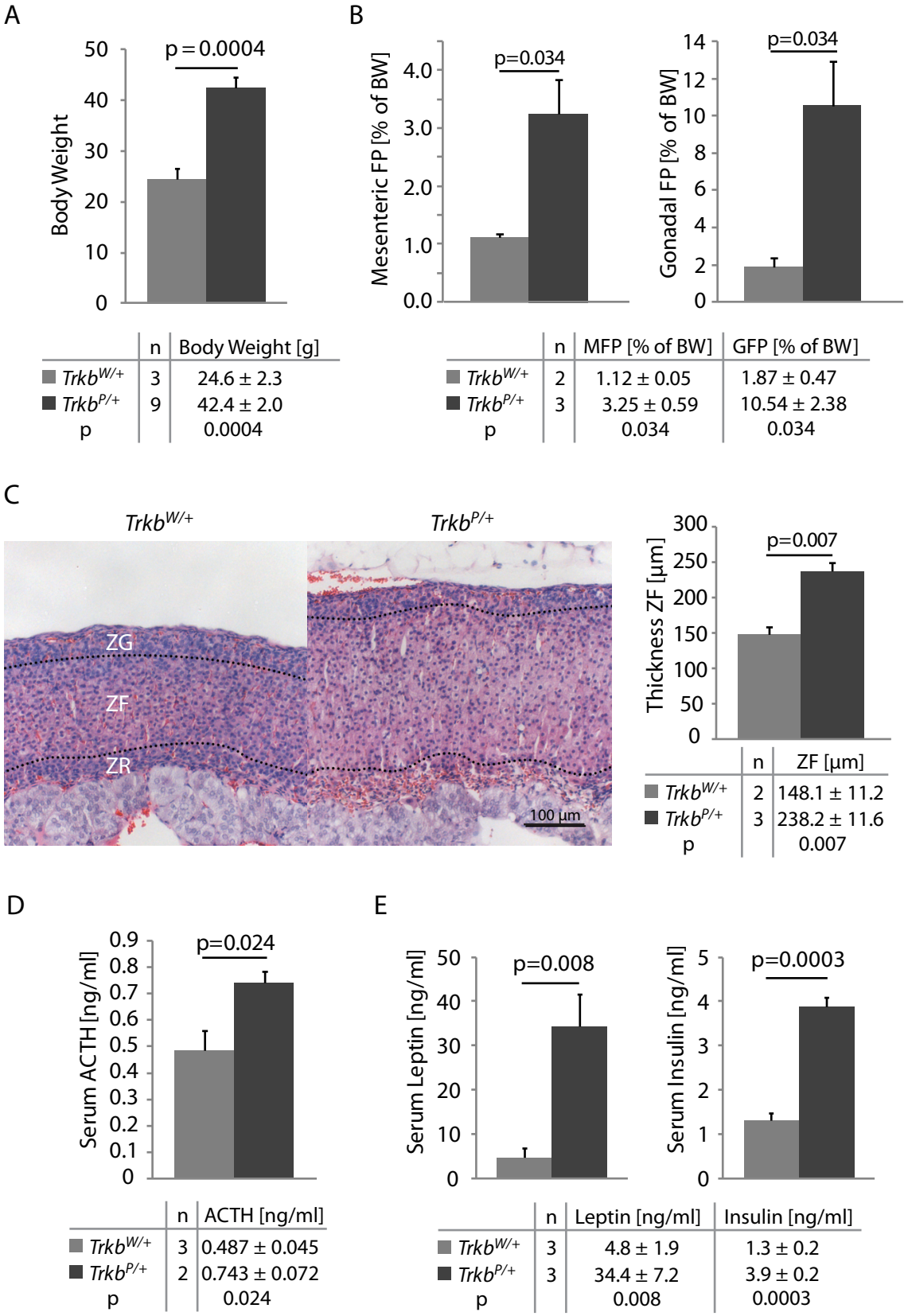

	n	Body Weight [g]
Trkb$^{W/+}$	3	24.6 ± 2.3
Trkb$^{P/+}$	9	42.4 ± 2.0
p		0.0004

	n	MFP [% of BW]	GFP [% of BW]
Trkb$^{W/+}$	2	1.12 ± 0.05	1.87 ± 0.47
Trkb$^{P/+}$	3	3.25 ± 0.59	10.54 ± 2.38
p		0.034	0.034

	n	ZF [µm]
Trkb$^{W/+}$	2	148.1 ± 11.2
Trkb$^{P/+}$	3	238.2 ± 11.6
p		0.007

	n	ACTH [ng/ml]
Trkb$^{W/+}$	3	0.487 ± 0.045
Trkb$^{P/+}$	2	0.743 ± 0.072
p		0.024

	n	Leptin [ng/ml]	Insulin [ng/ml]
Trkb$^{W/+}$	3	4.8 ± 1.9	1.3 ± 0.2
Trkb$^{P/+}$	3	34.4 ± 7.2	3.9 ± 0.2
p		0.008	0.0003

Figure 3.20 Mice with a heterozygous single point mutation of the PLC docking site (*Trkb*$^{P/+}$) mirror the phenotype of *Trkb*$^{CCK\text{-}KO}$ mice. Data is given in the tables as mean ± SEM with the number of mice used per line and the p-value. For data on *Trkb*^{SHC} mice see main text. A Body weight, B Visceral fat pad accumulations C Thickness of the zona fasiculata of the adrenal cortex D Serum ACTH levels E Serum leptin and insulin levels

In contrast, *Trkb*$^{P/+}$ mice were significantly heavier than *Trkb*$^{W/+}$ control mice (Figure 3.20 A, body weight of 7-8 months old female mice with data table, 5 months old female mice: *Trkb*$^{P/+}$ 35.8 ± 1.2 g vs *Trkb*$^{W/+}$ 27.6 ± 1.7 g, n = 2/4, p = 0.019; 5 months old male mice:, *Trkb*$^{P/+}$ 42.2 ± 1.3 g vs *Trkb*$^{W/+}$ 33.0 ± 0.6 g, n = 6/4, p = 0.0003) and this was associated with central obesity with increased mesenteric and gonadal fat pads (Figure 3.20 B with data table, 7 months old female mice).

Trkb$^{P/+}$ mice also showed hypertrophy of the zona fasciculata of the adrenal cortex (Figure 3.20 C, with data table) and elevated serum ACTH levels (Figure 3.20 D) clearly indicating chronic hypercortisolism. Furthermore, central obesity in *Trkb*$^{P/+}$ mice was accompanied by significantly increased serum leptin and insulin levels compared to *Trkb*$^{W/+}$ mice (Figure 3.20 E).

4 Discussion

4.1 Analysis of the *BAC-CCK-Cre* line

4.1.1 Recombination pattern and specificity in the *BAC-CCK-Cre* line

The recombination pattern of the *BAC-CCK-Cre* line was characterized by crossing the line to a reporter line that expresses EYFP under the Rosa26 promoter after Cre-mediated removal of a stop cassette. EYFP expression was analyzed in the brain, pituitary and adrenal by brightfield and confocal microscopy on DAB and fluorescence immunostained sections.

In the brain, the recombination pattern corresponds to the expression pattern published for CCK in literature. Recombination was detected in cortex, hippocampus, olfactory bulb, rostral striatum, thalamus, bed nucleus of the stria terminalis, hypothalamus, midbrain, brainstem and cerebellum. These areas were also found to express CCK in *in-situ* hybridization studies on rat brain (Hökfelt et al., 1985; Schiffmann and Vanderhaeghen, 1991) and by the Allen Brain Atlas project (Lein et al., 2007). The *BAC-CCK-Cre* line shows less recombined cells in the frontal regions of the cortex, the olfactory bulb and the amygdala and a more widespread recombination in the cerebellum than were detected in these studies but otherwise reflects the CCK-expression pattern well. The expression in the cerebellum might reflect CCK expression at an earlier developmental stage. Indeed, a more spread expression of CCK can be seen in P4 brains in pictures published by the Allen Brain Atlas project than in adult brains where it is restricted to Purkinje cells. A high number of recombined neurons was found in hypothalamic and caudal forebrain nuclei involved in control of energy intake or inhibitory control of the hypothalamic-adrenal-pituitary axis (HPA axis). This will be discussed in more detail in the chapters addressing these functions in $Trkb^{CCK\text{-}KO}$ mice.

Recombination was also analyzed at postnatal day 7 and embryonal stage E12.5. At P7, the pattern of recombination corresponds generally to the adult pattern and also to the expression pattern shown by the Allen Brain Atlas project for P4 and P14. Less recombined cells were seen in the cortex and hippocampus in comparison to adult

animals but CCK expression in the cortex was also reported to increase up to P21 (Burgunder and Young 3rd, 1990). At E12.5 expression was mainly found in the spinal cord and some recombined cells were visible in the future midbrain, hypothalamus and hindbrain. No recombination was found in the future cortex. CCK was published to be expressed in the spinal cord at this stage and in some regions in the brain, the earliest timepoint expression was detected in the cortex is E15.5 (Burgunder and Young 3rd, 1990; Giacobini and Wray, 2008), confirming our findings.

As serum ACTH and corticosterone levels were changed in $Trkb^{CCK\text{-}KO}$ mice recombination was analyzed in pituitary and adrenals of *BAC-CCK-Cre:R26R-EYFP* mice. The pituitary was reported to express TrkB (Kononen et al., 1994) but only very few CCK-positive cells at E17.5 (Giacobini and Wray, 2008). Accordingly, only single scattered recombined cells were found in the pituitary of *BAC-CCK-Cre:R26R-EYFP* mice precluding a causal role of the pituitary in the phenotype described here. Only few publications addressed expression of CCK in the adrenal and these reported the existence of few single CCK-positive nerve fibres and neuronal bodies in the medulla and cortex (Heym et al., 1995). We found numerous recombined cell bodies in the medulla but only few recombined cells in the adrenal cortex that were usually clustered around one column. This should have no influence on the phenotype seen in $Trkb^{CCK\text{-}KO}$ mice as TrkB is not expressed in the adrenal cortex (Schober et al., 1999).

The cellular specificity of Cre-mediated recombination in the *BAC-CCK-Cre:R26R-EYFP* line was verified by fluorescence colocalization studies on EYFP and CCK immunostained sections. Confocal pictures from different brain regions showed that EYFP expressing cells are generally CCK immunoreactive but that not all CCK-expressing cells were targeted. Colocalization was quantified in the peri-PVN as this is the region involved in the phenotype described here for $Trkb^{CCK\text{-}KO}$ mice. In the peri-PVN, 80% of CCK-expressing neurons were successfully targeted (showed Cre-mediated EYFP expression) and of the EYFP-expressing neurons 97% expressed CCK. This confirms that most CCK-expressing neurons recombine efficiently in the BAC-CCK-Cre line and that

recombination is restricted to CCK-expressing neurons. The 3% of EYFP expressing neurons in which CCK was not clearly detected might express CCK at too low levels to show staining or might have expressed CCK at an earlier stage. CCK was also reported to be difficult to detect by immunostaining in some neurons as it is only expressed at low levels and quickly transported into axons (see Introduction, chapter 1.2.2 and Mascagni et al, 2003). Thus, the cells only positive for EYFP are most probably not false positives but are not CCK immunoreactivity for the aforementioned reasons. Also the general absence of colocalization between EYFP and parvalbumin, a marker for an interneuron population that usually does not express CCK, confirms the specificity of recombination in the *BAC-CCK-Cre:R26R-EYFP* line.

CCK was described to be expressed in interneurons, however, expression was also reported in some pyramidal projection neurons in the cortex, hippocampus and amygdala (see Introduction, chapter 1.2.2). Colocalization of Cre-mediated EYFP expression and GABA in the *BAC-CCK-Cre:R26R-EYFP* line confirmed that most recombined neurons are GABAergic, but not all. Neurons with a pyramidal shape (a clearly visible apical dendrite) in the cortex and CA1 of the hippocampus did not express GABA. The recombined cortical neurons were found to be cortico-spinal motorneurons (CSMN), as they colocalize with the CSMN marker CTIP2. The recombined neurons in the CA1 were positive for a CamKII-CFP fusion protein that is only expressed in principal neurons. CCK expression in cortical projection neurons and CA1 pyramidal neurons has been reported (Burgunder and Young 3rd, 1990; Senatorov et al., 1995) and recombination in these neurons reflects the endogenous CCK expression. Colocalization of GABA and EYFP was quantified in the peri-PVN to verify whether targeted neurons in this region were GABAergic. The vast majority of recombined neurons (86%) in this region was GABAergic and of the GABA-positive cells 41% showed recombination, confirming that almost all of the CCK-expressing and half of the inhibitory interneurons in the peri-PVN were targeted in the *BAC-CCK-Cre* line.

In conclusion, recombination in the BAC-CCK-Cre line is found in all regions known to express CCK and is specific to CCK-expressing cells. Recombination occurs efficiently as it is already detected in the expected regions in embryos and young animals. Most recombined neurons are GABAergic with the exception of pyramidal neurons in the CA1 and projection neurons in the cortex, but this corresponds to the endogenous expression pattern published for CCK.

4.1.2 CCK-neuron specific ablation of *Trkb* by the *BAC-CCK-Cre* line

Trkb was specifically ablated from CCK-neurons by crossing the *BAC-CCK-Cre* line with a *Trkb-floxed* line. Successful removal of TrkB protein was verified by immunoblotting using lysates of cortex and hypothalamus of $Trkb^{CCK\text{-}WT}$ and $Trkb^{CCK\text{-}KO}$ mice. Full-length TrkB protein levels were significantly reduced to 25 % in the hypothalamus and also, even if not significantly, in the cortex of $Trkb^{CCK\text{-}KO}$ mice. As the hypothalamus contains a much higher proportion of recombined neurons than the cortex, a stronger reduction in TrkB protein levels in the hypothalamus is to be expected. Expression of truncated isoforms of TrkB was not affected as the loxP-sites of the *Trkb-floxed* line are downstream of the last exon expressed in the truncated forms.

Specific ablation of *Trkb* mRNA from recombined neurons was analyzed in the cortex and hippocampus by double-staining for *Trkb* mRNA by *in-situ* hybridization and for EGFP by immunofluorescence staining on brains of $BAC\text{-}CCK\text{-}Cre^{tg/+}$:$Z/EG\text{-}EGFP^{tg/+}$ and $Trkb^{CCK\text{-}KO}$:$Z/EG\text{-}EGFP^{tg/+}$. The Z/EG line was used in this case as we did not succeed in generating $Trkb^{CCK\text{-}KO}$::$R26R\text{-}EYFP^{tg/+}$ mice. On a wildtype background *Trkb* mRNA was found to be expressed in recombined neurons and absence of colocalization on a knockout background confirmed successful deletion of *Trkb* from these neurons. An analysis of ablation in hypothalamic neurons was not possible as only single recombined neurons were found in the Z/EG line in the hypothalamus, but the reduction in TrkB protein levels in the hypothalamus confirmed successful removal of TrkB in this region.

4.2 *Trkb*$^{CCK\text{-}KO}$ mice are viable and show no severe loss of neurons

Trkb$^{CCK\text{-}KO}$ mice are viable and did not show increased mortality from weaning age on up to seven month of age, the longest they were kept so far. Statistics on the gender and genotype of weaned animals show a small decrease in the number of heterozygous (*CCK-Cre*$^{tg/+}$,*Trkb*$^{lx/+}$) and homozygous (*CCK-Cre*$^{tg/+}$,*Trkb*$^{lx/lx}$) knockout mice and female mice reaching weaning age, most probably because too small numbers were analysed. No changes were found in the number of Cre-positive mice in comparison to wildtype mice or gender distribution.

Cresyl-Violet staining on brain sections showed that the gross morphology of *Trkb*$^{CCK\text{-}KO}$ brains is normal. Brain CCK levels were determined by CCK-ELISA on whole brain lysates and were also normal in *Trkb*$^{CCK\text{-}KO}$ mice. As recombination occurred in most CCK-expressing neurons and as CCK-neurons are the only source of CCK in the brain, this finding suggests that ablation of *Trkb* from CCK-neurons does not lead to significant neuronal loss or profound impairment of neuronal function. We had planned to investigate potential effects of *Trkb* ablation on numbers of CCK-neurons by cell counts in *BAC-CCK-Cre:R26R-EYFP* mice on wildtype and mutant background. However, this was not possible as we never obtained mice with the reporter allele on a knockout background. We did obtain Z/EG reporter mice on a knockout background that were used for the *Trkb in-situ* – EGFP double labelling, however, we did not want to rely on this line for cell counts, as it does not recombine efficiently. Another possibility would have been to use CCK immunostainings for cell counts. The weak signal of the CCK antibody is impossible to analyze automatically requiring counting by hand and we also had only small amounts of the antibody as newer lots or any other CCK antibody available were not specific. Nonetheless, the finding that *Trkb*$^{CCK\text{-}KO}$ mice have normal brain CCK levels is a reliable confirmation that CCK-neurons are present. Moreover, TrkB was shown to be rather involved in interneuron differentiation, synaptogenesis and synapse maintenance than survival. For instance, Trkb knockout mice were shown to have defects in interneuron differentiation but normal numbers of interneurons

(Carmona et al. 2006). Also specific deletion of *Trkb* from early postmitotic GABAergic neurons did not influence number and position of cortical interneurons but expression of specific markers (Sánchez-Huertas et al. 2011).

4.3 *Trkb*$^{CCK\text{-}KO}$ mice are obese but not hyperphagic

Trkb$^{CCK\text{-}KO}$ mice develop visible obesity in adulthood. Body weight of male *Trkb*$^{CCK\text{-}KO}$ mice was comparable to control groups up to three months of age but was significantly increased from four months of age on. Also female *Trkb*$^{CCK\text{-}KO}$ mice were significantly heavier at five months of age. This increase in body weight was due to increased accumulation of adipose tissue as central visceral fat pads, namely the mesenteric and gonadal fat pad, were significantly enlarged in five months old male and female *Trkb*$^{CCK\text{-}KO}$ mice.

BDNF/TrkB signalling has been implicated in the central control of energy intake. Obesity associated with hyperphagia (over-eating) was found in several models of *Bdnf* or *Trkb* deficiency such as TrkB hypomorphic mice, BDNF heterozygous mice and principal neuron-specific and VMH-specific BDNF knockout mice (Xu et al. 2003, Lyons et al. 1999, Rios et al. 2001, Unger et al. 2007, see also Introduction, chapter 1.3.2). Besides, the *BAC-CCK-Cre* line showed recombination in hypothalamic (VMH and DMH) and brainstem (DVC) regions involved in central control of food intake.

Therefore, we decided to next measure food intake in *Trkb*$^{CCK\text{-}KO}$ mice and control groups. We could not find any differences in food intake, circadian rhythm of food intake or accumulated food intake over several weeks in either male or female *Trkb*$^{CCK\text{-}KO}$ mice. Indeed, when tracking food intake and weight gain over one week, we found that *Trkb*$^{CCK\text{-}KO}$ mice gained significantly more weight during that week without eating more than the control group. The only difference ever found was in female mice in the first two hours after transferring them from home cages into metabolic cages. In this case, female *Trkb*$^{CCK\text{-}KO}$ mice did eat significantly more than female mice from control groups. This represents rather differences in stressed-induced behaviour than a general difference in control of energy intake.

Subtle changes in control of food intake might not be easy to detect on a normal diet. To assess whether *Trkb*$^{CCK\text{-}KO}$ mice were able to downregulate food intake in response to a high-calorie diet, mice were fed a high-fat diet for three weeks. High-fat diet induced a significant decrease in food intake and a significant increase in body weight in both the control group and *Trkb*$^{CCK\text{-}KO}$ mice. No differences were found in food intake or total weight gain between genotypes. *Trkb*$^{CCK\text{-}KO}$ mice gained significantly more weight after the first week of high-fat diet but not in the following weeks. This might rather be due to the fact that mice were at an age when *Trkb*$^{CCK\text{-}KO}$ mice would gain more weight anyway, than a different response to the high-fat diet.

These results show that control of energy intake is not affected in *Trkb*$^{CCK\text{-}KO}$ mice. *Trkb*$^{CCK\text{-}KO}$ mice are not hyperphagic, can decrease food intake in response to a high-calorie diet and the difference in body weight is not increased but obliterated by a high-fat diet. The absence of hyperphagia stands in contrast to other models of *Bdnf* or *Trkb* deficiency that are clearly hyperphagic. In these models, BDNF was found to be involved in anorectic signalling downstream of melanocortin in principal neurons in the VMH (Xu et al. 2003, Unger et al. 2007, see also Introduction chapter 1.3). As removal of *Trkb* from principal neurons does not induce obesity (observation in the *Trkb*$^{CamKII\text{-}Cre}$ line in our lab), one could hypothesize that BDNF might act on TrkB-expressing interneurons in the VMH to suppress food intake. The *BAC-CCK-Cre* line shows recombination in the CCK-positive subset of VMH interneurons, but the absence of hyperphagia in the *Trkb*$^{CCK\text{-}KO}$ mouse suggests BDNF does not act on these neurons to regulate food intake. The VMH also projects to the dorsal vagal complex (DVC) in the brainstem where BDNF and TrkB were shown to suppress food intake downstream of melanocortin signalling (Bariohay et al. 2005 and 2009, see also Introduction, chapter 1.3.2). Thus, BDNF from the VMH might rather act on the DVC than on hypothalamic nuclei. Recombined cells were found in the DVC in the *BAC-CCK-Cre* line but, as with the VMH, these neurons do not seem to be involved in BDNF/TrkB signalling downstream of melanocortin signalling as we do not see any deregulation of food intake in *Trkb*$^{CCK\text{-}KO}$ mice. In addition to its actions

downstream of melanocortin signalling in the VMH and DVC, BDNF was also implicated in the anorectic effect of corticotropin-releasing hormone (CRH) in the paraventricular nucleus of the hypothalamus (PVN). Infusion of BDNF into the PVN reduces food intake by upregulation of CRH and urocortin that both have an anorexigenic effect (via other ways than the HPA axis) (Toriya et al. 2010, see also Introduction chapter 1.3.2). This does not stand in contrast with our findings, as in this case BDNF acts on TrkB-expressing PVN neurons that do not show recombination in the *BAC-CCK-Cre* line.

In conclusion, obesity in $Trkb^{CCK\text{-}KO}$ mice is caused by other mechanisms than hyperphagia and BDNF/TrkB signalling in the CCK-positive subset of hypothalamic interneurons is not involved in control of energy intake.

Obesity in $Trkb^{CCK\text{-}KO}$ mice is associated with hyperleptinemia and hyperinsulinemia

Obesity is usually associated with high levels of the anorexic hormone leptin as leptin is secreted by adipocytes. However, obesity also induces leptin resistance, and therefore high leptin levels are not effective in suppressing food intake any more (see Introduction, chapter 1.3.1). To verify that obesity in $Trkb^{CCK\text{-}KO}$ mice was associated with an increase in leptin levels, serum leptin was determined in young lean and older obese $Trkb^{CCK\text{-}KO}$ mice and control groups as well as in the high-fat diet groups. Not yet obese $Trkb^{CCK\text{-}KO}$ mice had normal serum leptin levels whereas obese $Trkb^{CCK\text{-}KO}$ mice showed a significant increase. This confirms that, as expected, obesity in $Trkb^{CCK\text{-}KO}$ mice is associated with elevated serum leptin and leptin resistance. High-fat diet induced a profound increase of serum leptin in control group as well as $Trkb^{CCK\text{-}KO}$ mice even though levels were still significantly higher in $Trkb^{CCK\text{-}KO}$ mice.

Obesity is also often accompanied by elevated insulin levels and insulin resistance leading finally to deregulation of glucose metabolism and development of diabetes type II (see Introduction, chapter 1.3.1). Therefore, serum insulin and glucose levels were determined in the same groups as serum leptin. As for leptin, serum insulin was normal in lean but significantly elevated in obese $Trkb^{CCK\text{-}KO}$ mice. High-fat diet induced elevated insulin levels in the control as well as the knockout group, but was still significantly higher

in *Trkb*$^{CCK\text{-}KO}$ mice. Glucose was normal in young and only slightly but not significantly elevated in obese *Trkb*$^{CCK\text{-}KO}$ mice, but significantly elevated in *Trkb*$^{CCK\text{-}KO}$ mice on HFD in comparison to the control group. However, to assess whether glucose homeostasis is still functional a glucose tolerance test would be necessary.

Thus, obesity in *Trkb*$^{CCK\text{-}KO}$ mice is associated with hyperleptinemia and hyperinsulinemia and resistance to both hormones. Glucose levels are not significantly elevated in obese *Trkb*$^{CCK\text{-}KO}$ mice. The finding that leptin, insulin and glucose levels are significantly elevated in *Trkb*$^{CCK\text{-}KO}$ mice on HFD even though these mice do not weigh more than the control group suggests they may be more susceptible to metabolic changes.

4.4 HPA axis hyperactivity in *Trkb*$^{CCK\text{-}KO}$ mice

4.4.1 HPA axis hyperactivity and chronic hypercortisolism in *Trkb*$^{CCK\text{-}KO}$ mice

The *BAC-CCK-Cre* line showed recombination in hypothalamic nuclei associated with food intake control as well as in regions associated with control of HPA axis activity. BDNF and TrkB have been associated with HPA axis function, but so far none of the *Bdnf* or *Trkb* deficient or overexpressing mouse models show changes in HPA axis activity (see Introduction, chapter 1.42). This was particularly investigated in the principal neuron-specific knockout of *Trkb*, and these mice were found to have no differences in levels of HPA axis hormones (ACTH and corticosterone) and to be rather hyperactive than anxious or depressed (Zorner et al. 2003).

To investigate if TrkB signalling in CCK-interneurons might be involved in HPA axis regulation serum corticosterone and ACTH levels were measured in *Trkb*$^{CCK\text{-}KO}$ mice by ELISA or RIA. Both hormones have a circadian rhythm with the lowest levels at the start of the rest phase (morning in rodents – AM) and increased levels towards the end of the rest phase (afternoon-evening in rodents – PM). Serum ACTH was significantly elevated in five months old female *Trkb*$^{CCK\text{-}KO}$ mice at both time points, in male *Trkb*$^{CCK\text{-}KO}$ mice levels were elevated at both time points, but not significantly. Serum corticosterone was normal at basal levels but elevated in the afternoon in male *Trkb*$^{CCK\text{-}KO}$ mice. *Trkb*$^{CCK\text{-}}$

^{KO} female mice did not show elevated corticosterone levels, but, as shown later, show clear signs of hypercortisolism. It is inherently difficult to obtain reliable ACTH and corticosterone levels as both hormones show not only a circadian but also an ultradian rhythm with hourly bursts of secretion that have a higher amplitude in females (see Introduction, chapter 1.4.1 and Figure 1.4 B). This leads to high variations in hormone levels between individuals making it very difficult to acquire meaningful data. Moreover, handling during the experiments or events prior to the experiment can stress mice, resulting in altered ACTH and corticosterone levels. Therefore, changes in corticosterone levels of female *Trkb*$^{CCK\text{-}KO}$ mice might not have been detected here even if they are present as suggested by adrenal hypertrophy. Altogether, these results suggest increased HPA axis activity in *Trkb*$^{CCK\text{-}KO}$ mice.

HPA axis hyperactivity is often associated with increased hormonal responses to stress. Stress response was tested in *Trkb*$^{CCK\text{-}KO}$ mice and control groups by analyzing serum ACTH and corticosterone levels after a 20 minutes restraint stress. Both groups showed increased serum ACTH and corticosterone levels but no difference between genotypes was detected. Thus, the HPA axis response to restraint stress is not affected in *Trkb*$^{CCK\text{-}KO}$ mice. As will be discussed later, the HPA axis hyperactivity in *Trkb*$^{CCK\text{-}KO}$ mice is caused by decreased inhibitory input from local interneurons to the paraventricular nucleus of the hypothalamus (PVN). These interneurons were suggested to tonically inhibit PVN activity under normal but not any more under stressful conditions (Wamsteeker et al. 2010, see also Introduction chapter 1.4.1). Hence, impaired inhibitory input in *Trkb*$^{CCK\text{-}KO}$ mice would be expected to rather affect HPA axis activity under normal but not stressful conditions.

Chronic hypercortisolism can induce hypertrophy of the adrenal cortex due to the increased production of glucocorticoids in the zona fasciculata (see Introduction, chapter 1.4.1). Analysis of the adrenal cortex of *Trkb*$^{CCK\text{-}KO}$ mice and controls revealed that male and female *Trkb*$^{CCK\text{-}KO}$ mice had a significantly enlarged zona fasciculata. Diseases of chronic hypercortisolism as for instance Cushing's syndrome (see Introduction chapter

1.4.1) are also associated with increased central obesity and fat accumulation in the neck and shoulder region. Central obesity is present in *Trkb*$^{CCK\text{-}KO}$ mice as discussed in chapter 4.3. Pictures of fat accumulations in the neck/shoulder region of female and male *Trkb*$^{CCK\text{-}KO}$ mice revealed a clear increase in fat mass in female but not male *Trkb*$^{CCK\text{-}KO}$ mice.

Elevated serum ACTH and corticosterone levels in *Trkb*$^{CCK\text{-}KO}$ mice are thus associated with clear signs of chronic hypercortisolism confirming the presence of HPA axis hyperactivity in males and females.

HPA axis hyperactivity in *Trkb*$^{CCK\text{-}KO}$ mice is caused by changes in the central regulation as the adrenal cortex does not express TrkB and as only few cells were recombined in the pituitary,. The main central regulator of HPA axis activity is the PVN as it contains the parvocellular neurons that secret corticotropin releasing hormone (CRH) and arginine-vasopressin (AVP) to induce ACTH release from the pituitary (see Introduction, chapter 1.4.1). For this reason, CRH and AVP are also good markers for PVN activity. However, immunostainings for these peptides in the PVN are not very informative as both peptides are mainly located in vesicles in axon endings in the median eminence from where they are secreted into the portal blood stream. As both peptides are also secreted in response to stress, peptide content might be altered after handling mice for collection of tissues. As mRNA expression levels of both *Crh* and *Avp* reflect previous PVN activity (Watts 2005), *in-situ* hybridization for these two markers is generally used to assess PVN activity. A further marker for PVN activity is enkephalin. Enkephalin is mainly expressed in an unnamed nucleus lateral to the PVN and other neurons in the vicinity of the PVN and only under conditions of increased HPA axis activity also in the PVN itself (Dumont et al. 2000, Viau et al. 2002, Watts et al. 2005, see also Introduction, chapter 1.4.1).

Quantification of the *in-situ* hybridization signal revealed a small but significant elevation of PVN *Crh* mRNA expression in *Trkb*$^{CCK\text{-}KO}$ mice. *Penk* mRNA expression was significantly increased in *Trkb*$^{CCK\text{-}KO}$ mice and single *Penk* positive cells were found in the

PVN of *Trkb*$^{CCK\text{-}KO}$ mice but not in control mice. In contrast to this, *Avp* expression was reduced in the PVN of *Trkb*$^{CCK\text{-}KO}$ mice.

Elevated expression of *Crh* and *Penk* in the PVN and, in the case of *Penk*, the PVN surroundings, confirms increased activity of the PVN in *Trkb*$^{CCK\text{-}KO}$ mice. The increase in *Crh* expression seems small but, since only the density and not the area of staining increases, it could reflect increased expression in the same number of neurons as in control animals, rather than an increased number of *Crh* expressing cells. This kind of change is more difficult to detect by *in-situ* hybridization and might be easier to detect by quantitative real-time PCR. The PVN of mice is however so small that dissection by hand is impossible and would require the use of microdissection equipment. As CRH is a potent ACTH secretagogue, small changes in expression are sufficient to induce changes in ACTH secretion (Bradbury et al., 1974).

Glucocorticoids act in a negative feedback loop and suppress HPA axis activity in the pituitary and brain for instance by reducing *Crh* and *Avp* expression (Watts 2005, see also Introduction, chapter 1.4.1). *Crh* expression in the PVN and serum glucocorticoid concentration have usually an inverse relationship, particularly at glucocorticoid concentrations between 10 to 150 ng/ml (Watts 2005). Glucocorticoid receptor (GR) ablation from the pituitary impairs feedback inhibition at the pituitary but not the central level and results in elevated corticosterone levels but reduced expression of *Crh* in the PVN (Schmidt et al., 2009). The finding that *Crh* expression is not reduced in *Trkb*$^{CCK\text{-}KO}$ mice despite the elevated corticosterone levels confirms that central disregulation is the reason for HPA axis hyperactivity in these mice and indicates that this is linked to impaired feedback-inhibition of glucocorticoids at a central level.

Avp expression was reduced in *Trkb*$^{CCK\text{-}KO}$ mice as would be expected in individuals with elevated glucocorticoid levels. Thus, glucocorticoid feedback inhibition is able to suppress *Avp* expression in *Trkb*$^{CCK\text{-}KO}$ mice, but not *Crh* expression. Differential effects of glucocorticoids on *Avp* and *Crh* expression have been reported before. *Avp* expression was shown to react in a more sensitive way to changes in glucocorticoid levels (Watts

2005). On the other hand, analysis of GR knockout mice suggests that GR at the hypothalamic level might rather regulate *Crh* than *Avp* expression, as only CRH was elevated in these animals (Schmidt et al., 2009).

In conclusion, *Trkb*$^{CCK\text{-}KO}$ mice show hyperactivity of the HPA axis that leads to chronic hypercortisolism. HPA axis activity is associated with increased PVN activity and impaired glucocorticoid feedback inhibition. Involvement of BDNF/TrkB in GR signalling and possible mechanisms for increased PVN activity in *Trkb*$^{CCK\text{-}KO}$ mice will be discussed in chapter 4.4.5.

4.4.2 Chronic hypercortisolism is the reason for obesity in *Trkb*$^{CCK\text{-}KO}$ mice

In humans chronic hypercortisolism is generally caused by adrenal or pituitary tumours or exogenous glucocorticoid administration and can then lead to development of Cushing's syndrome. Cushing's syndrome is characterized by central obesity, fat accumulation in the shoulder/neck region, hyperleptinemia, hyperinsulinemia, risk for development of diabetes type II, adrenal hyperplasia, muscle atrophy, thinning skin, decreased bone density and psychological disturbances (see also Introduction, chapter 1.4.1). *Trkb*$^{CCK\text{-}KO}$ mice were found to develop a Cushing's syndrome-like phenotype, as they have hypercortisolism with several of these characteristics. Therefore, the central obesity found in *Trkb*$^{CCK\text{-}KO}$ mice is a consequence of HPA axis hyperactivity and chronic hypercortisolism and not, as in other models of *Bdnf* or *Trkb* deficiency, due to hyperphagia and deregulation of melanocortin signalling.

It is controversial whether Cushing's syndrome is associated with hyperphagia or only changes in food preference in humans as it is difficult to reliably measure food intake in patients. In contrast to our findings, chronic hypercortisolism can induce hyperphagia in rodent models. For instance, chronic exogenous administration of corticosterone in mice induced hyperphagia and obesity (Karatsoreos 2010). As CRH has an anorexigenic effect but will be suppressed in these animals by the elevated corticosterone levels, this does not reflect an orexigenic action of corticosterone, but rather the suppression of the anorexigenic effects of CRH (Nieuwenhuizen et al. 2008, see also Introduction, chapter

1.4.1). In *Trkb*$^{CCK\text{-}KO}$ elevated corticosterone levels are a consequence of impaired central glucocorticoid feedback. *Crh* expression is increased rather than decreased in these animals and thus the anorexigenic effect of CRH is maintained.

How do glucocorticoids induce accumulation of adipose tissue? Hypercortisolism has been associated with development of obesity due to the fact that Cushing's syndrome and the metabolic syndrome share several symptoms such as central obesity, hyperleptinemia, hyperinsulinemia, development diabetes type II, and hypertension (Peeke et al. 1995, Pasquali et al. 2006, Anagnostis et al. 2009, see also Introduction, chapter 1.4.1). Obese individuals show increased activity of glucocorticoids in peripheral tissues, especially adipose tissue (Pasquali et al. 2006, Anagnostis et al. 2009). This might be sufficient to induce obesity as increased availability of cortisol in adipose tissue of mice was shown to induce an increase in fat mass (Masuzaki et al. 2001). A further indication that glucocorticoids could induce obesity without altering food intake is the finding that glucocorticoids can upregulate the NPY (neuropeptide Y) receptor in adipose tissue resulting in central obesity under conditions of stress-induced NPY release.

Our model thus confirms that chronic exposure to increased glucocorticoid levels is sufficient to induce obesity with resistance to leptin and insulin in the absence of altered energy intake.

4.4.3 Behavioural changes in *Trkb*$^{CCK\text{-}KO}$ mice

CCK-interneurons as well as BDNF/TrkB signalling were implicated in emotional responses and anxiety behaviour (see Introduction, chapter 1.1.4 and 1.2.2). These behaviours depend on the limbic system that then interacts with the hypothalamus, for instance, to activate the HPA axis in response to psychological stressors (Alberts et al., 2002; Joëls and Baram, 2009). BDNF has been implicated in increased activity of the HPA axis in response to social stress (Shalev et al., 2009). The BAC-CCK-Cre line shows recombination in the limbic system, raising the possibility that *Trkb*$^{CCK\text{-}KO}$ mice show hyperactivity of the HPA axis due to increased anxiety behaviour.

Innate anxiety behaviour was tested in the light-dark box paradigm (DLT), the elevated-plus maze (EPM) and the open field (OF). The open field was repeated on four consecutive days to test the ability to habituate to a new environment. Habituation to the open field is reflected by decreased locomotion (see for instance van Gaalen et al. 2002).

Trkb$^{CCK\text{-}KO}$ mice did not show any changes in anxiety behaviour, but showed increased locomotion on day 2-4 in the open field and also increased rearing. This suggests increased exploratory behaviour and increased arousal. The fact that locomotion in the open field did not decrease in the *Trkb*$^{CCK\text{-}KO}$ group might indicate absence of habituation – either to the open field or to handling when mice were placed in the open field. Indeed, *Trkb*$^{CCK\text{-}KO}$ mice seem more aggressive when handled and bite more than other mice. This was particularly apparent during repeated behaviour testing which usually leads to mice getting used to handling. To test whether increased locomotion was due to handling or changes in environment we attempted to analyze locomotion in the home cage by inframot. However, the data obtained from this experiment could not be used due to high variations between individuals (most probably due to not properly calibrated detectors). As locomotion was not significantly higher in the light box during DLT nor in the first day of the open field, the hyperlocomotion observed on day 2 to 4 is rather due to increased arousal caused by repeated handling and changing of environment. A further indication that *Trkb*$^{CCK\text{-}KO}$ mice might react differently to changes in their environment comes from the observation that female *Trkb*$^{CCK\text{-}KO}$ mice ate more in the first two hours after being transferred to metabolic cages.

We therefore conclude that *Trkb*$^{CCK\text{-}KO}$ mice are not more anxious but rather easily aroused, aggressive and, under conditions of increased stress and arousal, hyperactive. This confirms that increased HPA axis output in *Trkb*$^{CCK\text{-}KO}$ mice is related to hypothalamic mechanisms rather than to changes in upstream circuits as the limbic system. Aggressive behaviour was not further studied in *Trkb*$^{CCK\text{-}KO}$ mice. A possible explanation for this observation could be disinhibition of nuclei involved in regulating aggressive behaviour. For instance, numerous recombined cells were found in the

periaqueductal gray and the inferior and superior colliculus in the midbrain, both regions in which GABAergic interneurons are known to suppress aversive behaviour (Brandão et al., 1999).

4.4.4 *Trkb*$^{P/+}$ mice phenocopy *Trkb*$^{CCK\text{-}KO}$ mice

Downstream signalling pathways of BDNF/TrkB are activated by binding of adaptor proteins to two docking sites in the intracellular domain of TrkB. The Ras/mitogen-activated protein kinase pathway and the phosphatidylinositol 3-kinase pathway are activated by SHC/FRS-2 recruitment to Y515, and the calcium/calmodulin kinase pathway is activated by binding of phospholipase C (PLC) to Y816 (see Introduction, chapter 1.1.2 and Figure 1.1).

To assess which of these sites was involved in regulation of HPA axis activity body weight and thickness of the zona fasciculata of the adrenal cortex were analyzed in mouse lines with single point mutations in either adaptor site (*Trkb*^{SHC} and *Trkb*^{PLC} mice). Heterozygous point mutants were used for this analysis, as they do not show the developmental abnormalities in the PNS that are seen in homozygous point mutants (Minichiello et al. 1998 and 2002, Medina et al 2004, Musumeci et al. 2009). Basal synaptic transmission is normal in these mice confirming the absence of developmental defects in the CNS as well. However, heterozygous mutant show deficits in learning suggesting that more complex functions of TrkB in the CNS require both copies of a wildtype TrkB allele (Musumeci et al. 2009).

Trkb$^{PLC/+}$, but not *Trkb*$^{SHC/+}$ mice showed increased body weight and an enlarged zona fasciculata suggesting involvement of the PLC but not the SHC adaptor site in the regulation of HPA axis activity. *Trkb*$^{PLC/+}$ mice were further analyzed for changes in serum ACTH, leptin and insulin levels as well as central fat accumulation. Comparable to *Trkb*$^{CCK\text{-}KO}$ mice, obesity in *Trkb*$^{PLC/+}$ mice was associated with enlarged central fat pads and elevated serum ACTH, leptin and insulin and ACTH levels.

In conclusion, regulation of HPA axis activity by TrkB is dependent on signalling via the PLC adaptor site. As heterozygous point mutants did not show any developmental

defects so far, this finding also suggests that HPA axis regulation by TrkB depends on adult mechanisms and is not a consequence of developmental defects.

4.4.5 Mechanism of HPA axis deregulation in *Trkb*$^{CCK\text{-}KO}$ mice

We have so far shown that hyperactivity of the HPA axis in *Trkb*$^{CCK\text{-}KO}$ mice is caused by increased activity of the PVN and is associated with impaired glucocorticoid feedback inhibition on central levels resulting in increased *Crh* expression. This function of TrkB is dependent on activation of the PLCγ1 activated signalling pathways and related to adult mechanisms rather than caused by a developmental defect. This chapter will address the question how TrkB signalling in CCK-positive neurons might be involved in the regulation of PVN activity.

A more detailed analysis of the recombination pattern around the PVN in the *BAC-Cck-Cre* line revealed that only few cells were recombined in the PVN itself. This stands in contrast to findings of Giacobini and colleagues that found strong expression of CCK in the PVN (Giacobini et al. 2008). However, other studies find only few positive cells in the PVN comparable to the recombination pattern seen in the *BAC-CCK-Cre* line (Schiffmann et al. 1991, Lein et al. 2007). Numerous recombined neurons were found rostral to the PVN in the bed nucleus of the stria terminalis, the medial preoptic area, in the peri-PVN (including the border of the PVN, a cluster in the rostromedial anterior hypothalamic nucleus, the subparaventricular zone and perifornical regions), and caudal to the PVN in the dorsomedial nucleus of the hypothalamus. A ring of GABAergic neurons that is located around the PVN, in exactly all of these regions, has been reported. Inhibitory neurons in this ring integrate glutamatergic and GABAergic inputs from limbic areas and exert tonic inhibition over the PVN that is only lifted under stressful conditions (Bowers et al. 1998, Herman et al. 2002, Cullinan et al. 1993 and 2008, Cole et al. 2002, Hewitt et al. 2009, Wamsteeker et al. 2010, see also Introduction, chapter 1.4.1). The majority of recombined neurons in this region in the *BAC-CCK-Cre* line are GABAergic suggesting that they are part of this inhibitory ring.

Consequently, increased PVN activity in *Trkb*$^{CCK\text{-}KO}$ mice is caused by reduced tonic inhibition of the PVN due to deletion of *Trkb* from local inhibitory interneurons. This is an interneuron-specific function of *Trkb,* as deletion of *Trkb* from principal neurons does not affect HPA axis function (Zorner et al. 2003). Therefore, involvement of principal neurons found to be recombined in the *BAC-CCK-Cre* line in the phenotype observed here could be excluded. TrkB was reported to be required for synapse assembly and maintenance in GABAergic neurons of the cerebellum (Chen et al. 2011). Thus, ablation of *Trkb* from hypothalamic CCK-interneurons might affect pre- and/or postsynapses in these neurons. A presynaptic defect would reduce the number or strength of GABAergic synapses onto PVN neurons. This could be investigated by triple labelling for CRH (to highlight PVN neurons), gephyrin, a marker for inhibitory postsynapses, and VGAT (vesicular GABA transporter), a marker for GABAergic presynapses. However, only few cells with a cytoplasmic CRH staining were detected in the PVN of sections stained for CRH. Injections with colchicine prior to tissue collection would increase CRH immunoreactivity as colchicine inhibits axonal transport. Unfortunately, colchicine was shown to alter dendritic length and spines which might alter synapse number and characteristics (Rho and Swanson, 1989). Postsynaptic effects of *Trkb* deletion could be investigated on a reporter background (to highlight CCK-interneurons) with colocalization of EGFP and markers for excitatory synapses like PSD-95 (postsynaptic density protein 95), presynaptic VGLUT1 (vesicular glutamate transporter 1) and markers for inhibitory synapses (gephyrin and VGAT as described above). For this analysis, we are still waiting to obtain reporter mice on the mutant background.

HPA axis activity is also tightly controlled by glucocorticoid feedback inhibition at pituitary and central levels (Watts 2005, see also Introduction chapter 1.4.1). Glucocorticoid feedback inhibition is mainly dependent on binding of the glucocorticoid receptor (GR), not the mineralocorticoid receptor (Ulrich-Lai et al. 2009, Joels et al. 2009), but the region and cell-type mediating this effect is still not established (see Introduction chapter 1.4.1). Recombined neurons in the peri-PVN of *BAC-CCK-Cre* mice

colocalize with the GR, raising the possibility that these neurons might integrate glucocorticoid negative feedback. Indeed, the absence of reduced *Crh* expression by elevated corticosterone levels in $Trkb^{CCK\text{-}KO}$ mice suggests impaired glucocorticoid feedback inhibition. TrkB was reported to interact directly with the GR via the N-terminal domain of the GR and this enhanced phosphorylation of PLCγ1 by BDNF/TrkB signalling (Numakawa et al. 2009). TrkB signalling via the PLC adaptor site is involved in inhibitory control of the HPA axis since we found that mice with a heterozygous single point mutation in this site develop the same phenotype as $Trkb^{CCK\text{-}KO}$ mice.

This strongly suggests, that TrkB interacts with the GR in inhibitory CCK-interneurons in the hypothalamus to mediate glucocorticoid feedback via PLCγ1 signalling. An action of glucocorticoids rather upstream than directly onto parvocellular neurons to suppress *Crh* expression has been suggested before. For instance, administration of corticosterone directly into the PVN had little effect on *Crh* expression (Watts 2005). Furthermore, the GR was shown to not only act via direct DNA binding but also by interaction with other receptors (TrkB for instance) in a DNA-binding independent mechanism. Mice with a mutation in the GR dimerization domain that is required for DNA binding showed no differences in *Crh* synthesis and ACTH secretion, suggesting that these functions are regulated by the GR via a DNA-binding independent mechanism. Therefore, we suggest that glucocorticoid feedback is integrated by upstream inhibitory CCK-interneurons in which the GR interacts with TrkB. Increased or decreased inhibitory input of these neurons into the PVN then decreases or increases parvocellular neuron activity. This alone might regulate *Crh* expression, as the *Crh* promotor contains a CRE (CREB-responsive element) that was shown to regulate *Crh* expression (Wölfl et al., 1999) and CREB is activated in PVN neurons in response to neuronal activity (Kovács and Sawchenko, 1996).

Gender differences were observed in several instances. The HPA axis is known to be differentially regulated in male and female rodents. For instance, female mice have

bigger adrenals with a thicker zona fasciculata (Bielohuby et al., 2007) and show increased corticosterone release under basal and stressful conditions (Lightman et al. 2010, see also Figure 1.4). This pattern is reversed by gonadectomy confirming the influence of sex hormones on HPA axis regulation (Seale et al., 2004). Increased expression of the GR and the GABA-synthesizing enzymes Gad65 and Gad67 in stress-responsive areas in male mice might allow for greater inhibitory modulation and feedback potential in males (Goel and Bale, 2010). Furthermore, a marked difference in the presynaptic innervation of the PVN, BST and amygdala was found between genders. Female mice showed higher synaptophysin staining in these areas and chronic stress reduced staining intensity in females but not males (Carvalho-Netto et al., 2011). Thus, the gender differences observed in this study are caused by known sex-dependent differences in the regulation of HPA axis activity.

4.5 Conclusion

In this study the role of the neurotrophin receptor TrkB in a specific subset of interneurons was investigated. For this, *Trkb* was specifically ablated from cholecystokinin (CCK)-expressing neurons by crossing a transgenic BAC-Cre mouse line that expresses Cre under the *Cck*-promotor to a *Trkb-floxed* mouse line. The *BAC-CCK-Cre* line showed particularly high recombination in hypothalamic nuclei involved in control of energy intake and regulation of the hypothalamic-pituitary-adrenal (HPA) axis. CCK-Cre specific *Trkb* knockout mice ($Trkb^{CCK\text{-}KO}$ mice) develop mature-onset central obesity with hyperleptinemia and increased insulin levels but show no signs of hyperphagia or other changes in food intake. The absence of hyperphagia stands in contrast to other models of *Bdnf* or *Trkb* deficiency and shows that BDNF/TrkB signalling in the CCK-positive subset of hypothalamic interneurons is not involved in control of energy intake. Disruption of TrkB signalling in CCK-positive interneurons induces instead hyperactivity of the HPA axis with elevated serum adrenocorticotropic hormone (ACTH) and corticosterone levels, hypercortisolism and hypertrophy of the adrenal cortex. Chronic hypercortisolism is known to induce central obesity and glucocorticoids

were suggested to increase accumulation of adipose tissue. Therefore, the central obesity found in *Trkb*$^{CCK\text{-}KO}$ mice is a consequence of HPA axis hyperactivity and confirms that chronic exposure to increased glucocorticoid levels is sufficient to induce obesity.

The main central regulator of HPA axis activity is the paraventricular nucleus of the hypothalamus (PVN). Expression of corticotropin-releasing hormone (*Crh*) and pro-enkephalin (*Penk*) is increased in the PVN of *Trkb*$^{CCK\text{-}KO}$ mice indicating increased PVN activity. The PVN is under tonic inhibition of local inhibitory interneurons that were targeted in the *BAC-CCK-Cre* line. Thus, deletion of *Trkb* from hypothalamic inhibitory CCK-interneurons leads to decreased inhibitory control over the PVN and hyperactivity of the HPA axis in *Trkb*$^{CCK\text{-}KO}$ mice.

HPA axis activity is also controlled by negative feedback inhibition of glucocorticoids via the glucocorticoid receptor (GR). Particularly *Crh* expression in the PVN is known to be reduced by elevated glucocorticoid levels. The finding that *Trkb*$^{CCK\text{-}KO}$ mice show increased *Crh* expression in the PVN despite elevated serum corticosterone levels is an indication for impaired hypothalamic glucocorticoid feedback in these animals. TrkB and the GR can interact directly enhancing BDNF-activated TrkB signalling through the PLC adaptor site of TrkB. Analysis of mice with a point mutation in the TrkB-PLC adaptor site revealed that these mice phenocopy *Trkb*$^{CCK\text{-}KO}$ mice. This suggests that TrkB interacts with the GR in CCK-interneurons to mediate glucocorticoid feedback via PLCγ1 signalling. In *Trkb*$^{CCK\text{-}KO}$ mice deletion of *Trkb* from these neurons impairs glucocorticoid feedback and reduces inhibitory input into PVN neurons resulting in HPA axis hyperactivity.

Thus, this study shows that CCK-expressing inhibitory interneurons in the hypothalamus regulate PVN and HPA axis activity. Furthermore, we found a hitherto unknown role of TrkB in mediating central glucocorticoid feedback inhibition in these interneurons.

4.6 Outlook

Further studies will investigate possible effects of *Trkb* deletion on pre- and postsynapses of hypothalamic interneurons. Inhibitory synapses onto CRH-expressing PVN neurons and synapses onto targeted hypothalamic CCK-interneurons will be analyzed as discussed in chapter 4.4.5. The *BAC-CCK-Cre* line used here shows recombination from developmental stages on. The finding that $Trkb^{PLC/+}$ mice share the same phenotype suggests that the mechanisms involved in TrkB-mediated regulation of HPA axis activity are independent of development as these mice were shown to have no developmental deficits in synaptic transmission. An inducible Cre-line could be used to exclude developmental effects and to study how TrkB is involved in maintenance of GABAergic synapses. To further investigate TrkB functions in CCK-interneurons it would also be interesting to compare the transcriptome of CCK-positive interneurons in mutant and wildtype mice.

Several regions involved in inhibitory control of the PVN were targeted in the *BAC-CCK-Cre* line, such as the bed nucleus of the stria terminalis, the medial preoptic area, the peri-PVN and the DMH. The wide recombination in this line prevents a more detailed analysis of the involvement of the single regions in control of PVN activity. More restrictive Cre-lines might be used here, but no specific markers are known for the single nuclei yet. Another possibility would be to inject viral vectors containing a Cre-cassette into single regions.

The *BAC-CCK-Cre* line used for this study might also be used to study other functions of CCK-neurons. For instance, we found recombination in numerous brain regions in which no function for CCK-neurons is known. Furthermore, CCK-neuron specific functions of other proteins could be studied by crossing other floxed lines to the *BAC-CCK-Cre* line.

ABBREVIATIONS

ACTH	adrenocorticotropic hormone
AHN	anterior hypothalamic area, see also dmAHN
Akt	protein kinase B, PKB
AIS	axon initial segment
AMPA	alpha-amino-3-hydroxy-5-methyl-4-isoxazole propionate
AMPAR	AMPA receptor
ARC	arcuate nucleus
AVP	arginine-vasopressin
BDNF	brain-derived neurotrophic factor
BST	bed nucleus of the stria terminalis
CamK	Ca^{2+}/calmodulin-dependent protein kinase
CCK	cholecystokinin
CGE	caudal ganglionic eminence
CR	calretinin
CREB	cAMP responsive element binding protein
CRH	corticotropin-releasing hormone
DAB	3'3- diaminobenzidine
DAG	diacylglycerol
DIG	digoxigenin
dmAHN	dorsomedial AHN
DMH	dorsomedial hypothalamus
EDTA	ethylene diaminetetraacetic acid
EIA	enzyme immunoassay
ELISA	enzyme-linked immunosorbent assay
ERK	extracellular signal-regulated kinsase, a MAP kinase
EtOH	ethanol
FRS2	fibroblast growth factor receptor substrate 2
GABA	γ-aminobutyric acid
Gad	glutamate decarboxylase
GEF	guanine nucleotide exchange factor
GLUR	glutamate receptor
GR	glucocorticoid receptor
GRB2	growth factor receptor-bound protein 2
GTP	guanosine triphosphate
HFD	high fat diet
HPA axis	hypothalamic-pituitary-adrenal axis
IP3	inositol 1,4,5-trisphosphate
LGE	lateral ganglionic eminence
LHA	lateral hypothalamus
LTP	long-term potentiation

MAPK	mitogen-activated protein kinase
MEK	MAP kinase kinase
MEKK	MAP kinase kinase kinase
MGE	medial ganglionic eminence
NGF	nerve growth factor
NMDA	N-methyl D-aspartate
NMDAR	NMDA receptor
NPY	neuropeptide Y
NT	neurotrophin
NTS	nucleus tractus solitarius
o/n	over night
p75NTR	p75 neurotrophin receptor
PDK-1	inositide-dependent protein kinase
PENK	pro-enkephalin
PI3K	phosphatidylinositol 3-kinase
PKB	protein kinase B
PLC	phospholipase C
POA	preoptic area
POMC	pro-opiomelanocortin
PTB	phosphotyrosine-binding domain
PV	parvalbumin
PVN	paraventricular nucleus of the hypothalamus
Ras	rat sarcoma
RIA	radioimmunoassay
RSK	ribosomal s6 kinase
RT	room temperature
SH2	Src homology 2 protein domain
SHC	Sh2-domain containing
SOS	son of sevenless (a GEF)
SST	somatostatin
Trk	tropomyosin-receptor kinase
VIP	vasointestinal peptide
(v/v)	volume per volume
(w/v)	weight per volume

REFERENCES

Abramoff MD, Magalhaes PJ, Ram SJ (2004) *Image Processing with ImageJ*. Biophotonics International 11:36–42.

Aguado F, Carmona MA, Pozas E, Aguiló A, Martínez-Guijarro FJ, Alcántara S, Borrell V, Yuste R, Ibañez CF, Soriano E (2003) *BDNF regulates spontaneous correlated activity at early developmental stages by increasing synaptogenesis and expression of the K+/Cl- co-transporter KCC2.* Development 130:1267–1280.

Alberts, Johnson, Lewis, Raff, Roberts, Walter (2002) *Molecular Biology of the Cell*, 4th ed. New York: Garland Science.

Alcántara S, Frisén J, del Río J a, Soriano E, Barbacid M, Silos-Santiago I (1997) *TrkB signaling is required for postnatal survival of CNS neurons and protects hippocampal and motor neurons from axotomy-induced cell death*. J Neurosci 17:3623–3633.

Anagnostis P, Athyros VG, Tziomalos K, Karagiannis A, Mikhailidis DP (2009) *Clinical review: The pathogenetic role of cortisol in the metabolic syndrome: a hypothesis*. J Clin Endocrinol Metab 94:2692–2701.

Ascoli GA et al. (2008) *Petilla terminology: nomenclature of features of GABAergic interneurons of the cerebral cortex*. Nat Rev Neurosci 9:557–568.

Baldelli P, Hernandez-Guijo J-M, Carabelli V, Carbone E (2005) *Brain-derived neurotrophic factor enhances GABA release probability and nonuniform distribution of N- and P/Q-type channels on release sites of hippocampal inhibitory synapses*. J Neurosci 25:3358–3368.

Balthasar N et al. (2005) *Divergence of melanocortin pathways in the control of food intake and energy expenditure*. Cell 123:493–505.

Barbacid M (1995) *Structural and functional properties of the TRK family of neurotrophin receptors.* Ann N Y Acad Sci 766:442–458.

Bariohay B, Lebrun B, Moyse E, Jean A (2005) *Brain-derived neurotrophic factor plays a role as an anorexigenic factor in the dorsal vagal complex*. Endocrinology 146:5612–5620.

Bariohay B, Roux J, Tardivel C, Trouslard J, Jean A, Lebrun B (2009) *Brain-derived neurotrophic factor/tropomyosin-related kinase receptor type B signaling is a*

downstream effector of the brainstem melanocortin system in food intake control. Endocrinology 150:2646–2653.

Beinfeld MC (2001) *An introduction to neuronal cholecystokinin*. Peptides 22:1197–1200.

Belgardt BF, Brüning JC (2010) *CNS leptin and insulin action in the control of energy homeostasis*. Ann N Y Acad Sci 1212:97–113.

Ben-Ari Y (2001) *Developing networks play a similar melody*. Trends Neurosci 24:353–360.

Berger S, Wolfer DP, Selbach O, Alter H, Erdmann G, Reichardt HM, Chepkova AN, Welzl H, Haas HL, Lipp H-P, Schütz G (2006) *Loss of the limbic mineralocorticoid receptor impairs behavioral plasticity*. PNAS 103:195–200.

Berghuis P, Dobszay MB, Sousa KM, Schulte G, Mager PP, Härtig W, Görcs TJ, Zilberter Y, Ernfors P, Harkany T (2004) *Brain-derived neurotrophic factor controls functional differentiation and microcircuit formation of selectively isolated fast-spiking GABAergic interneurons*. Eur J Neurosci 20:1290–1306.

Berghuis P, Dobszay MB, Wang X, Spano S, Ledda F, Sousa KM, Schulte G, Ernfors P, Mackie K, Paratcha G, Hurd YL, Harkany T (2005) *Endocannabinoids regulate interneuron migration and morphogenesis by transactivating the TrkB receptor*. PNAS 102:19115–19120.

Bibel M, Barde YA (2000) *Neurotrophins: key regulators of cell fate and cell shape in the vertebrate nervous system*. Genes Dev 14:2919–2937.

Bibel M, Hoppe E, Barde YA (1999) *Biochemical and functional interactions between the neurotrophin receptors trk and p75NTR*. EMBO J 18:616–622.

Bielohuby M, Herbach N, Wanke R, Maser-Gluth C, Beuschlein F, Wolf E, Hoeflich A (2007) *Growth analysis of the mouse adrenal gland from weaning to adulthood: time- and gender-dependent alterations of cell size and number in the cortical compartment*. Am J Physiol Endocrinol Metab 293:E139–E146.

Blackshaw S, Scholpp S, Placzek M, Ingraham H, Simerly R, Shimogori T (2010) *Molecular pathways controlling development of thalamus and hypothalamus: from neural specification to circuit formation*. J Neurosci 30:14925–14930.

von Bohlen und Halbach O, Minichiello L, Unsicker K (2008) *TrkB but not trkC receptors are necessary for postnatal maintenance of hippocampal spines*. Neurobiol Aging 29:1247–1255.

Bonni A, Brunet A, West AE, Datta SR, Takasu MA, Greenberg ME (1999) *Cell survival promoted by the Ras-MAPK signaling pathway by transcription-dependent and -independent mechanisms.* Science 286:1358–1362.

Bowers G, Cullinan WE, Herman JP (1998) *Region-specific regulation of glutamic acid decarboxylase (GAD) mRNA expression in central stress circuits*. J Neurosci 18:5938–5947.

Boyle MP, Brewer J a, Funatsu M, Wozniak DF, Tsien JZ, Izumi Y, Muglia L (2005) *Acquired deficit of forebrain glucocorticoid receptor produces depression-like changes in adrenal axis regulation and behavior.* PNAS 102:473–478.

Boyle MP, Kolber BJ, Vogt SK, Wozniak DF, Muglia L (2006) *Forebrain glucocorticoid receptors modulate anxiety-associated locomotor activation and adrenal responsiveness.* J Neurosci 26:1971–1978.

Bradbury MW, Burden J, Hillhouse EW, Jones MT (1974) *Stimulation electrically and by acetylcholine of the rat hypothalamus in vitro*. J Physiol 239:269–283.

Brandão ML, Anseloni VZ, Pandóssio JE, De Araújo JE, Castilho VM (1999) *Neurochemical mechanisms of the defensive behavior in the dorsal midbrain.* Neurosci Biobehav Rev 23:863–875.

Brigadski T, Hartmann M, Lessmann V (2005) *Differential vesicular targeting and time course of synaptic secretion of the mammalian neurotrophins*. J Neurosci 25:7601–7614.

Brunet A, Bonni A, Zigmond MJ, Lin MZ, Juo P, Hu LS, Anderson MJ, Arden KC, Blenis J, Greenberg ME (1999) *Akt promotes cell survival by phosphorylating and inhibiting a Forkhead transcription factor*. Cell 96:857–868.

Brunet A, Kanai F, Stehn J, Xu J, Sarbassova D, Frangioni JV, Dalal SN, DeCaprio JA, Greenberg ME, Yaffe MB (2002) *14-3-3 transits to the nucleus and participates in dynamic nucleocytoplasmic transport.* J Cell Biol 156:817–828.

Burgunder JM, Young 3rd WS (1990) *Cortical neurons expressing the cholecystokinin gene in the rat: distribution in the adult brain, ontogeny, and some of their projections.* J Comp Neurol 300:26–46.

Butte MJ (2001) *Neurotrophic factor structures reveal clues to evolution, binding, specificity, and receptor activation*. Cell Mol Life Sci 58:1003–1013.

Carmona MA, Martínez A, Soler A, Blasi J, Soriano E, Aguado F (2003) *Ca(2+)-evoked synaptic transmission and neurotransmitter receptor levels are impaired in the forebrain of trkb (-/-) mice.* Mol Cell Neurosci 22:210–226.

Carmona MA, Pozas E, Martinez A, Espinosa-Parrilla JF, Soriano E, Aguado F (2006) *Age-dependent spontaneous hyperexcitability and impairment of GABAergic function in the hippocampus of mice lacking trkB*. Cereb Cortex 16:47–63.

Carvalho-Netto EF, Myers B, Jones K, Solomon MB, Herman JP (2011) *Sex differences in synaptic plasticity in stress-responsive brain regions following chronic variable stress.* Physiol Behav 104:242–247.

Cellerino A, Maffei L, Domenici L (1996) *The distribution of brain-derived neurotrophic factor and its receptor trkB in parvalbumin-containing neurons of the rat visual cortex.* Eur J Neurosci 8:1190–1197.

Chen AI, Nguyen CN, Copenhagen DR, Badurek S, Minichiello L, Ranscht B, Reichardt LF (2011) *TrkB (tropomyosin-related kinase B) controls the assembly and maintenance of GABAergic synapses in the cerebellar cortex*. J Neurosci 31:2769–2780.

Chen KS, Nishimura MC, Armanini MP, Crowley C, Spencer SD, Phillips HS (1997) *Disruption of a single allele of the nerve growth factor gene results in atrophy of basal forebrain cholinergic neurons and memory deficits*. J Neurosci 17:7288–7296.

Cole RL, Sawchenko PE (2002) *Neurotransmitter regulation of cellular activation and neuropeptide gene expression in the paraventricular nucleus of the hypothalamus.* J Neurosci 22:959–969.

Cone RD (2005) *Anatomy and regulation of the central melanocortin system*. Nat Neurosci 8:571–578.

Cone RD, Cowley MA, Butler AA, Fan W, Marks DL, Low MJ (2001) *The arcuate nucleus as a conduit for diverse signals relevant to energy homeostasis*. Int J Obes Relat Metab Disord 25 Suppl 5:S63–S67.

Conover JC, Erickson JT, Katz DM, Bianchi LM, Poueymirou WT, McClain J, Pan L, Helgren M, Ip NY, Boland P (1995) *Neuronal deficits, not involving motor neurons, in mice lacking BDNF and/or NT4*. Nature 375:235–238.

Corbit KC, Foster DA, Rosner MR (1999) *Protein kinase Cdelta mediates neurogenic but not mitogenic activation of mitogen-activated protein kinase in neuronal cells.* Mol Cell Biol 19:4209–4218.

Cowley MA, Pronchuk N, Fan W, Dinulescu DM, Colmers WF, Cone RD (1999) *Integration of NPY, AGRP, and melanocortin signals in the hypothalamic paraventricular nucleus: evidence of a cellular basis for the adipostat*. Neuron 24:155–163.

Cowley MA, Smart JL, Rubinstein M, Cerdán MG, Diano S, Horvath TL, Cone RD, Low MJ (2001) *Leptin activates anorexigenic POMC neurons through a neural network in the arcuate nucleus*. Nature 411:480–484.

Crowley C, Spencer SD, Nishimura MC, Chen KS, Pitts-Meek S, Armanini MP, Ling LH, McMahon SB, Shelton DL, Levinson AD (1994) *Mice lacking nerve growth factor display perinatal loss of sensory and sympathetic neurons yet develop basal forebrain cholinergic neurons.* Cell 76:1001–1011.

Cullinan WE, Herman JP, Watson SJ (1993) *Ventral subicular interaction with the hypothalamic paraventricular nucleus: evidence for a relay in the bed nucleus of the stria terminalis.* J Comp Neurol 332:1–20.

Cullinan WE, Ziegler DR, Herman JP (2008) *Functional role of local GABAergic influences on the HPA axis.* Brain Struct Funct 213:63–72.

Dalvi PS, Nazarians-Armavil A, Tung S and Belsham DD (2011) *Immortalized neurons for the study of hypothalamic function*. Am J Physiol Regul Integr Comp Physiol 300, R1030-52.

Datta SR, Dudek H, Tao X, Masters S, Fu H, Gotoh Y, Greenberg ME (1997) *Akt phosphorylation of BAD couples survival signals to the cell-intrinsic death machinery.* Cell 91:231–241.

Datta SR, Katsov A, Hu L, Petros A, Fesik SW, Yaffe MB, Greenberg ME (2000) *14-3-3 proteins and survival kinases cooperate to inactivate BAD by BH3 domain phosphorylation.* Mol Cell 6:41–51.

DeFelipe J (1999) *Chandelier cells and epilepsy*. Brain 122 (Pt 1:1807–1822.

Dickie M (1975) *Keeping Records. In Biology of the Laboratory Mouse* (Green E, ed)., 1st ed. New York: Dover Publications.

Douville E, Downward J (1997) *EGF induced SOS phosphorylation in PC12 cells involves P90 RSK-2.* Oncogene 15:373–383.

Drake CT, Milner TA, Patterson SL (1999) *Ultrastructural localization of full-length trkB immunoreactivity in rat hippocampus suggests multiple roles in modulating activity-dependent synaptic plasticity*. J Neurosci 19:8009–8026.

Drolet G, Rivest S (2001) *Corticotropin-releasing hormone and its receptors; an evaluation at the transcription level in vivo*. Peptides 22:761–767.

Duan W (2003) *Reversal of Behavioral and Metabolic Abnormalities, and Insulin Resistance Syndrome, by Dietary Restriction in Mice Deficient in Brain-Derived Neurotrophic Factor*. Endocrinology 144:2446–2453.

Dumont EC, Kinkead R, Trottier JF, Gosselin I, Drolet G (2000) *Effect of chronic psychogenic stress exposure on enkephalin neuronal activity and expression in the rat hypothalamic paraventricular nucleus.* J Neurochem 75:2200–2211.

Eckel RH, Alberti KGMM, Grundy SM, Zimmet PZ (2010) *The metabolic syndrome.* Lancet 375:181–183.

Eide FF, Vining ER, Eide BL, Zang K, Wang XY, Reichardt LF (1996) *Naturally occurring truncated trkB receptors have dominant inhibitory effects on brain-derived neurotrophic factor signaling.* J Neurosci 16:3123–3129.

Elmariah SB, Crumling M a, Parsons TD, Balice-Gordon RJ (2004) *Postsynaptic TrkB-mediated signaling modulates excitatory and inhibitory neurotransmitter receptor clustering at hippocampal synapses*. J Neurosci 24:2380–2393.

Ernfors P, Lee KF, Jaenisch R (1994) *Mice lacking brain-derived neurotrophic factor develop with sensory deficits*. Nature 368:147–150.

Fagan AM, Zhang H, Landis S, Smeyne RJ, Silos-Santiago I, Barbacid M (1996) *TrkA, but not TrkC, receptors are essential for survival of sympathetic neurons in vivo.* J Neurosci 16:6208–6218.

Fan G, Copray S, Huang EJ, Jones K, Yan Q, Walro J, Jaenisch R, Kucera J (2000) *Formation of a full complement of cranial proprioceptors requires multiple neurotrophins*. Dev Dyn 218:359–370.

Fariñas I, Jones KR, Backus C, Wang XY, Reichardt LF (1994) *Severe sensory and sympathetic deficits in mice lacking neurotrophin-3.* Nature 369:658–661.

Fariñas I, Jones KR, Tessarollo L, Vigers AJ, Huang E, Kirstein M, de Caprona DC, Coppola V, Backus C, Reichardt LF, Fritzsch B (2001) *Spatial shaping of cochlear*

innervation by temporally regulated neurotrophin expression. J Neurosci 21:6170–6180.

Felig F, Frohman LA (2001) *Endocrinology & Metabolism*, 4th ed. McGraw-Hill Medical.

Fernandez-Rodriguez E, Stewart PM, Cooper MS (2009) *The pituitary-adrenal axis and body composition.* Pituitary 12:105–115.

Fink H, Rex A, Voits M, Voigt JP (1998) *Major biological actions of CCK--a critical evaluation of research findings.* Exp Brain Res 123:77–83.

Finkbeiner S, Tavazoie SF, Maloratsky a, Jacobs KM, Harris KM, Greenberg ME (1997) *CREB: a major mediator of neuronal neurotrophin responses*. Neuron 19:1031–1047.

Freund TF (2003) *Interneuron Diversity series: Rhythm and mood in perisomatic inhibition.* Trends Neurosci 26:489–495.

Freund TF, Katona I (2007) *Perisomatic inhibition*. Neuron 56:33–42.

Fryer RH, Kaplan DR, Feinstein SC, Radeke MJ, Grayson DR, Kromer LF (1996) *Developmental and mature expression of full-length and truncated TrkB receptors in the rat forebrain*. J Comp Neurol 374:21–40.

Gao Q, Horvath TL (2008) *Neuronal control of energy homeostasis*. FEBS Lett 582:132–141.

Gelman DM, Marín O (2010) *Generation of interneuron diversity in the mouse cerebral cortex*. Eur J Neurosci 31:2136–2141.

Giacobini P, Wray S (2008) *Prenatal expression of cholecystokinin (CCK) in the central nervous system (CNS) of mouse*. Neurosci Lett 438:96–101.

Givalois L, Arancibia S, Alonso G, Tapia-Arancibia L (2004a) *Expression of brain-derived neurotrophic factor and its receptors in the median eminence cells with sensitivity to stress*. Endocrinology 145:4737–4747.

Givalois L, Marmigère F, Rage F, Ixart G, Arancibia S, Tapia-Arancibia L (2001) *Immobilization stress rapidly and differentially modulates BDNF and TrkB mRNA expression in the pituitary gland of adult male rats*. Neuroendocrinology 74:148–159.

Givalois L, Naert G, Rage F, Ixart G, Arancibia S, Tapia-Arancibia L (2004b) *A single brain-derived neurotrophic factor injection modifies hypothalamo-pituitary-adrenocortical axis activity in adult male rats.* Mol Cell Neurosci 27:280–295.

Goel N, Bale TL (2010) *Sex differences in the serotonergic influence on the hypothalamic-pituitary-adrenal stress axis*. Endocrinology 151:1784–1794.

Gorba T, Wahle P (1999) *Expression of TrkB and TrkC but not BDNF mRNA in neurochemically identified interneurons in rat visual cortex in vivo and in organotypic cultures*. Eur J Neurosci 11:1179–1190.

Groenink L, Dirks A, Verdouw PM, Schipholt M, Veening JG, van der Gugten J, Olivier B (2002) *HPA axis dysregulation in mice overexpressing corticotropin releasing hormone*. Biol Psychiatry 51:875–881.

Gropp E, Shanabrough M, Borok E, Xu AW, Janoschek R, Buch T, Plum L, Balthasar N, Hampel B, Waisman A, Barsh GS, Horvath TL, Brüning JC (2005) *Agouti-related peptide-expressing neurons are mandatory for feeding.* Nat Neurosci 8:1289–1291.

Gärtner A, Polnau DG, Staiger V, Sciarretta C, Minichiello L, Thoenen H, Bonhoeffer T, Korte M, Gartner A (2006) *Hippocampal long-term potentiation is supported by presynaptic and postsynaptic tyrosine receptor kinase B-mediated phospholipase Cgamma signaling.* J Neurosci 26:3496–3504.

Hashimoto T, Bergen SE, Nguyen QL, Xu B, Monteggia LM, Pierri JN, Sun Z, Sampson AR, Lewis DA (2005) *Relationship of brain-derived neurotrophic factor and its receptor TrkB to altered inhibitory prefrontal circuitry in schizophrenia.* J Neurosci 25:372–383.

Hefti F, Hartikka J, Knusel B (1989) *Function of neurotrophic factors in the adult and aging brain and their possible use in the treatment of neurodegenerative diseases*. Neurobiol Aging 10:515–533.

Heinrichs SC, Menzaghi F, Pich EM, Hauger RL, Koob GF (1993) *Corticotropin-releasing factor in the paraventricular nucleus modulates feeding induced by neuropeptide Y*. Brain Res 611:18–24.

Hendry SH, Jones EG, DeFelipe J, Schmechel D, Brandon C, Emson PC (1984) *Neuropeptide-containing neurons of the cerebral cortex are also GABAergic*. PNAS 81:6526–6530.

Herman JP (2003) *Central mechanisms of stress integration: hierarchical circuitry controlling hypothalamo–pituitary–adrenocortical responsiveness.* Front Neuroendocrinol 24:151–180.

Herman JP, Flak JN, Jankord R (2008) *Chronic stress plasticity in the hypothalamic paraventricular nucleus*. Prog Brain Res 170:353–364.

Herman JP, Mueller NK (2006) *Role of the ventral subiculum in stress integration*. Behav Brain Res 174:215–224.

Herman JP, Tasker JG, Ziegler DR, Cullinan WE (2002) *Local circuit regulation of paraventricular nucleus stress integration: glutamate-GABA connections*. Pharmacol Biochem Behav 71:457–468.

Hewitt SA, Bains JS (2006) *Brain-derived neurotrophic factor silences GABA synapses onto hypothalamic neuroendocrine cells through a postsynaptic dynamin-mediated mechanism*. J Neurophysiol 95:2193–2198.

Hewitt SA, Wamsteeker JI, Kurz EU, Bains JS (2009) *Altered chloride homeostasis removes synaptic inhibitory constraint of the stress axis*. Nat Neurosci 12:438–443.

Heym C, Braun B, Shuyi Y, Klimaschewski L, Colombo-Benkmann M (1995) *Immunohistochemical correlation of human adrenal nerve fibres and thoracic dorsal root neurons with special reference to substance P*. Histochem Cell Biol 104:233–243.

Holgado-Madruga M, Moscatello DK, Emlet DR, Dieterich R, Wong AJ (1997) *Grb2-associated binder-1 mediates phosphatidylinositol 3-kinase activation and the promotion of cell survival by nerve growth factor*. PNAS 94:12419–12424.

Holtzman DM, Kilbridge J, Li Y, Cunningham ET, Lenn NJ, Clary DO, Reichardt LF, Mobley WC (1995) *TrkA expression in the CNS: evidence for the existence of several novel NGF-responsive CNS neurons*. J Neurosci 15:1567–1576.

Huang EJ, Reichardt LF (2001) *Neurotrophins: roles in neuronal development and function*. Annu Rev Neurosci 24:677–736.

Huang EJ, Reichardt LF (2003) *Trk receptors: roles in neuronal signal transduction*. Annu Rev Biochem 72:609–642.

Huang YZ, Pan E, Xiong Z-Q, McNamara JO (2008) *Zinc-mediated transactivation of TrkB potentiates the hippocampal mossy fiber-CA3 pyramid synapse*. Neuron 57:546–558.

Huang ZJ, Di Cristo G, Ango F (2007) *Development of GABA innervation in the cerebral and cerebellar cortices*. Nat Rev Neurosci 8:673–686.

Huang ZJ, Kirkwood A, Pizzorusso T, Porciatti V, Morales B, Bear MF, Maffei L, Tonegawa S (1999) *BDNF regulates the maturation of inhibition and the critical period of plasticity in mouse visual cortex*. Cell 98:739–755.

Hökfelt T, Skirboll L, Everitt B, Meister B, Brownstein M, Jacobs T, Faden A, Kuga S, Goldstein M, Markstein R (1985) *Distribution of cholecystokinin-like immunoreactivity in the nervous system. Co-existence with classical neurotransmitters and other neuropeptides.* Ann N Y Acad Sci 448:255–274.

Jankord R, Herman JP (2008) *Limbic regulation of hypothalamo-pituitary-adrenocortical function during acute and chronic stress*. Ann N Y Acad Sci 1148:64–73.

Jin X, Hu H, Mathers PH, Agmon A (2003) *Brain-derived neurotrophic factor mediates activity-dependent dendritic growth in nonpyramidal neocortical interneurons in developing organotypic cultures.* J Neurosci 23:5662–5673.

Johnson D, Lanahan A, Buck CR, Sehgal A, Morgan C, Mercer E, Bothwell M, Chao M (1986) *Expression and structure of the human NGF receptor*. Cell 47:545–554.

Jonas P, Bischofberger J, Fricker D, Miles R (2004) *Interneuron Diversity series: Fast in, fast out--temporal and spatial signal processing in hippocampal interneurons*. Trends Neurosci 27:30–40.

Jones KR, Fariñas I, Backus C, Reichardt LF (1994) *Targeted disruption of the BDNF gene perturbs brain and sensory neuron development but not motor neuron development.* Cell 76:989–999.

Joëls M, Baram TZ (2009) *The neuro-symphony of stress*. Nat Rev Neurosci 10:459–466.

Kandel ER, Schwartz JH, Jessell TM (2000) *Principles of Neural Science*, 4th ed. McGraw-Hill Medical.

Kao S, Jaiswal RK, Kolch W, Landreth GE (2001) *Identification of the mechanisms regulating the differential activation of the mapk cascade by epidermal growth factor and nerve growth factor in PC12 cells.* J Biol Chem 276:18169–18177.

Karatsoreos IN, Bhagat SM, Bowles NP, Weil ZM, Pfaff DW, McEwen BS (2010) *Endocrine and physiological changes in response to chronic corticosterone: a potential model of the metabolic syndrome in mouse*. Endocrinology 151:2117–2127.

Kenchappa RS, Zampieri N, Chao MV, Barker PA, Teng HK, Hempstead BL, Carter BD (2006) *Ligand-dependent cleavage of the P75 neurotrophin receptor is necessary for NRIF nuclear translocation and apoptosis in sympathetic neurons*. Neuron 50:219–232.

Kernie SG, Liebl DJ, Parada LF (2000) *BDNF regulates eating behavior and locomotor activity in mice.* EMBO J 19:1290–1300.

Kimball SR, Farrell PA, Jefferson LS (2002) *Role of insulin in translational control of protein synthesis in skeletal muscle by amino acids or exercise*. J Appl Physiol 93:1168–1180.

Klausberger T, Somogyi P (2008) *Neuronal diversity and temporal dynamics: the unity of hippocampal circuit operations*. Science 321:53–57.

Klein R, Martin-Zanca D, Barbacid M, Parada LF (1990) *Expression of the tyrosine kinase receptor gene trkB is confined to the murine embryonic and adult nervous system.* Development 109:845–850.

de Kloet ER, Joëls M, Holsboer F (2005) *Stress and the brain: from adaptation to disease*. Nat Rev Neurosci 6:463–475.

Kohl MM, Paulsen O (2010) *The roles of GABAB receptors in cortical network activity.* Advances in Pharmacology 58:205–229.

Kolber BJ, Wieczorek L, Muglia L (2008) *Hypothalamic-pituitary-adrenal axis dysregulation and behavioral analysis of mouse mutants with altered glucocorticoid or mineralocorticoid receptor function.* Stress 11:321–338.

Kononen J, Soinila S, Persson H, Honkaniemi J, Hökfelt T, Pelto-Huikko M (1994) *Neurotrophins and their receptors in the rat pituitary gland: regulation of BDNF and trkB mRNA levels by adrenal hormones.* Brain Res Mol Brain Res 27:347–354.

Korte M, Staiger V, Griesbeck O, Thoenen H, Bonhoeffer T (1996) *The involvement of brain-derived neurotrophic factor in hippocampal long-term potentiation revealed by gene targeting experiments.* J Physiol 90:157–164.

Kovács KJ, Sawchenko PE (1996) *Sequence of stress-induced alterations in indices of synaptic and transcriptional activation in parvocellular neurosecretory neurons.* J Neurosci 16:262–273.

Kuo LE, Kitlinska JB, Tilan JU, Li L, Baker SB, Johnson MD, Lee EW, Burnett MS, Fricke ST, Kvetnansky R, Herzog H, Zukowska Z (2007) *Neuropeptide Y acts directly in the periphery on fat tissue and mediates stress-induced obesity and metabolic syndrome*. Nat Med 13:803–811.

Lebrun B, Bariohay B, Moyse E, Jean A (2006) *Brain-derived neurotrophic factor (BDNF) and food intake regulation: a minireview.* Auton Neurosci 126-127:30–38.

Lee R, Kermani P, Teng KK, Hempstead BL (2001) *Regulation of cell survival by secreted proneurotrophins.* Science 294:1945–1948.

Leevers SJ, Vanhaesebroeck B, Waterfield MD (1999) *Signalling through phosphoinositide 3-kinases: the lipids take centre stage.* Current Opin Cell Biol 11:219–225.

Lein ES et al. (2007) *Genome-wide atlas of gene expression in the adult mouse brain.* Nature 445:168–176.

Letinic K, Zoncu R, Rakic P (2002) *Origin of GABAergic neurons in the human neocortex.* Nature 417:645–649.

Levi-Montalcini R, Angeletti PU (1968) *Nerve growth factor.* Physiol Rev 48:534–569.

Levi-Montalcini R, Booker B (1960) *Destruction of the sympathetic ganglia in mammals by an antiserum to a nerve-growth protein.* PNAS 46:384–391.

Lewis DA, Hashimoto T, Volk DW (2005) *Cortical inhibitory neurons and schizophrenia.* Nat Rev Neurosci 6:312–324.

Lightman SL, Conway-Campbell BL (2010) *The crucial role of pulsatile activity of the HPA axis for continuous dynamic equilibration.* Nat Rev Neurosci 11:710–718.

Lillie R (1965) *Histopathologic Technis and Practical Histochemistry*, 3rd ed. New York: McGraw-Hill Book Co.

Linnarsson S, Björklund A, Ernfors P (1997) *Learning deficit in BDNF mutant mice.* Eur J Neurosci 9:2581–2587.

Liu X, Ernfors P, Wu H, Jaenisch R (1995) *Sensory but not motor neuron deficits in mice lacking NT4 and BDNF.* Nature 375:238–241.

Liu X, Jaenisch R (2000) *Severe peripheral sensory neuron loss and modest motor neuron reduction in mice with combined deficiency of brain-derived neurotrophic factor, neurotrophin 3 and neurotrophin 4/5.* Dev Dyn 218:94–101.

Lo CM, Samuelson LC, Chambers JB, King A, Heiman J, Jandacek RJ, Sakai RR, Benoit SC, Raybould HE, Woods SC, Tso P (2008) *Characterization of mice lacking the gene for cholecystokinin.* Am J Physiol Regul Integr Comp Physiol 294:R803–R810.

Lobe CG, Koop KE, Kreppner W, Lomeli H, Gertsenstein M, Nagy A (1999) *Z/AP, a double reporter for cre-mediated recombination.* Dev Biol 208:281–292.

Lupien SJ, McEwen BS, Gunnar MR, Heim C (2009) *Effects of stress throughout the lifespan on the brain, behaviour and cognition.* Nat Rev Neurosci 10, 434-45.

Luquet S, Perez FA, Hnasko TS, Palmiter RD (2005) *NPY/AgRP neurons are essential for feeding in adult mice but can be ablated in neonates*. Science 310:683–685.

Lyons WE, Mamounas LA, Ricaurte GA, Coppola V, Reid SW, Bora SH, Wihler C, Koliatsos VE, Tessarollo L (1999) *Brain-derived neurotrophic factor-deficient mice develop aggressiveness and hyperphagia in conjunction with brain serotonergic abnormalities.* PNAS 96:15239–15244.

Ma L, Reis G, Parada LF, Schuman EM (1999) *Neuronal NT-3 is not required for synaptic transmission or long-term potentiation in area CA1 of the adult rat hippocampus.* Learn Mem 6:267–275.

Maccaferri G, Lacaille JC (2003) *Interneuron Diversity series: Hippocampal interneuron classifications--making things as simple as possible, not simpler*. Trends Neurosci 26:564–571.

Maggirwar SB, Sarmiere PD, Dewhurst S, Freeman RS (1998) *Nerve growth factor-dependent activation of NF-kappaB contributes to survival of sympathetic neurons.* J Neurosci 18:10356–10365.

Marmigère F, Givalois L, Rage F, Arancibia S, Tapia-Arancibia L (2003) *Rapid induction of BDNF expression in the hippocampus during immobilization stress challenge in adult rats.* Hippocampus 13:646–655.

Martinowich K, Manji H, Lu B (2007) *New insights into BDNF function in depression and anxiety*. Nat Neurosci 10:1089–1093.

Martyn JAJ, Kaneki M, Yasuhara S (2008) *Obesity-induced insulin resistance and hyperglycemia: etiologic factors and molecular mechanisms.* Anesthesiology 109:137–148.

Marín O, Rubenstein JL (2001) *A long, remarkable journey: tangential migration in the telencephalon.* Nat Rev Neurosci 2:780–790.

Mascagni F, McDonald AJ (2003) *Immunohistochemical characterization of cholecystokinin containing neurons in the rat basolateral amygdala.* Brain Res 976:171–184.

Masuzaki H, Paterson J, Shinyama H, Morton NM, Mullins JJ, Seckl JR, Flier JS (2001) *A transgenic model of visceral obesity and the metabolic syndrome.* Science 294:2166–2170.

Matsuo S, Ichikawa H, Silos-Santiago I, Arends JJ, Henderson TA, Kiyomiya K, Kurebe M, Jacquin MF (2000) *Proprioceptive afferents survive in the masseter muscle of trkC knockout mice*. Neuroscience 95:209–216.

McAllister AK, Lo DC, Katz LC (1995) *Neurotrophins regulate dendritic growth in developing visual cortex*. Neuron 15:791–803.

McDonald NQ, Lapatto R, Murray-Rust J, Gunning J, Wlodawer A, Blundell TL (1991) *New protein fold revealed by a 2.3-A resolution crystal structure of nerve growth factor*. Nature 354:411–414.

Medina DL, Sciarretta C, Calella AM, Von Bohlen Und Halbach O, Unsicker K, Minichiello L (2004) *TrkB regulates neocortex formation through the Shc/PLCgamma-mediated control of neuronal migration*. Embo J 23:3803–3814.

Mendell LM (1999) *Neurotrophin action on sensory neurons in adults: an extension of the neurotrophic hypothesis*. Pain Suppl 6:S127–S132.

Miller L (2010) *Analyzing gels and western blots with ImageJ*. Available at: http://lukemiller.org/index.php/2010/11/analyzing-gels-and-western-blots-with-image-j/ [Accessed July 12, 2011].

Minichiello L (2009) *TrkB signalling pathways in LTP and learning*. Nat Rev Neurosci 10:850–860.

Minichiello L, Calella AM, Medina DL, Bonhoeffer T, Klein R, Korte M (2002) *Mechanism of TrkB-mediated hippocampal long-term potentiation*. Neuron 36:121–137.

Minichiello L, Casagranda F, Tatche RS, Stucky CL, Postigo A, Lewin GR, Davies AM, Klein R (1998) *Point mutation in trkB causes loss of NT4-dependent neurons without major effects on diverse BDNF responses*. Neuron 21:335–345.

Minichiello L, Klein R (1996) *TrkB and TrkC neurotrophin receptors cooperate in promoting survival of hippocampal and cerebellar granule neurons*. Genes Dev 10:2849–2858.

Minichiello L, Korte M, Wolfer D, Kuhn R, Unsicker K, Cestari V, Rossi-Arnaud C, Lipp HP, Bonhoeffer T, Klein R, Kühn R (1999) *Essential role for TrkB receptors in hippocampus-mediated learning*. Neuron 24:401–414.

Minichiello L, Piehl F, Vazquez E, Schimmang T, Hokfelt T, Represa J, Klein R (1995) *Differential effects of combined trk receptor mutations on dorsal root ganglion and inner ear sensory neurons*. Development 121:4067–4075.

Miyoshi G, Fishell G (2010) *GABAergic Interneuron Lineages Selectively Sort into Specific Cortical Layers during Early Postnatal Development.* Cereb Cortex 21(4):845-52.

Monteggia LM, Luikart B, Barrot M, Theobold D, Malkovska I, Nef S, Parada LF, Nestler EJ (2007) *Brain-derived neurotrophic factor conditional knockouts show gender differences in depression-related behaviors.* Biol Psychiatry 61:187–197.

Morozov YM, Torii M, Rakic P (2009) *Origin, early commitment, migratory routes, and destination of cannabinoid type 1 receptor-containing interneurons.* Cereb Cortex 19 Suppl 1:i78–i89.

Morton GJ, Cummings DE, Baskin DG, Barsh GS, Schwartz MW (2006) *Central nervous system control of food intake and body weight.* Nature 443:289–295.

Morton GJ and Schwartz MW (2011) *Leptin and the central nervous system control of glucose metabolism.* Physiol Rev 91, 389-411.

Mott DD, Dingledine R (2003) *Interneuron Diversity series: Interneuron research--challenges and strategies.* Trends Neurosci 26:484–488.

Mowla SJ, Pareek S, Farhadi HF, Petrecca K, Fawcett JP, Seidah NG, Morris SJ, Sossin WS, Murphy RA (1999) *Differential sorting of nerve growth factor and brain-derived neurotrophic factor in hippocampal neurons.* J Neurosci 19:2069–2080.

Musumeci G, Sciarretta C, Rodriguez-Moreno A, Al Banchaabouchi M, Negrete-Diaz V, Costanzi M, Berno V, Egorov AV, von Bohlen Und Halbach O, Cestari V, Delgado-Garcia JM, Minichiello L (2009) *TrkB modulates fear learning and amygdalar synaptic plasticity by specific docking sites.* J Neurosci 29:10131–10143.

Müller MB, Holsboer F (2006) *Mice with mutations in the HPA-system as models for symptoms of depression.* Biol Psychiatry 59:1104–1115.

Naert G, Ixart G, Maurice T, Tapia-Arancibia L, Givalois L (2010) *Brain-derived neurotrophic factor and hypothalamic-pituitary-adrenal axis adaptation processes in a depressive-like state induced by chronic restraint stress.* Mol Cell Neurosci.

Naert G, Ixart G, Tapia-Arancibia L, Givalois L (2006) *Continuous i.c.v. infusion of brain-derived neurotrophic factor modifies hypothalamic-pituitary-adrenal axis activity, locomotor activity and body temperature rhythms in adult male rats.* Neuroscience 139:779–789.

Nakajima T, Sato M, Akaza N, Umezawa Y (2008) *Cell-based fluorescent indicator to visualize brain-derived neurotrophic factor secreted from living neurons*. ACS Chemical Biology 3:352–358.

Nieuwenhuizen AG, Rutters F (2008) *The hypothalamic-pituitary-adrenal-axis in the regulation of energy balance*. Physiol Behav 94:169–177.

Njå A, Purves D (1978) *The effects of nerve growth factor and its antiserum on synapses in the superior cervical ganglion of the guinea-pig*. J Physiol 277:53–75.

Novak A, Guo C, Yang W, Nagy A, Lobe CG (2000) *Z/EG, a double reporter mouse line that expresses enhanced green fluorescent protein upon Cre-mediated excision*. Genesis 28:147–155.

Numakawa T, Kumamaru E, Adachi N, Yagasaki Y, Izumi A, Kunugi H (2009) *Glucocorticoid receptor interaction with TrkB promotes BDNF-triggered PLC-gamma signaling for glutamate release via a glutamate transporter*. PNAS 106:647–652.

Nunzi MG, Gorio A, Milan F, Freund TF, Somogyi P, Smith AD (1985) *Cholecystokinin-immunoreactive cells form symmetrical synaptic contacts with pyramidal and nonpyramidal neurons in the hippocampus*. J Comp Neurol 237:485–505.

Nykjaer A, Lee R, Teng KK, Jansen P, Madsen P, Nielsen MS, Jacobsen C, Kliemannel M, Schwarz E, Willnow TE, Hempstead BL, Petersen CM (2004) *Sortilin is essential for proNGF-induced neuronal cell death*. Nature 427:843–848.

Pascual M, Acsady L, Rocamora N, Freund TF, Soriano E (1999) *Expression of neurotrophins in hippocampal interneurons immunoreactive for the neuropeptides somatostatin, neuropeptide-Y, vasoactive intestinal polypeptide and cholecystokinin*. Neuroscience 89:1089–1101.

Pasquali R, Vicennati V, Cacciari M, Pagotto U (2006) *The hypothalamic-pituitary-adrenal axis activity in obesity and the metabolic syndrome*. Ann N Y Acad Sci 1083:111–128.

Patterson SL, Abel T, Deuel TA, Martin KC, Rose JC, Kandel ER (1996) *Recombinant BDNF rescues deficits in basal synaptic transmission and hippocampal LTP in BDNF knockout mice*. Neuron 16:1137–1145.

Patterson SL, Grover LM, Schwartzkroin PA, Bothwell M (1992) *Neurotrophin expression in rat hippocampal slices: a stimulus paradigm inducing LTP in CA1 evokes increases in BDNF and NT-3 mRNAs*. Neuron 9:1081–1088.

Patterson SL, Pittenger C, Morozov A, Martin KC, Scanlin H, Drake CT, Kandel ER (2001) *Some forms of cAMP-mediated long-lasting potentiation are associated with release of BDNF and nuclear translocation of phospho-MAP kinase*. Neuron 32:123–140.

Peeke PM, Chrousos GP (1995) *Hypercortisolism and Obesity*. Ann N Y Acad Sci 771:665–676.

Pelleymounter MA, Cullen MJ, Wellman CL (1995) *Characteristics of BDNF-Induced Weight Loss*. Exp Neurol 238:229–238.

Polleux F, Whitford KL, Dijkhuizen PA, Vitalis T, Ghosh A (2002) *Control of cortical interneuron migration by neurotrophins and PI3-kinase signaling.* Development 129:3147–3160.

Pozzo-Miller LD, Gottschalk W, Zhang L, McDermott K, Du J, Gopalakrishnan R, Oho C, Sheng ZH, Lu B (1999) *Impairments in high-frequency transmission, synaptic vesicle docking, and synaptic protein distribution in the hippocampus of BDNF knockout mice.* J Neurosci 19:4972–4983.

Price CJ, Hoyda TD, Ferguson AV (2008) *The area postrema: a brain monitor and integrator of systemic autonomic state.* Neuroscientist 14:182–194.

Rage F, Givalois L, Marmigère F, Tapia-Arancibia L, Arancibia S (2002) *Immobilization stress rapidly modulates BDNF mRNA expression in the hypothalamus of adult male rats.* Neuroscience 112:309–318.

Rajagopal R, Chao MV (2006) *A role for Fyn in Trk receptor transactivation by G-protein-coupled receptor signaling.* Mol Cell Neurosci 33:36–46.

Rasband WS (2011) *ImageJ*, http://imagej.nih.gov/ij/, Bethesda, Maryland, USA.

Rehfeld JF, Bungaard JR, Friis-Hansen L, Goetze JP (2003) *On the tissue-specific processing of procholecystokinin in the brain and gut--a short review*. J Physiol Pharmacol 54 Suppl 4:73–79.

Reichardt HM, Kaestner KH, Tuckermann J, Kretz O, Wessely O, Bock R, Gass P, Schmid W, Herrlich P, Angel P, Schütz G (1998) *DNA binding of the glucocorticoid receptor is not essential for survival.* Cell 93:531–541.

Reichardt LF (2006) *Neurotrophin-regulated signalling pathways*. Philos Trans R Soc Lond B Biol Sci 361:1545–1564.

Rho JH, Swanson LW (1989*) A morphometric analysis of functionally defined subpopulations of neurons in the paraventricular nucleus of the rat with observations on the effects of colchicine.* J Neurosci 9:1375–1388.

Riccio A, Ahn S, Davenport CM, Blendy JA, Ginty DD (1999) *Mediation by a CREB family transcription factor of NGF-dependent survival of sympathetic neurons.* Science 286:2358–2361.

Richard D, Huang Q, Timofeeva E (2000) *The corticotropin-releasing hormone system in the regulation of energy balance in obesity.* Int J Obes Relat Metab Disord 24 Suppl 2:S36–S39.

Rico B, Xu B, Reichardt LF (2002) *TrkB receptor signaling is required for establishment of GABAergic synapses in the cerebellum*. Nat Neurosci 5:225–233.

Rios M, Fan G, Fekete C, Kelly J, Bates B, Kuehn R, Lechan RM, Jaenisch R (2001) *Conditional deletion of brain-derived neurotrophic factor in the postnatal brain leads to obesity and hyperactivity*. Mol Endocrinol 15:1748–1757.

Rivera C, Voipio J, Payne JA, Ruusuvuori E, Lahtinen H, Lamsa K, Pirvola U, Saarma M, Kaila K (1999) *The K+/Cl- co-transporter KCC2 renders GABA hyperpolarizing during neuronal maturation*. Nature 397:251–255.

Rotzinger S, Vaccarino FJ (2003) *Cholecystokinin receptor subtypes: role in the modulation of anxiety-related and reward-related behaviours in animal models.* J Psychiatry Neurosci 28:171–181.

Saiardi A, Borrelli E (1998) *Absence of dopaminergic control on melanotrophs leads to Cushing's-like syndrome in mice*. Mol Endocrinol 12:1133–1139.

Saito N, Shirai Y (2002) *Protein kinase C gamma (PKC gamma): function of neuron specific isotype.* J Biochem 132:683–687.

Schaaf MJ, Hoetelmans RW, de Kloet ER, Vreugdenhil E (1997) *Corticosterone regulates expression of BDNF and trkB but not NT-3 and trkC mRNA in the rat hippocampus.* J Neurosci Res 48:334–341.

Schecterson LC, Bothwell M (2010) *Neurotrophin receptors: Old friends with new partners.* Dev Neurobiol 70:332–338.

Schiffmann SN, Vanderhaeghen JJ (1991) *Distribution of cells containing mRNA encoding cholecystokinin in the rat central nervous system*. J Comp Neurol 304:219–233.

Schimmang T, Minichiello L, Vazquez E, San Jose I, Giraldez F, Klein R, Represa J (1995) *Developing inner ear sensory neurons require TrkB and TrkC receptors for innervation of their peripheral targets*. Development 121:3381–3391.

Schmidt MV, Sterlemann V, Wagner K, Niederleitner B, Ganea K, Liebl C, Deussing JM, Berger S, Schütz G, Holsboer F, Müller MB (2009) *Postnatal glucocorticoid excess due to pituitary glucocorticoid receptor deficiency: differential short- and long-term consequences.* Endocrinology 150:2709–2716.

Schober A, Wolf N, Kahane N, Kalcheim C, Krieglstein K, Unsicker K (1999) *Expression of neurotrophin receptors trkB and trkC and their ligands in rat adrenal gland and the intermediolateral column of the spinal cord.* Cell Tissue Res 296:271–279.

Schule C, Zill P, Baghai TC, Eser D, Zwanzger P, Wenig N, Rupprecht R, Bondy B (2006) *Brain-derived neurotrophic factor Val66Met polymorphism and dexamethasone/CRH test results in depressed patients*. Psychoneuroendocrinology 31:1019–1025.

Schwartz MW, Woods SC, Porte D, Seeley RJ, Baskin DG (2000) *Central nervous system control of food intake*. Nature 404:661–671.

Schwartz PM, Borghesani PR, Levy RL, Pomeroy SL, Segal RA (1997) *Abnormal cerebellar development and foliation in BDNF-/- mice reveals a role for neurotrophins in CNS patterning*. Neuron 19:269–281.

Schäfer T, Schwab ME, Thoenen H (1983) *Increased formation of preganglionic synapses and axons due to a retrograde trans-synaptic action of nerve growth factor in the rat sympathetic nervous system.* J Neurosci 3:1501–1510.

Seale JV, Wood SA, Atkinson HC, Bate E, Lightman SL, Ingram CD, Jessop DS, Harbuz MS (2004) *Gonadectomy reverses the sexually diergic patterns of circadian and stress-induced hypothalamic-pituitary-adrenal axis activity in male and female rats*. J Neuroendocrinol 16:516–524.

Seidah NG, Benjannet S, Pareek S, Chrétien M, Murphy RA (1996) *Cellular processing of the neurotrophin precursors of NT3 and BDNF by the mammalian proprotein convertases.* FEBS Lett 379:247–250.

Senatorov VV, Trudeau VL, Hu B (1995) *Expression of cholecystokinin mRNA in corticothalamic projecting neurons: a combined fluorescence in situ hybridization and retrograde tracing study in the ventrolateral thalamus of the rat*. Brain Res Mol Brain Res 30:87–96.

Shalev I, Lerer E, Israel S, Uzefovsky F, Gritsenko I, Mankuta D, Ebstein RP, Kaitz M (2009) *BDNF Val66Met polymorphism is associated with HPA axis reactivity to psychological stress characterized by genotype and gender interactions*. Psychoneuroendocrinology 34:382–388.

Shu XQ, Mendell LM (1999) *Neurotrophins and hyperalgesia*. PNAS 96:7693–7696.

Skaper SD (2008) *The biology of neurotrophins, signalling pathways, and functional peptide mimetics of neurotrophins and their receptors*. CNS Neurol Disord Drug Targets 7:46–62.

Sloviter RS, Nilaver G (1987) *Immunocytochemical localization of GABA-, cholecystokinin-, vasoactive intestinal polypeptide-, and somatostatin-like immunoreactivity in the area dentata and hippocampus of the rat.* J Comp Neurol 256:42–60.

Smeyne RJ, Klein R, Schnapp A, Long LK, Bryant S, Lewin A, Lira SA, Barbacid M (1994) *Severe sensory and sympathetic neuropathies in mice carrying a disrupted Trk/NGF receptor gene*. Nature 368:246–249.

Soderling TR (2000) *CaM-kinases: modulators of synaptic plasticity*. Curr Opin Neurobiol 10:375–380.

Somogyi P, Klausberger T (2005) *Defined types of cortical interneurone structure space and spike timing in the hippocampus*. J Physiol 562:9–26.

Son GH, Chung S, Kim K (2011) *The adrenal peripheral clock: Glucocorticoid and the circadian timing system.* Front Neuroendocrinol. [in press – September 2011]

Spiegelman BM, Flier JS (2001) *Obesity and the regulation of energy balance*. Cell 104:531–543.

Spina M, Merlo-Pich E, Chan RK, Basso AM, Rivier J, Vale W, Koob GF (1996) *Appetite-suppressing effects of urocortin, a CRF-related neuropeptide.* Science 273:1561–1564.

Srinivas S, Watanabe T, Lin CS, William CM, Tanabe Y, Jessell TM, Costantini F (2001) *Cre reporter strains produced by targeted insertion of EYFP and ECFP into the ROSA26 locus*. BMC Dev Biol 1:4.

Stenzel-Poore MP, Cameron VA, Vaughan J, Sawchenko PE, Vale WW (1992) *Development of Cushing's syndrome in corticotropin-releasing factor transgenic mice.* Endocrinology 130:3378–3386.

Sternson SM, Shepherd GMG, Friedman JM (2005) *Topographic mapping of VMH --> arcuate nucleus microcircuits and their reorganization by fasting*. Nat Neurosci 8:1356–1363.

Swanson J-D, Carlson JE, Guiltinan MJ (2006) *Use of image analysis software as a tool to visualize non-radioactive signals in plant in situ analysis*. Plant Molecular Biology Reporter 24:105–105.

Sánchez-Huertas C, Rico B (2011) *CREB-Dependent Regulation of GAD65 Transcription by BDNF/TrkB in Cortical Interneurons*. Cereb Cortex 21:777–788.

Tapia-Arancibia L, Rage F, Givalois L, Arancibia S (2004) *Physiology of BDNF: focus on hypothalamic function*. Front Neuroendocrinol 25:77–107.

Teng HK, Teng KK, Lee R, Wright S, Tevar S, Almeida RD, Kermani P, Torkin R, Chen Z-Y, Lee FS, Kraemer RT, Nykjaer A, Hempstead BL (2005) *ProBDNF induces neuronal apoptosis via activation of a receptor complex of p75NTR and sortilin*. J Neurosci 25:5455–5463.

Teng KK, Felice S, Kim T, Hempstead BL (2010) *Understanding proneurotrophin actions: Recent advances and challenges*. Dev Neurobiol 70:350–359.

Tessarollo L, Tsoulfas P, Martin-Zanca D, Gilbert DJ, Jenkins NA, Copeland NG, Parada LF (1993) *trkC, a receptor for neurotrophin-3, is widely expressed in the developing nervous system and in non-neuronal tissues*. Development 118:463–475.

Toriya M, Maekawa F, Maejima Y, Onaka T, Fujiwara K, Nakagawa T, Nakata M, Yada T (2010) *Long-term infusion of brain-derived neurotrophic factor reduces food intake and body weight via a corticotrophin-releasing hormone pathway in the paraventricular nucleus of the hypothalamus*. J Neuroendocrinol 22:987–995.

Tricoire L, Pelkey K a, Erkkila BE, Jeffries BW, Yuan X, McBain CJ (2011) *A Blueprint for the Spatiotemporal Origins of Mouse Hippocampal Interneuron Diversity*. J Neurosci 31:10948–10970.

Tronche F, Kellendonk C, Kretz O, Gass P, Anlag K, Orban PC, Bock R, Klein R, Schütz G (1999) *Disruption of the glucocorticoid receptor gene in the nervous system results in reduced anxiety*. Nat Gen 23:99–103.

Tucker KL, Meyer M, Barde YA (2001) *Neurotrophins are required for nerve growth during development*. Nat Neurosci 4:29–37.

Uehara Y, Shimizu H, Ohtani K, Sato N, Mori M (1998) *Hypothalamic corticotropin-releasing hormone is a mediator of the anorexigenic effect of leptin*. Diabetes 47:890–893.

Ulrich-Lai YM, Herman JP (2009) *Neural regulation of endocrine and autonomic stress responses*. Nat Rev Neurosci 10:397–409.

Unger TJ, Calderon GA, Bradley LC, Sena-Esteves M, Rios M (2007) *Selective deletion of Bdnf in the ventromedial and dorsomedial hypothalamus of adult mice results in hyperphagic behavior and obesity*. J Neurosci 27:14265–14274.

Urfer R, Tsoulfas P, O'Connell L, Shelton DL, Parada LF, Presta LG (1995) *An immunoglobulin-like domain determines the specificity of neurotrophin receptors.* EMBO J 14:2795–2805.

Vanderhaeghen JJ, Lotstra F, De Mey J, Gilles C (1980) *Immunohistochemical localization of cholecystokinin- and gastrin-like peptides in the brain and hypophysis of the rat*. PNAS 77:1190–1194.

Viau V, Sawchenko PE (2002) *Hypophysiotropic neurons of the paraventricular nucleus respond in spatially, temporally, and phenotypically differentiated manners to acute vs. repeated restraint stress: rapid publication*. J Comp Neurol 445:293–307.

Vilar M, Charalampopoulos I, Kenchappa RS, Reversi A, Klos-Applequist JM, Karaca E, Simi A, Spuch C, Choi S, Friedman WJ, Ericson J, Schiavo G, Carter BD, Ibáñez CF (2009a) *Ligand-independent signaling by disulfide-crosslinked dimers of the p75 neurotrophin receptor*. J Cell Sci 122:3351–3357.

Vilar M, Charalampopoulos I, Kenchappa RS, Simi A, Karaca E, Reversi A, Choi S, Bothwell M, Mingarro I, Friedman WJ, Schiavo G, Bastiaens PIH, Verveer PJ, Carter BD, Ibáñez CF (2009b) *Activation of the p75 neurotrophin receptor through conformational rearrangement of disulphide-linked receptor dimers*. Neuron 62:72–83.

Vinberg M, Trajkovska V, Bennike B, Knorr U, Knudsen GM, Kessing LV (2009) *The BDNF Val66Met polymorphism: relation to familiar risk of affective disorder, BDNF levels and salivary cortisol.* Psychoneuroendocrinology 34:1380–1389.

Volpi S, Rabadan-Diehl C, Aguilera G (2004) *Vasopressinergic regulation of the hypothalamic pituitary adrenal axis and stress adaptation*. Stress 7:75–83.

Wamsteeker JI, Bains JS (2010) *A synaptocentric view of the neuroendocrine response to stress.* Eur J Neurosci 32:2011–2021.

Wang C, Bomberg E, Billington C, Levine A, Kotz CM (2007) *Brain-derived neurotrophic factor in the hypothalamic paraventricular nucleus reduces energy intake*. Am J Physiol Regul Integr Comp Physiol 293:R1003–R1012.

Wang F, Herzmark P, Weiner OD, Srinivasan S, Servant G, Bourne HR (2002) *Lipid products of PI(3)Ks maintain persistent cell polarity and directed motility in neutrophils*. Nat Cell Biol 4:513–518.

Wang Y, Sheen VL, Macklis JD (1998) *Cortical interneurons upregulate neurotrophins in vivo in response to targeted apoptotic degeneration of neighboring pyramidal neurons.* Exp Neurol 154:389–402.

de Wardener HE (2001) *The hypothalamus and hypertension*. Physiol Rev 81:1599–1658.

Watanabe T, Orth DN (1987) *Detailed Kinetic Analysis of Adrenocorticotropin Secretion by Dispersed Rat Anterior Pituitary Cells in a Microperifusion System: Effects of Ovine Corticotropin-Releasing Factor and Arginine Vasopressin*. Endocrinology 121:1133–1145.

Watts AG (2005) *Glucocorticoid regulation of peptide genes in neuroendocrine CRH neurons: a complexity beyond negative feedback*. Front Neuroendocrinol 26:109–130.

Westphal CH, Muller L, Zhou A, Zhu X, Bonner-Weir S, Schambelan M, Steiner DF, Lindberg I, Leder P (1999) *The neuroendocrine protein 7B2 is required for peptide hormone processing in vivo and provides a novel mechanism for pituitary Cushing's disease*. Cell 96:689–700.

Wonders C, Anderson S a (2005) *Cortical interneurons and their origins*. Neuroscientist 11:199–205.

Woo NH, Lu B (2006) *Regulation of cortical interneurons by neurotrophins: from development to cognitive disorders*. Neuroscientist 12:43–56.

Wu C, Cui B, He L, Chen L, Mobley WC (2009) *The coming of age of axonal neurotrophin signaling endosomes*. J Proteomics 72:46–55.

Wu C, Lai CF, Mobley WC (2001) *Nerve growth factor activates persistent Rap1 signaling in endosomes.* J Neurosci 21:5406–5416.

Wölfl S, Martinez C, Majzoub JA (1999) *Inducible binding of cyclic adenosine 3',5'-monophosphate (cAMP)-responsive element binding protein (CREB) to a cAMP-responsive promoter in vivo.* Mol Endocrinol 13:659–669.

Xie CW, Sayah D, Chen QS, Wei WZ, Smith D, Liu X (2000) *Deficient long-term memory and long-lasting long-term potentiation in mice with a targeted deletion of neurotrophin-4 gene.* PNAS 97:8116–8121.

Xing J, Kornhauser JM, Xia Z, Thiele EA, Greenberg ME (1998) *Nerve growth factor activates extracellular signal-regulated kinase and p38 mitogen-activated protein kinase pathways to stimulate CREB serine 133 phosphorylation.* Mol Cell Biol 18:1946–1955.

Xu B, Goulding EH, Zang K, Cepoi D, Cone RD, Jones KR, Tecott LH, Reichardt LF (2003a) *Brain-derived neurotrophic factor regulates energy balance downstream of melanocortin-4 receptor*. Nat Neurosci 6:736–742.

Xu B, Zang K, Ruff NL, Zhang YA, McConnell SK, Stryker MP, Reichardt LF (2000) *Cortical degeneration in the absence of neurotrophin signaling: dendritic retraction and neuronal loss after removal of the receptor TrkB*. Neuron 26:233–245.

Xu Q, de la Cruz E, Anderson SA (2003b) *Cortical interneuron fate determination: diverse sources for distinct subtypes?* Cereb Cortex 13:670–676.

Yamada M, Ohnishi H, Sano S i, Nakatani A, Ikeuchi T, Hatanaka H (1997) *Insulin receptor substrate (IRS)-1 and IRS-2 are tyrosine-phosphorylated and associated with phosphatidylinositol 3-kinase in response to brain-derived neurotrophic factor in cultured cerebral cortical neurons.* J Biol Chem 272:30334–30339.

Yamashita H, Avraham S, Jiang S, Dikic I, Avraham H (1999) *The Csk homologous kinase associates with TrkA receptors and is involved in neurite outgrowth of PC12 cells.* J Biol Chem 274:15059–15065.

Yuan XB, Jin M, Xu X, Song YQ, Wu CP, Poo MM, Duan S (2003) *Signalling and crosstalk of Rho GTPases in mediating axon guidance*. Nat Cell Biol 5:38–45.

Zachrisson O, Falkenberg T, Lindefors N (1996) *Neuronal coexistence of trkB and glutamic acid decarboxylase67 mRNAs in rat hippocampus*. Brain Res Mol Brain Res 36:169–173.

Zhang Y, Proenca R, Maffei M, Barone M, Leopold L, Friedman JM (1994) *Positional cloning of the mouse obese gene and its human homologue*. Nature 372:425–432.

Zorner B, Wolfer DP, Brandis D, Kretz O, Zacher C, Madani R, Grunwald I, Lipp H-P, Klein R, Henn FA, Gass P, Zörner B (2003) *Forebrain-specific trkB-receptor knockout mice: behaviorally more hyperactive than "depressive"*. Biol Psychiatry 54:972–982.